UNIVERSITY OF SOUTHERN CALIFORNIA

BUILDING PERIODS FOR USE IN EARTHQUAKE RESISTANT DESIGN CODES – EARTHQUAKE RESPONSE DATA COMPILATION AND ANALYSIS OF TIME AND AMPLITUDE VARIATIONS

Final Project Report

Submitted to U.S. Geological Survey External Research Program

Project No. 05HQGR027

(12/01/2004—11/30/2005)

Principal Investigator:

Maria I. Todorovska
University of Southern California
Civil Engineering Department
Los Angeles, CA 90089-2531
Tel. (213) 740-0616; fax. (213) 744-1426
E-mail: mtodorov@usc.edu;
URL: http://www-rcf.usc.edu/~mtodorov/

Other contributors:

M. D. Trifunac
T.-Y Hao
Y. Al Rjoub

Los Angeles
October 3, 2007

BUILDING PERIODS FOR USE IN EARTHQUAKE RESISTANT DESIGN CODES – EARTHQUAKE RESPONSE DATA COMPILATION AND ANALYSIS OF TIME AND AMPLITUDE VARIATIONS

Final Project Report

Submitted to U.S. Geological Survey External Research Program

Project No. 05HQGR027

(12/01/2004—11/30/2005)

Principal Investigator:
Maria I. Todorovska
University of Southern California
Civil Engineering Department
Los Angeles, CA 90089-2531
Tel. (213) 740-0616; fax. (213) 744-1426
E-mail: mtodorov@usc.edu;
URL: http://www-rcf.usc.edu/~mtodorov/

Other contributors:
M. D. Trifunac
T.-Y Hao
Y. Al Rjoub

ABSTRACT

Estimation of the frequencies of buildings from actual earthquake response data, and understanding how they vary with time and depending on the level of shaking is important for the improvement of the building codes, as the design base shear coefficient and the response amplitudes are estimated based on the building frequency.

This project contributed new strong motion data of the response of 21 buildings in the Los Angeles area (instrumented by USGS or "code" buildings) to the 1994 Northridge earthquake and its aftershocks, which were digitized and processed for this project. Although the number of recorded aftershocks in many of these buildings was large (up to about 80), only a small number of records were found to be useable for analysis of the building frequencies, because of the small signal to noise ratio at long periods.

The "instantaneous" building-foundation-soil system frequency and amplitude of response were estimated by two methods—zero crossing analysis, and Gabor transform time-frequency

analysis, and were plotted on same graphs to find the trends of the variation of frequency as function of amplitude of response for all recorded events. Despite the scatter, the data shows clear dependence of the observed building frequencies on the amplitudes of response. The frequency decreased during the largest event and recovered during the aftershocks, but for some of the buildings there was a permanent reduction. For angles of response up to 10 mili radians (including rigid body motion and deflection due to deformation of the structure, which could not be separated), the building periods during the small amplitude responses ($T_{\min}$) did not exceed 3.3 s, and during the largest amplitude responses ($T_{\max}$) did not exceed 4.5 s. Alternatively, the building frequencies during the largest motions ($f_{\min}$) did not exceed 3 Hz, and during the small motions ($f_{\max}$) did not exceed 3.5 Hz. The observed changes in period of vibration ($\Delta T / T_{\min}$) approached 50%, in frequency of vibration ($\Delta f / f_{\max}$) approached 35%, and in stiffness (of the soil-structure system) ($\Delta k / k_{\max}$) approached 55%. Large scatter was observed in the correlation plots of these changes with the maximum amplitudes of response, which is believed to be mostly due to variations among the buildings in structural material (reinforced concrete vs. steal), structural type (ductile vs. nonductile frame), foundation type, and local soil conditions (which would determine the degree to which the response was influenced by the soil-structure interaction), and whether the building was damaged by the earthquake. This information was not readily available for the majority of the buildings in this set (the "code" buildings). A detailed analysis of the causes of the observed changes, and separate analysis for different groups of buildings (depending on type, local soil conditions, etc.) was beyond the scope of this project.

ACKNOWLEDGEMENTS

This work was supported by U.S. Geological Survey External Research Program (Grants No. 03HQGR0013, and 05HQGR027). All views presented are solely those of the authors and do not necessarily represent the official views of the U.S. Government. The authors are also grateful to Chris Stephens of the U.S. Geological Survey for kindly supplying film records for this project from the National Strong Motion Program archives.

TABLE OF CONTENTS

ABSTRACT i

ACKNOWLEDGEMENTS iii

1. INTRODUCTION 1

2. STRONG MOTION DATA 5

3. METHODOLOGY 10

3.1 Estimation of Instantaneous Frequency during an Earthquake 10

3.2 Illustrations of Instantaneous Frequency for Selected Earthquake Records 13

3.3 Estimation of Tends in Time and Amplitude Variations of Frequency for Multiple Earthquakes 20

4. RESULTS AND ANALYSIS 23

5. DISCUSSION AND CONCLUSIONS 38

APPENDIX A: STRONG MOTION DATA RELEASED (pp. 17)

APPENDIX B: DETAILED RESULTS FOR TIME AND AMPITUDE VARIATIONS OF THE INSTANTANEOUS BUILDING-FOUNDATION-SOIL SYSTEM FREQUENCY (pp. 85)

1. INTRODUCTION

In most earthquake resistant design codes, the design shear forces are quantified using the seismic coefficient $C(T)$, where T is the "fundamental vibration period of the building," and various scaling factors that depend on the seismic zone, type of structure, soil site conditions, importance of the structure etc. As the building period cannot be measured for a particular structure before its construction, most codes provide simplified empirical formulae for its estimation, based on past experience and recorded response of existing buildings. The problem of estimation of T has been considered by many investigators, based on theory [Biot 1942], small amplitude ambient and forced vibration tests of full-scale structures [Carder 1936], and recorded earthquake response [Li and Mau 1979].

The most reliable are the estimates of building periods obtained from recorded earthquake response. Such data are, however, extremely limited, both in quantity and in quality. The number of well-documented instrumented buildings that have recorded at least one strong earthquake is typically less than 100. When the recorded data is grouped by structural systems (moment resistant frame, shear wall etc.) and building materials (reinforced concrete, steal, etc.), the number of records per group becomes too small to control the accuracy of regression analyses, or to separate "good" from "bad" empirical models [Goel and Chopra 1997; Stewart et al. 1999]. This problem is further complicated by the nonlinearity of the foundation soil even for very small strains [Hudson 1970; Luco et al. 1987]. During strong earthquake shaking, the apparent period of the soil-foundation-structure system can lengthen significantly [Udwadia and Trifunac 1974], and it may or may not return to its pre earthquake value. Environmental factors, such as temperature and heavy rainfall have also been found to cause small but systematic temporary changes [Clinton et al. 2006; Todorovska and Al Rjoub 2006]. All of these factors contribute to the scatter in empirical regression analyses of building periods, and to ambiguity in choosing a representative T for evaluation of $C(T)$ [Trifunac 1999; 2000].

For further improvements and developments of the building codes, it is essential to understand the amplitude dependent period lengthening (as function of the level of response of the structure and strain in the soil), and estimate its range. This can be best accomplished by analysis of building periods from multiple earthquake recordings in buildings—of both small and

large levels of shaking. The first step towards this goal is to augment the database of multiple earthquake records in buildings, which is very limited, because most buildings records have been recorded on film, and typically only those with larger amplitudes have been digitized and released. Data of small amplitude response is being generated fast from instrumented buildings with a digital recording system, but it may take many years before they record larger amplitude response. Hence, as far as the building design codes are considered, the use of small amplitude data from newly instrumented buildings is quite limited. While small amplitude data are useful in those buildings in which large amplitude response has already been recorded by analog recorders, replaced by the digital system, smaller amplitude analog recordings of past earthquakes are also very valuable—for understanding of the variations of building periods with time, as the changes may be temporary or permanent. In the Los Angeles metropolitan area, there have been many small earthquakes and aftershocks of larger earthquakes that have been recorded in buildings and archived but not digitized and released.

To this effect, this two-year project was initiated at the University of Southern California, funded by the U.S. Geological Survey External Research Program, with the objectives to:

(1) Augment the pool of processed building response data, in particular with multiple recordings corresponding to different levels of shaking, by digitizing and processing records in buildings of aftershocks of the 1994 Northridge earthquake, of the main event not yet processed or processed inadequately, and of other earthquakes to complement the Northridge data set.

(2) Augment the knowledge base on the variations of the building periods during earthquakes as a function of the level of response and time, with the ultimate objective to improve the code formulae for estimation of building periods.

The scope of this project included only records archived by the U.S. Geological Survey, and only buildings with multiple records one of which at least is a significant event. The objective of the analysis of the variations of the building periods was to find out the trends and quantify the changes for the subset of buildings and amplitudes of response covered by the data used for this project. Detailed analysis of these changes as function of the building structural type, type of

foundation, and local soil conditions is out of the scope of this project, as such information is not readily available for many of the buildings (in particular for the "code" buildings).

This report presents results for 21 buildings for which the earthquake records satisfied the requirement for this analysis. Results for the first set of 7 buildings can be found in Todorovska et al. [2004a,b], and a summary of the results for the 21 buildings can be found in Todorovska et al. [2006], which was presented at the First European Conference on Earthquake Engineering and Seismology (a joint event of the 13th ECEE and 30th General Assembly of the ESC), which was held in Geneva, Switzerland, 3-8 September 2006. The paper was presented as part of the special *debate* session entitled "By how much does the natural frequency of structures decrease during seismic response?", which was chaired by Dr. Todorovska, the Principal Investigator of this project. The session created significant interest, being attended by more than 100 individuals, and resulting in a community web site where researchers can post results on this topic (URL: http://www.usc.edu/dept/civil_eng/Earthquake_eng/ECEES_STS-E10/). The interest in this session also motivated a NATO Workshop, organized by M. Mucciareli and M. Herak, and held in Dubrovnik in September of 2007.

This report is organized as follows. Chapter 2 presents a summary of the processed data for this project, Chapter 3 presents the methodology used for estimation of instantaneous frequency from building response data and illustrations, Chapter 4 presents a summary of the results for the building periods, and Chapter 5 presents the conclusions. Appendix A lists the strong motion data released, Appendix B presents detailed results for each building of the variation of the building frequencies as function of the amplitudes of response (expressed as deflection angle) for a series of instances of time, which were used to "read" the range of the variations of the building frequencies and the corresponding amplitudes of response. The strong motion data is posted on USC web, and can be accessed via the project web page at

http://www.usc.edu/dept/civil_eng/Earthquake_eng/USGS_build/

or directly by ftp from ftp://cwis.usc.edu/pub/todorovs/USGS_build/ .

2. STRONG MOTION DATA

The data processed and analyzed was recorded in buildings in the Los Angeles metropolitan area that have been instrumented either by the USGS and partner organizations, or by the building owner (as required by the Los Angeles and state building codes), the latter being commonly referred to as "code" buildings. The data from these buildings have been archived by USGS, and are referred to in this paper as "USGS instrumented buildings," identified by their station number. Figure 1 shows a map of the Los Angeles metropolitan area and locations of such buildings that were instrumented at the time of the 1994 Northridge earthquake.

The sensors in these buildings have been either three-component SMA-1 or multi-channel CR-1 accelerographs, both recording on film. Many of the "code" buildings (about 30 buildings total) have only one instrument, at the roof, due to a change in the original ordinance for Los Angeles, such that only one instrument at the roof was required, which lead to removal or neglect of the instruments at the ground floor and intermediate levels. This unfortunate fact limits considerably the use of these records, especially for analyses of soil-structure interaction. The recorded (absolute) roof motions *can* be used to estimate the apparent building period, as approximations of the relative roof motion near the first system frequency.

After the Northridge earthquake, the analog strong motion instrumentation is being gradually replaced by digital, and additional buildings are being instrumented. For some of these buildings, motions of smaller local earthquakes and distant larger earthquakes have been recorded and released. The recorded levels of response for these events, however, are much smaller than those for the Northridge earthquake. Figure 2.1 also shows the epicenters of earthquakes that have been recorded in these buildings. The Northridge main event was followed by a large number of aftershocks (9 of these had M > 5, and 55 had M > 4). Many of these larger magnitude aftershocks, as well as smaller magnitude but closer aftershocks, were recorded in the instrumented buildings. The aftershock of March 20, 1994 (M = 5.2; "aftershock 392") was the one recorded by the largest number of (ground motion) stations [Todorovska et al., 1999]. The Northridge sequence was recorded on several films archived separately. The largest number of recorded aftershocks known to the authors of this paper is 86—at station USGS #5455, and about

60 at several other stations. Unfortunately, it turned out that the number of aftershock records useable for estimation of the building apparent frequency was small—up to 11.

This paper shows results for 21 buildings for which there were three or more adequate records of both strong and weak shaking (mostly the 1994 Northridge sequence or the Whittier-Narrows sequence) to estimate the apparent building frequency. These stations are marked by open (yellow) dots in Fig. 2.1. The stations marked by solid rectangles, less than three "adequate" records for such analysis were known to exist, and were not included in this analysis.

Table 2.1 shows a list of earthquakes recorded in "USGS" instrumented buildings. For the Northridge sequence, only the aftershocks are shown for which there is an adequate record that has been used in the analysis presented in this paper. For most of the buildings, the contributing aftershocks have not been identified, and are assigned a *negative* aftershock number. For this analysis, however, the amplitude of response and their chronological order were sufficient. This table also lists the 2001 West Hollywood earthquake (M = 4.2), which occurred close to many of the instrumented buildings (see Fig. 2.1), and which were likely recorded by these buildings.

Table 2.2 shows a list of the 21 buildings that were analyzed in this study. The buildings are identified by their USGS station number and street address. For each building the number of stories, N, is shown and the number of records used in this study separately for the two horizontal components of recorded motion. It is noted that due to small signal to noise ratio at the long period, many small amplitude aftershock records had to be disregarded.

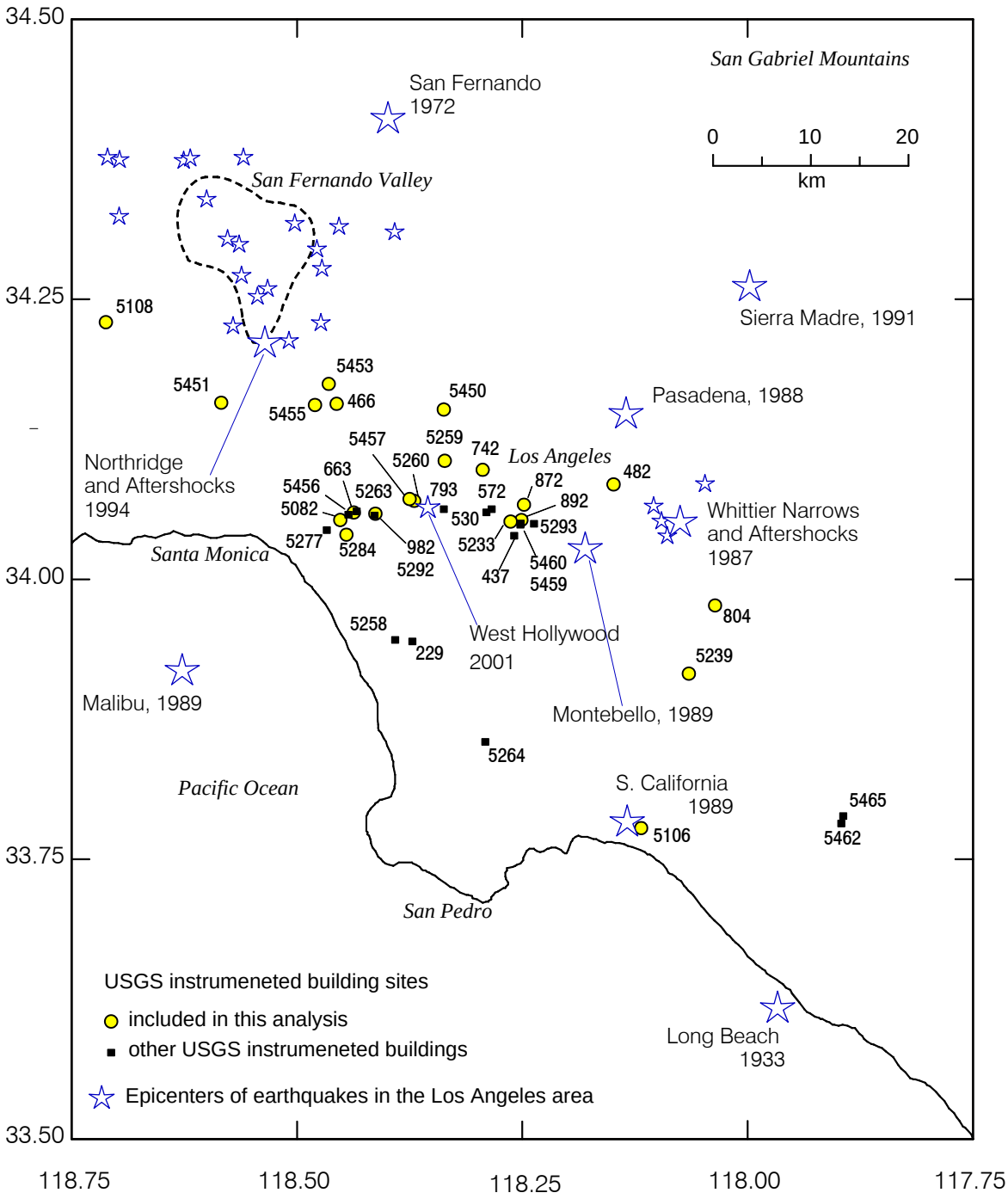

Figure 2.1 Locations of instrumented buildings in the Los Angeles metropolitan area at the time of the 1994 Northridge earthquake, for which the data is archived by USGS. The building sites are identified by their station number.

Table 2.1. Earthquakes recorded by USGS instrumented buildings (1971 to 2001).

Event	Date	Time	M_L	Latitude	Longitude	Depth (km)
San Fernando	02/09/1971	06:00	6.6	34 24 42N	118 24 00W	--
Whittier-Narrows	10/01/1987	14:42	5.9	34 03 10N	118 04 34W	14.5
Whittier-Narrows, 12th Aft.	10/04/1987	10:59	5.3	34 04 01N	118 06 19W	13.0
Whittier-Narrows, 13th Aft.	02/03/1988	15:25	4.7	34 05 13N	118 02 52W	16.7
Pasadena	12/03/1988	11:38	4.9	34 08 56N	118 08 05W	13.3
Malibu	01/19/1989	06:53	5.0	33 55 07N	118 37 38W	11.8
Montebello	06/12/1989	16:57	4.4	34 01 39N	118 10 47W	15.6
Upland	02/28/1990	23:43	5.2	34 08 17N	117 42 10W	5.3
Sierra Madre	06/28/1991	14:43	5.8	34 15 45N	117 59 52W	12.0
Landers	06/28/1992	11:57	7.5	34 12 06N	116 26 06W	5.0
Big Bear	06/28/1992	15:05	6.5	34 12 06N	116 49 36W	5.0
Northridge	01/17/1994	12:30	6.7	34 12 48N	118 32 13W	18.4
Northridge, Aft. #1	01/17/1994	12:31	5.9	34 16 45N	118 28 25W	0.0
Northridge, Aft. #7	01/17/1994	12:39	4.9	34 15 39N	118 32 01W	14.8
Northridge, Aft. #9	01/17/1994	12:40	5.2	34 20 29N	118 36 05W	0.0
Northridge, Aft. #100	01/17/1994	17:56	4.6	34 13 39N	118 34 20W	19.2
Northridge, Aft. #129	01/17/1994	20:46	4.9	34 18 04N	118 33 55W	9.5
Northridge, Aft. #142	01/17/1994	23:33	5.6	34 19 34N	118 41 54W	9.8
Northridge, Aft. #151	01/18/1994	00:43	5.2	34 22 35N	118 41 53W	11.3
Northridge, Aft. #253	01/19/1994	21:09	5.1	34 22 43N	118 42 42W	14.4
Northridge, Aft. #254	01/19/1994	21:11	5.1	34 22 40N	118 37 10W	11.4
Northridge, Aft. #336	01/29/1994	11:20	5.1	34 18 21N	118 34 43W	1.1
Northridge, Aft. #392	03/20/1994	21:20	5.2	34 13 52N	118 28 30W	13.1
Hector Mine	10/16/1999	09:46	7.1	34 36 00N	116 16 12W	3.0
West Hollywood	09/09/2001	23:59	4.2	34 04 30N	118 22 44W	3.7

Table 2.2 List of buildings analyzed in this study.

Station No.	N	Street address	Comp.	No. rec.	Comp.	No. rec.
0466	13	LOS ANGELES, 15250 VENTURA BLVD.	N00E	3	W00N	3
0482	12	ALHAMBRA, 900 S. FREMONT	NS	5	EW	5
0663	12	LOS ANGELES, 10751 WILSHIRE Blvd.	S72W	3	S18E	2
0742	8	LOS ANGELES, 1526 N.EDGEMONT ST.,	E00S	12	N00E	10
0793	11	LOS ANGELES, 4929 WILSHITE BLVD.	S00W	5	E00S	6
0804	10	7215 BRIGHT AVE., BASEMENT, WHITTIER, CA	NS	2	EW	2
0872	8	LOS ANGELES, 1111 SUNSET Blvd.	N12W	3	S78W	3
0892	55	LOS ANGELES, 333 S. HOPE ST.	N83E	2	W83N	2
5082	6	LOS ANGELES, WADSWORTH V.A. HOSPITAL	N35W	2	S55W	2
5106	11	LONG BEACH VA HOSPITAL	NS	3	EW	3
5108	6	SANTA SUSANA, ETEC Bldg 462	E00S	9	N00E	7
5233	32	1100 WILSHIRE, LOS ANGELES, CA	N62W	2	S28W	2
5239	7	12440 IMPERIAL HWY, NORWALK, CA	N90E	5	S00W	5
5259	8	LOS ANGELES, 2005 N. HIGHLAND AVE.	N00E	8	W00N	6
5260	12	LOS ANGELES, 444 S. SAN VINCENTE	W65N	7	S65W	9
5263	19	LOS ANGELES, 10660 WILSHIRE BLVD.	E70S	5	N70E	3
5450	9	BURBANK, 3601 WEST OLIVE AVE.	N00E	5	W00N	5
5451	12	LOS ANGELES, 6301 OWENSMOUTH AVE.	N00E	3	W00N	3
5453	9	LOS ANGELES, 5805 SEPULVEDA BLVD.	N00E	4	W00N	8
5455	13	LOS ANGELES, 16000 VENTURA BLVD.	E30S	5	N30E	5
5457	10	LOS ANGELES, 8436 WEST 3rd ST.	N00E	8	S00W	7

3. METHODOLOGY

3.1 Estimation of Instantaneous Frequency during an Earthquake

The instantaneous frequency was estimated by two methods: (a) zero-crossing analysis, and (b) from the ridge of the Gabor transform, both applied to the relative roof displacement—when there was a record at the base, or to the absolute displacement—when only the roof response was recorded—considered as an approximation of the relative displacement in the neighborhood of the first system frequency. Both methods were applied to the filtered displacement, such that it contained only motion in the neighborhood of the first system frequency, hence resembling a chirp signal. The zero-crossing analysis consists of measuring the time between consecutive zero crossings of the displacement, and assuming this time interval to be a half of the system period [Trifunac et al. 2001a,b,c,d,e; Hao et al. 2004]. The Gabor transform method is summarized in the remaining part of this section, and a more detailed description can be found in [Todorovska 2001; Todorovska and Trifunac 2007a].

The Gabor transform is a complex-valued time-frequency distribution, which represents a projection of the signal onto a series of Gabor wavelets. For a signal $f(t) \in L_2(R)$, the Gabor transform is

$$G_f(b,\omega) = \int_{-\infty}^{\infty} f(t)\bar{g}_{(b,\omega)}(t)dt, \quad \infty < b < \infty, |\omega| > 0 \tag{3.1.1}$$

where b is time, and ω is circular frequency. The Gabor wavelet, $g_{(b,\omega)}(t)$ is a complex exponential modulated by a Gaussian envelope with a constant shape

$$g_{(b,\omega)}(t) = \exp\left[-\frac{(t-b)^2}{2\sigma^2}\right]\exp\left[i\omega(t-b)\right] \tag{3.1.2}$$

and has Fourier Transform

$$\begin{aligned}\hat{g}_{(b,\omega)}(\xi) &= \exp\left[-i\xi b\right]\hat{g}_{(0,\omega)}(\xi) \\ &= \exp\left[-i\xi b\right]\sqrt{2\pi}\sigma\exp\left[-\frac{1}{2}(\xi-\omega)^2\sigma^2\right]\end{aligned} \tag{3.1.3}$$

Figure 3.1.1 shows the real and imaginary parts of a Gabor wavelet (left) and its Fourier transform (right) for $b = 0$ and $\omega = 2\pi$. Up to a phase shift, the Gabor transform is identical to a moving window analysis with a Gaussian time window.

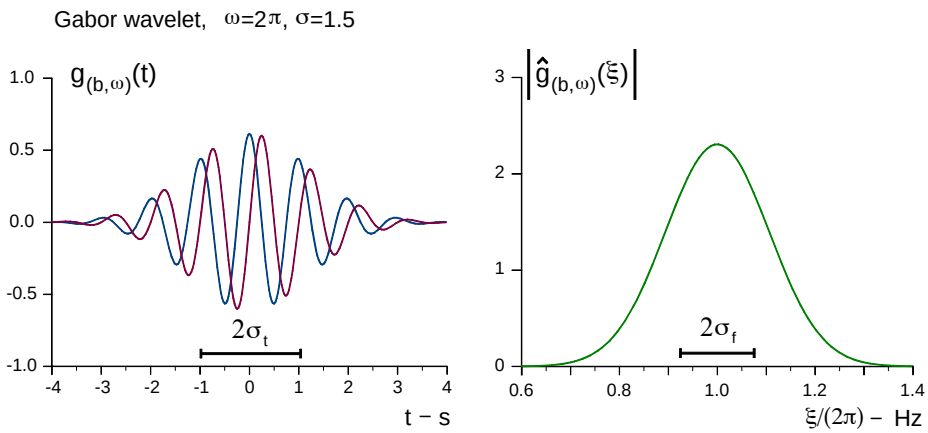

Figure 3.1.1 A Gabor wavelet for $b = 0$ and $\omega = 2\pi$, in the time domain (left) and in the frequency domain (right).

The shape of the Gabor wavelet is determined by parameter σ, which is a measure of the spread of the Gaussian window and hence determines its effective length. This parameter is preset for the entire transform, which distinguishes the Gabor transform from the continuous complex wavelet transform with a Morlet wavelet, which is a projection of the function onto a family of wavelets of variable length. As it can be seen from Fig. 3.1.1, the Gabor wavelet is localized both in time and in frequency. The smaller the spread of the Gaussian envelope—the better the localization in time, and the smaller the spread of $\hat{g}_{(b,\omega)}(\xi)$—the better the localization in frequency. As it can be seen from eqns (3.1.2) and (3.1.3), the better the localization in time, the poorer the localization in frequency, which is formally described by the Heisenberg uncertainty principle, stating that a signal cannot be arbitrarily well localized both in time and in frequency, i.e. the product of the spread in time, σ_t and the spread in frequency, σ_ω is bounded

$$\sigma_t \cdot \sigma_\omega = C \leq \frac{1}{2} \tag{3.1.4}$$

The constant C is the smallest for a Gaussian window, which provides best possible localization *both* in time and in frequency. In eqn (3.1.4), the spreads in time and in frequency, σ_t and σ_ω,

are such that σ_t^2 and σ_ω^2 are the variances of the Gabor wavelet and of its Fourier transform, and in terms of parameter σ

$$\sigma_t^2 = \frac{1}{2}\sigma^2 \quad \Leftrightarrow \quad \sigma_t = 0.71\sigma$$

(3.1.5)

$$\sigma_\omega^2 = \frac{1}{2}\frac{1}{\sigma^2} \quad \Leftrightarrow \quad \sigma_\omega = 0.71\frac{1}{\sigma} \tag{3.1.6}$$

which gives

$$\sigma_t \cdot \sigma_\omega = \frac{1}{2} \tag{3.1.7}$$

The instantaneous frequency was determined from the *ridge* of the magnitude of the Gabor transform—a surface on the time-frequency plane, and the corresponding amplitude was estimated from the *skeleton* of the transform. The ridge is the collocation of points (t,ω) where the magnitude of the transform (i.e. the energy of the signal) is maximum, and the skeleton is the value of the transform along the ridge. This method is the most robust and efficient from all methods based on time-frequency distributions for signals that are "noisy" but the amplitude of the noise is relatively small compared to the signal [Todorovska 2001]. The complex wavelet transform with the Morlet wavelet was initially considered, which is essentially a Gabor transform with a window that varies depending on the frequency so that it always contains same number of wavelengths. The results by both methods were found to be very similar, and no advantage was seen in using a variable window, as the observed changes of the building frequency are relatively small—well within an order of magnitude. Using constant window was convenient in the estimation of the resolution of the method. The Gabor transform was used with spread $\sigma = 1.5$.

It should be noted here that the spreads in time and frequency, σ_t and σ_ω, of the Gabor wavelet used define the *resolution* of the method, namely, the method *cannot* resolve frequencies closer than σ_ω, and the estimate of "instantaneous" frequency at a time *t* is the weighted average of the frequency within the time widow of the Gabor wavelet, rather than exactly at time *t*.

Another important fact in interpretation of the results by both the zero-crossing analysis and Gabor analysis is that they are both based on the premise that the signal—relative building response in our case—can be represented (uniquely) as the product

$$f(t) = A(t)\cos\Phi(t) \tag{3.1.8}$$

where the amplitude $A(t)$ varies *very slowly* with time compared to the oscillations of $\cos\Phi(t)$, in which case the instantaneous frequency can be obtained by differentiating $\Phi(t)$

$$\omega(t) = \frac{d\Phi}{dt} \tag{3.1.9}$$

Such signals are called *asymptotic*. Hence, these methods are most accurate when the asymptoticity condition is satisfied and produce artifacts when it is violated. Longer window of the Gabor wavelet (larger σ) would smooth variations due to such artifacts.

3.2 Illustrations of Instantaneous Frequency for Selected Earthquake Records

The methodology for estimation of the instantaneous frequency of building-soil systems is illustrated in Figs 3.2.1 through 3.2.5 for five records. Figure 3.2.1 shows results for component N11E of the record of the 1971 San Fernando earthquake at station USGS 466 (Los Angeles, 15250 Ventura Blvd.), Fig. 3.2.2—for component N00E of the record of the 1994 Northridge earthquake at station USGS 5450 (Burbank, 3601 West Olive Ave.), Fig. 3.2.3—for component W00N of the record of the 1994 Northridge earthquake at station USGS 5451 (Los Angeles, 6301 Owensmouth Ave.), Fig. 3.2.4—for component N00E of the record of the 1994 Northridge earthquake at station USGS 5453 (Los Angeles, 5805 Sepulveda Blvd.), and Fig. 3.2.5—for component E30S of the record of the 1994 Northridge earthquake at station USGS 5455 (Los Angeles, 1600 Ventura Blvd.). For each record, the plot on the left hand side shows the Fourier spectrum of the relative roof displacement (solid line), or its approximation by the absolute displacement when only a roof record was available, the Fourier spectrum of acceleration at the ground floor (dashed line)—if available, and a smooth approximation of the relative (or absolute) roof displacement spectrum by the marginal Gabor transform distribution (the smooth line). There are three plots in the right hand side, as follows. The plot on the top shows the time history of the roof relative (or absolute) displacement (solid line), and of the ground floor

displacement (dashed line) if available, for the "broad-band" data, which is the output of the standard data processing. The plot in the middle shows the same time histories but for the "narrow-band" data, which is the broad-band data filtered so that it contains only the frequencies in the neighborhood of the first building-soil system frequency. The cut-off and role-off frequencies, in Hz, of the Ormsby filters used are shown in the upper right corner of these plots. The plot in the bottom shows the instantaneous frequency versus time estimated by the zero-crossing analysis (open circles), and Gabor analysis (with $\sigma = 1.5$ for all the records). The shaded rectangle in this plot has width $2\sigma_t$ and height $2\sigma_\omega$ and is a measure of the resolution of the Gabor analysis. The Gabor transform at a point (t, f) in the time frequency plane is the weighed average of the components of the function (effectively) within such a rectangle centered at that point. The method cannot resolve frequencies that are closer than σ_ω, and estimates in time that are closer than σ_t. The resolution in frequency can be increased only if the resolution in time is decreased (by increasing the time window of the Gabor wavelet, and consequently—σ_t), and vice versa.

The results in Figures 3.2.1 through 3.2.5 show that the estimates by the zero-crossing and from the ridge of the Gabor transform are consistent. The estimates by the latter method are smoother, as the Gabor transform is a smoothing operator. The zero-crossing method is not accurate when the oscillations of the signal depart too much from a "pure" harmonic, and these estimates are not shown. Both methods are most accurate when the amplitude of the signal is large and does not vary significantly during one cycle of oscillation, least accurate when the amplitude is small and varies significantly during one cycle, and are arbitrary when the amplitude is practically zero. Figures 3.2.1 and 3.2.4 show a significant change (decrease) in the system frequency for these buildings during a single earthquake, of about 30%, Figure 3.2.2 indicates a change of about 17%, while Fig. 3.2.5 shows no significant change. It is interesting to see whether the changes of frequency are permanent (indicating possible damage), or temporary (possibly due to changes in the soil, changes in the bonding condition along the contact surface between the foundation and the soil, e.g. formation of gaps between the foundation and the soil, foundation partial uplift, etc.). The answer to this important question can be explored through records from consecutive earthquakes, the results of which are shown in Chapter 4.

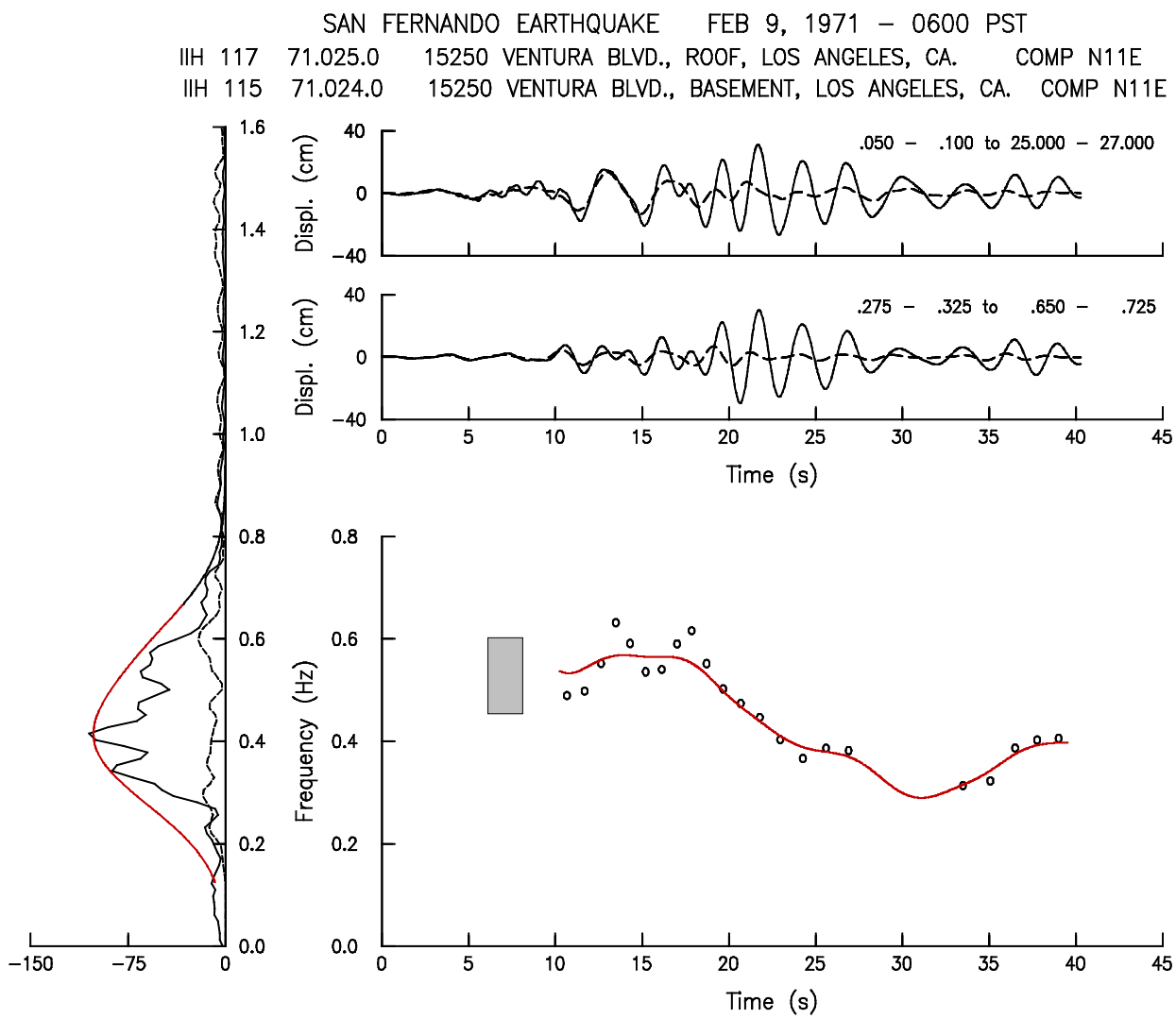

Figure 3.2.1 Estimation of the instantaneous frequency for component N11E of the record of the 1971 San Fernando earthquake at station USGS 466 (Los Angeles, 15250 Ventura Blvd.). Left: Fourier spectrum of the relative roof displacement (solid line), of acceleration at the ground floor (dashed line), and a smooth approximation of the relative roof displacement spectrum by the marginal Gabor transform distribution (the red line). Time history of the roof relative displacement (solid line), and of the ground floor displacement (dashed line), for the "broad-band" data (right-top), and for the filtered data (right-middle). Right-bottom: instantaneous frequency versus time estimated by the zero-crossing method (open circles), and from the ridge of the Gabor transform (with $\sigma = 1.5$). The shaded rectangle has width $2\sigma_t$ and height $2\sigma_\omega$, and is a measure of the resolution of the Gabor transform method.

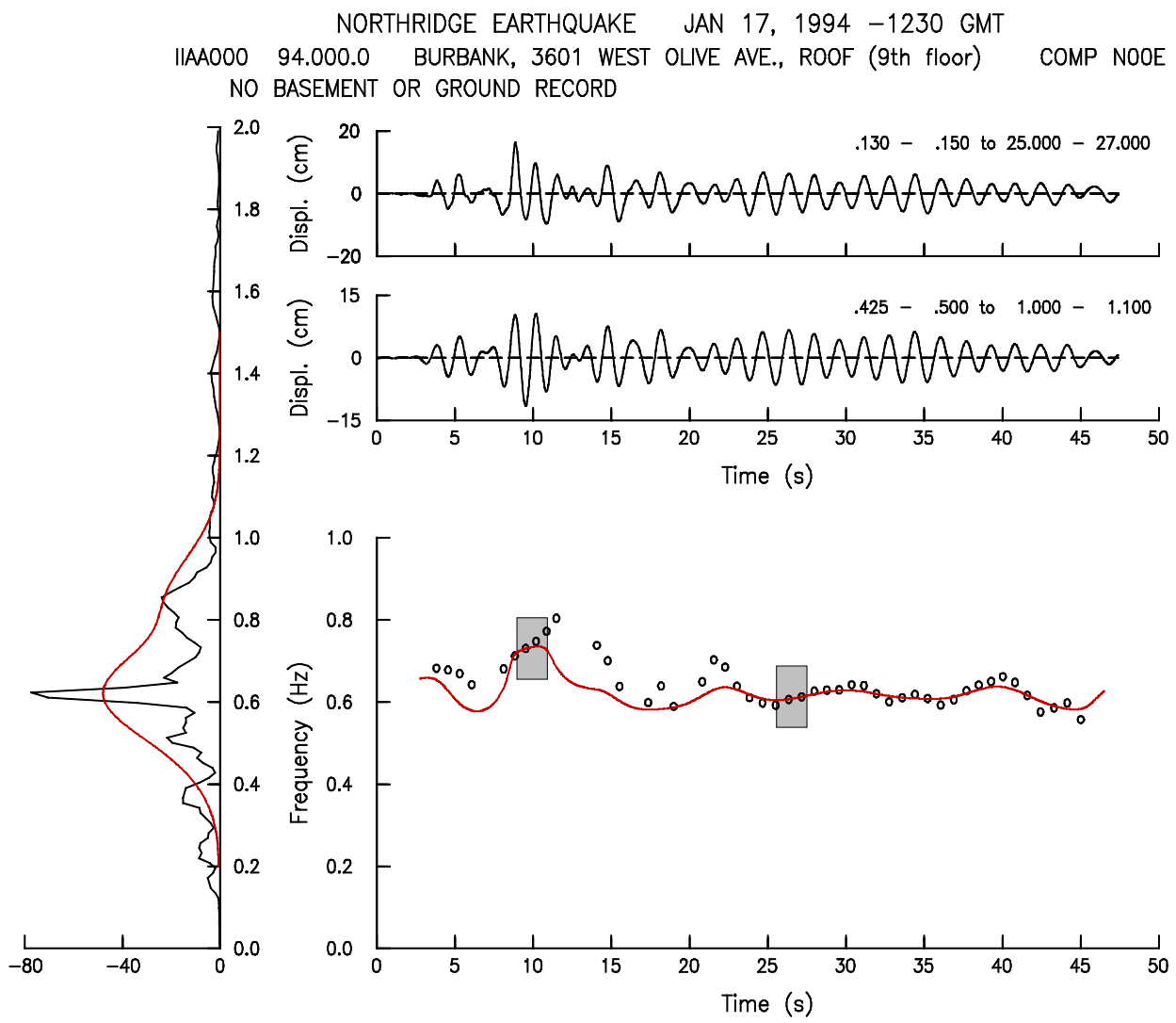

Figure 3.2.2 Same as Fig. 3.2.1 but for component N00E of the record of the 1994 Northridge earthquake at station USGS 5450 (Burbank, 3601 West Olive Ave.).

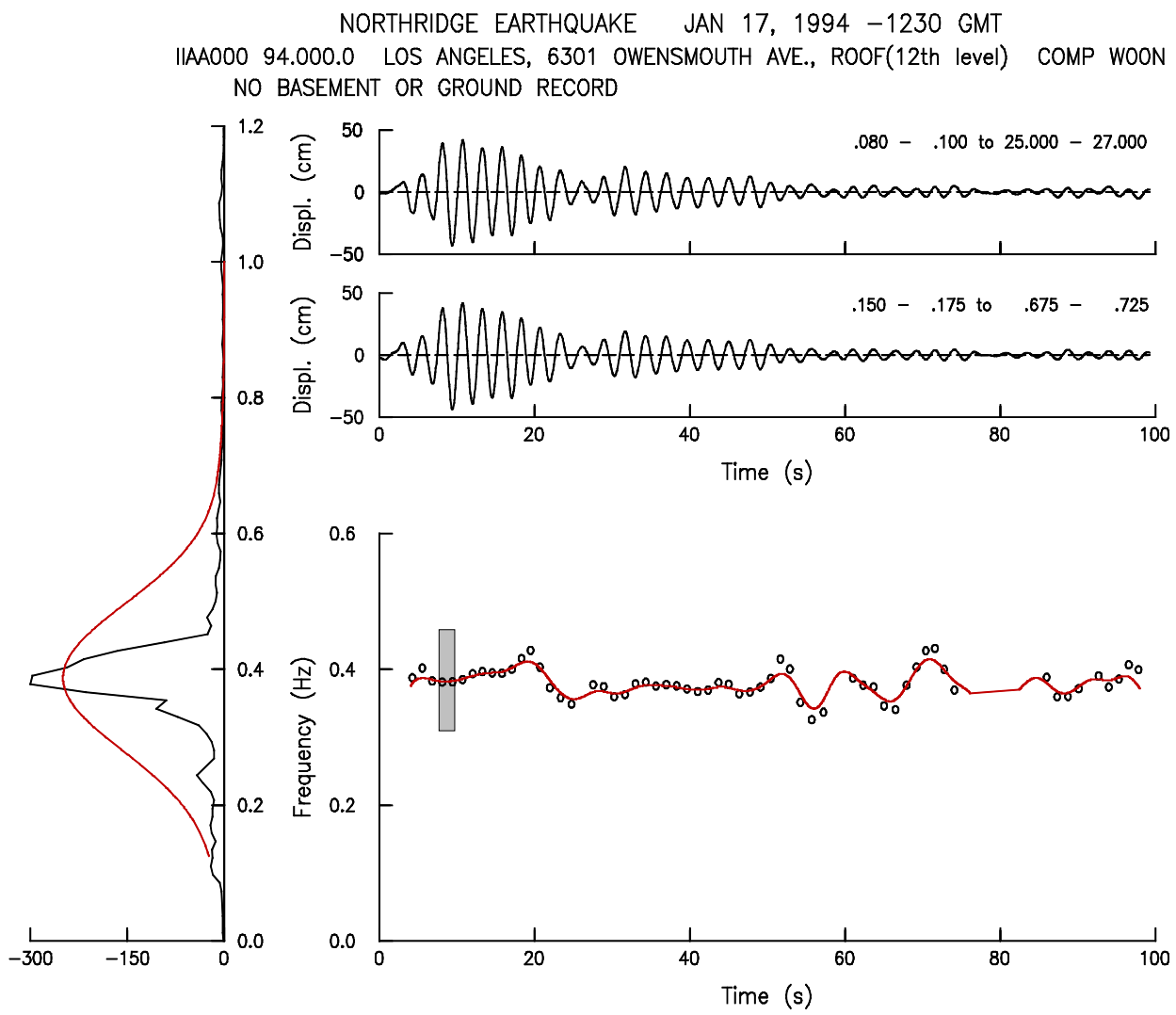

Figure 3.2.3 Same as Fig. 3.2.1 but for component W00N of the record of the 1994 Northridge earthquake at station USGS 5451 (Los Angeles, 6301 Owensmouth Ave.).

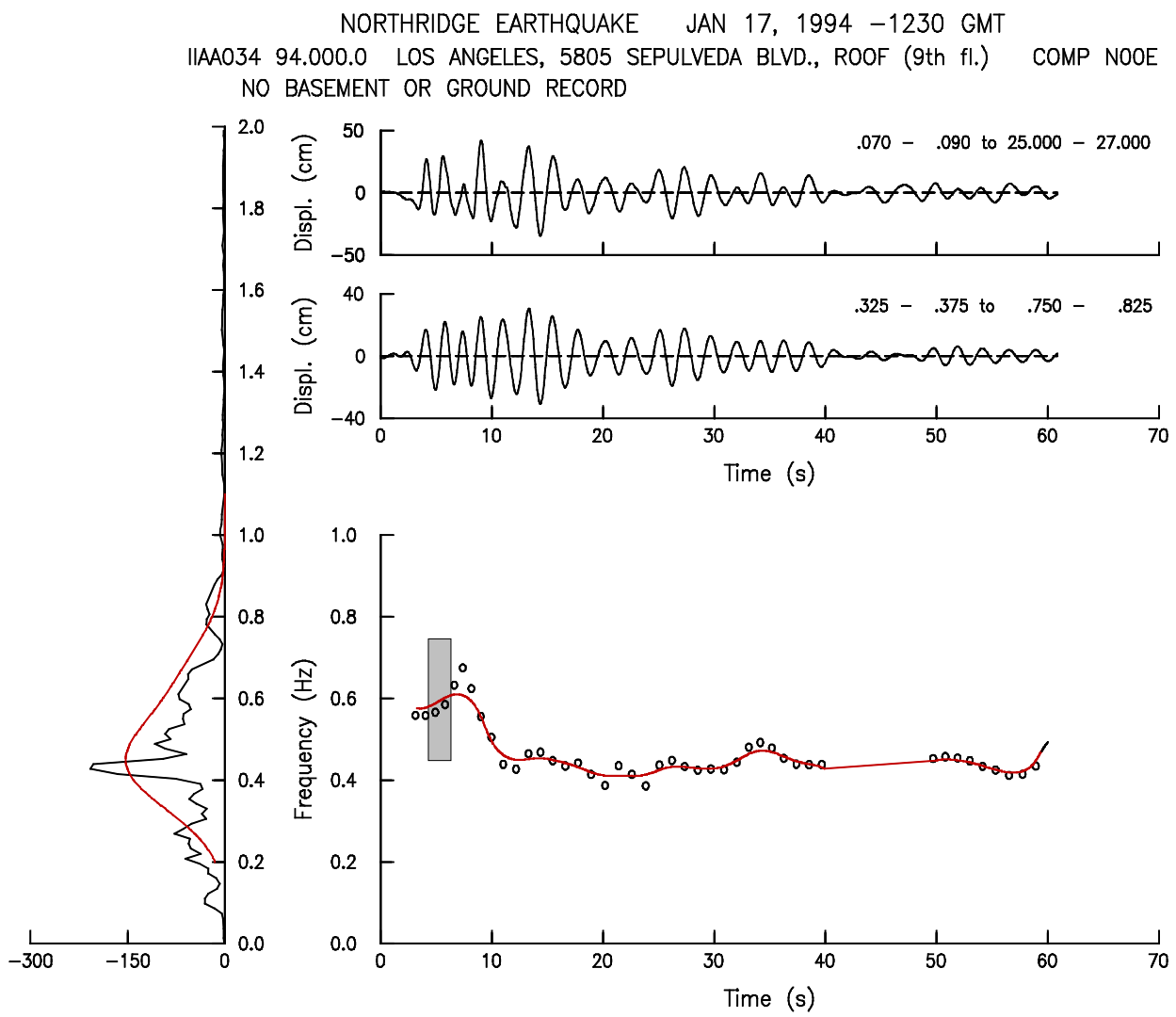

Figure 3.2.4 Same as Fig. 3.2.1 but for component N00E of the record of the 1994 Northridge earthquake at station USGS 5453 (Los Angeles, 5805 Sepulveda Blvd.).

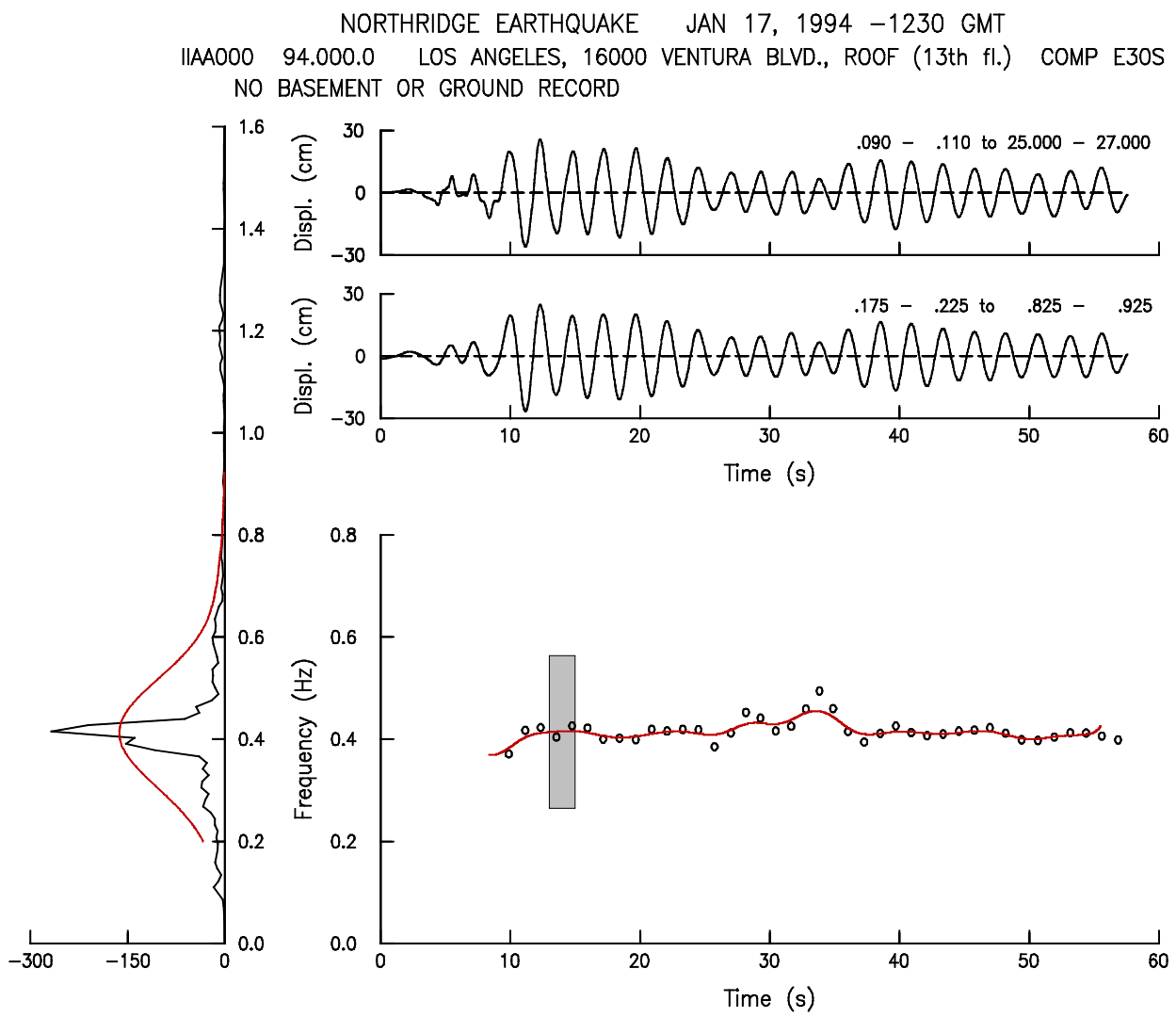

Figure 3.2.5 Same as Fig. 3.2.1 but for component E30S of the record of the 1994 Northridge earthquake at station USGS 5455 (Los Angeles, 1600 Ventura Blvd.).

3.3 Estimation of Tends in Time and Amplitude Variations of Frequency for Multiple Earthquakes

The trends in the variation of the building frequency for multiple earthquakes were analyzed from plots like the sample ones shown in Fig. 3.3.1 for building USGS 5108. The plot on the left corresponds to the first horizontal component of motion and the one on the right to the second horizontal component of motion. In each plot, the horizontal axis corresponds to the instantaneous frequency, the vertical axis corresponds to the amplitude of response (of the filtered signal) expressed as a rocking angle in radians, and each point corresponds to a particular instant in time. The rocking angle was computed by dividing the amplitude of the relative (roof minus base) response, if motion at the base was recorded, or otherwise the absolute horizontal response of the roof or top floor by the building height. The floor height varies within a building, and the average floor height varies from one building to another. In this report, an average floor height of 12.5 feet was assumed (1 foot = 30.48 cm). It is noted here that this rocking angle includes the *rigid body* rocking, which could not be separated because of insufficient number of instruments at the base, in addition to motion resulting from *deflection* of the structure. Each line corresponds to a particular earthquake, and connects points corresponding to consecutive instants of time during that earthquake.

In the plots in Fig. 3.3.1, the instantaneous frequency and amplitudes of response were computed by zero-crossings analysis. For each of the buildings, such plots were drawn also based on results of the Gabor transform analysis. Generally, the plots based on the Gabor transform analysis have curves for each earthquake that are piecewise smoother over intervals of time, but have jumps between the time intervals, while the plots based on zero-crossings analysis have scatter within the time intervals. While there is intrinsic uncertainty in the estimate of the "instantaneous" frequency and amplitude, due to the Heisenberg-Gabor uncertainty principle, the scatter observed in estimates using real data (of earthquakes recorded in real buildings) exceeds substantially the theoretical uncertainty, and is due primarily to violations of the assumption that the signal (the relative or absolute roof displacement) is asymptotic, which is the basic assumption for virtually all nonparametric methods for estimation of instantaneous frequency [Todorovska 2001; Todorovska and Trifunac 2007a]. Asymptotic signals are such signals whose variation in time is mostly due to change in phase rather than change in amplitude. The

asymptoticity assumption is violated most in the instants when the amplitudes of the signal are small and the amplitude modulation varies significantly. This can be seen in the plots in Figs 3.2.1 through 3.2.5.

In the plots showing results for the zero-crossing method, the first and last point shown for a particular earthquake are marked respectively by an open and a closed circle. The backbone curve, drawn by hand, indicates roughly the trend of the variation of the system frequency as function of the amplitude of response. From Fig. 3.3.1, it can be seen that for the largest motions (during the 1994 Northridge earthquake), the system frequency is the lowest, but it recovers during the aftershock shaking.

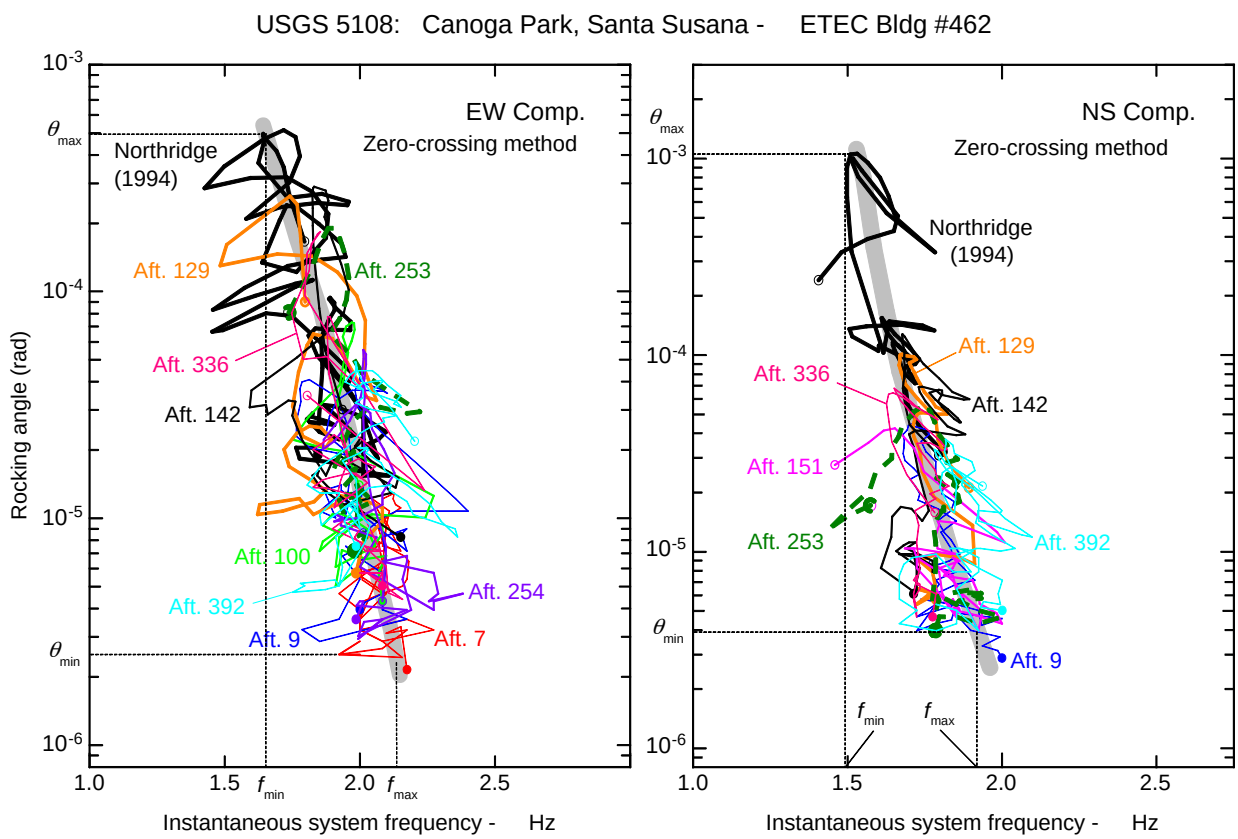

Figure 3.3.1 Instantaneous frequency versus amplitude of motion for station USGS 5108.

Results like those in Fig. 3.3.2 for all the 21 buildings and for both zero-crossings and Gabor transform analysis are shown in Appendix B. The "backbone" curves were used a guidance in reading from the plots the minimum and maximum frequency for all events, $f_{\min}$ and $f_{\max}$, and the range of amplitudes of the angle of response, $\theta_{\max}$ and $\theta_{\min}$. However, not all readings of these values are on the corresponding "backbone" curve. Chapter 4 shows a summary of the readings for all the buildings.

4. RESULTS AND ANALYSIS

This chapter presents a summary of the results for all 21 buildings, and an analysis of the observed trends. Appendix B shows detailed results of the variations of the building (system) frequencies with amplitude of the roof response.

Despite the considerable scatter in these plots, for all the buildings, the frequency was the smallest during the largest motions, and recovered during the aftershocks. A common trend seen for most stations during the largest event is a decrease of the frequency some time *after* the largest amplitudes of response. For few of the buildings, some permanent drop of the frequency occurred during the large events, indicating damage. Such drop can be seen in Fig. 3.2.1, showing instantaneous frequency analysis for the N11E component of response of USGS 466 during the 1971 San Fernando earthquake. This building, located at 15250 Ventura Blvd., Los Angeles, is the Bank of California building, which was damaged by that earthquake and repaired. The readings for this building shown in this summary exclude the San Fernando earthquake, and reflect only the variation of frequency during the Northridge earthquake and its aftershocks.

Table 4.1 shows a summary of the results for the instantaneous frequency $f_{\min}$ and $f_{\max}$, and for the range of amplitudes of angle of response, $\theta_{\max}$ and $\theta_{\min}$, for all 21 buildings. These values supersede those reported in [Todorovska at al. 2004, 2006], and reflect some revisions. The percentage changes in frequency $\Delta f / f_{\max} = (f_{\max} - f_{\min}) / f_{\max}$ is also shown as well as of (system) stiffness $\Delta k / k_{\max}$ based on the assumption that $k \sim f^2$. Table 4.2 is same as Table 4.1 except that the system periods, $T = 1/f$, are shown instead of the system frequencies. In both tables, the percentage changes were computed using as reference the values corresponding to the small amplitude response.

Table 4.1 Maximum and minimum system frequencies and maximum and minimum rocking angles for 21 instrumented buildings. The corresponding percentage changes in system frequency and stiffness are also shown.

Station No.	No. floors	Comp.	No. rec.	f_{max} Hz	f_{min} Hz	$\Delta f / f_{max}$ %	$\Delta k / k_{max}$ %	θ_{max} $\times 10^{-3}$ rad	θ_{min} $\times 10^{-3}$ rad	Comp.	No. rec.	f_{max} Hz	f_{min} Hz	$\Delta f / f_{max}$ %	$\Delta k / k_{max}$ %	θ_{max} $\times 10^{-3}$ rad	θ_{min} $\times 10^{-3}$ rad
0466	13	N00E	3	0.38	0.31	18.4	33.4	4.746	0.123	W00N	3	0.3	0.22	26.7	46.2	4.664	0.316
0482	12	NS	5	0.52	0.45	13.5	25.1	1.660	0.059	EW	5	0.51	0.46	9.8	18.6	2.818	0.115
0663	12	S72W	3	0.52	0.51	1.9	3.8	3.449	0.058	S18E	2	0.525	0.5	4.8	9.3	2.000	0.115
0742	8	E00S	12	2.52	2.15	14.7	27.2	0.400	0.002	N00E	10	1.69	1.18	30.2	51.2	1.820	0.005
0793	11	S00W	5	0.98	0.79	19.4	35.0	2.754	0.006	E00S	6	0.92	0.72	21.7	38.8	2.344	0.008
0804	10	NS	2	0.8	0.68	15.0	27.8	0.540	0.009	EW	2	1.22	1.14	6.6	12.7	1.000	0.017
0872	8	N12W	3	0.63	0.57	9.5	18.1	1.698	0.042	S78W	3	0.76	0.63	17.1	31.3	2.359	0.015
0892	55	N83E	2	0.53	0.52	1.9	3.7	0.240	0.010	W83N	2	0.53	0.52	1.9	3.7	0.158	0.013
5082	6	N35W	2	1.16	1.01	12.9	24.2	1.820	0.013	S55W	2	1.19	0.94	21.0	37.6	1.622	0.016
5106	11	NS	3	1.84	1.73	6.0	11.6	0.331	0.006	EW	3	1.85	1.76	4.9	9.5	0.260	0.010
5108	6	E00S	9	2.13	1.65	22.5	40.0	0.496	0.003	N00E	7	1.9	1.5	21.1	37.7	1.056	0.004
5233	32	N62W	2	0.62	0.46	25.8	45.0	0.630	0.015	S28W	2	0.65	0.48	26.2	45.5	0.468	0.007
5239	7	N90E	5	0.9	0.81	10.0	19.0	0.920	0.005	S00W	5	0.82	0.76	7.3	14.1	1.622	0.004
5259	8	N00E	8	1.95	1.51	22.6	40.0	1.023	0.002	W00N	6	3.62	2.89	20.2	36.3	0.219	0.002
5260	12	W65N	7	0.83	0.71	14.5	26.8	2.720	0.016	S65W	9	0.8	0.68	15.0	27.8	4.169	0.020
5263	19	E70S	5	0.61	0.49	19.7	35.5	2.239	0.013	N70E	3	0.62	0.42	32.3	54.1	1.585	0.014
5450	9	N00E	5	0.69	0.61	11.6	21.8	3.088	0.039	W00N	5	0.67	0.58	13.4	25.1	5.166	0.038
5451	12	N00E	3	0.33	0.24	27.3	47.1	7.384	0.180	W00N	3	0.406	0.36	11.3	21.4	9.573	0.134
5453	9	N00E	4	0.615	0.415	32.5	54.5	7.870	0.061	W00N	8	0.78	0.67	14.1	26.2	4.881	0.026
5455	13	E30S	5	0.45	0.41	8.9	17.0	5.394	0.056	N30E	5	0.43	0.36	16.3	29.9	5.361	0.099
5457	10	N00E	8	0.68	0.57	16.2	29.7	6.340	0.029	S00W	7	0.87	0.69	20.7	37.1	3.625	0.013

Table 4.2 Same as Table 4.1 except that the system periods are shown instead of the system frequencies.

Station No.	No. floors	Comp.	No. rec.	T_{max} Hz	T_{min} Hz	$\Delta T / T_{min}$ %	$\Delta k / k_{max}$ %	θ_{max} $\times 10^{-3}$ rad	θ_{min} $\times 10^{-3}$ rad	Comp.	No. rec.	T_{max} Hz	T_{min} Hz	$\Delta T / T_{min}$ %	$\Delta k / k_{max}$ %	θ_{max} $\times 10^{-3}$ rad	θ_{min} $\times 10^{-3}$ rad
0466	13	N00E	3	2.63	3.23	22.58	33.4	4.746	0.123	W00N	3	3.33	4.55	36.36	46.2	4.664	0.316
0482	12	NS	5	1.92	2.22	15.56	25.1	1.660	0.059	EW	5	1.96	2.17	10.87	18.6	2.818	0.115
0663	12	S72W	3	1.92	1.96	1.96	3.8	3.449	0.058	S18E	2	1.90	2.00	5.00	9.3	2.000	0.115
0742	8	E00S	12	0.40	0.47	17.21	27.2	0.400	0.002	N00E	10	0.59	0.85	43.22	51.2	1.820	0.005
0793	11	S00W	5	1.02	1.27	24.05	35.0	2.754	0.006	E00S	6	1.09	1.39	27.78	38.8	2.344	0.008
0804	10	NS	2	1.25	1.47	17.65	27.8	0.540	0.009	EW	2	0.82	0.88	7.02	12.7	1.000	0.017
0872	8	N12W	3	1.59	1.75	10.53	18.1	1.698	0.042	S78W	3	1.32	1.59	20.63	31.3	2.359	0.015
0892	55	N83E	2	1.89	1.92	1.92	3.7	0.240	0.010	W83N	2	1.89	1.92	1.92	3.7	0.158	0.013
5082	6	N35W	2	0.86	0.99	14.85	24.2	1.820	0.013	S55W	2	0.84	1.06	26.60	37.6	1.622	0.016
5106	11	NS	3	0.54	0.58	6.36	11.6	0.331	0.006	EW	3	0.54	0.57	5.11	9.5	0.260	0.010
5108	6	E00S	9	0.47	0.61	29.09	40.0	0.496	0.003	N00E	7	0.53	0.67	26.67	37.7	1.056	0.004
5233	32	N62W	2	1.61	2.17	34.78	45.0	0.630	0.015	S28W	2	1.54	2.08	35.42	45.5	0.468	0.007
5239	7	N90E	5	1.11	1.23	11.11	19.0	0.920	0.005	S00W	5	1.22	1.32	7.89	14.1	1.622	0.004
5259	8	N00E	8	0.51	0.66	29.14	40.0	1.023	0.002	W00N	6	0.28	0.35	25.26	36.3	0.219	0.002
5260	12	W65N	7	1.20	1.41	16.90	26.8	2.720	0.016	S65W	9	1.25	1.47	17.65	27.8	4.169	0.020
5263	19	E70S	5	1.64	2.04	24.49	35.5	2.239	0.013	N70E	3	1.61	2.38	47.62	54.1	1.585	0.014
5450	9	N00E	5	1.45	1.64	13.11	21.8	3.088	0.039	W00N	5	1.49	1.72	15.52	25.1	5.166	0.038
5451	12	N00E	3	3.03	4.17	37.50	47.1	7.384	0.180	W00N	3	2.46	2.78	12.78	21.4	9.573	0.134
5453	9	N00E	4	1.63	2.41	48.19	54.5	7.870	0.061	W00N	8	1.28	1.49	16.42	26.2	4.881	0.026
5455	13	E30S	5	2.22	2.44	9.76	17.0	5.394	0.056	N30E	5	2.33	2.78	19.44	29.9	5.361	0.099
5457	10	N00E	8	1.47	1.75	19.30	29.7	6.340	0.029	S00W	7	1.15	1.45	26.09	37.1	3.625	0.013

The results summarized in Tables 4.1 and 4.2 are shown graphically in Figs. 4.1 through 4.11, as follows. Figure 4.1 shows the building periods versus the number of floors. All except 3 buildings in this set have up to 13 stories, one has 19 stories, one has 32 stories, and one has 55 stories. Different symbols are used for the maximum and minimum observed values, and for the two horizontal components of motion. It can be seen that the periods during the small amplitude responses ($T_{\min}$) did not exceed 3.3 s, and during the largest amplitude responses ($T_{\max}$) did not exceed 4.5 s. The line shows the period estimated by the simple code formula $T = N/10$, where N is the number of stories. It can be seen that this simple formula predicts well the periods for the 19-story building, and overestimates significantly the periods of the 32 and 55-story buildings. For most of the other buildings ($N \leq 13$), the simple code formula underestimates the periods.

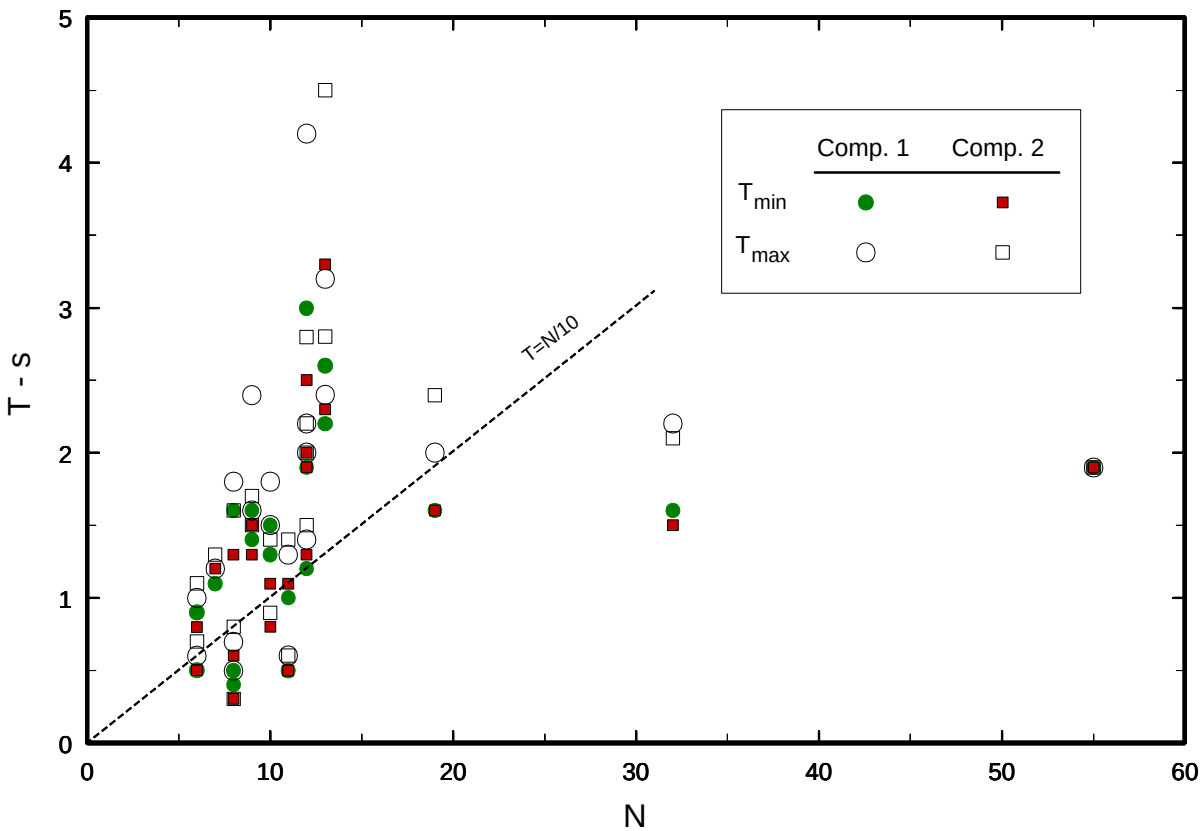

Fig. 4.1 Minimum and maximum periods versus number of floors *N*.

The next group of three figures (Fig. 4.2, 4.3 and 4.4) shows the observed periods, frequencies and maximum response angles, as follows.

Figure 4.2 shows the observed minimum (top) and maximum (bottom) periods for the 21 buildings. The values for the first horizontal component are shown on the *x*-axis and for the second component are shown on the *y*-axis. The label next to each symbol is the USGS station number. As mentioned earlier, it can be seen that $T_{\min}$ did not exceed 3.3 s, and $T_{\max}$ did not exceed 4.5 s. The largest observed values for both $T_{\min}$ and $T_{\max}$ are for building USGS 0466, which is 13-story. The next largest values are for building USGS 5451, which is 12-story, and for which $T_{\max}$ exceeded 4 s for one of the components of motion.

Similarly, Fig. 4.3 shows the observed values of $f_{\max}$ and $f_{\min}$. It can be seen that $f_{\min}$ did not exceed 3 Hz, and $f_{\max}$ did not exceed 3.5 Hz.

Figure 4.4 shows the maximum observed angles of deflection $\theta_{\max}$ for all 21 buildings. It can be seen that $\theta_{\max}$ did not exceed 10 mili radians, and was the largest for USGS 5451.

The next group of three figures (Fig. 4.5, 4.6 and 4.7) shows the observed percentage changes in period $\Delta T / T_{\min}$, frequency $\Delta f / f_{\max} = 1 - f_{\min} / f_{\max}$, and stiffness $\Delta k / k_{\max} = 1 - (f_{\min} / f_{\max})^2$. It can be seen that $\Delta T / T_{\min}$ approached 50%, $\Delta f / f_{\max}$ approached 35%, and $\Delta k / k_{\max}$ approached 55%.

Finally, the last group of figures (Fig. 4.8, 4.9 and 4.10) shows correlation plots between the observed changes in the system properties (period, frequency and stiffness) and maximum deflection angle $\theta_{\max}$ for all 21 buildings. The top parts show results for the first horizontal component if motion, and the bottom parts show results for the second horizontal component of motion, and each point is labeled by the respective station number. Figures 4.11 and 4.12 show, on same plots, results for both components of motion, respectively of the changes in frequency and in stiffness. It can be seen from these plots that, while in general the percentage changes are larger for larger deflection angle, there is lot of scatter in the data to fit a meaningful single trend.

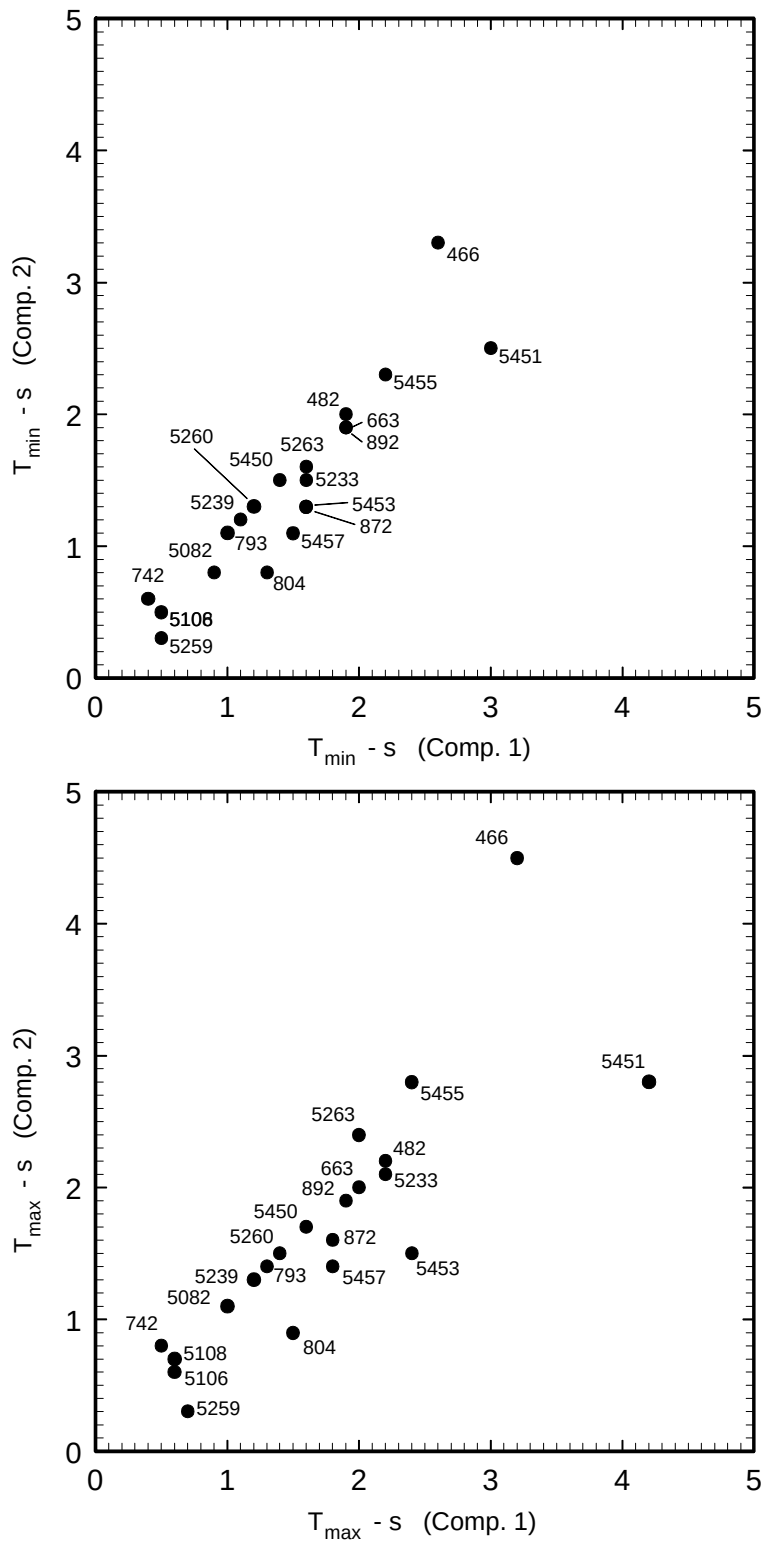

Fig. 4.2 Observed minimum (top) and maximum (bottom) periods for the 21 buildings. The values for the first horizontal component are shown on the x-axis and for the second component are shown on the y-axis.

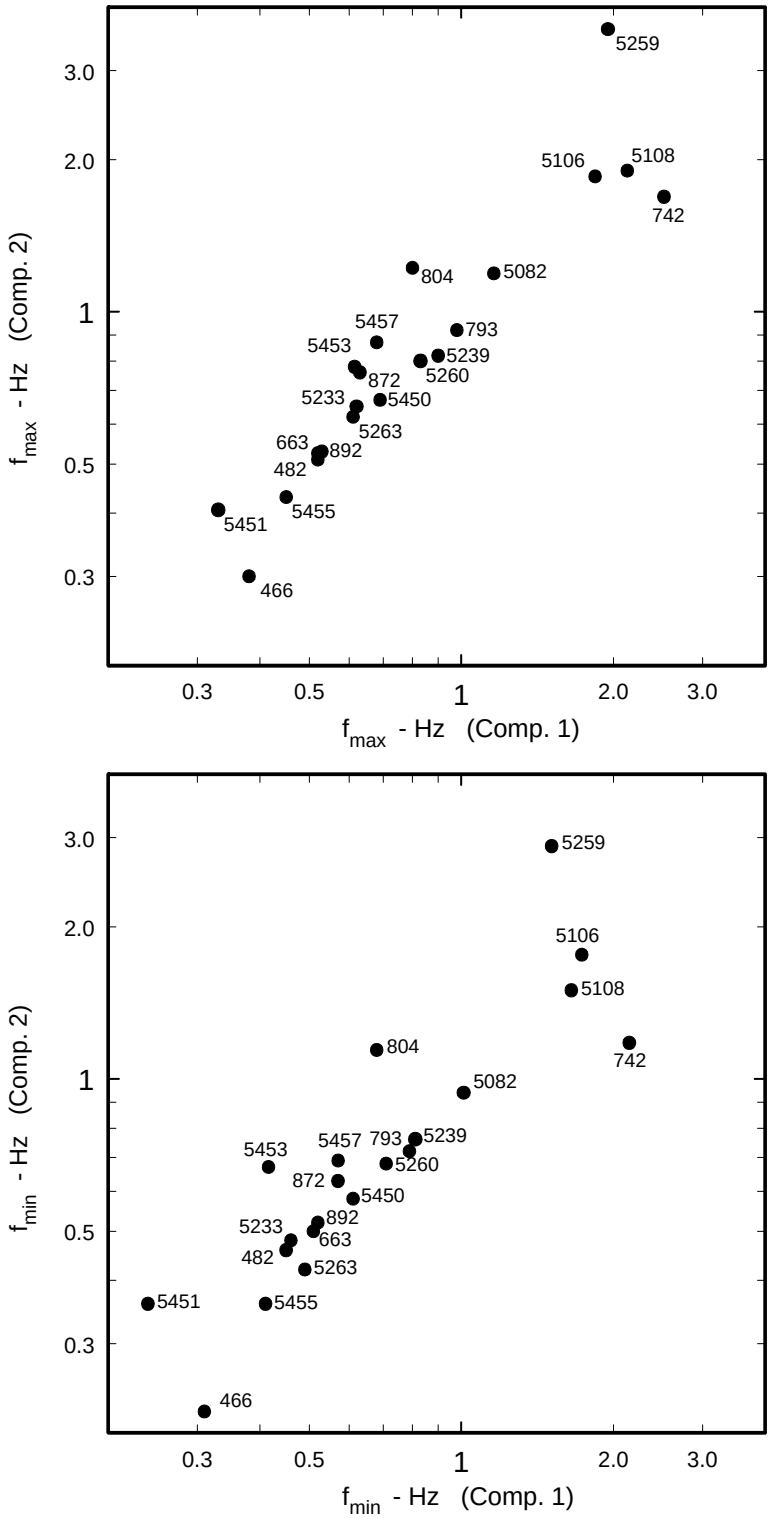

Fig. 4.3 Observed maximum (top) and minimum (bottom) frequencies for the 21 buildings. The values for the first horizontal component are shown on the x-axis and for the second component are shown on the y-axis.

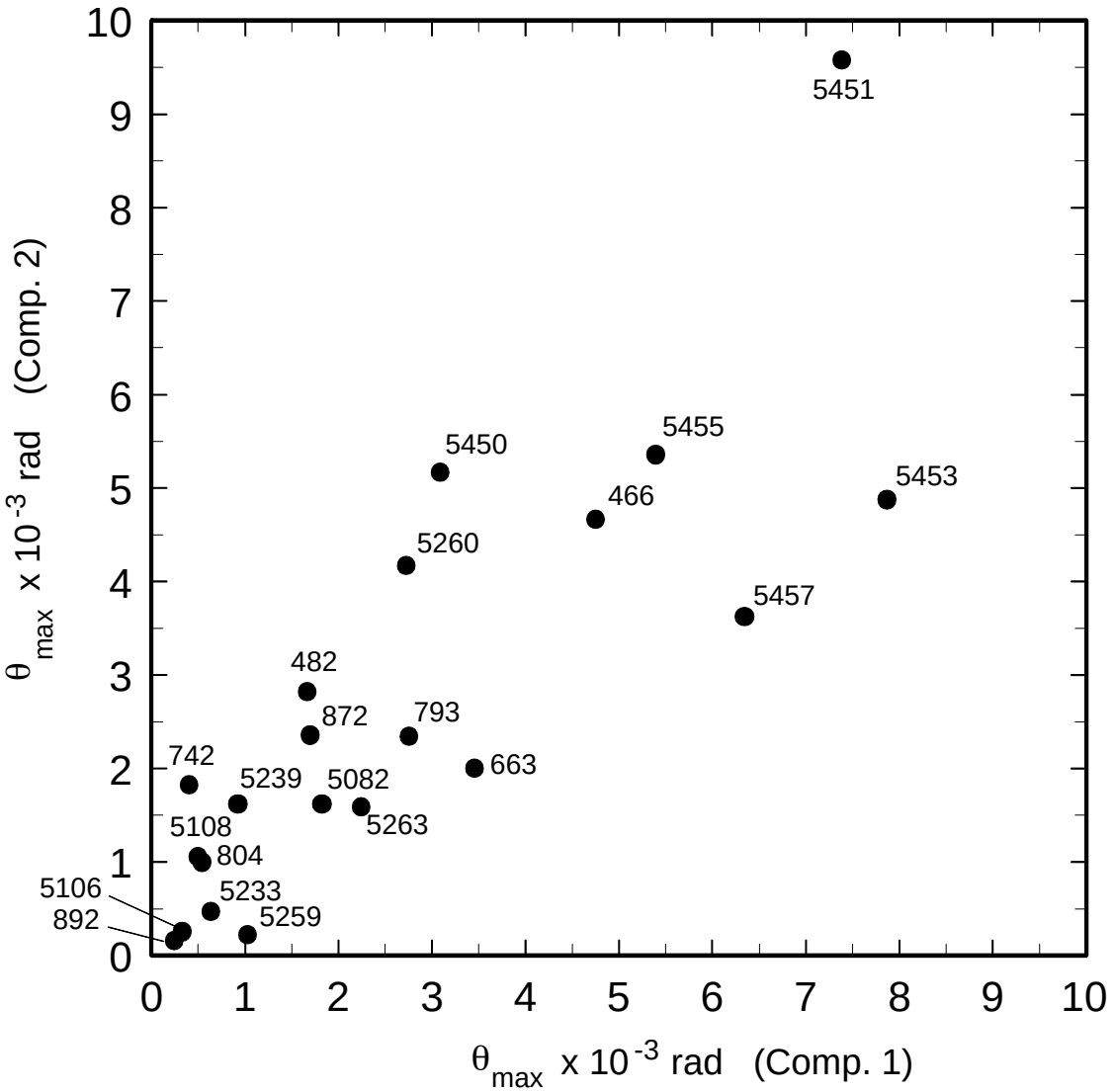

Fig. 4.4 Observed minimum (top) and maximum (bottom) angles of response for the 21 buildings. The values for the first horizontal component are shown on the x-axis and for the second component are shown on the y-axis.

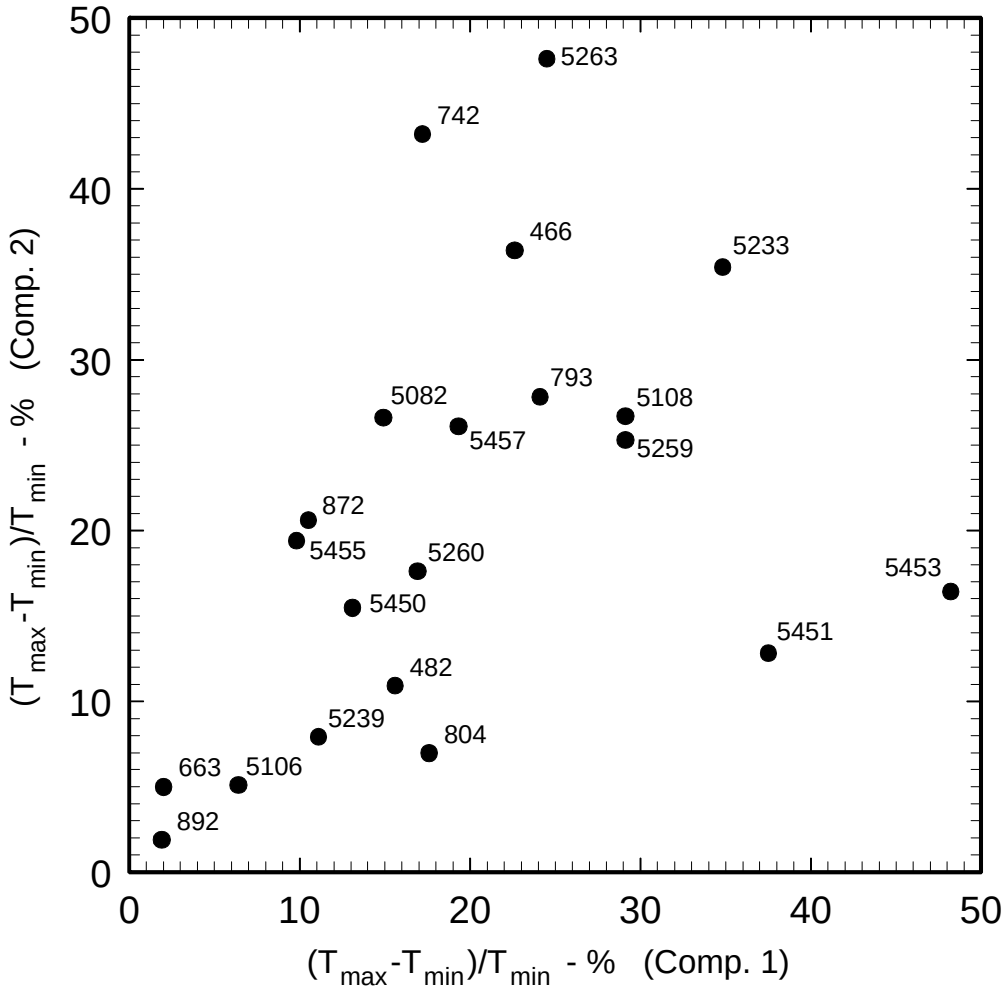

Fig. 4.5 Observed percentage changes in the periods of vibration, *T*, for the 21 buildings. The values for the first horizontal component are shown on the x-axis and for the second component are shown on the y-axis.

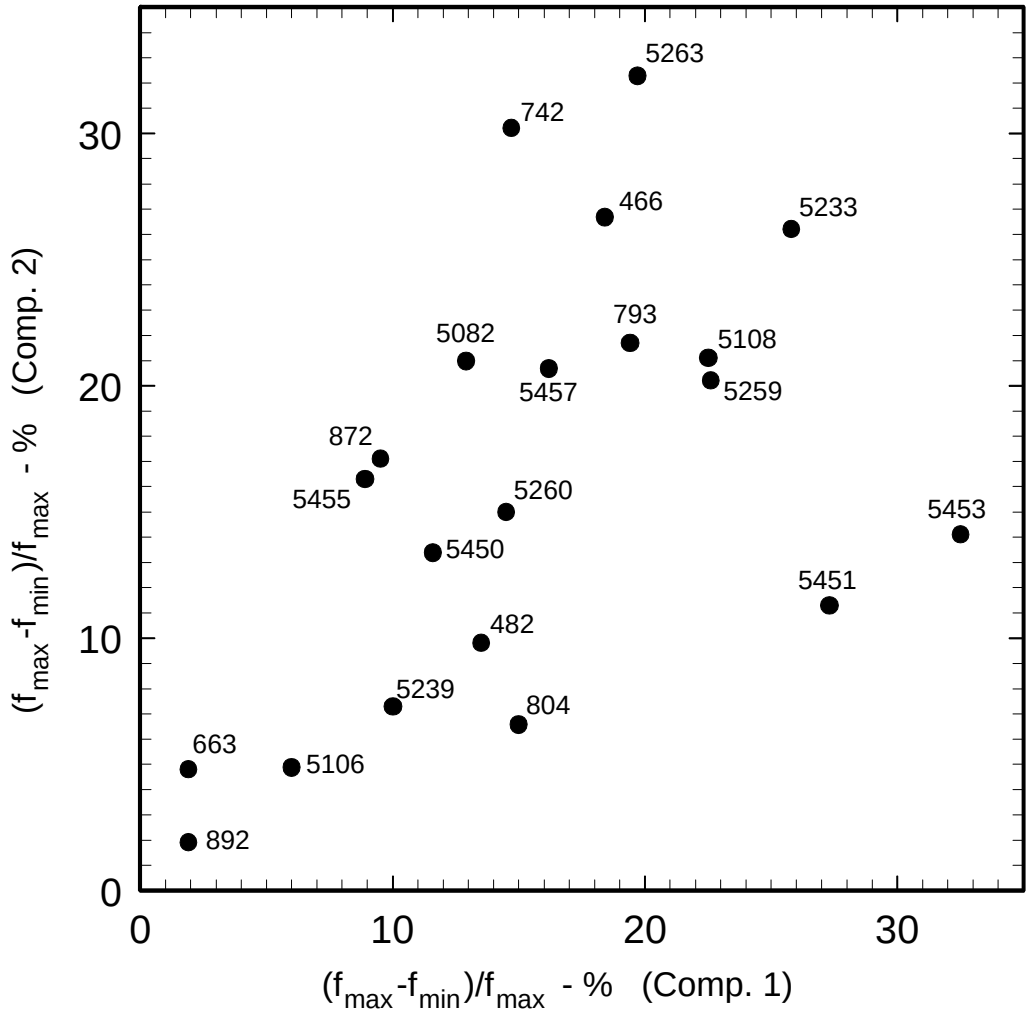

Fig. 4.6 Observed percentage changes in the frequencies of vibration, *f*, for the 21 buildings. The values for the first horizontal component are shown on the x-axis and for the second component are shown on the y-axis.

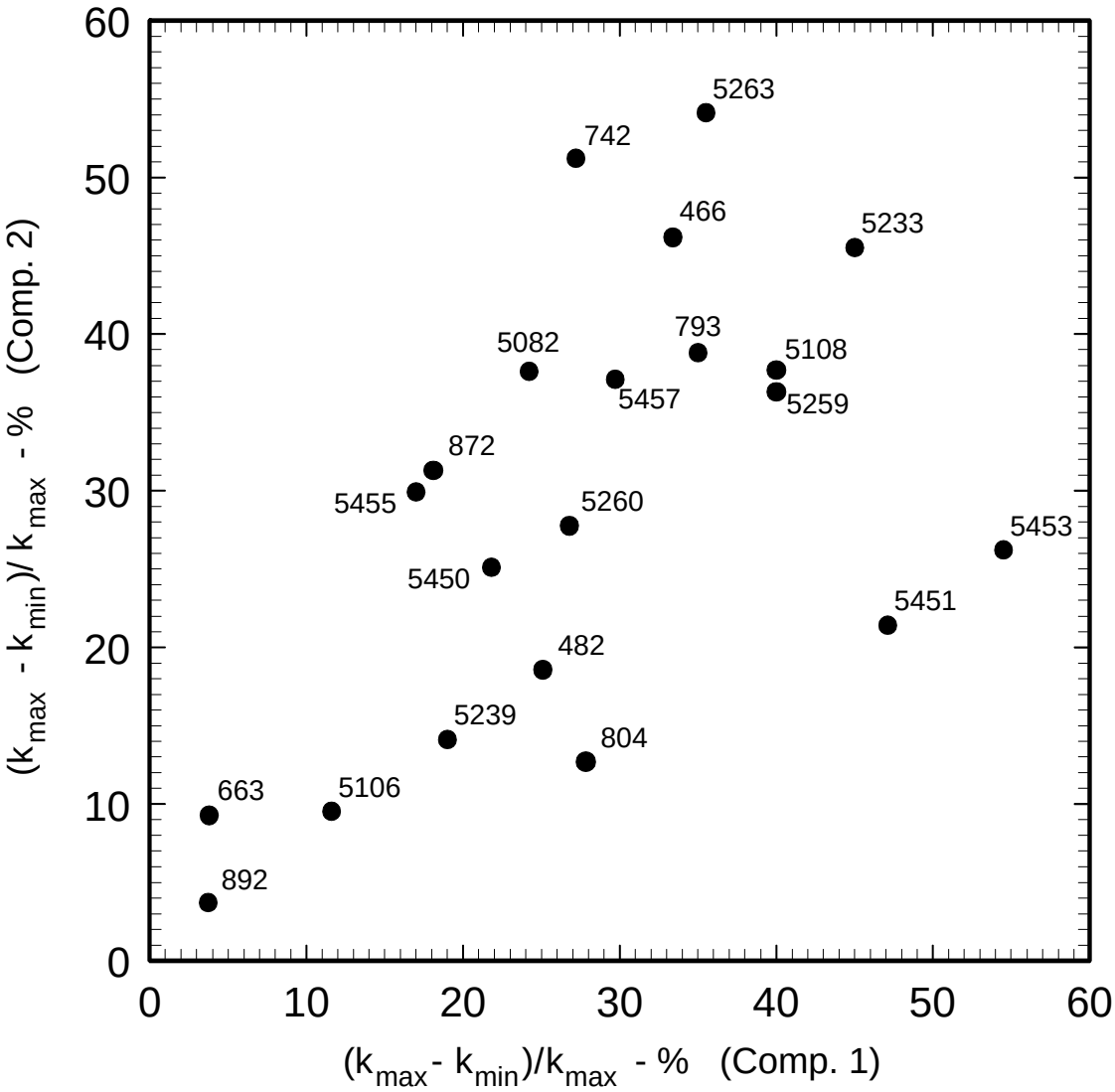

Fig. 4.7 Observed percentage changes in system stiffness, *k*, inferred from the change in frequency, for the 21 buildings. The values for the first horizontal component are shown on the x-axis and for the second component are shown on the y-axis.

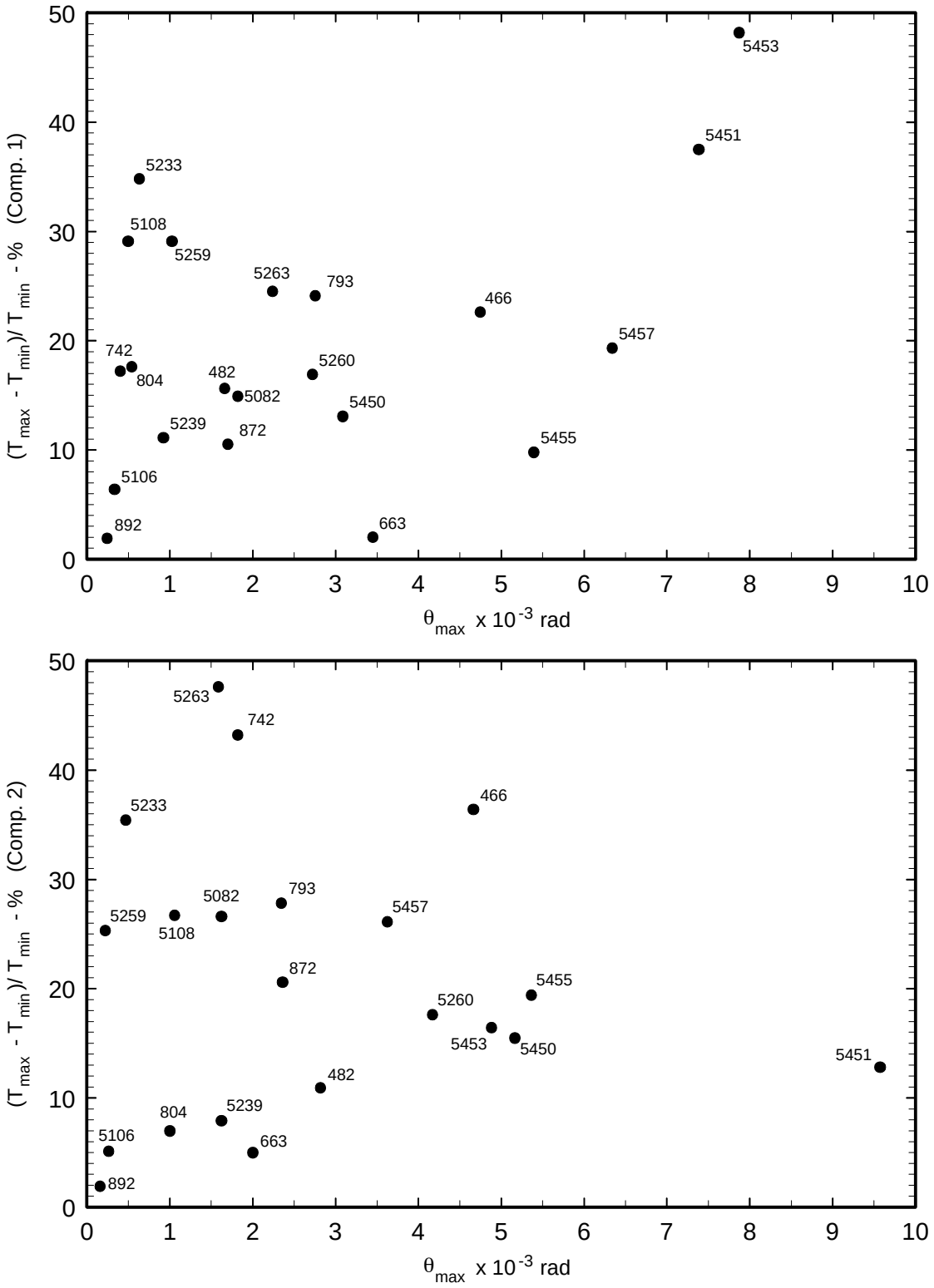

Fig. 4.8 Percentage change in period of vibration versus maximum deflection angle for components 1 (top) and 2 (bottom).

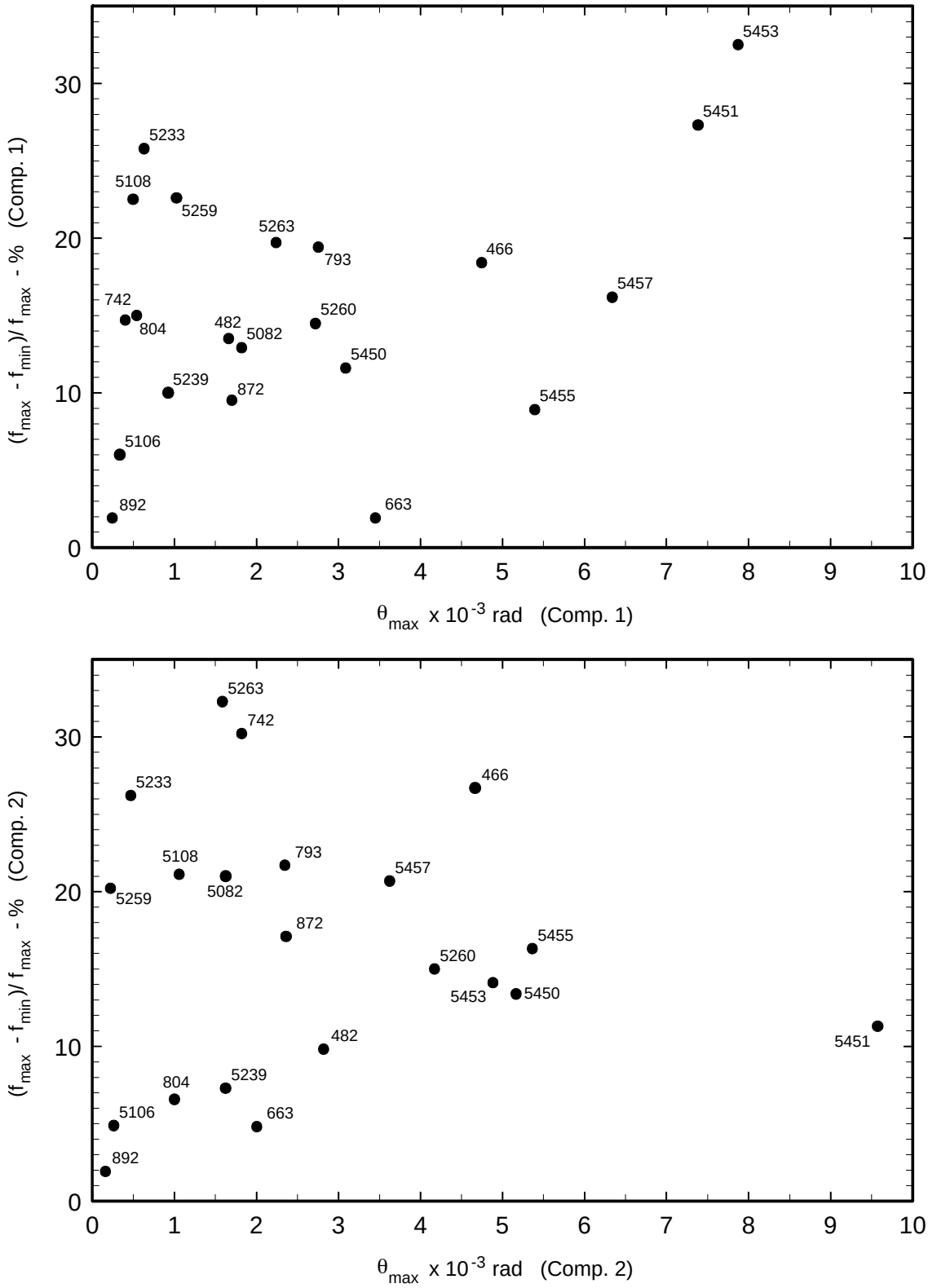

Fig. 4.9 Percentage change in frequency of vibration versus maximum deflection angle for components 1 (top) and 2 (bottom).

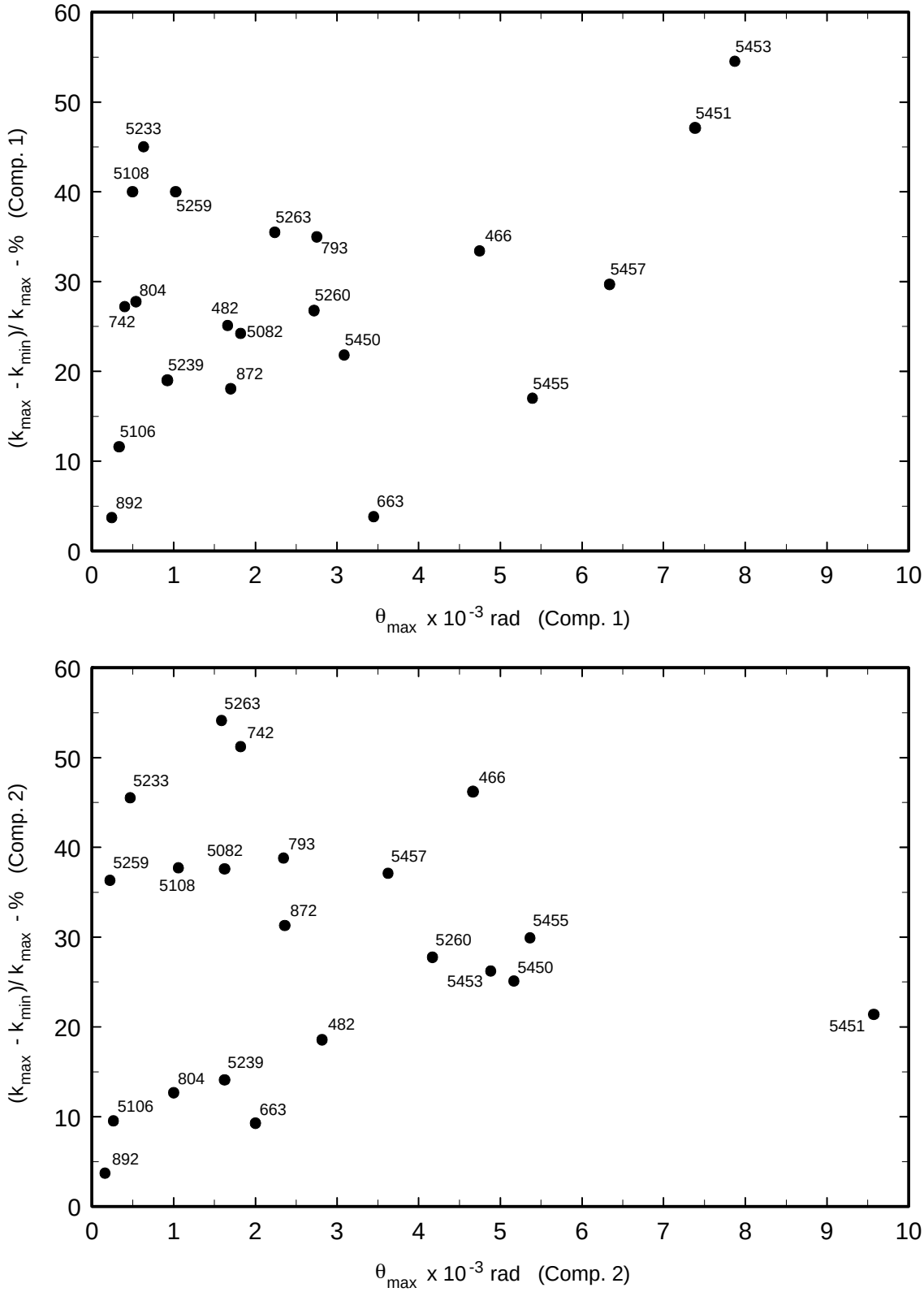

Fig. 4.10 Percentage change in system stiffness versus maximum deflection angle for components 1 (top) and 2 (bottom).

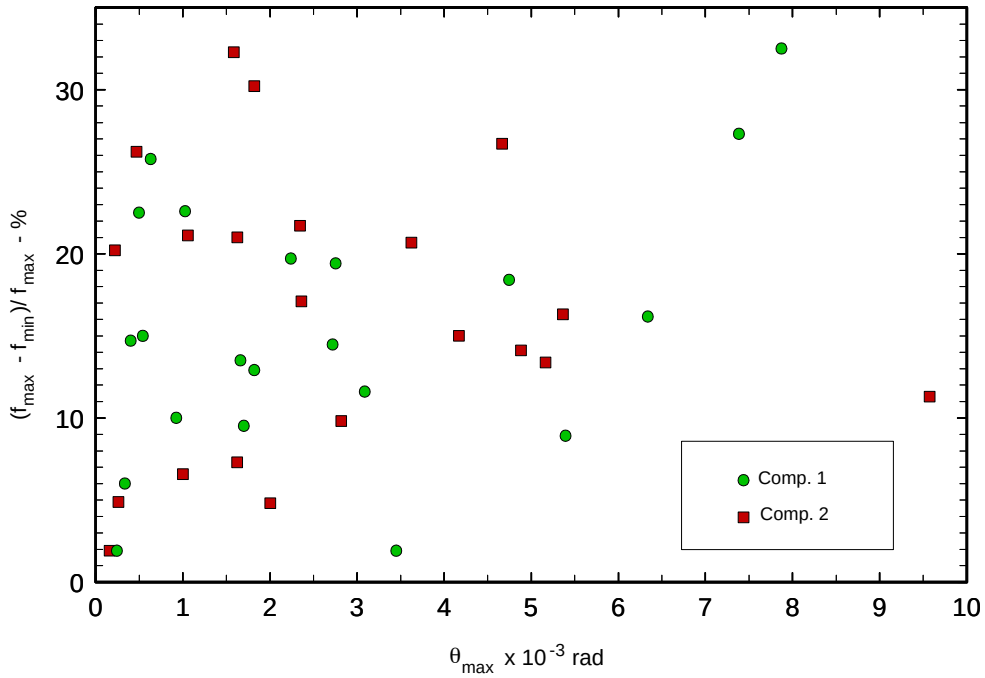

Fig. 4.11 Percentage change in frequency of vibration versus maximum deflection angle for both components of motion.

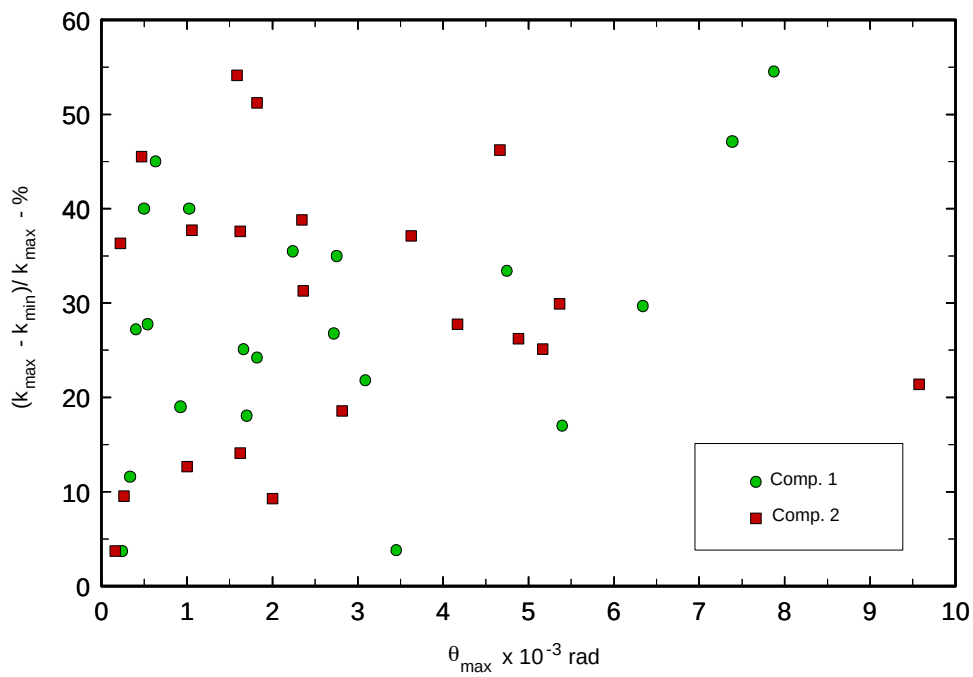

Fig. 4.12 Percentage change in stiffness versus maximum deflection angle for both components of motion.

5. DISCUSSION AND CONCLUSIONS

Results are shown of the variations of the building periods (frequencies) as function of the level of response for 21 buildings in the Los Angeles area. For each building, records of several earthquakes were used, including at least one significant earthquake. Most of the records analyzed are of the 1994 Northridge earthquake and its aftershocks.

The majority of these buildings are "code" buildings, and only the response on the roof or top floor was recorded. Consequently, for these buildings only the absolute motion on the roof was known, which was used as a proxy for the relative motion. Further, it was not possible to separate the roof motion that is due to rigid body rocking of the building due to insufficient instrumentation. As a consequence, the measured deflection angles are not due to deformation of the building only, but include also the contribution from rigid body motion. Further, the frequencies measured by this Fourier type of analysis are those of the building-foundation-soil system, and depend both on the properties of the soil and of the building. Consequently, it was not possible to decipher to what degree the observed changes are due to changes in the building as opposed to changes in the soil, which would be necessary in order to develop empirical predictive formulae for the change. These physical constraints in the way the data was recorded certainly contributed to the scatter in the observed percentage change in the frequencies of vibration as function of the maximum deflection angle (Fig. 4.8 through 4.12), as well as the imprecision in the estimation of instantaneous frequency. Most of the scatter, however, is likely due to variations among the different buildings in structural material (reinforced concrete vs. steal), structural type (ductile vs. nonductile frame), foundation type, and local soil conditions (which would determine the degree to which the response was influenced by the soil-structure interaction), and whether the building was damaged by the earthquake. This information is not readily available for majority of the buildings analyzed, which are "code" buildings, but is traceable and should be compiled in order to derive improved predictive formulae for the building periods of vibration for the building codes. Also, much is to be learned from detailed studies of selected buildings with more complete instrumentation, which would help interpret the trends for the data from roof instrument only. Examples of such studies can be found in [Todorovska and Trifunac 2007a,b,c; Trifunac et al. 2007), which include estimation of the building fixed-base frequency from only two horizontal records (ground floor and roof) by travel

time analysis. The same type of analysis should be completed for the well instrumented buildings in this set, as well as for other instrumented buildings.

Despite the scatter, a clear dependence of the observed building frequencies on the amplitudes of response was observed. The frequency decreased during the largest event and recovered during the aftershocks, but for some of the buildings there was a permanent reduction. For angles of response up to 10 mili radians, the periods during the small amplitude responses ($T_{\min}$) did not exceed 3.3 s, and during the largest amplitude responses ($T_{\max}$) did not exceed 4.5 s. Alternatively, the building frequencies during the largest motions ($f_{\min}$) did not exceed 3 Hz, and during the small motions ($f_{\max}$) did not exceed 3.5 Hz. The observed changes in period of vibration $\Delta T / T_{\min}$ approached 50%, in frequency of vibration $\Delta f / f_{\max}$ approached 35%, and in stiffness (of the soil-structure system) $\Delta k / k_{\max}$ approached 55%.

6. REFERENCES

[1] Biot MA (1942). Analytical and experimented methods in engineering seismology, *Trans., ASCE*, 68, 365-409.

[2] Carder DS (1936). Vibration observations, Chapter 5, in *Earthquake Investigations in California 1934-1935*, U.S. Dept. of Commerce, Coast and Geological Survey, *Special Publication No. 201*, Washington D.C.

[3] Clinton JF, Bradford SK, Heaton TH, Favela J (2005). The observed wander of the natural frequencies in a structure, *Bulletin of Seismological Society of America*, 96(1):237-57.

[4] Goel RK, Chopra AK (1997). Period formulas for concrete shear wall buildings, *J. of Structural Eng.*, ASCE, 124(4), 426-433.

[5] Hao TY, Trifunac MD, Todorovska MI (2004). Instrumented buildings of University of Southern California—strong motion data, metadata and soil-structure system frequencies, Report CE 04-01, Dept. of Civil Engrg., Univ. of Southern California, Los Angeles, California, pp. 558.

[6] Hudson DE (1970). Dynamic tests of full scale structures, Chapter 7, 127-149, in *Earthquake Engineering*, Edited by R.L. Wiegel, Prentice Hall, N.J.

[7] Li Y, Mau ST (1979). Learning from recorded earthquake motions in buildings, *J. of Structural Engrg*, ASCE, 123(1), 62-69.

[8] Luco JE, Trifunac MD, Wong HL (1987). On the apparent change in dynamic behavior of a nine story reinforced concrete building, *Bull. Seism. Soc. Amer.*, 77(6), 1961-1983.

[9] Stewart JP, Seed RB, Fenves GL (1999). Seismic soil-structure interaction in buildings II: Empirical findings, *J. of Geotech. Geoenvir. Engrg*, ASCE, 125(1), 38-48.

[10] Todorovska MI (2001). Estimation of instantaneous frequency of signals using the continuous wavelet transform, Report CE 01-07, Dept. of Civil Engrg., Univ. of Southern California, Los Angeles, California, pp. 55.

[11] Todorovska MI, Al Rjoub Y (2006). Effects of rainfall on soil-structure system frequency: examples based on poroelasticity and a comparison with full-scale measurements, *Soil Dynamics and Earthquake Engrg*, 26(6-7), 694-707.

[12] Todorovska MI, Trifunac MD (2007a). Earthquake damage detection in the Imperial County Services Building I: the data and time-frequency analysis, *Soil Dynamics and Earthquake Engrg*, 27(6), 564–576.

[13] Todorovska MI, Trifunac MD (2007b). Earthquake damage detection in the Imperial County Services Building II: analysis of novelties via wavelets, submitted for publication.

[14] Todorovska MI, Trifunac MD (2007c). Earthquake damage detection in the Imperial County Services Building III: analysis of wave travel times via impulse response functions, *Soil Dynamics and Earthquake Engrg,* in press, doi:10.1016/j.soildyn.2007.07.001.

[15] Todorovska MI, Hao T-Y, Trifunac MD (2004a). Building periods for use in earthquake resistant design codes - earthquake response data compilation and analysis of time and amplitude variations, Report CE 04-02, Dept. of Civil Engrg., Univ. of Southern California, Los Angeles, California, pp. 272.

[16] Todorovska MI, Hao T-Y, Trifunac MD (2004b). Time and amplitude variations of building-soil system frequencies during strong earthquake shaking for selected buildings in the Los Angeles, *Proc. Third UJNR Workshop on Soil-Structure Interaction*, Menlo Park, California, March 29-30, 2004, pp. 22.

[17] Todorovska MI, Trifunac MD, Hao TY (2006). Variations of apparent building frequencies - lessons from full-scale earthquake observations, *Proc. First European Conference on Earthquake Engineering and Seismology* (a joint event of the 13th ECEE & 30th General Assembly of the ESC), Geneva, Switzerland, 3-8 September 2006, Paper Number: 1547, pp. 9.

[18] Todorovska MI, Trifunac MD, Lee VW, Stephens CD, Fogleman KA, Davis C, Tognazzini R (1999). The ML = 6.4 Northridge, California, Earthquake and Five M > 5 Aftershocks Between 17 January and 20 March 1994 - Summary of Processed Strong Motion Data, *Report CE 99-01*, Dept. of Civil Engrg., Univ. of Southern California, Los Angeles, California.

[19] Todorovska MI, Trifunac MD (2007d). Impulse response analysis of the Van Nuys 7-story hotel during 11 earthquakes and earthquake damage detection, *Structural Control and Health Monitoring*, in press, DOI: 10.1002/stc.208.

[20] Trifunac MD (1999). Comments on "Period formulas for concrete shear wall buildings," *J. Struct. Eng.*, ASCE, 125(7), 797-798.

[21] Trifunac MD (2000). Comments on "Seismic soil-structure interaction in buildings I: analytical models, and II: empirical findings," *J. Geotech. Geoenvir. Engrg*, ASCE, 126(7), 668-670.

[22] Trifunac MD, Ivanovic SS, Todorovska MI (2001a). Apparent periods of a building I: Fourier analysis, *J. of Struct. Engrg*, ASCE, 127(5), 517-526).

[23] Trifunac MD, Ivanovic SS, Todorovska MI (2001b). Apparent periods of a building II: time-frequency analysis, *J. of Struct. Engrg*, ASCE, 127(5), 527-537.

[24] Trifunac MD, Hao TY, Todorovska MI (2001c). Response of a 14-story reinforced concrete structure to nine earthquakes: 61 years of observation in the Hollywood Storage Building. Report CE 01-02, Dept. of Civil Engrg., Univ. of Southern California, Los Angeles, California, pp. 88.

[25] Trifunac MD, Hao TY, Todorovska MI (2001d). On energy flow in earthquake response, Report CE 01-03, Dept. of Civil Engrg., Univ. of Southern California, Los Angeles, California.

[26] Trifunac MD, Hao TY, Todorovska MI (2001e). Energy of earthquake response as a design tool, *Proc. 13th Mexican National Conf. on Earthquake Engineering*, Guadalajara, Mexico.

[27] Trifunac MD, Todorovska MI, Manić MI, Bulajić BĐ (2007). Variability of the fixed-base and soil-structure system frequencies of a building – the case of Borik-2 building, Structural Control and Health Monitoring, submitted for publication.

[28] Udwadia FE, Trifunac MD (1974). Time and amplitude dependent response of structures, *Earthquake Engrg and Structural Dynamics*, 2, 359-378.

APPENDIX A:

STRONG MOTION DATA RELEASED

This appendix presents lists of strong motion data used for the analysis in this report that have been processed for this project. The digitization and processing methods used are described in Lee and Trifunac [1990]. The other records that were used are either from the collection of building records of the 1971 San Fernando earthquake, or have been processed by or for the USGS Strong Motion Program, which has released or will be releasing these records. The list of stations below shows the table number used in this appendix, the USGS station number, the number of floors, the street address, the number of earthquakes analyzed, the number of earthquakes for which records are released, and the number of components of motion released.

Web documents and FTP site with data file:

Project web page: http://www.usc.edu/dept/civil_eng/Earthquake_eng/USGS_build/

FTP site with data file: ftp://cwis.usc.edu/pub/todorovs/USGS_build/

The data files can be accessed either using the links in the project web page or directly by FTP.

List of stations

Table No.	Station No.	N floors	Street address	No. Rec. used	No. Rec. rel.	No. Comp. Rel.
A.01	0466	13	LOS ANGELES, 15250 VENTURA BLVD., Roof	3	2	6
A.02	0482	12	ALHAMBRA, 900 S. FREMONT, 12-chanel array	5	2	24
A.03	0663	12	LOS ANGELES, 10751 WILSHIRE Blvd., Roof	3	3	9
A.04	0742	8	LOS ANGELES, 1526 N.EDGEMONT ST., Roof	12	12	36
A.05	0793	11	LOS ANGELES, 4929 WILSHIRE BLVD., Roof	6	5	15
A.06	0804	10	WHITTIER, 7215 BRIGHT AVE., Basement, Roof	2	0	0
A.07	0872	8	LOS ANGELES, 1111 SUNSET Blvd., Bsmnt, 4th and 8th fl.	3	1	9
A.08	0892	55	LOS ANGELES, 333 S. HOPE ST., 5th fl.	2	2	6
A.09	5082	6	LOS ANGELES, WADSWORTH V.A. HOSPITAL, 9-chanel array	2	2	18
A.10	5106	11	LONG BEACH VA HOSPITAL, structural array	3	0	0
A.11	5108	6	SANTA SUSANA, ETEC Bldg 462, 1st and 6th fl.	9	11	66
A.12	5233	32	LOS ANGELES, 1100 WILSHIRE, 12-chanel array	2	1	12
A.13	5239	7	NORWALK, 12440 IMPERIAL HWY, structural array	5	0	0
A.14	5259	8	LOS ANGELES, 2005 N. HIGHLAND AVE., Roof	8	8	24
A.15	5260	12	LOS ANGELES, 444 S. SAN VINCENTE, Roof	9	8	24
A.16	5263	19	LOS ANGELES, 10660 WILSHIRE BLVD., Roof	5	5	15
A.17	5450	9	BURBANK, 3601 WEST OLIVE AVE., Roof	5	5	15
A.18	5451	12	LOS ANGELES, 6301 OWENSMOUTH AVE., Roof	3	3	9
A.19	5453	9	LOS ANGELES, 5805 SEPULVEDA BLVD., Roof	8	9	27
A.10	5455	13	LOS ANGELES, 16000 VENTURA BLVD., Roof	5	6	18
A.21	5457	10	LOS ANGELES, 8436 WEST 3rd ST., Roof	8	9	27

References:

V.W. Lee and M.D. Trifunac (1990). Automatic Digitization and Processing of Accelerograms Using PC. *Report No. 90-03*, Dept. of Civil Engrg., Univ. of Southern California.

Table A.01 List of processed records at station USGS 0466

USGS: 0466 SMA-1 185	LOS ANGELES, 15250 VENTURA BLVD., ROOF (13th floor)					34.157∞N 117.476∞W	
File Name	Ref No.	Log No.	Earthquake	Distance [km]	Duration [s]	Comp	Peak Acc. [g]
v1x0000.dat	IAA000	94.000.0	NORTHRIDGE EARTHQUAKE	9.0	59.7	N00E	0.550
						UP	0.394
						W00N	0.257
v1x0001.dat	IAA001	94.000.1	NORTHRIDGE EARTHQUAKE (aft. -1)	15.9	33.2	N00E	0.151
						UP	0.097
						W00N	0.054

Table A.02 List of processed records at station USGS 0482

USGS: 0482 CR-1 316	ALHAMBRA, 900 S. FREMONT					34.085∞N 118.149∞W	
File Name	Ref No.	Log No.	Earthquake	Distance [km]	Duration [s]	Comp.	Peak Acc. [g]
v1x4700.dat	IFA164	94.470.0	NORTHRIDGE EARTHQUAKE	38.4	137.5	Ch01	0.099
						Ch02	0.149
						Ch03	0.128
						Ch04	0.250
						Ch05	0.141
						Ch06	0.201
						Ch07	0.582
						Ch08	0.380
						Ch09	0.392
						Ch10	0.126
						Ch11	0.114
						Ch12	0.176
v1x0131.dat	IFA031	94.013.1	NORTHRIDGE EARTHQUAKE (aft. 392)	34.1	71.6	Ch01	0.025
						Ch02	0.014
						Ch03	0.013
						Ch04	0.017
						Ch05	0.034
						Ch06	0.014
						Ch07	0.032
						Ch08	0.094
						Ch09	0.028
						Ch10	0.032
						Ch11	0.014
						Ch12	0.024

Table A.03 List of processed records at station USGS 0663

USGS: 0663 SMA-1 552	LOS ANGELES, 10751 WILSHIRE Blvd., Roof (12th level)					34.06∞N 118.438∞W	
File Name	Ref No.	Log No.	Earthquake	Distance [km]	Duration [s]	Comp.	Peak Acc. [g]
v1X0000.DAT	IAA005	94.000.0	NORTHRIDGE EARTHQUAKE	19.4	102.6	S72W	0.390
						UP	0.392
						S18E	0.319
v1X0015.DAT	IAA005	94.001.5	NORTHRIDGE EARTHQUAKE (aft. -15)	27.0	30.9	S72W	0.015
						UP	0.029
						S18E	0.028
v1X0016.DAT	IAA005	94.001.6	NORTHRIDGE EARTHQUAKE (aft. -16)	27.0	38.9	S72W	0.044
						UP	0.048
						S18E	0.028

Table A.04 List of processed records at station USGS 0742

USGS: 0742 SMA-1 923	LOS ANGELES, 1526 N.EDGEMONT ST., ROOF (8th floor)					34.098∞N 118.294∞W	
File Name	Ref No.	Log No.	Earthquake	Distance [km]	Duration [s]	Comp.	Peak Acc. [g]
v1x0000.dat	IAA000	94.000.0	NORTHRIDGE EARTHQUAKE	25.8	44.2	E00S	0.832
						UP	0.241
						N00E	0.691
v1x0001.dat	IAA001	94.000.1	NORTHRIDGE EARTHQUAKE (aft. -1)	28.6	22.3	E00S	0.315
						UP	0.086
						N00E	0.112
v1x0003.dat	IAA003	94.000.3	NORTHRIDGE EARTHQUAKE (aft. -3)	28.6	19.6	E00S	0.048
						UP	0.025
						N00E	0.049
v1x0004.dat	IAA004	94.000.4	NORTHRIDGE EARTHQUAKE (aft. -4)	28.6	20.4	E00S	0.029
						UP	0.021
						N00E	0.046
v1x0005.dat	IAA005	94.000.5	NORTHRIDGE EARTHQUAKE (aft. -5)	28.6	14.7	E00S	0.058
						UP	0.017
						N00E	0.034
v1x0008.dat	IAA008	94.000.8	NORTHRIDGE EARTHQUAKE (aft. -8)	28.6	17.1	E00S	0.126
						UP	0.026
						N00E	0.029
v1x0011.dat	IAA011	94.001.1	NORTHRIDGE EARTHQUAKE (aft. -11)	28.6	22.4	E00S	0.109
						UP	0.018
						N00E	0.033
v1x0012.dat	IAA012	94.001.2	NORTHRIDGE EARTHQUAKE (aft. -12)	28.6	24.3	E00S	0.099
						UP	0.026
						N00E	0.053
v1x0013.dat	IAA013	94.001.3	NORTHRIDGE EARTHQUAKE (aft. -13)	28.6	14.9	E00S	0.036
						UP	0.022
						N00E	0.016
v1x0014.dat	IAA014	94.001.4	NORTHRIDGE EARTHQUAKE (aft. -14)	28.6	14.6	E00S	0.020
						UP	0.010
						N00E	0.012
v1x0019.dat	IAA019	94.001.9	NORTHRIDGE EARTHQUAKE (aft. -19)	28.6	20.8	E00S	0.060
						UP	0.012
						N00E	0.021
v1x0020.dat	IAA020	94.002.0	NORTHRIDGE EARTHQUAKE (aft. -20)	28.6	18.9	E00S	0.028
						UP	0.010
						N00E	0.015

Table A.05 List of processed records at station USGS 0793

USGS: 0793 SMA-1 931	LOS ANGELES, 4929 WILSHIRE BLVD. ROOF (11th Floor)					34.063∞N 118.337∞W	
File Name	Ref No.	Log No.	Earthquake	Distance [km]	Duration [s]	Comp.	Peak Acc. [g]
v1x0000.dat	IAA000	94.000.0	NORTHRIDGE EARTHQUAKE	24.9	104.7	S00W	0.396
						UP	0.304
						E00S	0.331
v1x0004.dat	IAA004	94.000.4	NORTHRIDGE EARTHQUAKE (aft. -4)	29.7	34.3	S00W	0.018
						UP	0.023
						E00S	0.021
v1x0007.dat	IAA007	94.000.7	NORTHRIDGE EARTHQUAKE (aft. -7)	29.7	27.6	S00W	0.023
						UP	0.023
						E00S	0.018
v1x0008.dat	IAA008	94.000.8	NORTHRIDGE EARTHQUAKE (aft. -8)	29.7	31.8	S00W	0.032
						UP	0.028
						E00S	0.031
v1x0103.dat	IAA103	94.010.3	NORTHRIDGE EARTHQUAKE (aft. -103)	29.7	23.9	S00W	0.007
						UP	0.024
						E00S	0.014
v1x0104.dat	IAA104	94.010.4	NORTHRIDGE EARTHQUAKE (aft. -104)	29.7	41.2	S00W	0.051
						UP	0.080
						E00S	0.040

Table A.06 List of processed records at station USGS 0804

Records have or will be distributed by USGS.

Table A.07 List of processed records at station USGS 0872 (Basement, 4th and 8th floor)

USGS: 0872 SMA-1 1074	LOS ANGELES, 1111 SUNSET Blvd. (Basement)					34.067∞N 118.248∞W	
File Name	Ref No.	Log No.	Earthquake	Distance [km]	Duration [s]	Comp.	Peak Acc. [g]
v1X8200.DAT	IAA000	94.820.0	NORTHRIDGE EARTHQUAKE	31.2	34.2	N12W UP S78W	0.128 0.061 0.133

USGS: 0872 SMA-1 1075	LOS ANGELES, 1111 SUNSET Blvd. (4th floor)					34.067∞N 118.248∞W	
File Name	Ref No.	Log No.	Earthquake	Distance [km]	Duration [s]	Comp.	Peak Acc. [g]
v1X8300.DAT	IAA000	94.830.0	NORTHRIDGE EARTHQUAKE	31.2	34.2	N12W UP S78W	0.173 0.090 0.178

USGS: 0872 SMA-1 1076	LOS ANGELES, 1111 SUNSET Blvd. Roof (8th floor)					34.067∞N 118.248∞W	
File Name	Ref No.	Log No.	Earthquake	Distance [km]	Duration [s]	Comp.	Peak Acc. [g]
v1X8400.DAT	IAA000	94.840.0	NORTHRIDGE EARTHQUAKE	31.2	34.2	N12W UP S78W	0.219 0.159 0.230

Table A.08 List of processed records at station USGS 0892

USGS: 0892 SMA-1 1631	LOS ANGELES, 333 S. HOPE ST., 55th Floor					34.053∞N 118.251∞W	
File Name	Ref No.	Log No.	Earthquake	Distance [km]	Duration [s]	Comp.	Peak Acc. [g]
v1x0000.dat	IAA000	94.000.0	NORTHRIDGE EARTHQUAKE	31.8	63.9	N83E	0.113
						UP	0.301
						W83N	0.202
v1x0001.dat	IAA001	94.000.1	NORTHRIDGE EARTHQUAKE (aft. -1)	35.0	27.4	N83E	0.016
						UP	0.058
						W83N	0.029

Table A.09 List of processed records at station USGS 5082

USGS: 5082 CR-1 233	LOS ANGELES, WADSWORTH V.A. HOSPITAL (Struct. Array)					34.053∞N 118.452∞W	
File Name	Ref No.	Log No.	Earthquake	Distance [km]	Duration [s]	Comp.	Peak Acc. [g]
v1X4900.DAT	IAA001	94.490.0	NORTHRIDGE EARTHQUAKE	19.4	113.3	Ch01	0.511
						Ch02	0.415
						Ch03	0.444
						Ch04	0.456
						Ch05	0.461
						Ch06	0.443
						Ch07	0.207
						Ch08	0.210
						Ch09	0.102
v1X0140.DAT	IAA002	94.014.0	NORTHRIDGE EARTHQUAKE (aft. 392)	19.9	54.9	Ch01	0.115
						Ch02	0.096
						Ch03	0.092
						Ch04	0.099
						Ch05	0.113
						Ch06	0.065
						Ch07	0.085
						Ch08	0.052
						Ch09	0.027

Table A.10 List of processed records at station USGS 5106

Records have or will be distributed by USGS.

Table A.11 List of processed records at station USGS 5108 (1st and 6th floor)

USGS: 5108 SMA 1277	SANTA SUSANA, ETEC Bldg 462 (1st Floor)					34.230∞N 118.712∞W	
File Name	Ref No.	Log No.	Earthquake	Distance [km]	Duration [s]	Comp	Peak Acc. [g]
V1X0300.dat	IAA013	94.030.0	NORTHRIDGE EARTHQUAKE	16.3	60.1	E00S	0.236
						UP	0.226
						N00E	0.335
V1X0301.dat	IAA014	94.030.1	NORTHRIDGE EARTHQUAKE (aft. 7)	16.8	34.2	E00S	0.023
						UP	0.010
						N00E	0.022
V1X0302.dat	IAA015	94.030.2	NORTHRIDGE EARTHQUAKE (aft. 9)	16.1	43.1	E00S	0.037
						UP	0.019
						N00E	0.032
V1X0304.dat	IAA018	94.030.4	NORTHRIDGE EARTHQUAKE (aft. 100)	12.9	37.6	E00S	0.030
						UP	0.015
						N00E	0.023
V1X0305.dat	IAA019	94.030.5	NORTHRIDGE EARTHQUAKE (aft. 129)	15.7	42.8	E00S	0.151
						UP	0.045
						N00E	0.181
V1X0306.dat	IAA020	94.030.6	NORTHRIDGE EARTHQUAKE (aft. 142)	10.9	46.5	E00S	0.043
						UP	0.047
						N00E	0.061
V1X0307.dat	IAA021	94.030.7	NORTHRIDGE EARTHQUAKE (aft. 151)	16.4	31.8	E00S	0.016
						UP	0.010
						N00E	0.024
V1X0308.dat	IAA022	94.030.8	NORTHRIDGE EARTHQUAKE (aft. 253)	16.5	43.1	E00S	0.036
						UP	0.024
						N00E	0.039
V1X0309.dat	IAA023	94.030.9	NORTHRIDGE EARTHQUAKE (aft. 254)	18.5	43.9	E00S	0.027
						UP	0.016
						N00E	0.021
V1X0310.dat	IAA024	94.031.0	NORTHRIDGE EARTHQUAKE (aft. 336)	14.9	42.7	E00S	0.096
						UP	0.036
						N00E	0.090
V1X0311.dat	IAA025	94.031.1	NORTHRIDGE EARTHQUAKE (aft. 392)	16.5	41.8	E00S	0.047
						UP	0.021
						N00E	0.047

USGS: 5108 SMA 1276	SANTA SUSANA, ETEC Bldg 462 (6th Floor)					34.230∞N 118.712∞W	
File Name	Ref No.	Log No.	Earthquake	Distance [km]	Duration [s]	Comp	Peak Acc. [g]
V1X8900.dat	IAA001	94.890.0	NORTHRIDGE EARTHQUAKE	16.3	59.8	E00S	0.392
						UP	0.398
						N00E	0.595
V1X8901.dat	IAA002	94.890.1	NORTHRIDGE EARTHQUAKE (aft. 7)	16.8	34.2	E00S	0.019
						UP	0.018
						N00E	0.019
V1X8902.dat	IAA003	94.890.2	NORTHRIDGE EARTHQUAKE (aft. 9)	16.1	43.1	E00S	0.032
						UP	0.040
						N00E	0.045
V1X8904.dat	IAA005	94.890.4	NORTHRIDGE EARTHQUAKE (aft. 100)	12.9	37.6	E00S	0.039
						UP	0.027
						N00E	0.025
V1X8905.dat	IAA006	94.890.5	NORTHRIDGE EARTHQUAKE (aft. 129)	15.7	42.8	E00S	0.165
						UP	0.106
						N00E	0.127
V1X8906.dat	IAA007	94.890.6	NORTHRIDGE EARTHQUAKE (aft. 142)	10.9	46.0	E00S	0.129
						UP	0.071
						N00E	0.075
V1X8907.dat	IAA008	94.890.7	NORTHRIDGE EARTHQUAKE (aft. 151)	16.4	34.9	E00S	0.021
						UP	0.017
						N00E	0.035
V1X8908.dat	IAA009	94.890.8	NORTHRIDGE EARTHQUAKE (aft. 253)	16.5	43.1	E00S	0.089
						UP	0.051
						N00E	0.046
V1X8909.dat	IAA010	94.890.9	NORTHRIDGE EARTHQUAKE (aft. 254)	18.5	43.9	E00S	0.034
						UP	0.031
						N00E	0.025
V1X8910.dat	IAA011	94.891.0	NORTHRIDGE EARTHQUAKE (aft. 336)	14.9	42.7	E00S	0.089
						UP	0.074
						N00E	0.070
V1X8911.dat	IAA012	94.891.1	NORTHRIDGE EARTHQUAKE (aft. 392)	16.5	41.8	E00S	0.043
						UP	0.037
						N00E	0.038

Table A.12 List of processed records at station USGS 5233

USGS: 5233 CR-1 270	LOS ANGELES, 1100 WILSHIRE (Struct. Array)					34.052∞N 118.263∞W	
File Name	Ref No.	Log No.	Earthquake	Distance [km]	Duration [s]	Comp.	Peak Acc. [g]
v1X1000.DAT	IFA147	94.100.0	NORTHRIDGE EARTHQUAKE	31.0	149.3	Ch01	0.153
						Ch02	0.219
						Ch03	0.145
						Ch04	0.152
						Ch05	0.273
						Ch06	0.156
						Ch07	0.142
						Ch08	0.350
						Ch09	0.156
						Ch10	0.171
						Ch11	0.151
						Ch12	0.192

Table A.13 List of processed records at station USGS 5239

Records have or will be distributed by USGS.

Table A.14 List of processed records at station USGS 5259

USGS: 5259 SMA-1 2691	LOS ANGELES, 2005 N. HIGHLAND AVE. ROOF (8th floor)					34.106∞N 118.336∞W	
File Name	Ref No.	Log No.	Earthquake	Distance [km]	Duration [s]	Comp.	Peak Acc. [g]
v1x0000.dat	IAA000	94.000.0	NORTHRIDGE EARTHQUAKE	22.0	58.9	N00E	0.376
						UP	0.191
						W00N	0.415
v1x0001.dat	IAA001	94.000.1	NORTHRIDGE EARTHQUAKE (aft. -1)	25.6	41.6	N00E	0.068
						UP	0.046
						W00N	0.148
v1x0003.dat	IAA003	94.000.3	NORTHRIDGE EARTHQUAKE (aft. -3)	25.6	87.1	N00E	0.015
						UP	0.016
						W00N	0.048
v1x0015.dat	IAA015	94.001.5	NORTHRIDGE EARTHQUAKE (aft. -15)	25.6	32.9	N00E	0.015
						UP	0.013
						W00N	0.046
v1x0016.dat	IAA016	94.001.6	NORTHRIDGE EARTHQUAKE (aft. -16)	25.6	39.1	N00E	0.044
						UP	0.019
						W00N	0.103
v1x0026.dat	IAA026	94.002.6	NORTHRIDGE EARTHQUAKE (aft. -26)	25.6	32.8	N00E	0.013
						UP	0.006
						W00N	0.025
v1x0105.dat	IAA105	94.010.5	NORTHRIDGE EARTHQUAKE (aft. -105)	25.6	25.0	N00E	0.014
						UP	0.007
						W00N	0.022
v1x0110.dat	IAA110	94.011.0	NORTHRIDGE EARTHQUAKE (aft. -110)	25.6	41.8	N00E	0.084
						UP	0.090
						W00N	0.134

Table A.15 List of processed records at station USGS 5260

USGS: 5260 SMA-1 5701	LOS ANGELES, 444 S. SAN VINCENTE, ROOF (12th floor)					34.071∞N 118.374∞W	
File Name	Ref No.	Log No.	Earthquake	Distance [km]	Duration [s]	Comp.	Peak Acc. [g]
v1x0000.dat	IAA000	94.000.0	NORTHRIDGE EARTHQUAKE	21.8	51.4	W65N	0.544
						UP	0.330
						S65W	0.631
v1x0001.dat	IAA001	94.000.1	NORTHRIDGE EARTHQUAKE (aft. -1)	27.5	31.7	W65N	0.170
						UP	0.144
						S65W	0.108
v1x0002.dat	IAA002	94.000.2	NORTHRIDGE EARTHQUAKE (aft. -2)	27.5	13.4	W65N	0.018
						UP	0.013
						S65W	0.013
v1x0014.dat	IAA014	94.001.4	NORTHRIDGE EARTHQUAKE (aft. -14)	27.5	27.7	W65N	0.072
						UP	0.045
						S65W	0.078
v1x0015.dat	IAA015	94.001.5	NORTHRIDGE EARTHQUAKE (aft. -15)	27.5	17.7	W65N	0.023
						UP	0.017
						S65W	0.045
v1x0021.dat	IAA021	94.002.1	NORTHRIDGE EARTHQUAKE (aft. -21)	27.5	18.7	W65N	0.042
						UP	0.039
						S65W	0.047
v1x0106.dat	IAA106	94.010.6	NORTHRIDGE EARTHQUAKE (aft. -106)	27.5	16.9	W65N	0.034
						UP	0.019
						S65W	0.044
v1x0110.dat	IAA110	94.011.0	NORTHRIDGE EARTHQUAKE (aft. -110)	27.5	31.9	W65N	0.153
						UP	0.240
						S65W	0.143

Table A.16 List of processed records at station USGS 5263

USGS: 5263 SMA-1 4235	LOS ANGELES, 10660 WILSHIRE BLVD., ROOF (19th floor)					34.061∞N 118.434∞W	
File Name	Ref No.	Log No.	Earthquake	Distance [km]	Duration [s]	Comp.	Peak Acc. [g]
v1x0000.dat	IAA000	94.000.0	NORTHRIDGE EARTHQUAKE	19.4	110.8	E70S	0.514
						UP	0.488
						N70E	1.054
v1x0012.dat	IAA012	94.001.2	NORTHRIDGE EARTHQUAKE (aft. -12)	27.0	45.8	E70S	0.057
						UP	0.055
						N70E	0.073
v1x0014.dat	IAA014	94.001.4	NORTHRIDGE EARTHQUAKE (aft. -14)	27.0	39.4	E70S	0.040
						UP	0.023
						N70E	0.039
v1x0106.dat	IAA106	94.010.6	NORTHRIDGE EARTHQUAKE (aft. -106)	27.0	31.9	E70S	0.034
						UP	0.018
						N70E	0.053
v1x0108.dat	IAA108	94.010.8	NORTHRIDGE EARTHQUAKE (aft. -108)	27.0	48.3	E70S	0.231
						UP	0.224
						N70E	0.277

Table A.17 List of processed records at station USGS 5450

USGS: 5450 SMA-1 6146	BURBANK, 3601 WEST OLIVE AVE., ROOF (9th floor)					34.152∞N 118.337∞W	
File Name	Ref No.	Log No.	Earthquake	Distance [km]	Duration [s]	Comp	Peak Acc. [g]
v1x0000.dat	IAA000	94.000.0	NORTHRIDGE EARTHQUAKE	19.6	47.4	N00E	0.644
						UP	1.060
						W00N	0.508
v1x0001.dat	IAA001	94.000.1	NORTHRIDGE EARTHQUAKE (aft. -1)	21.4	21.9	N00E	0.069
						UP	0.065
						W00N	0.085
v1x0005.dat	IAA005	94.000.5	NORTHRIDGE EARTHQUAKE (aft. -5)	21.4	16.3	N00E	0.024
						UP	0.031
						W00N	0.027
v1x0013.dat	IAA013	94.001.3	NORTHRIDGE EARTHQUAKE (aft. -13)	21.4	21.8	N00E	0.036
						UP	0.041
						W00N	0.031
v1x0014.dat	IAA014	94.001.4	NORTHRIDGE EARTHQUAKE (aft. -14)	21.4	11.6	N00E	0.020
						UP	0.014
						W00N	0.011

Table A.18 List of processed records at station USGS 5451

USGS: 5451 SMA-1 4048	LOS ANGELES, 6301 OWENSMOUTH AVE., ROOF (12th level)					34.185∞N 118.584∞W	
File Name	Ref No.	Log No.	Earthquake	Distance [km]	Duration [s]	Comp	Peak Acc. [g]
v1x0000.dat	IAA000	94.000.0	NORTHRIDGE EARTHQUAKE	5.4	99.2	N00E	0.552
						UP	0.477
						W00N	0.373
v1x0026.dat	IAA026	94.002.6	NORTHRIDGE EARTHQUAKE (aft. -26)	15.55	41.5	N00E	0.077
						UP	0.068
						W00N	0.073
v1x0115.dat	IAA115	94.011.5	NORTHRIDGE EARTHQUAKE (aft. -115)	15.55	38.3	N00E	0.034
						UP	0.090
						W00N	0.045

Table A.19 List of processed records at station USGS 5453

USGS: 5453 SMA-1 7073	LOS ANGELES, 5805 SEPULVEDA BLVD., ROOF (9th floor)					34.175∞N 118.465∞W	
File Name	Ref No.	Log No.	Earthquake	Distance [km]	Duration [s]	Comp	Peak Acc. [g]
v1X0000.DAT	IAA034	94.000.0	NORTHRIDGE EARTHQUAKE	7.9	60.9	N00E	0.735
						UP	0.488
						W00N	0.663
v1X0001.DAT	IAA034	94.000.1	NORTHRIDGE EARTHQUAKE (aft. -1)	14.0	30.6	N00E	0.231
						UP	0.104
						W00N	0.130
v1X0007.DAT	IAA034	94.000.7	NORTHRIDGE EARTHQUAKE (aft. -7)	14.0	18.1	N00E	0.026
						UP	0.015
						W00N	0.023
v1X0024.DAT	IAA034	94.002.4	NORTHRIDGE EARTHQUAKE (aft. -24)	14.0	21.1	N00E	0.040
						UP	0.021
						W00N	0.053
v1X0026.DAT	IAA034	94.002.6	NORTHRIDGE EARTHQUAKE (aft. -26)	14.0	23.2	N00E	0.057
						UP	0.047
						W00N	0.086
v1X0029.DAT	IAA034	94.002.9	NORTHRIDGE EARTHQUAKE (aft. -29)	14.0	23.2	N00E	0.041
						UP	0.017
						W00N	0.044
v1X0103.DAT	IAA103	94.010.3	NORTHRIDGE EARTHQUAKE (aft. -103)	14.0	24.5	N00E	0.045
						UP	0.017
						W00N	0.037
v1X0104.DAT	IAA104	94.010.4	NORTHRIDGE EARTHQUAKE (aft. -104)	14.0	19.1	N00E	0.017
						UP	0.015
						W00N	0.031
v1X0115.DAT	IAA115	94.011.5	NORTHRIDGE EARTHQUAKE (aft. -115)	14.0	26.9	N00E	0.055
						UP	0.019
						W00N	0.065

Table A.20 List of processed records at station USGS 5455

USGS: 5455 SMA-1 4270	LOS ANGELES, 16000 VENTURA BLVD., ROOF (13th floor)					34.156∞N 118.480∞W	
File Name	Ref No.	Log No.	Earthquake	Distance [km]	Duration [s]	Comp	Peak Acc. [g]
v1x0000.dat	IAA000	94.000.0	NORTHRIDGE EARTHQUAKE	8.2	57.6	E30S	0.358
						UP	0.337
						N30E	0.394
v1x0001.dat	IAA001	94.000.1	NORTHRIDGE EARTHQUAKE (aft. -1)	15.9	28.2	E30S	0.070
						UP	0.087
						N30E	0.104
v1x0007.dat	IAA007	94.000.7	NORTHRIDGE EARTHQUAKE (aft. -7)	15.9	23.1	E30S	0.018
						UP	0.033
						N30E	0.016
v1x0022.dat	IAA022	94.002.2	NORTHRIDGE EARTHQUAKE (aft. -22)	15.9	20.9	E30S	0.033
						UP	0.072
						N30E	0.029
v1x0025.dat	IAA025	94.002.5	NORTHRIDGE EARTHQUAKE (aft. -25)	15.9	34.7	E30S	0.043
						UP	0.056
						N30E	0.057
v1x0046.dat	IAA046	94.004.6	NORTHRIDGE EARTHQUAKE (aft. -46)	15.9	19.2	E30S	0.029
						UP	0.045
						N30E	0.041

Table A.21 List of processed records at station USGS 5457

USGS: 5457 SMA 5491	LOS ANGELES, 8436 WEST 3rd ST., Roof (10th floor)					34.072∞N 118.375∞W	
File Name	Ref No.	Log No.	Earthquake	Distance [km]	Duration [s]	Comp	Peak Acc. [g]
v1x0000.dat	IAA030	94.000.0	NORTHRIDGE EARTHQUAKE	21.7	53.2	N00E	0.658
						UP	0.253
						S90W	0.547
v1x0001.dat	IAA030	94.000.1	NORTHRIDGE EARTHQUAKE (aft. -1)	27.4	28.1	N00E	0.102
						UP	0.093
						S90W	0.262
v1x0004.dat	IAA030	94.000.4	NORTHRIDGE EARTHQUAKE (aft. -4)	27.4	20.3	N00E	0.014
						UP	0.022
						S90W	0.017
v1x0008.dat	IAA030	94.000.8	NORTHRIDGE EARTHQUAKE (aft. -8)	27.4	22.5	N00E	0.031
						UP	0.023
						S90W	0.057
v1x0009.dat	IAA030	94.000.9	NORTHRIDGE EARTHQUAKE (aft. -9)	27.4	27.5	N00E	0.053
						UP	0.032
						S90W	0.053
v1x0010.dat	IAA030	94.001.0	NORTHRIDGE EARTHQUAKE (aft. -10)	27.4	18.7	N00E	0.018
						UP	0.015
						S90W	0.014
v1x0013.dat	IAA030	94.001.3	NORTHRIDGE EARTHQUAKE (aft. -13)	27.4	21.6	N00E	0.027
						UP	0.014
						S90W	0.032
v1x0017.dat	IAA030	94.001.7	NORTHRIDGE EARTHQUAKE (aft. -17)	27.4	20.5	N00E	0.018
						UP	0.014
						S90W	0.021
v1x0019.dat	IAA030	94.001.9	NORTHRIDGE EARTHQUAKE (aft. -19)	27.4	30.9	N00E	0.100
						UP	0.124
						S90W	0.185

APPENDIX B:

DETAILED RESULTS FOR TIME AND AMPITUDE VARIATIONS OF THE INSTANTANEOUS BUILDING-FOUNDATION-SOIL SYSTEM FREQUENCY

This appendix documents the results of variations of instantaneous building frequency for the 21 buildings. For each building, 4 plots are shown (parts a,b,c,d of the respective figure). The first two correspond to first horizontal component of motion, and the second two – to the second component of motion. For each component, the first plot is based on results using zero-crossing analysis, and the second plot is based on results using Gabor transform analysis.

Figure No.	Station No.	N	Street address	Comp.	No. rec.	Comp.	No. rec.
B.01	0466	13	LOS ANGELES, 15250 VENTURA BLVD.	N00E	3	W00N	3
B.02	0482	12	ALHAMBRA, 900 S. FREMONT	NS	5	EW	5
B.03	0663	12	LOS ANGELES, 10751 WILSHIRE Blvd.	S72W	3	S18E	2
B.04	0742	8	LOS ANGELES, 1526 N.EDGEMONT ST.,	E00S	12	N00E	10
B.05	0793	11	LOS ANGELES, 4929 WILSHITE BLVD.	S00W	5	E00S	6
B.06	0804	10	7215 BRIGHT AVE., BASEMENT, WHITTIER, CA	NS	2	EW	2
B.07	0872	8	LOS ANGELES, 1111 SUNSET Blvd.	N12W	3	S78W	3
B.08	0892	55	LOS ANGELES, 333 S. HOPE ST.	N83E	2	W83N	2
B.09	5082	6	LOS ANGELES, WADSWORTH V.A. HOSPITAL	N35W	2	S55W	2
B.10	5106	11	LONG BEACH VA HOSPITAL	NS	3	EW	3
B.11	5108	6	SANTA SUSANA, ETEC Bldg 462	E00S	9	N00E	7
B.12	5233	32	1100 WILSHIRE, LOS ANGELES, CA	N62W	2	S28W	2
B.13	5239	7	12440 IMPERIAL HWY, NORWALK, CA	N90E	5	S00W	5
B.14	5259	8	LOS ANGELES, 2005 N. HIGHLAND AVE.	N00E	8	W00N	6
B.15	5260	12	LOS ANGELES, 444 S. SAN VINCENTE	W65N	7	S65W	9
B.16	5263	19	LOS ANGELES, 10660 WILSHIRE BLVD.	E70S	5	N70E	3
B.17	5450	9	BURBANK, 3601 WEST OLIVE AVE.	N00E	5	W00N	5
B.18	5451	12	LOS ANGELES, 6301 OWENSMOUTH AVE.	N00E	3	W00N	3
B.19	5453	9	LOS ANGELES, 5805 SEPULVEDA BLVD.	N00E	4	W00N	8
B.10	5455	13	LOS ANGELES, 16000 VENTURA BLVD.	E30S	5	N30E	5
B.21	5457	10	LOS ANGELES, 8436 WEST 3rd ST.	N00E	8	S00W	7

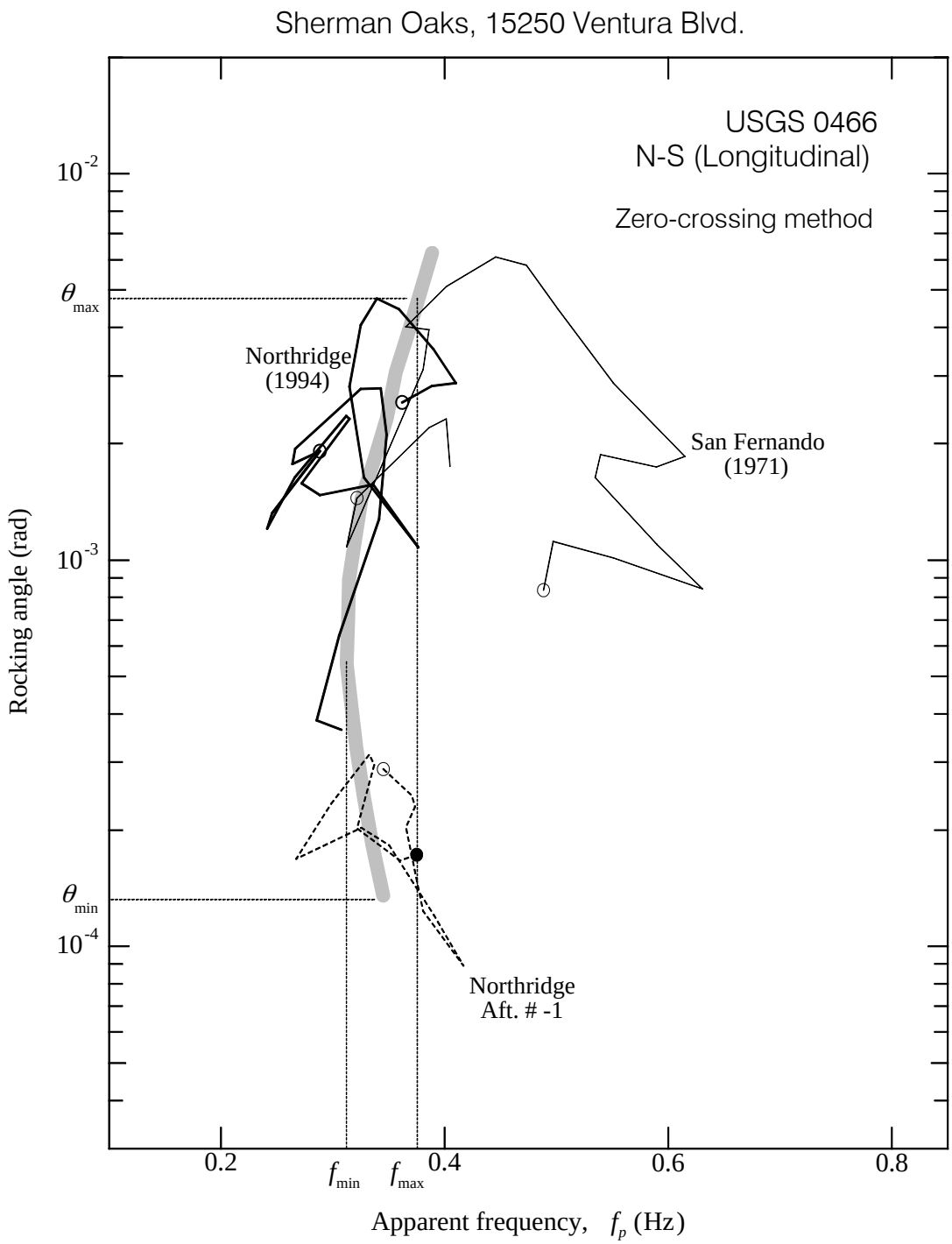
Sherman Oaks, 15250 Ventura Blvd.
USGS 0466
N-S (Longitudinal)
Zero-crossing method
10^{-2}
θ_{max}
Northridge
(1994)
San Fernando
(1971)
10^{-3}
Rocking angle (rad)
θ_{min}
10^{-4}
Northridge
Aft. # -1
0.2
f_{min}
f_{max}
0.4
0.6
0.8
Apparent frequency, f_p (Hz)

Figure B.01a

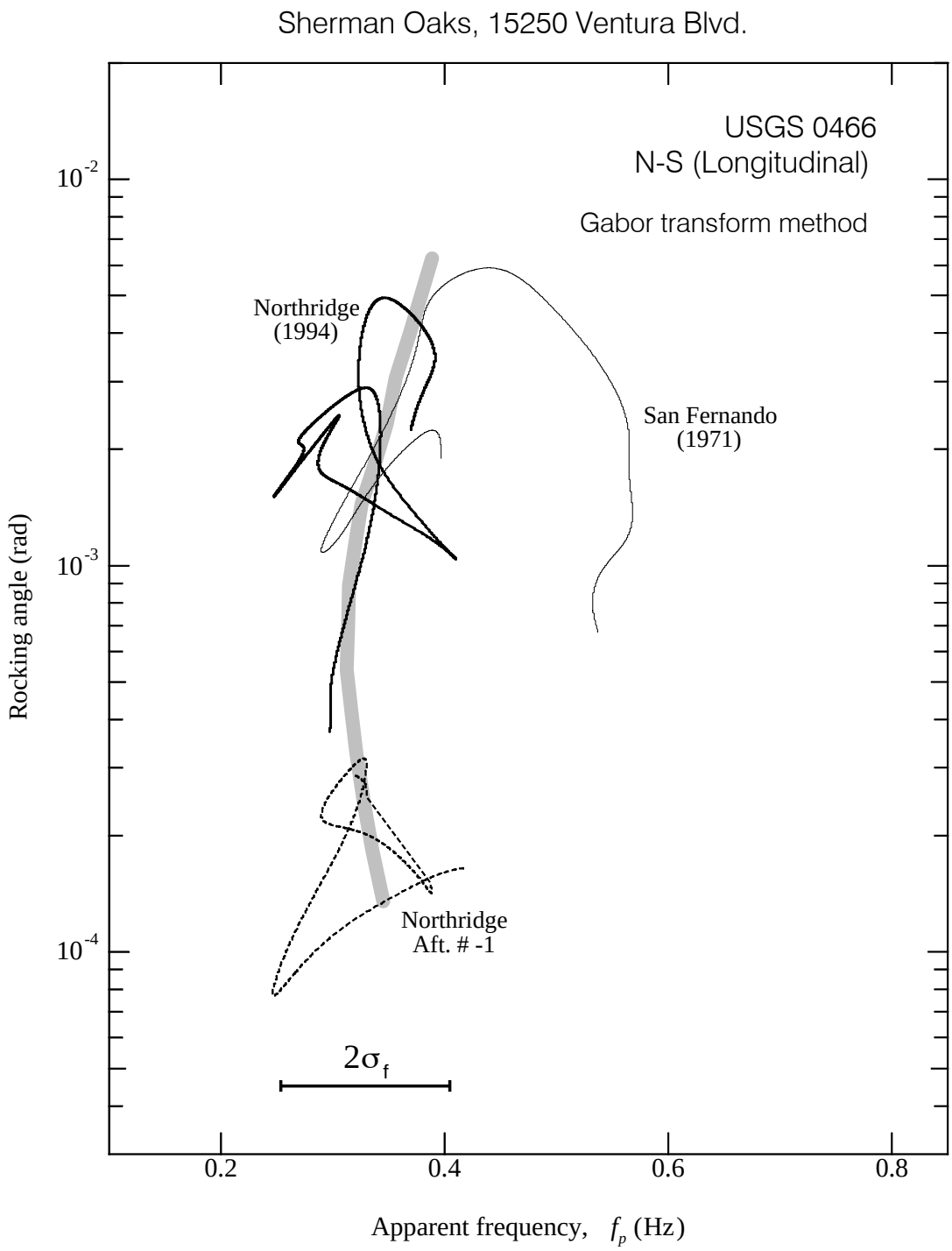
Sherman Oaks, 15250 Ventura Blvd.
USGS 0466
N-S (Longitudinal)
Gabor transform method
Northridge
(1994)
San Fernando
(1971)
Northridge
Aft. # -1
2σf
10-2
10-3
10-4
Rocking angle (rad)
0.2
0.4
0.6
0.8
Apparent frequency, fp (Hz)

Figure B.01b.

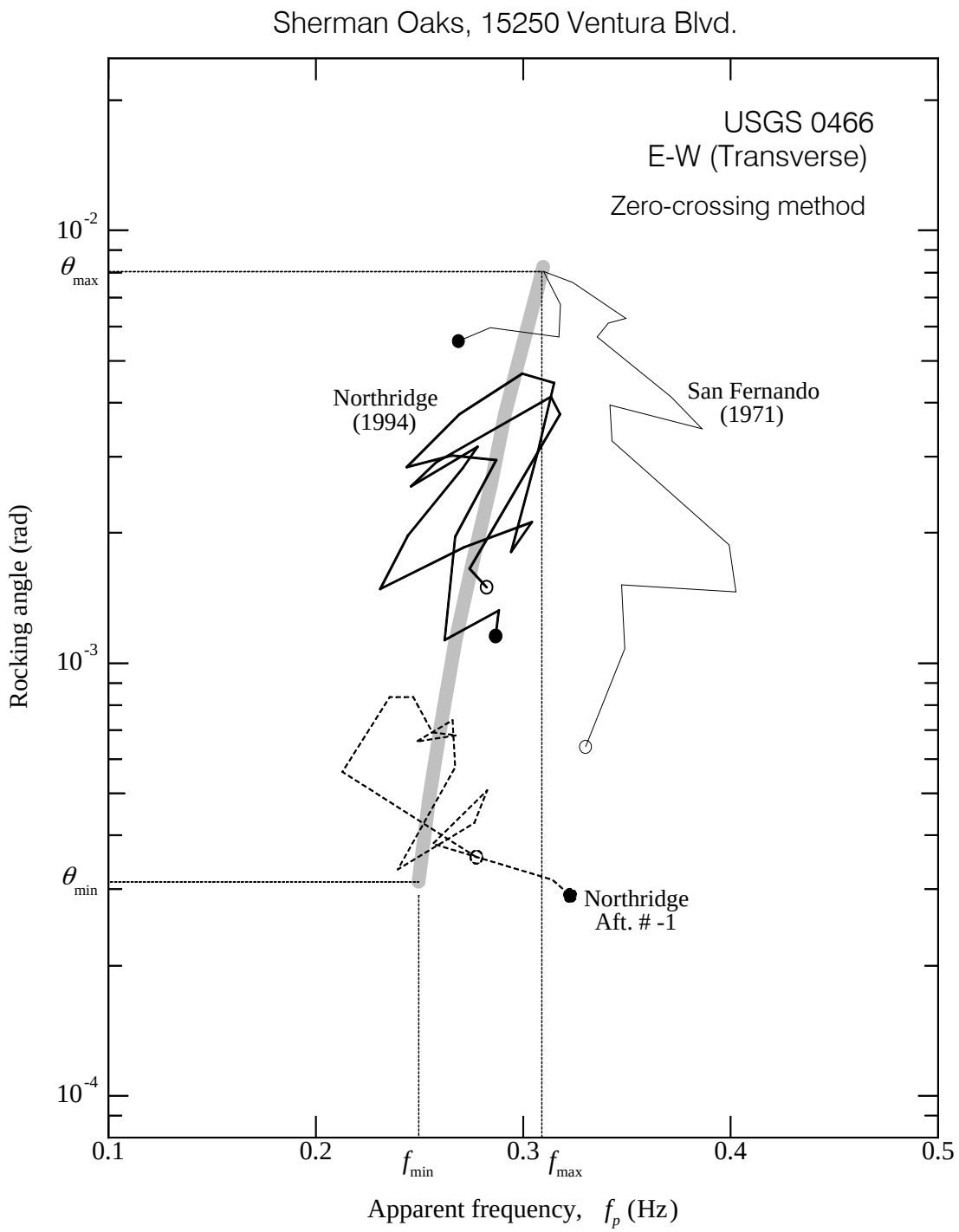
Sherman Oaks, 15250 Ventura Blvd.
USGS 0466
E-W (Transverse)
Zero-crossing method
10^{-2}
θ_{max}
10^{-3}
θ_{min}
10^{-4}
Rocking angle (rad)
Northridge
(1994)
San Fernando
(1971)
Northridge
Aft. # -1
0.1
0.2
0.3
0.4
0.5
f_{min}
f_{max}
Apparent frequency, f_p (Hz)

Figure B.01c

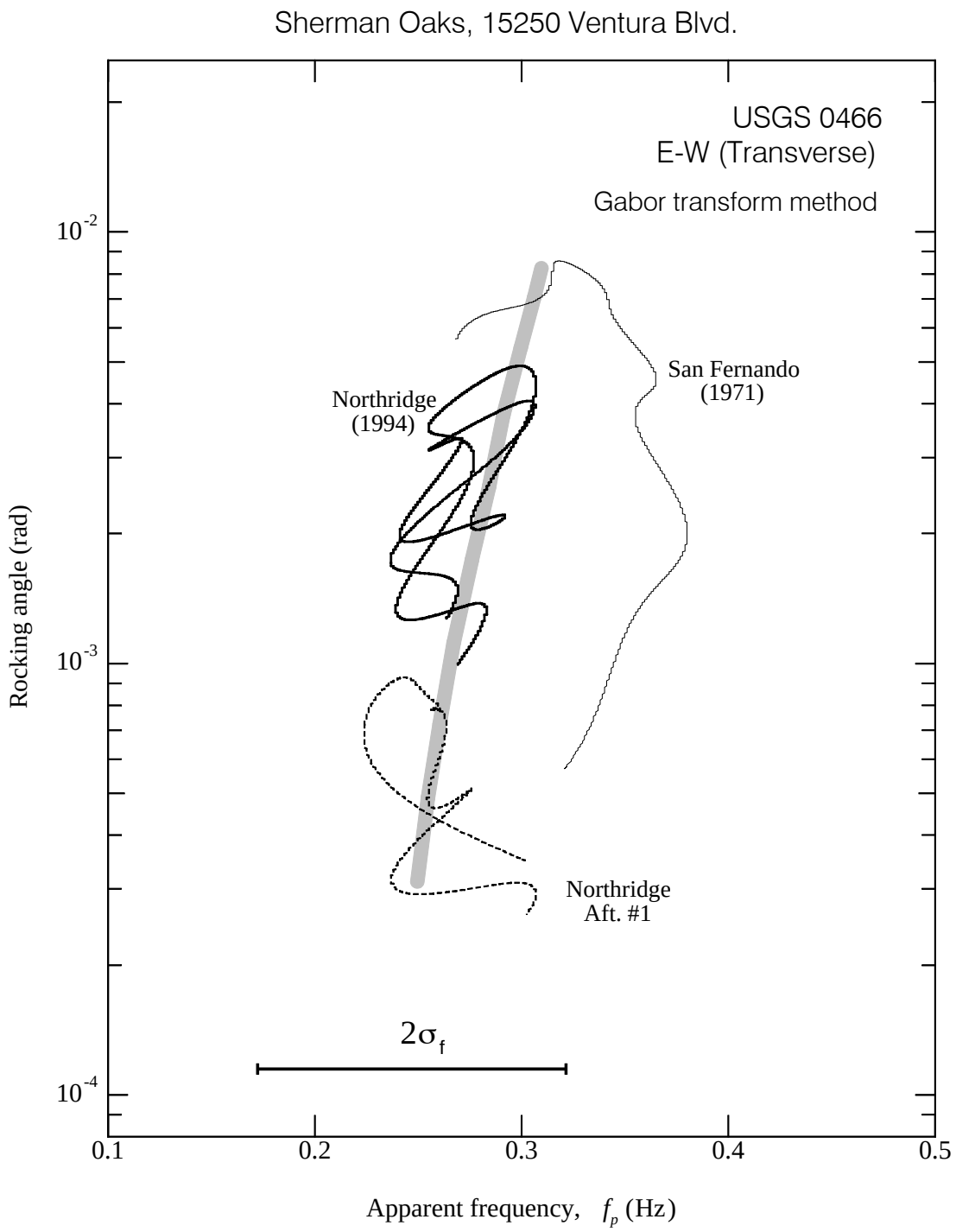
Sherman Oaks, 15250 Ventura Blvd.
USGS 0466
E-W (Transverse)
Gabor transform method
San Fernando
(1971)
Northridge
(1994)
Northridge
Aft. #1
2σf
10-2
10-3
10-4
Rocking angle (rad)
0.1
0.2
0.3
0.4
0.5
Apparent frequency, fp (Hz)

Figure B.01d.

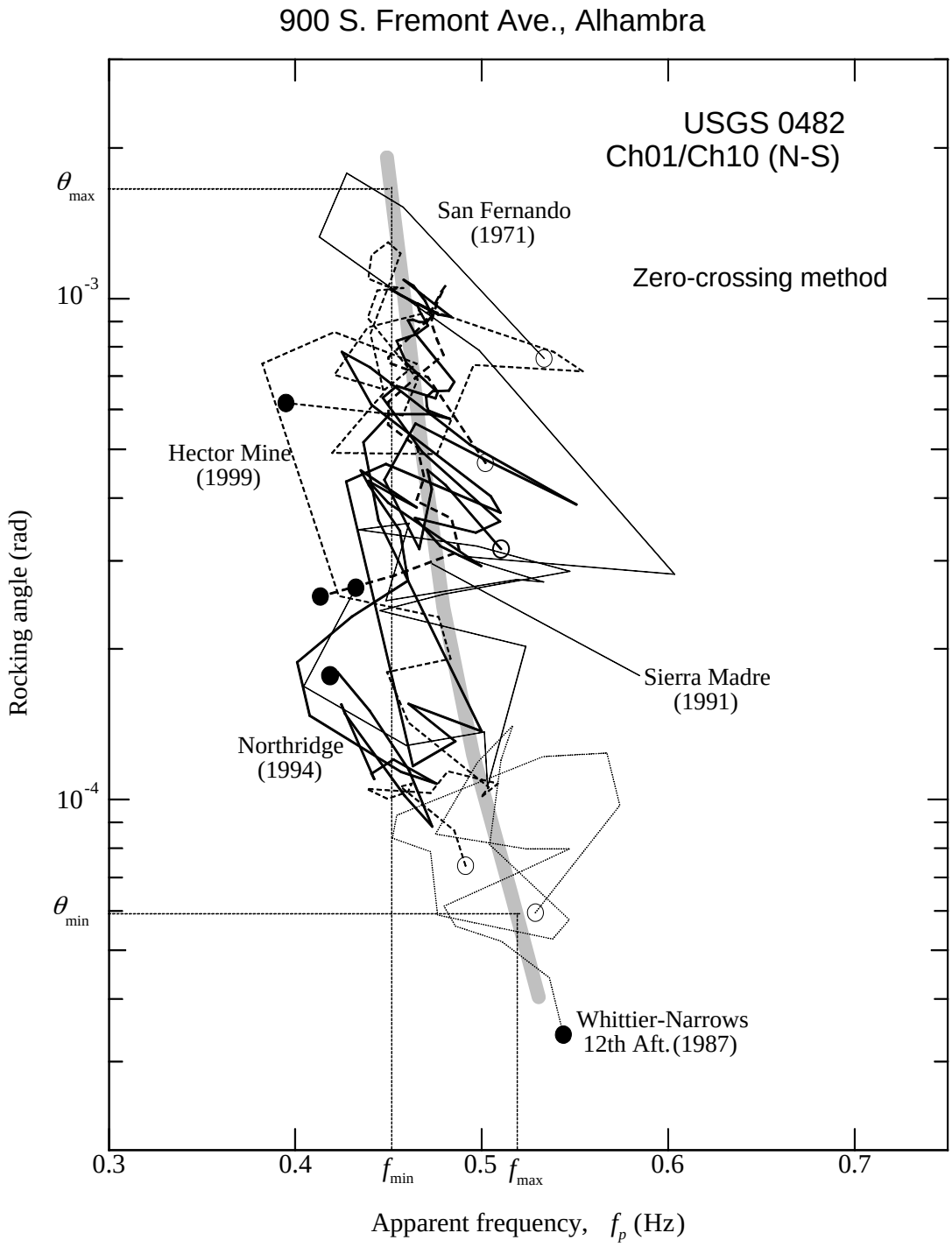
900 S. Fremont Ave., Alhambra
USGS 0482
Ch01/Ch10 (N-S)
Zero-crossing method
San Fernando
(1971)
Hector Mine
(1999)
Sierra Madre
(1991)
Northridge
(1994)
Whittier-Narrows
12th Aft. (1987)
θmax
10-3
10-4
θmin
Rocking angle (rad)
0.3
0.4
fmin
0.5
fmax
0.6
0.7
Apparent frequency, fp (Hz)

Figure B.02a

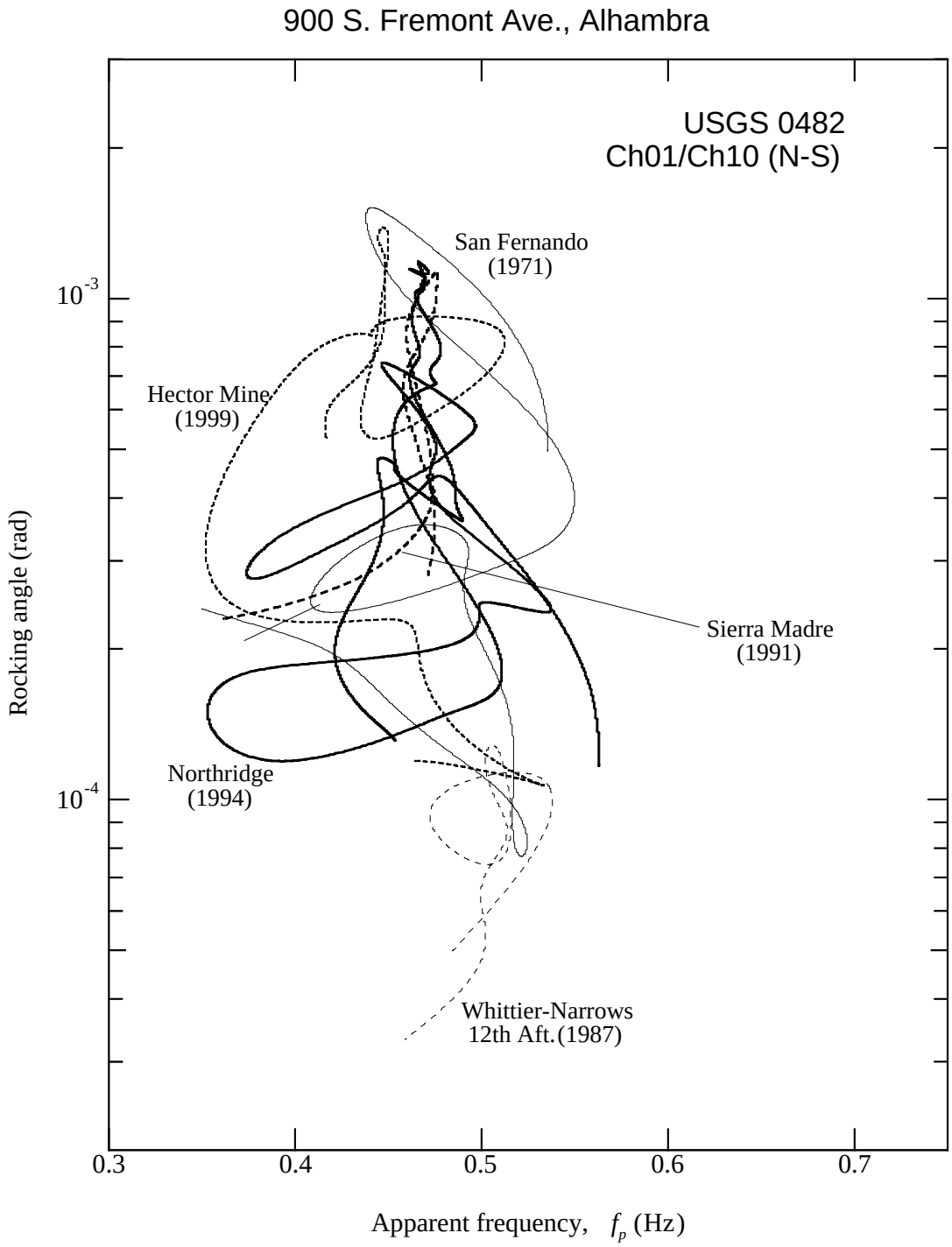
900 S. Fremont Ave., Alhambra
USGS 0482
Ch01/Ch10 (N-S)
San Fernando
(1971)
Hector Mine
(1999)
Sierra Madre
(1991)
Northridge
(1994)
Whittier-Narrows
12th Aft.(1987)
Rocking angle (rad)
10^-3
10^-4
0.3
0.4
0.5
0.6
0.7
Apparent frequency, f_p (Hz)

Figure B.02b

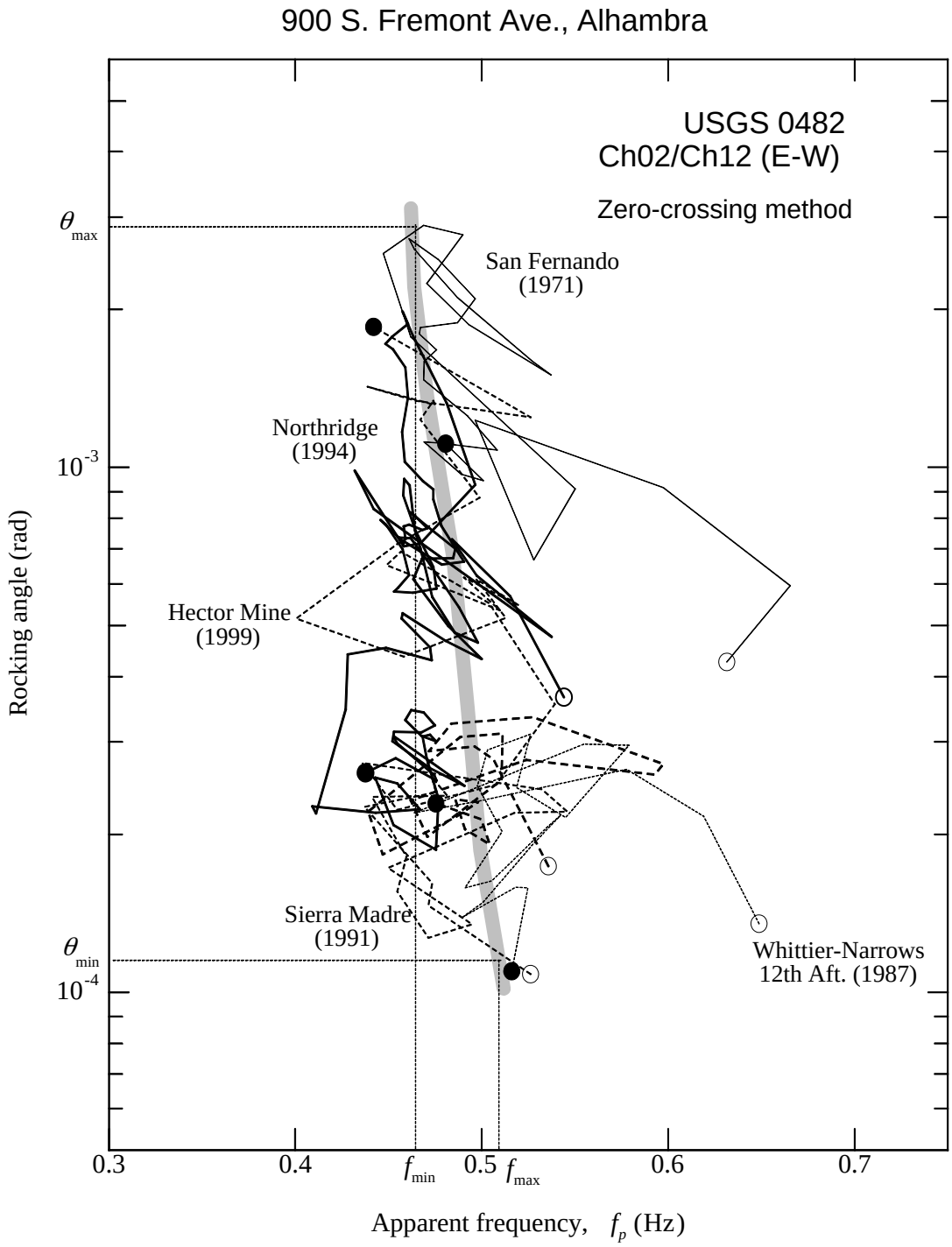
900 S. Fremont Ave., Alhambra
USGS 0482
Ch02/Ch12 (E-W)
Zero-crossing method
θ_{max}
10^{-3}
θ_{min}
10^{-4}
Rocking angle (rad)
San Fernando
(1971)
Northridge
(1994)
Hector Mine
(1999)
Sierra Madre
(1991)
Whittier-Narrows
12th Aft. (1987)
0.3
0.4
f_{min}
0.5
f_{max}
0.6
0.7
Apparent frequency, f_p (Hz)

Figure B.02c

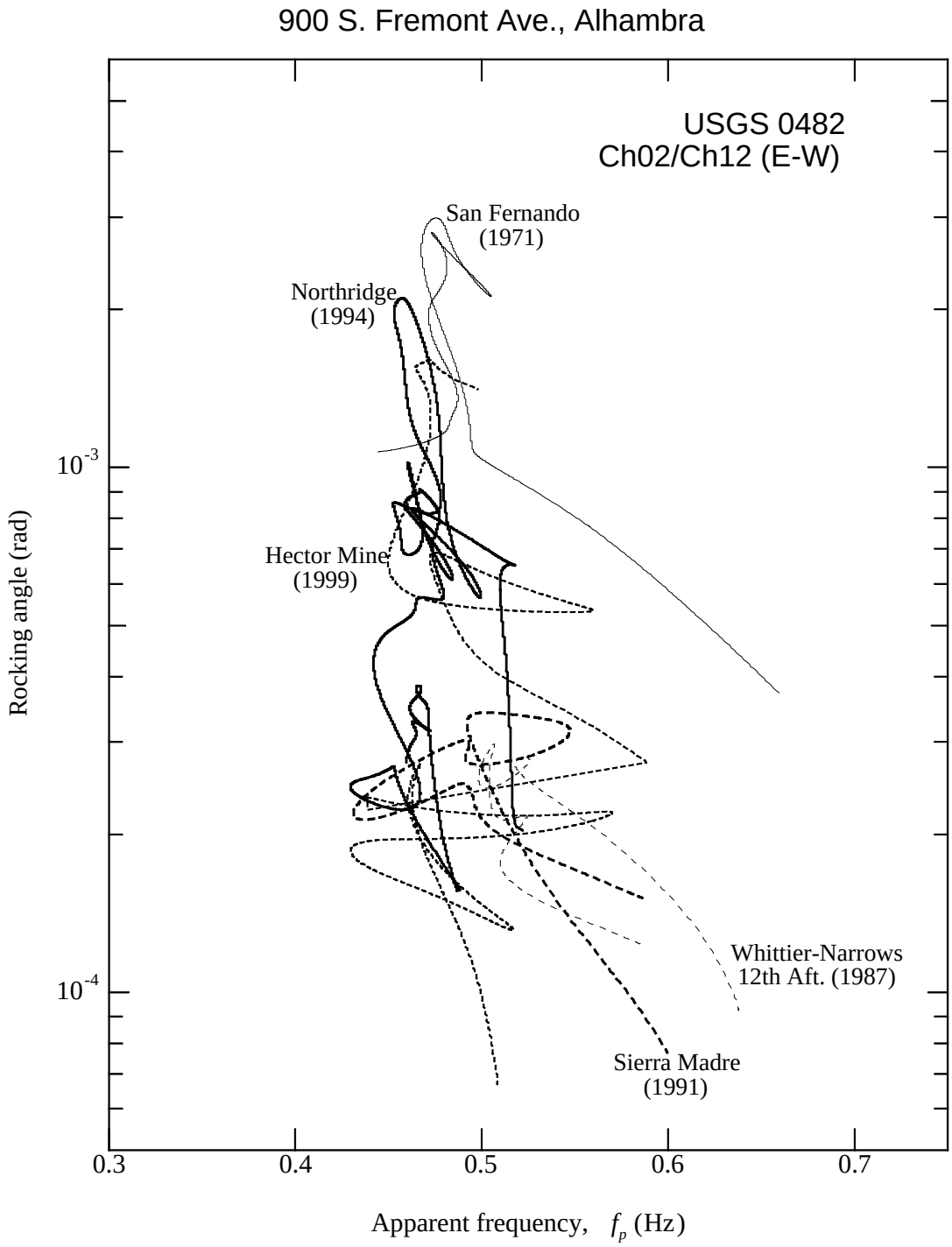
900 S. Fremont Ave., Alhambra
USGS 0482
Ch02/Ch12 (E-W)
San Fernando
(1971)
Northridge
(1994)
Hector Mine
(1999)
Whittier-Narrows
12th Aft. (1987)
Sierra Madre
(1991)
Rocking angle (rad)
10-3
10-4
0.3
0.4
0.5
0.6
0.7
Apparent frequency, fp (Hz)

Figure B.02d

10751 Wilshire Blvd.

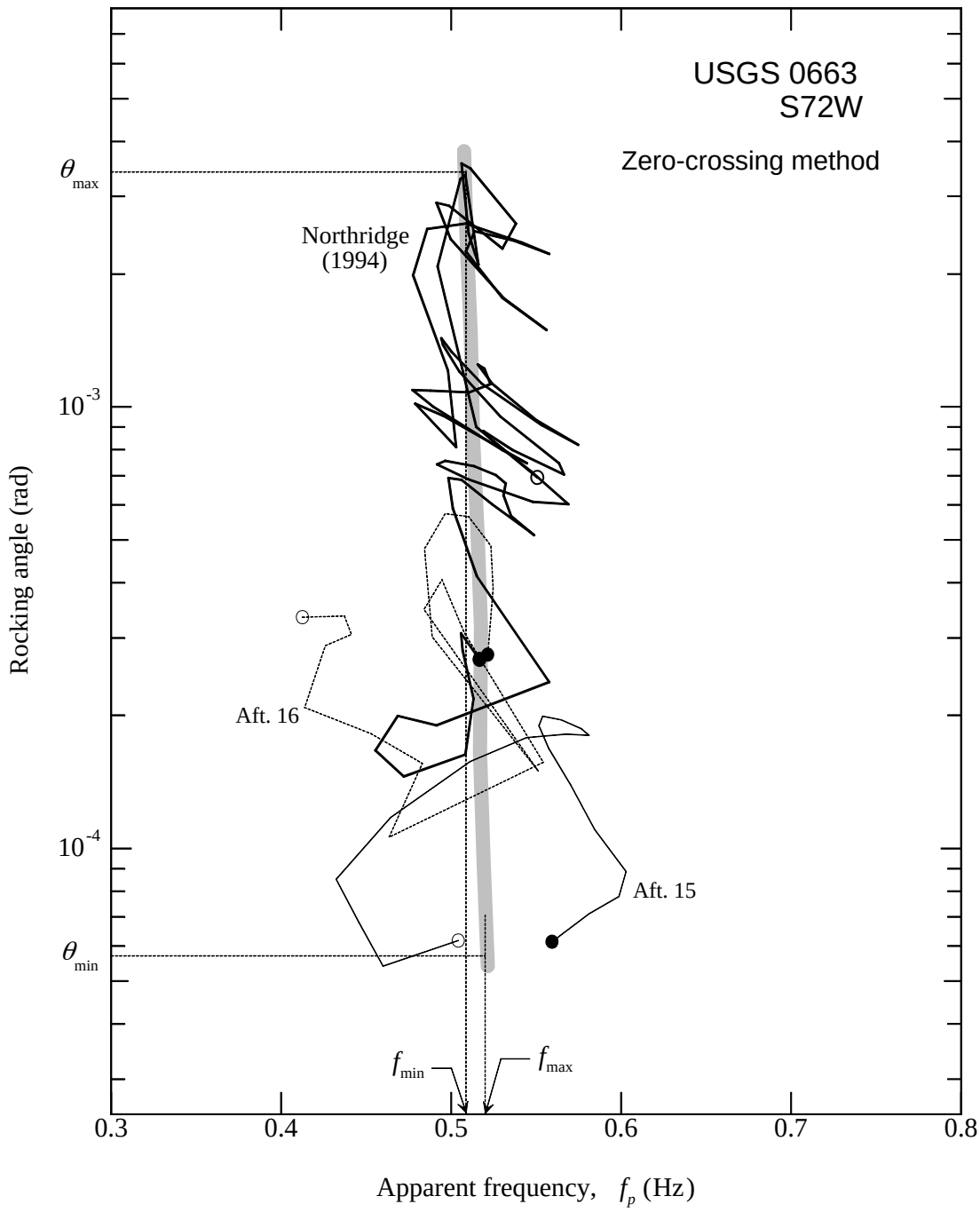

Figure B.03a

10751 Wilshire Blvd.

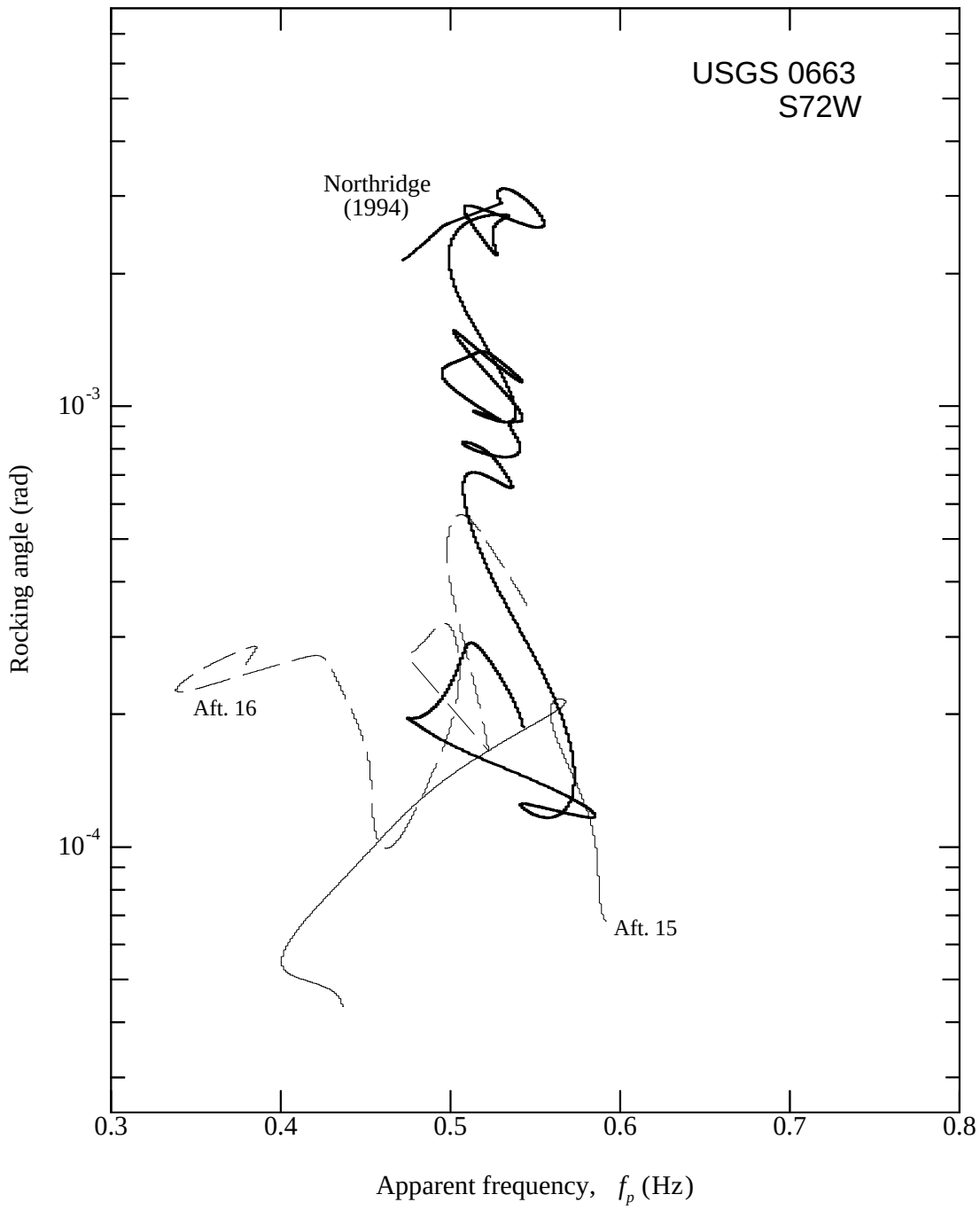

Figure B.03b

10751 Wilshire Blvd.

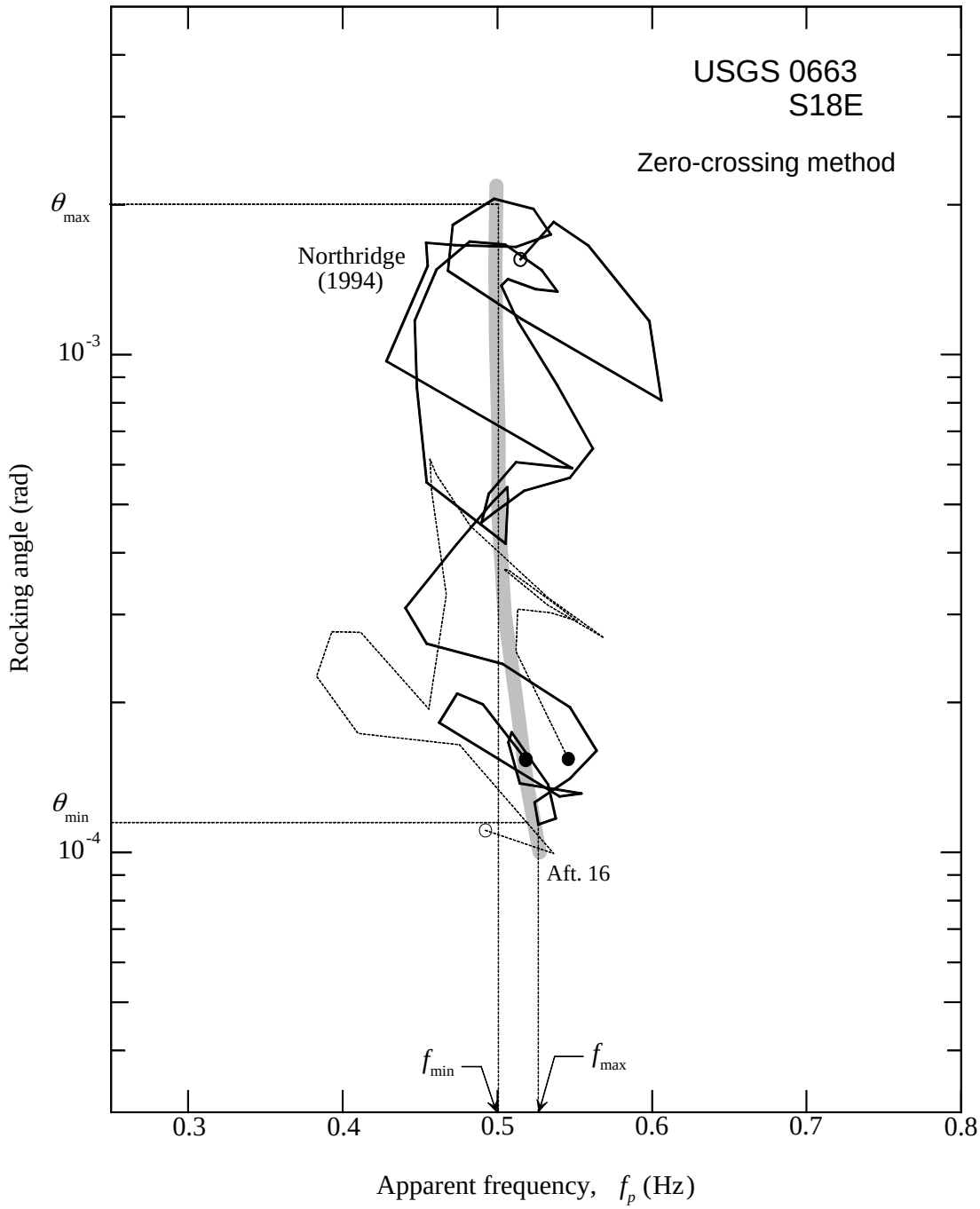

Figure B.03c

10751 Wilshire Blvd.

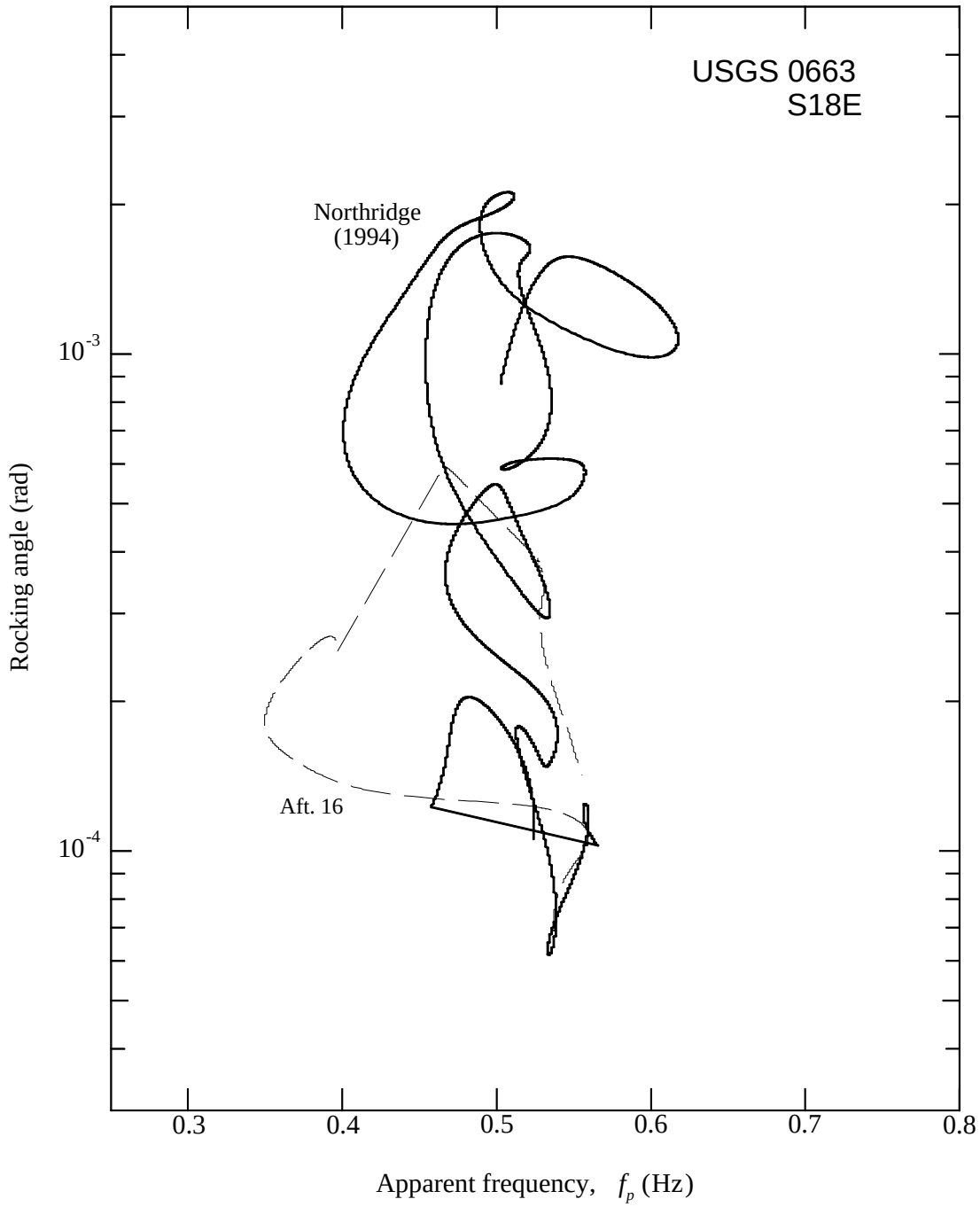

Figure B.03d

1526 N. Edgemont St.

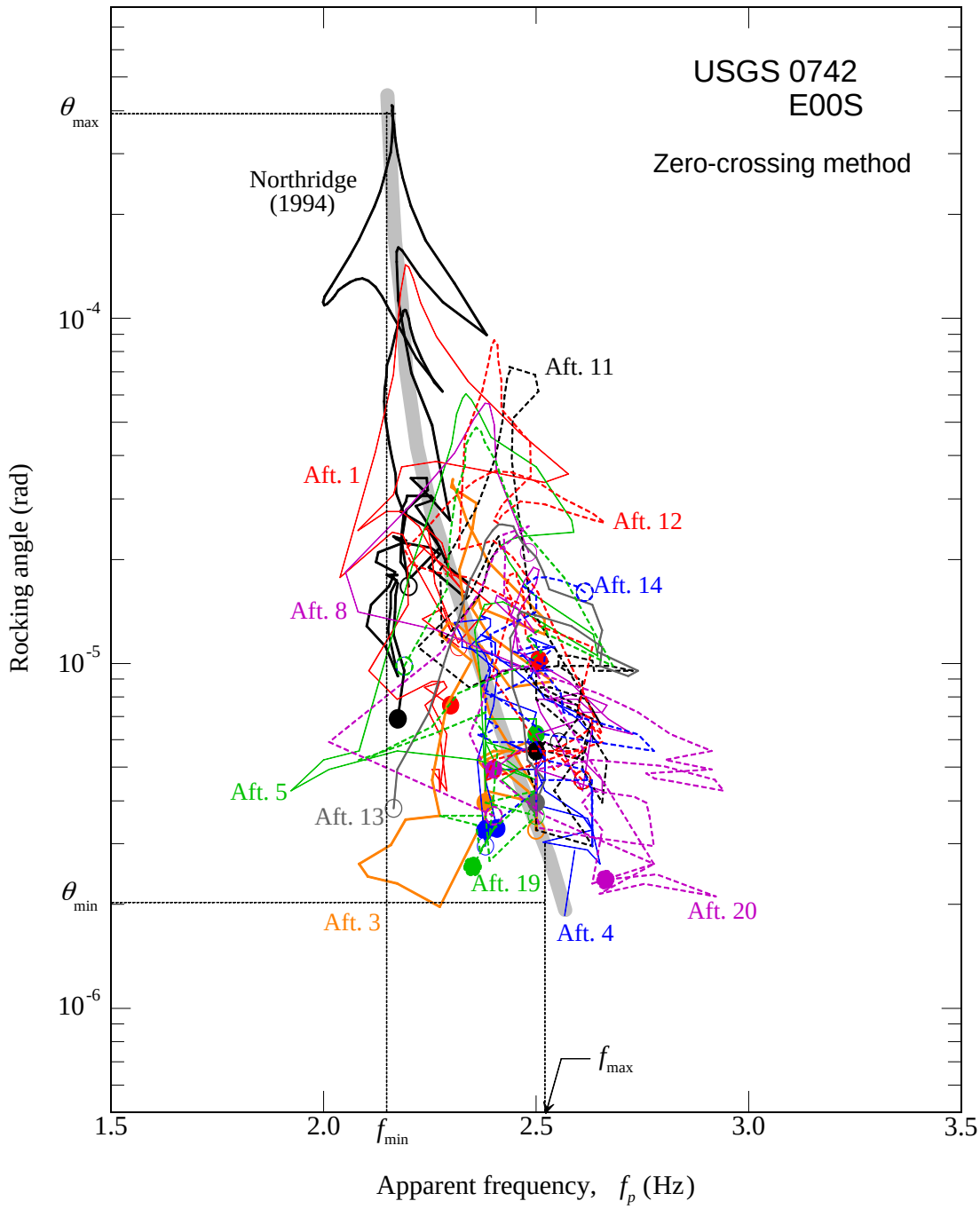

Figure B.04a

1526 N. Edgemont St.

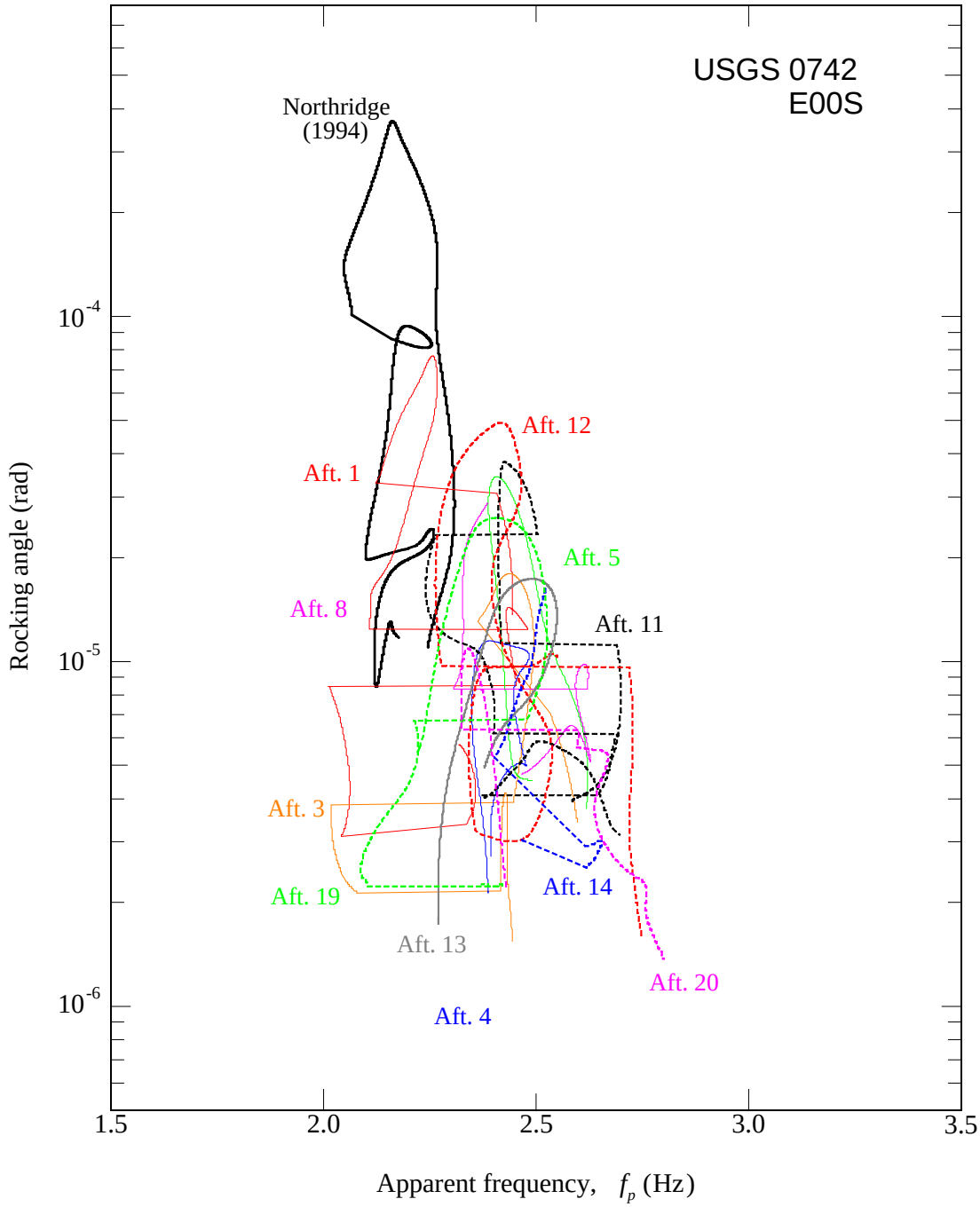

Figure B.04b

1526 N. Edgemont St.

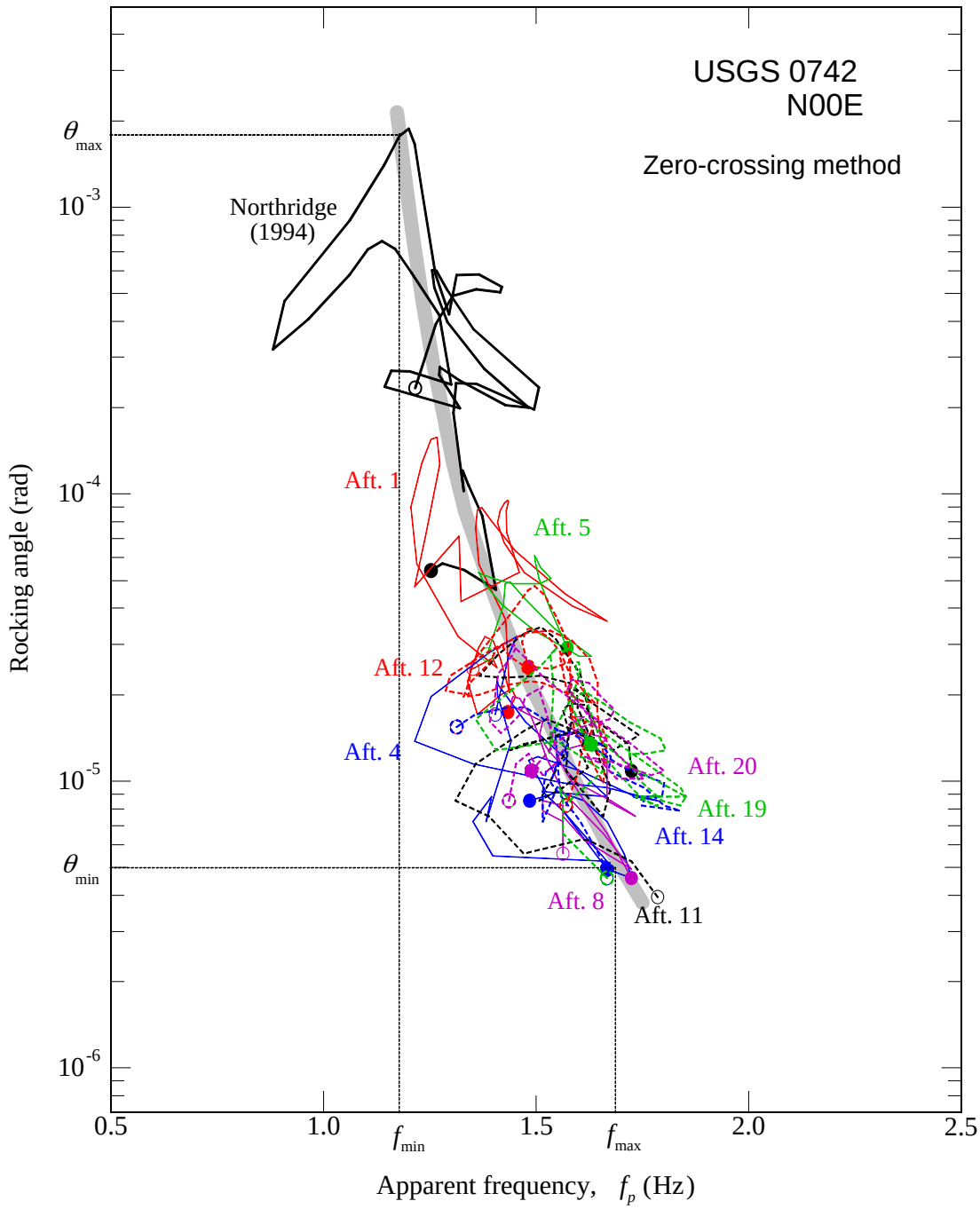

Figure B.04c

1526 N. Edgemont St.

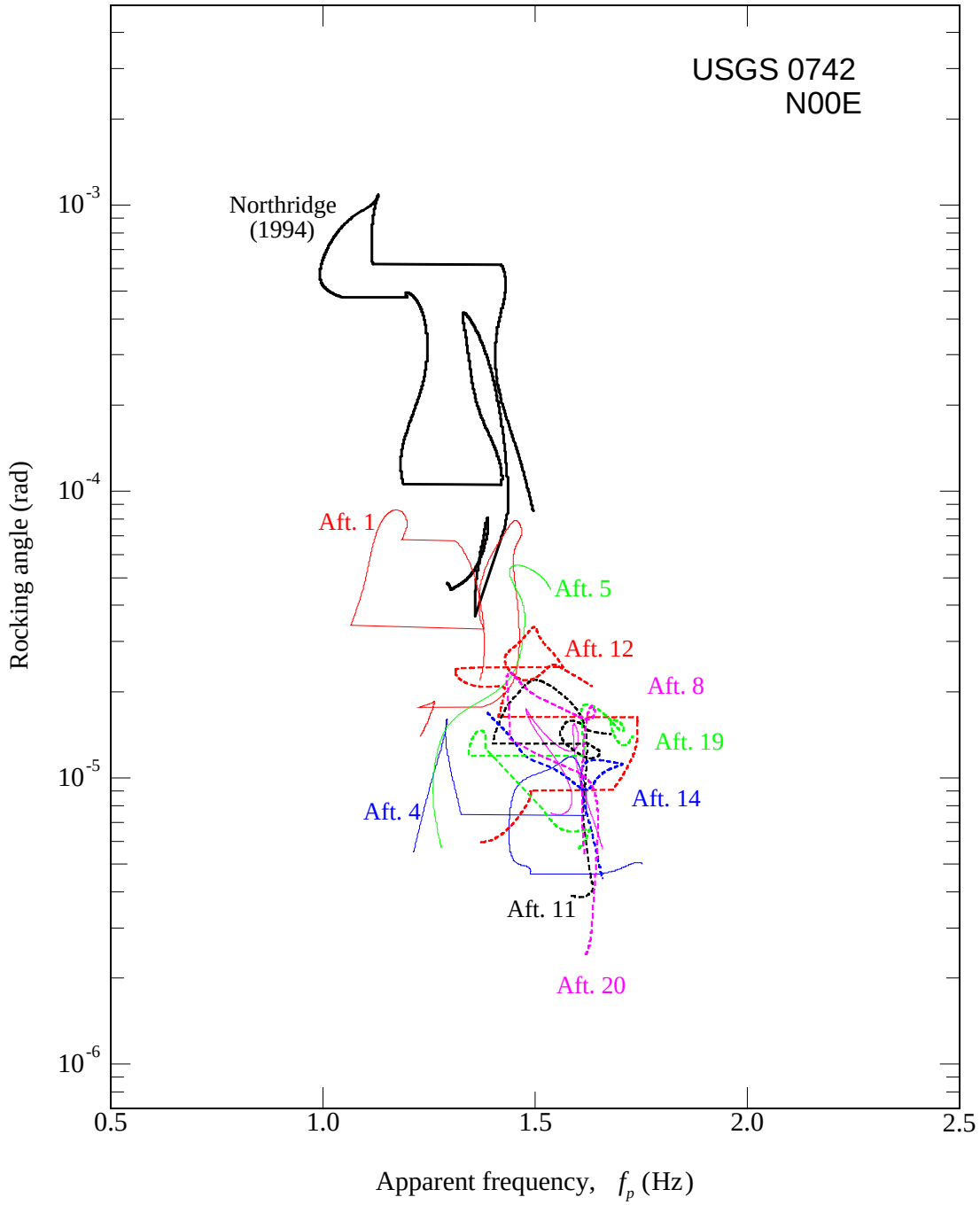

Figure B.04d

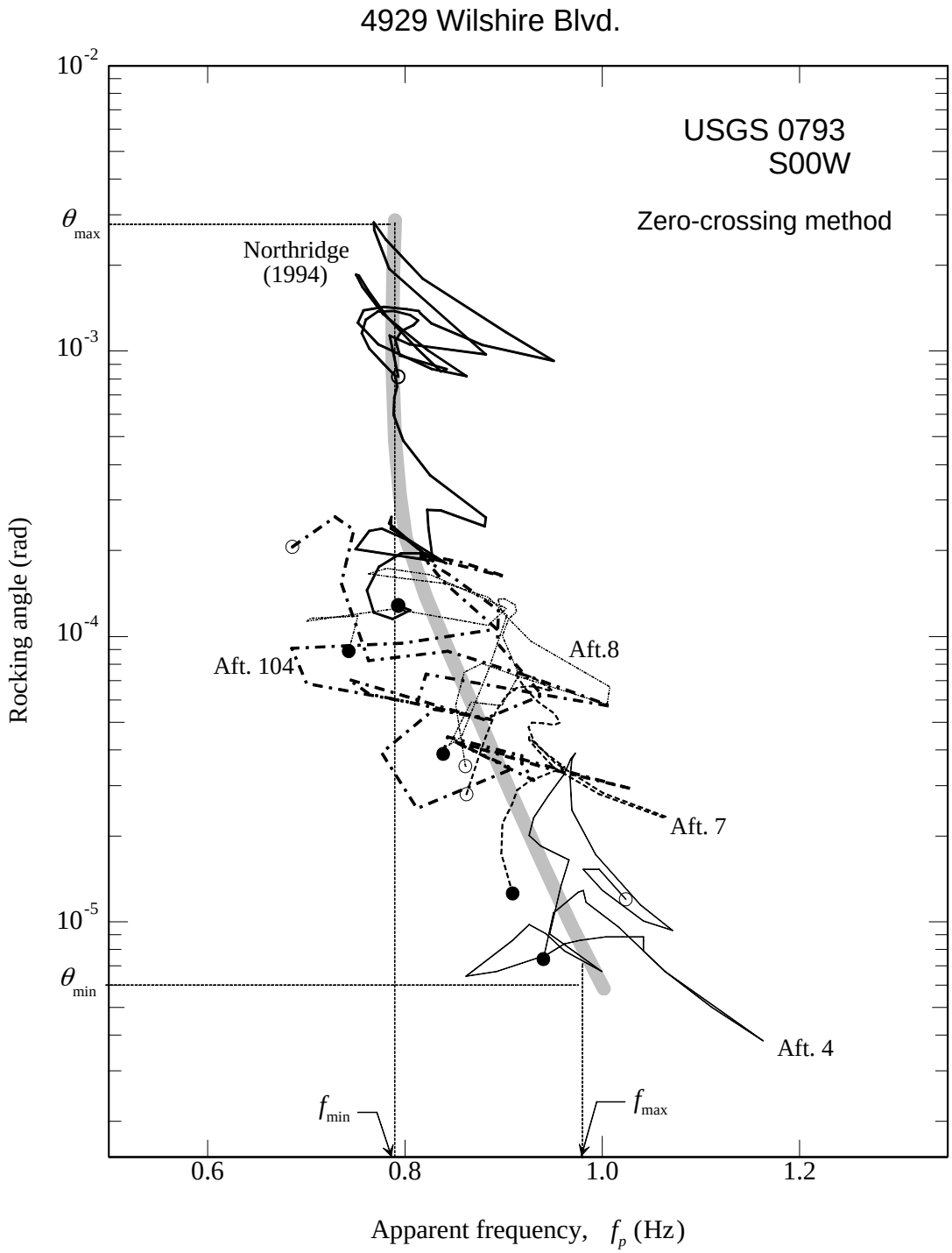
4929 Wilshire Blvd.
USGS 0793
S00W
Zero-crossing method
Northridge
(1994)
Aft. 104
Aft.8
Aft. 7
Aft. 4
θ_{max}
θ_{min}
f_{min}
f_{max}
10^{-2}
10^{-3}
10^{-4}
10^{-5}
Rocking angle (rad)
0.6
0.8
1.0
1.2
Apparent frequency, f_p (Hz)

Figure B.05a

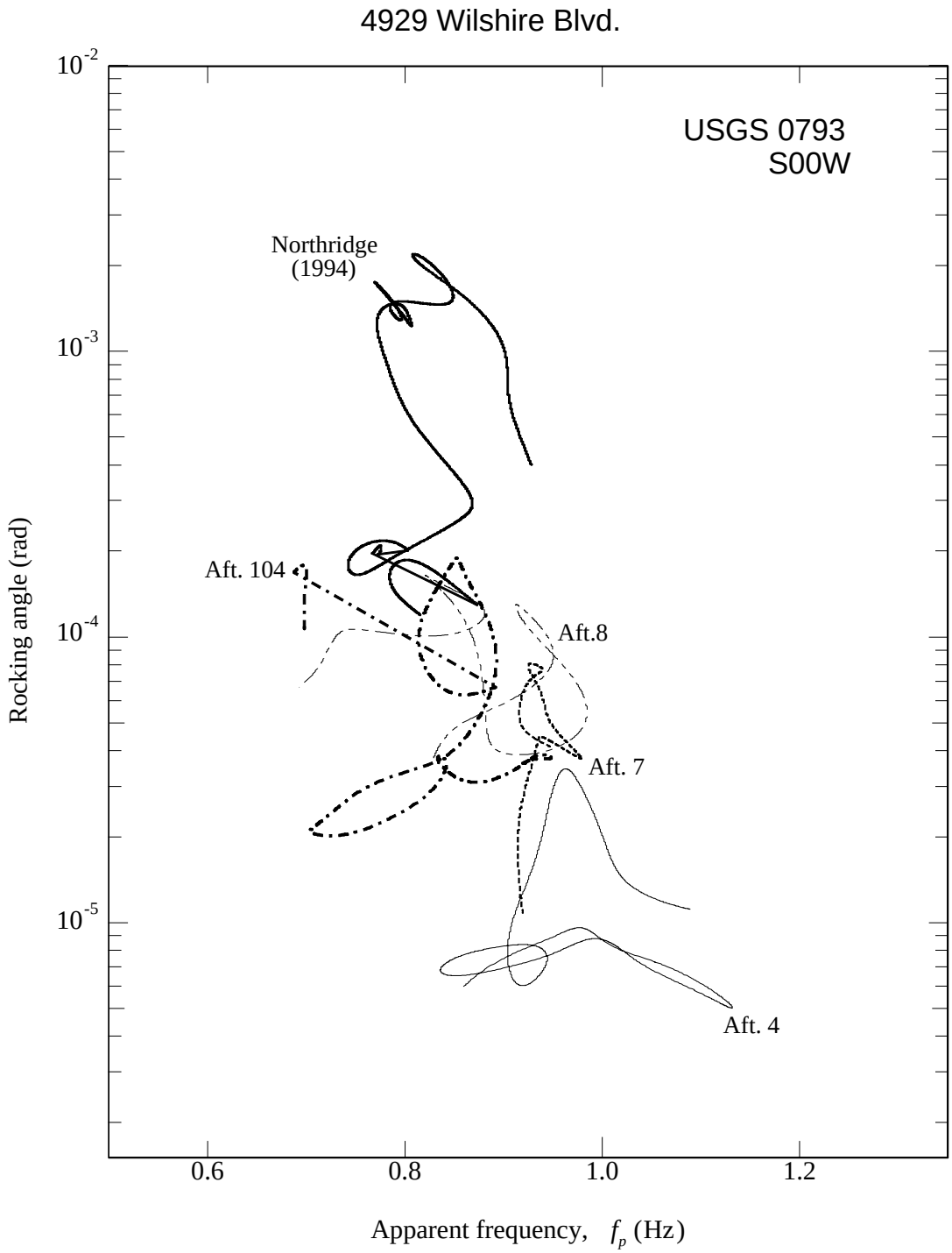
4929 Wilshire Blvd.
USGS 0793
S00W
Northridge
(1994)
Aft. 104
Aft.8
Aft. 7
Aft. 4
Rocking angle (rad)
Apparent frequency, f_p (Hz)
10^{-2}
10^{-3}
10^{-4}
10^{-5}
0.6
0.8
1.0
1.2

Figure B.05b

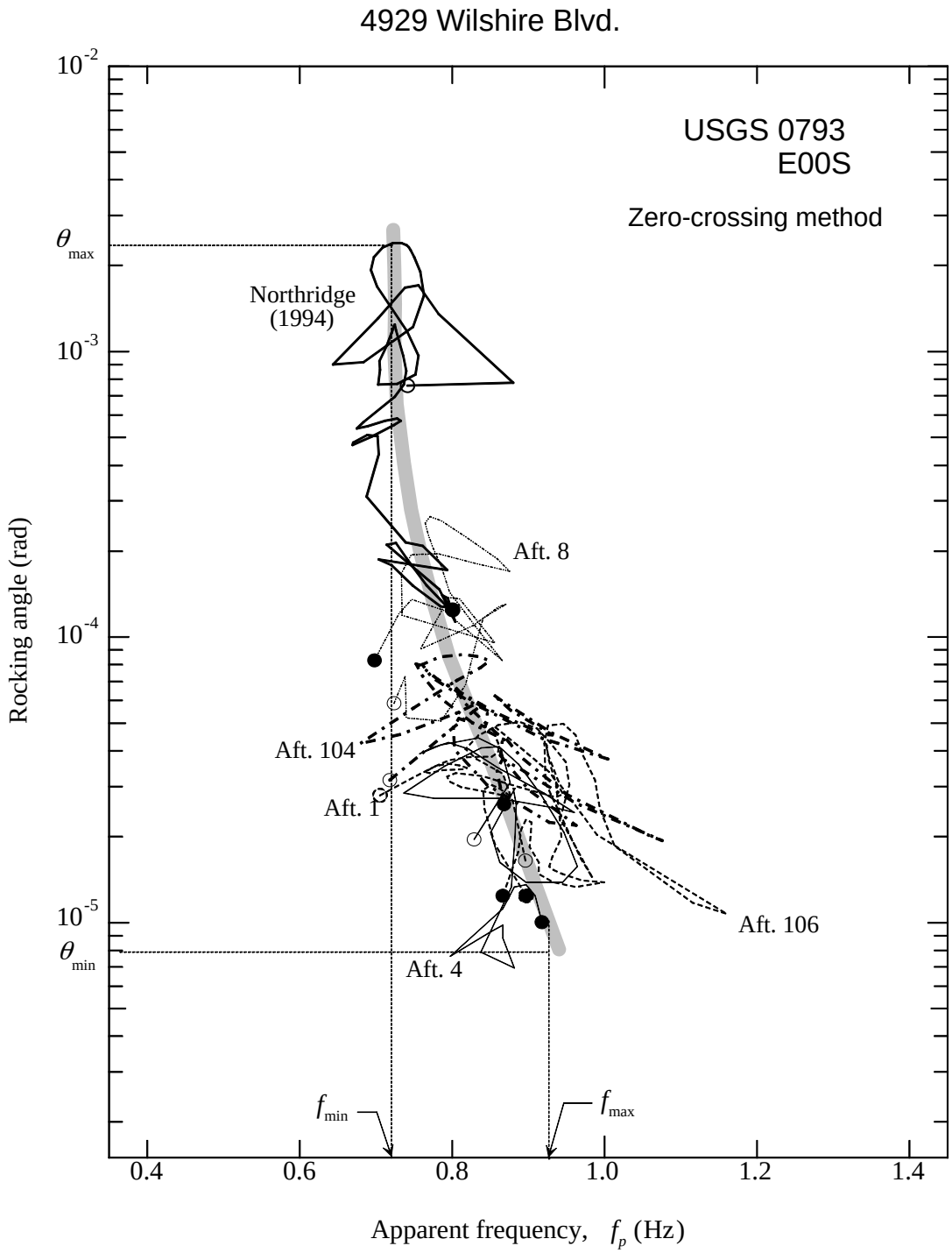
4929 Wilshire Blvd.
USGS 0793
E00S
Zero-crossing method
Northridge
(1994)
Aft. 8
Aft. 104
Aft. 1
Aft. 4
Aft. 106
θ_{max}
θ_{min}
f_{min}
f_{max}
10^{-2}
10^{-3}
10^{-4}
10^{-5}
Rocking angle (rad)
0.4
0.6
0.8
1.0
1.2
1.4
Apparent frequency, f_p (Hz)

Figure B.05c

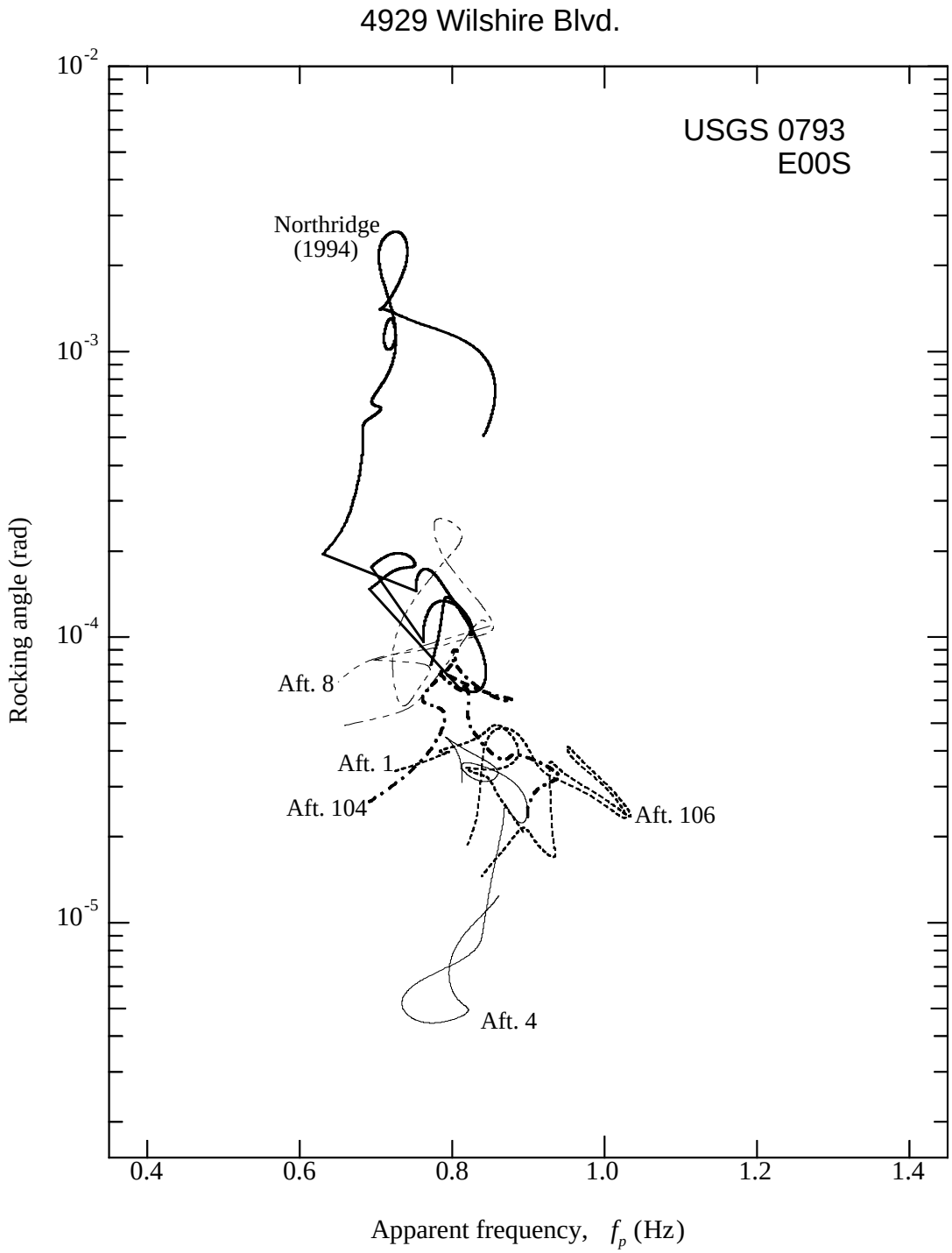
4929 Wilshire Blvd.
USGS 0793
E00S
Northridge
(1994)
Aft. 8
Aft. 1
Aft. 104
Aft. 106
Aft. 4
Rocking angle (rad)
Apparent frequency, f_p (Hz)
10^{-2}
10^{-3}
10^{-4}
10^{-5}
0.4
0.6
0.8
1.0
1.2
1.4

Figure B.05d

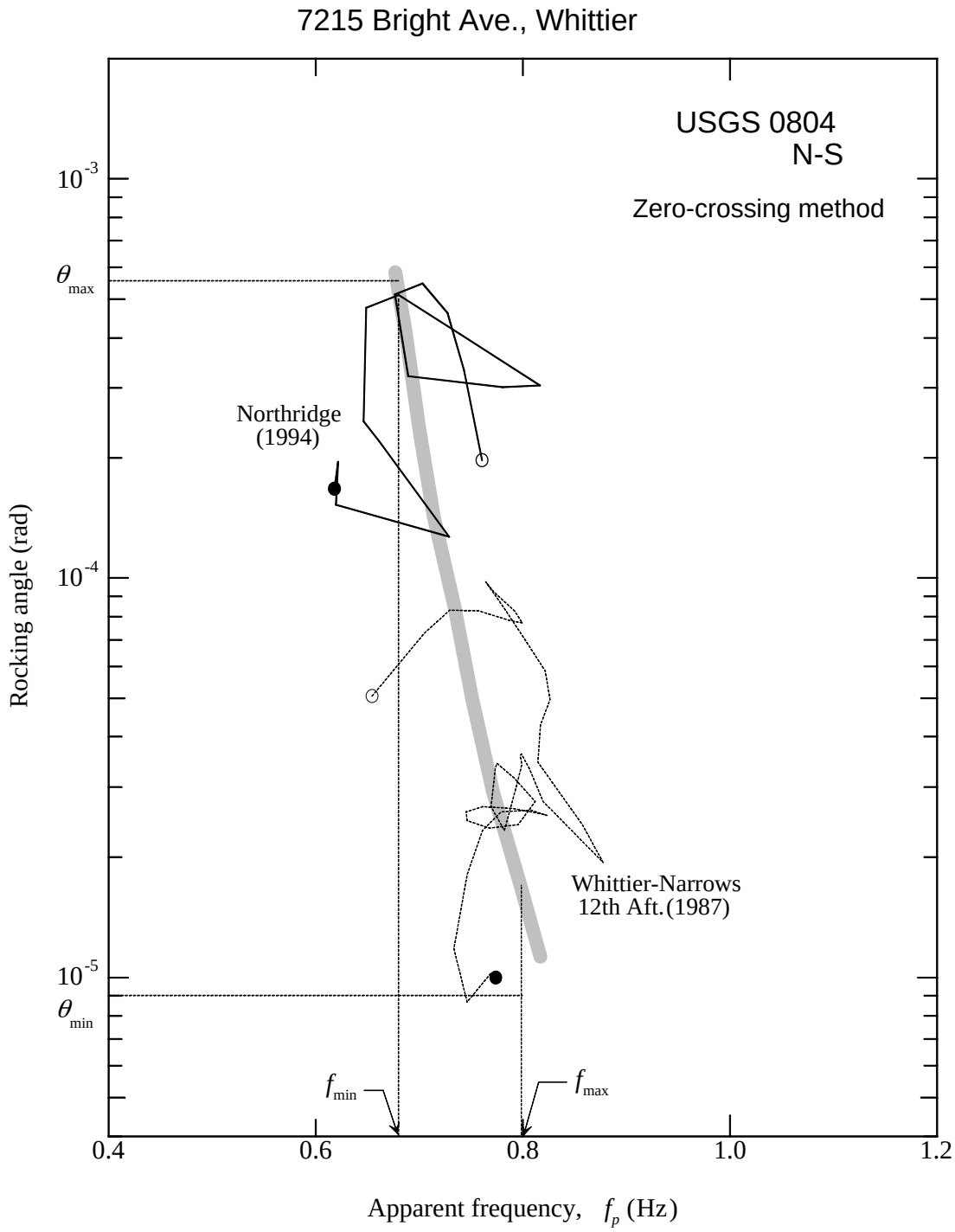
7215 Bright Ave., Whittier
USGS 0804
N-S
Zero-crossing method
10^{-3}
θ_{max}
Northridge
(1994)
10^{-4}
Whittier-Narrows
12th Aft.(1987)
10^{-5}
θ_{min}
f_{min}
f_{max}
0.4
0.6
0.8
1.0
1.2
Rocking angle (rad)
Apparent frequency, f_p (Hz)

Figure B.06a

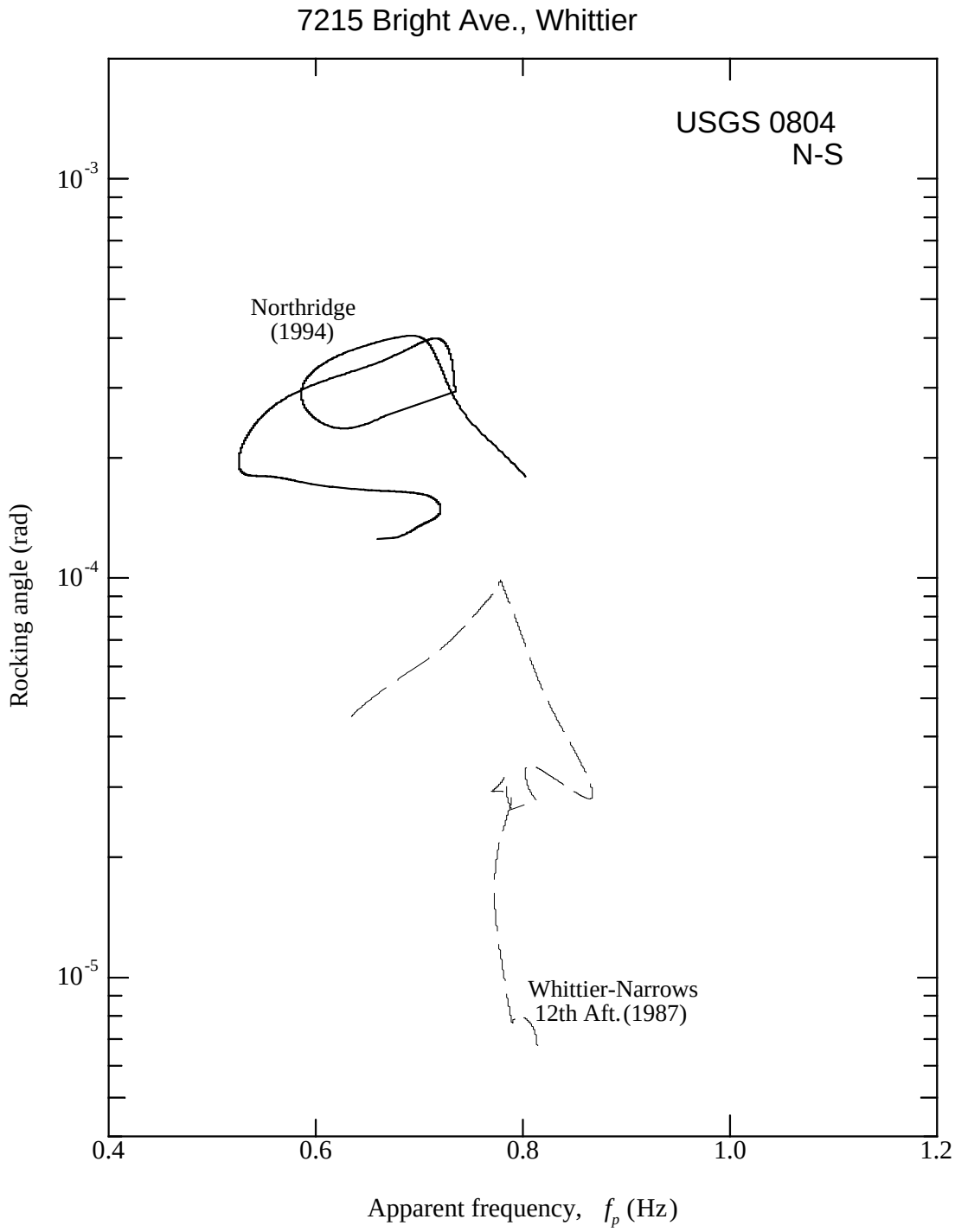
7215 Bright Ave., Whittier
USGS 0804
N-S
Northridge
(1994)
Whittier-Narrows
12th Aft. (1987)
Rocking angle (rad)
10^-3
10^-4
10^-5
0.4
0.6
0.8
1.0
1.2
Apparent frequency, f_p (Hz)

Figure B.06b

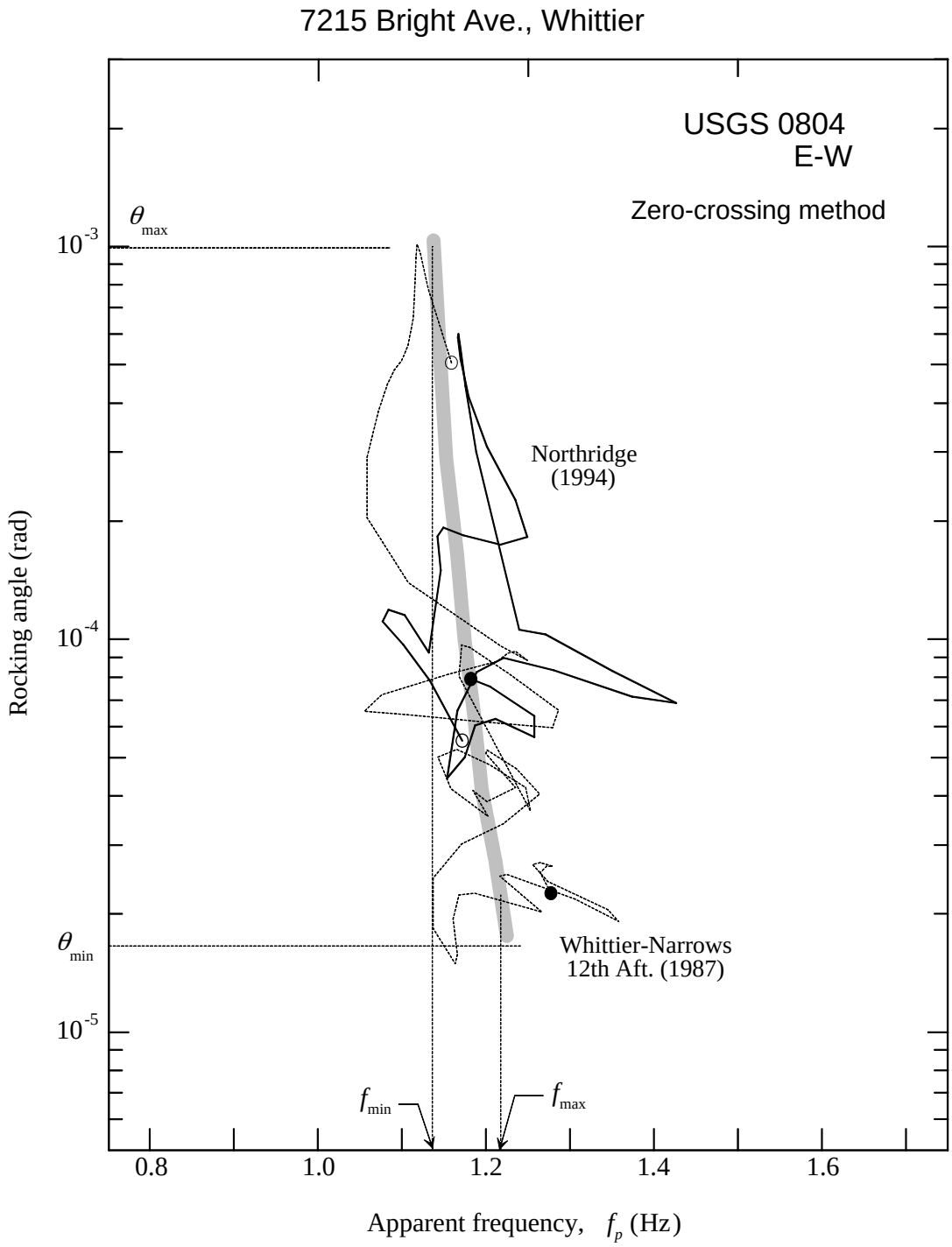
7215 Bright Ave., Whittier
USGS 0804
E-W
Zero-crossing method
θ_{max}
10^{-3}
10^{-4}
θ_{min}
10^{-5}
Rocking angle (rad)
Northridge
(1994)
Whittier-Narrows
12th Aft. (1987)
f_{min}
f_{max}
0.8
1.0
1.2
1.4
1.6
Apparent frequency, f_p (Hz)

Figure B.06c

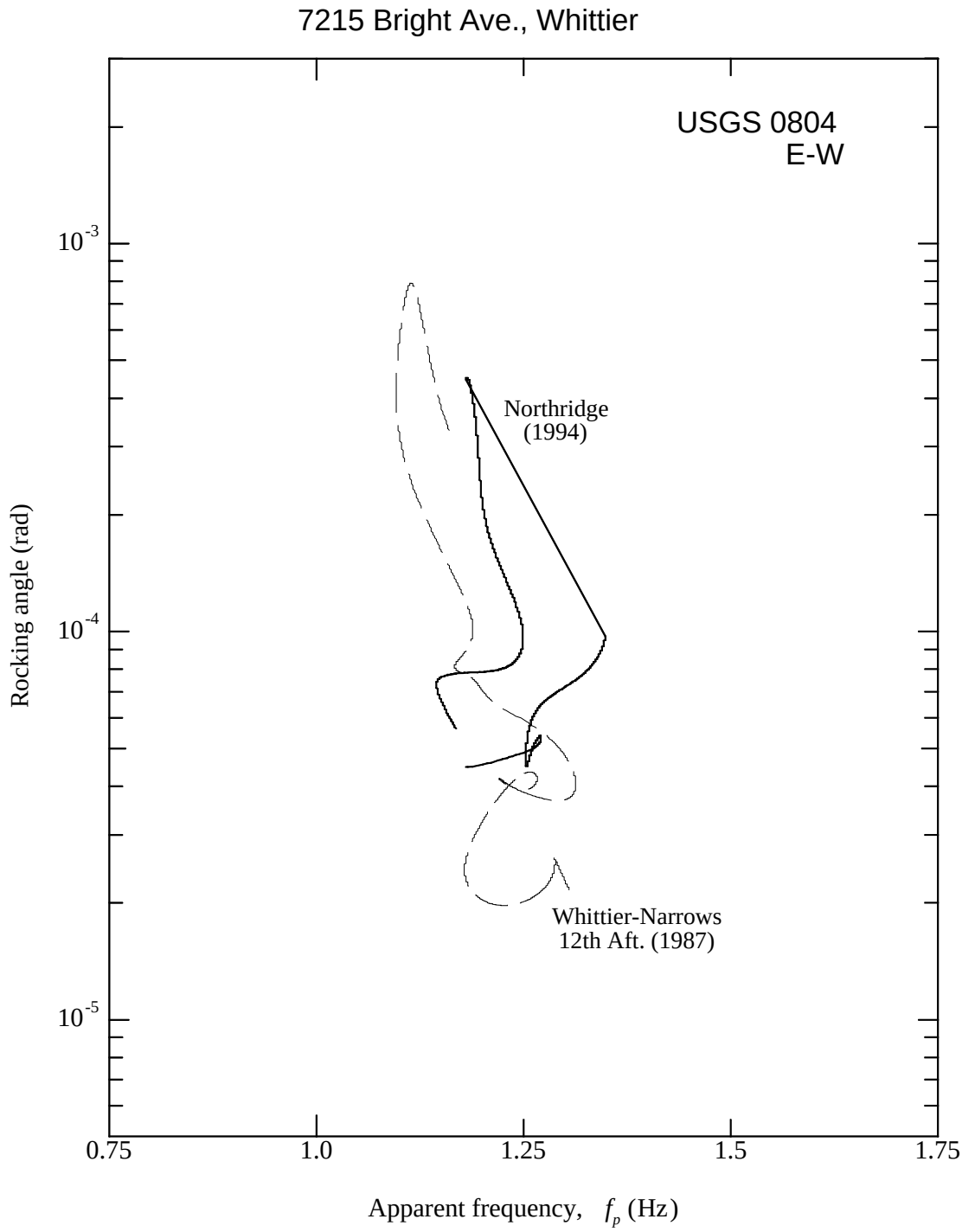
7215 Bright Ave., Whittier
USGS 0804
E-W
Northridge
(1994)
Whittier-Narrows
12th Aft. (1987)
Rocking angle (rad)
10-3
10-4
10-5
0.75
1.0
1.25
1.5
1.75
Apparent frequency, fp (Hz)

Figure B.06d

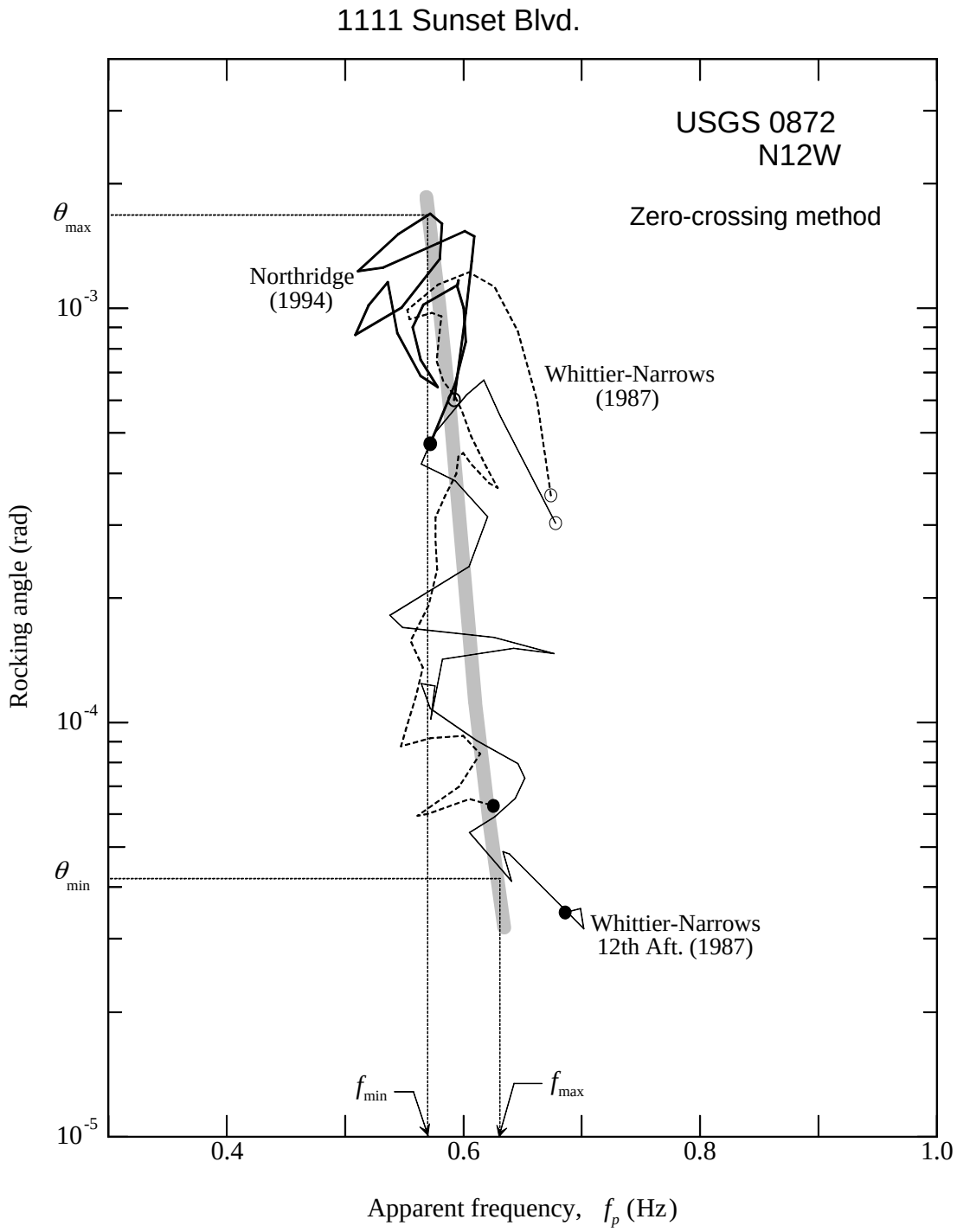
1111 Sunset Blvd.
USGS 0872
N12W
Zero-crossing method
θ_{max}
θ_{min}
Northridge
(1994)
Whittier-Narrows
(1987)
Whittier-Narrows
12th Aft. (1987)
f_{min}
f_{max}
10^{-3}
10^{-4}
10^{-5}
0.4
0.6
0.8
1.0
Rocking angle (rad)
Apparent frequency, f_p (Hz)

Figure B.07a

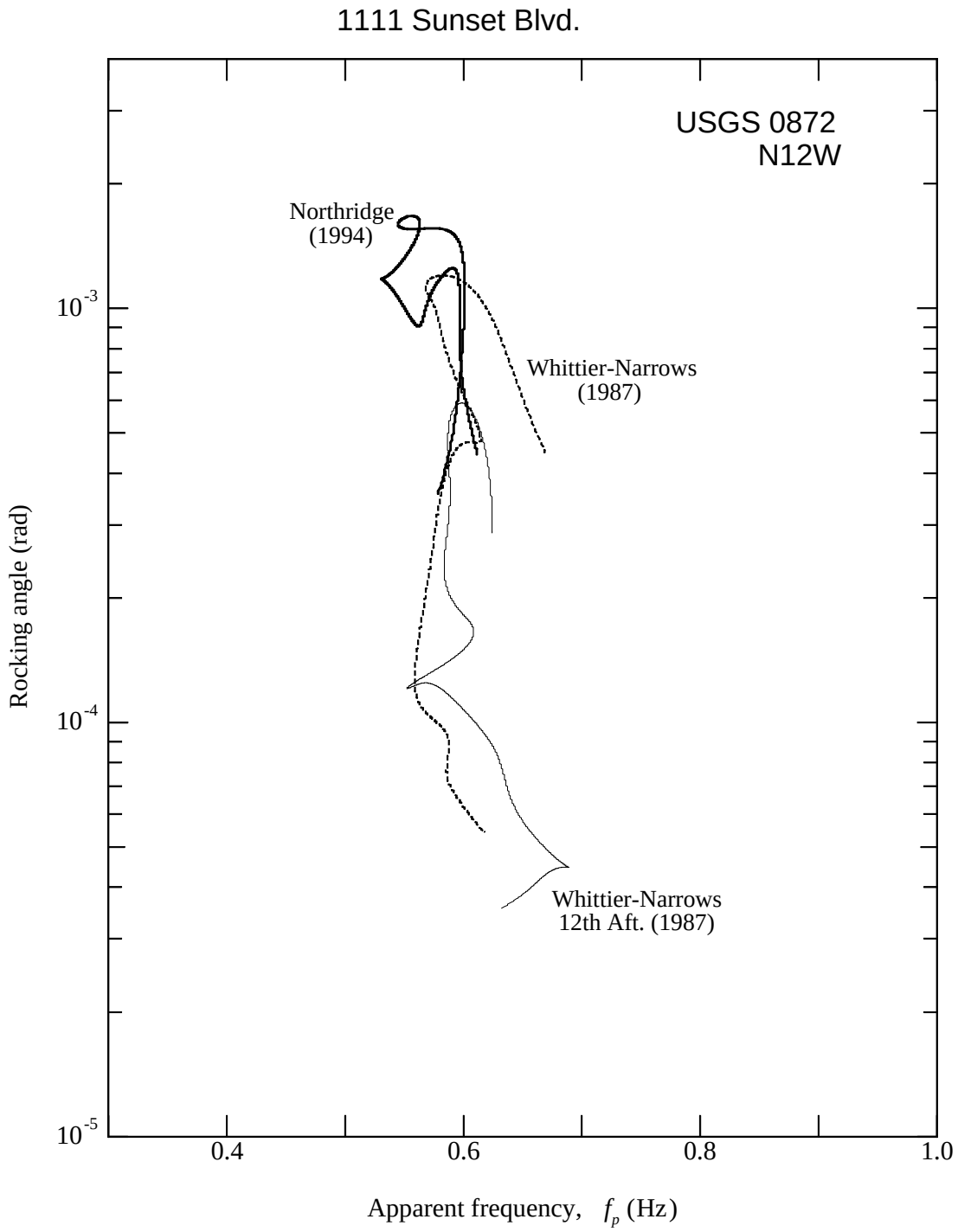
1111 Sunset Blvd.
USGS 0872
N12W
Northridge
(1994)
Whittier-Narrows
(1987)
Whittier-Narrows
12th Aft. (1987)
Rocking angle (rad)
10-3
10-4
10-5
0.4
0.6
0.8
1.0
Apparent frequency, fp (Hz)

Figure B.07b

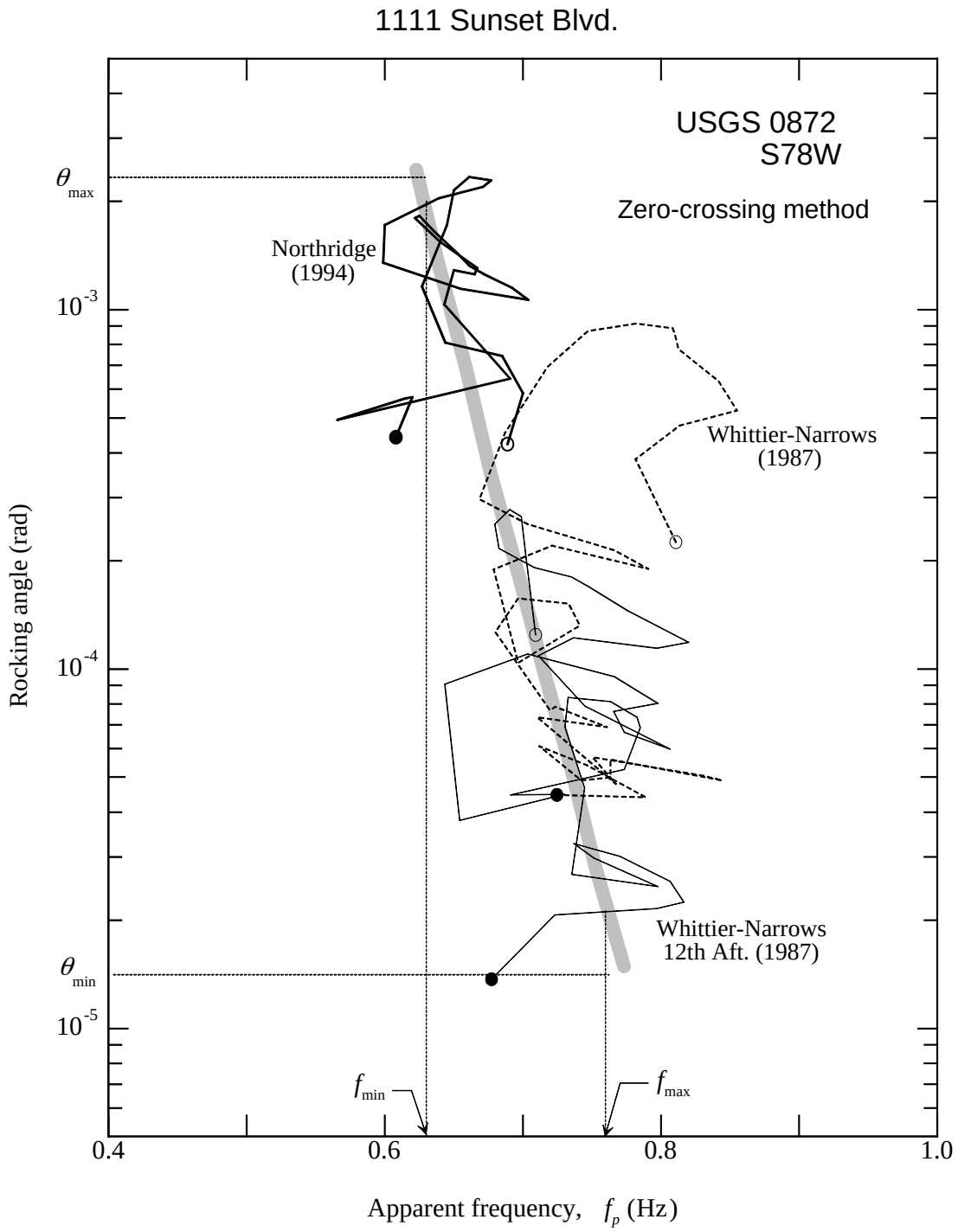
1111 Sunset Blvd.
USGS 0872
S78W
Zero-crossing method
Northridge
(1994)
Whittier-Narrows
(1987)
Whittier-Narrows
12th Aft. (1987)
θ_{max}
θ_{min}
10^{-3}
10^{-4}
10^{-5}
f_{min}
f_{max}
0.4
0.6
0.8
1.0
Rocking angle (rad)
Apparent frequency, f_p (Hz)

Figure B.07c

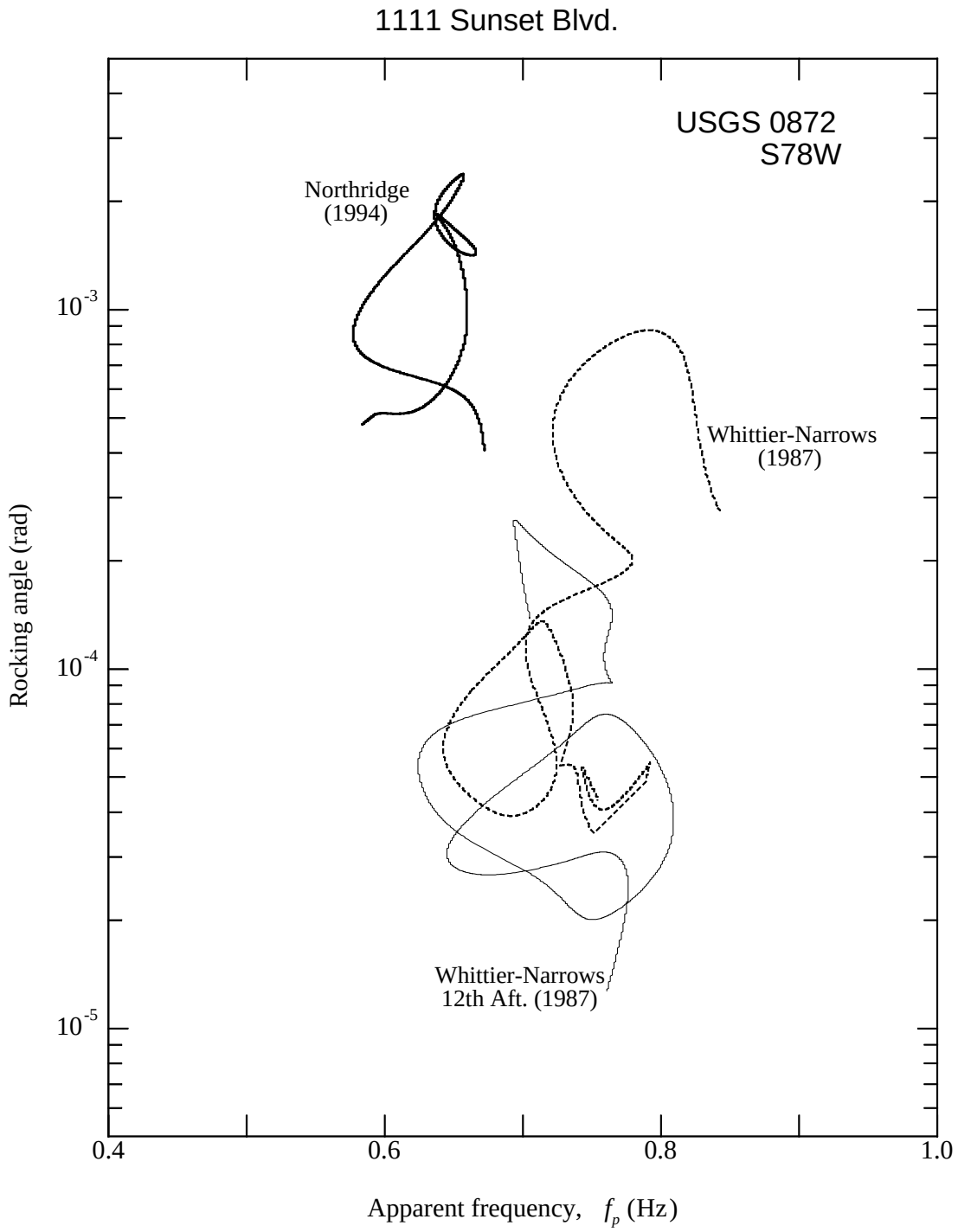
1111 Sunset Blvd.
USGS 0872
S78W
Northridge
(1994)
Whittier-Narrows
(1987)
Whittier-Narrows
12th Aft. (1987)
Rocking angle (rad)
10-3
10-4
10-5
0.4
0.6
0.8
1.0
Apparent frequency, fp (Hz)

Figure B.07d

333 S. Hope St.

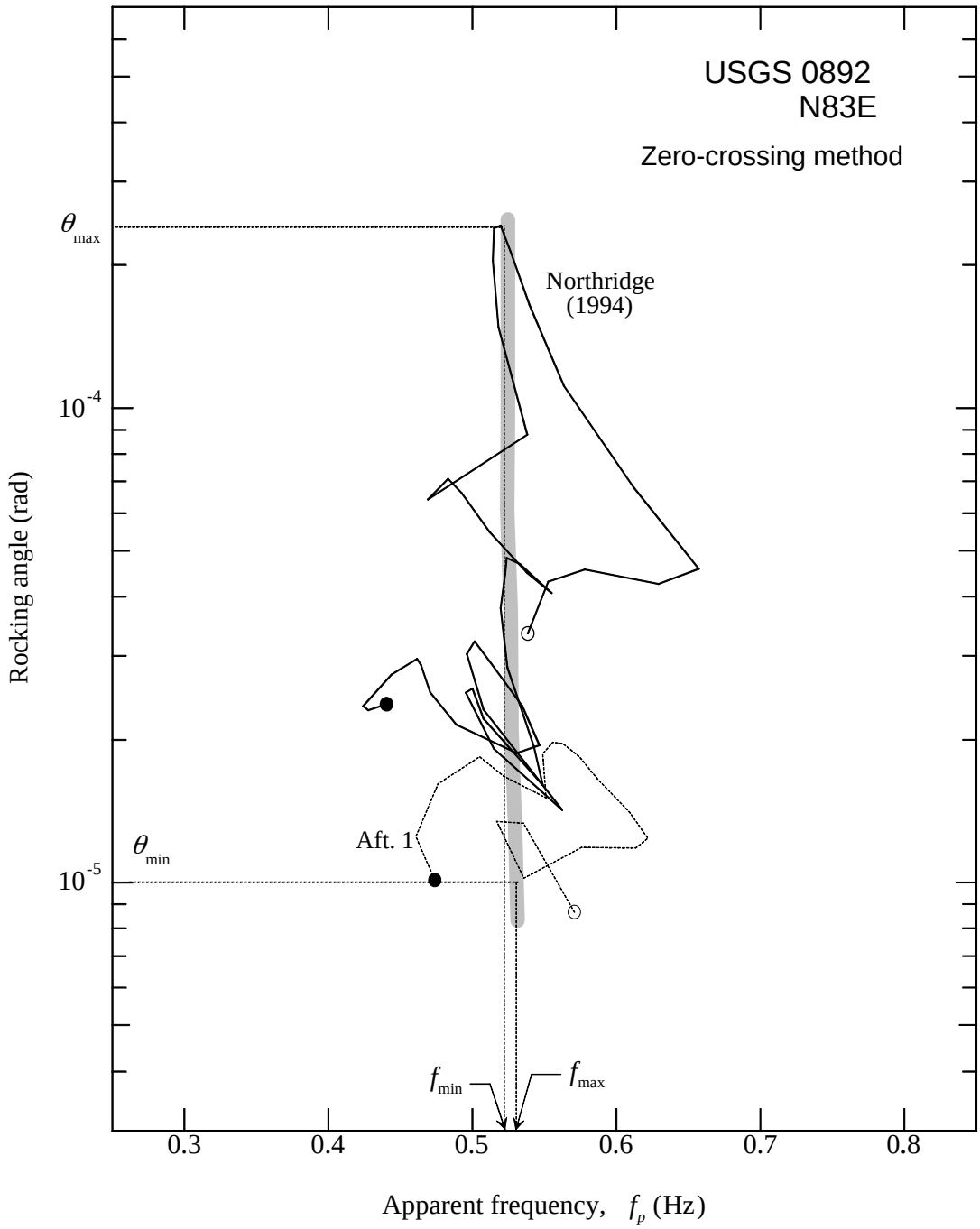

Figure B.08a

333 S. Hope St.

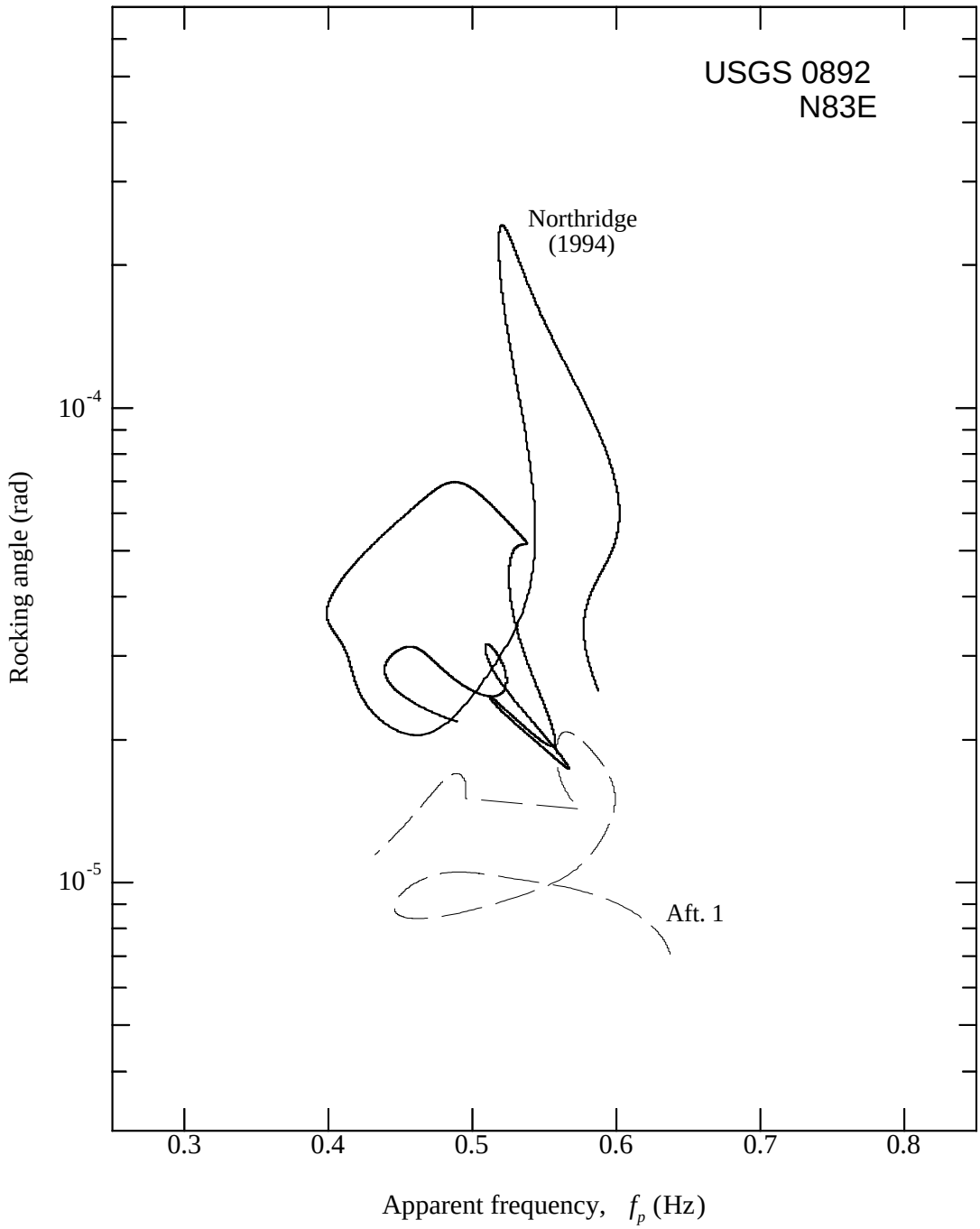

Figure B.08b

333 S. Hope St.

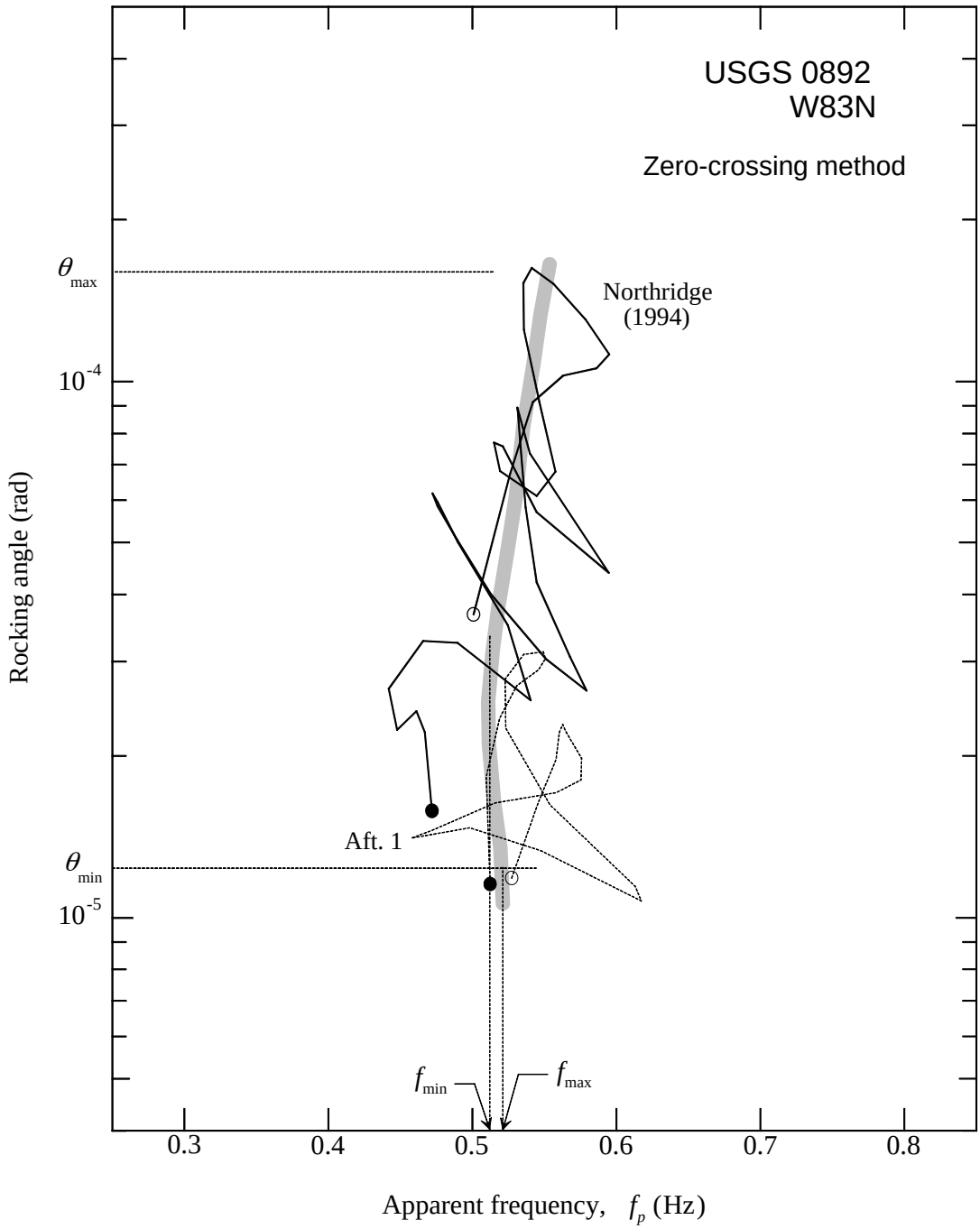

Figure B.08c

333 S. Hope St.

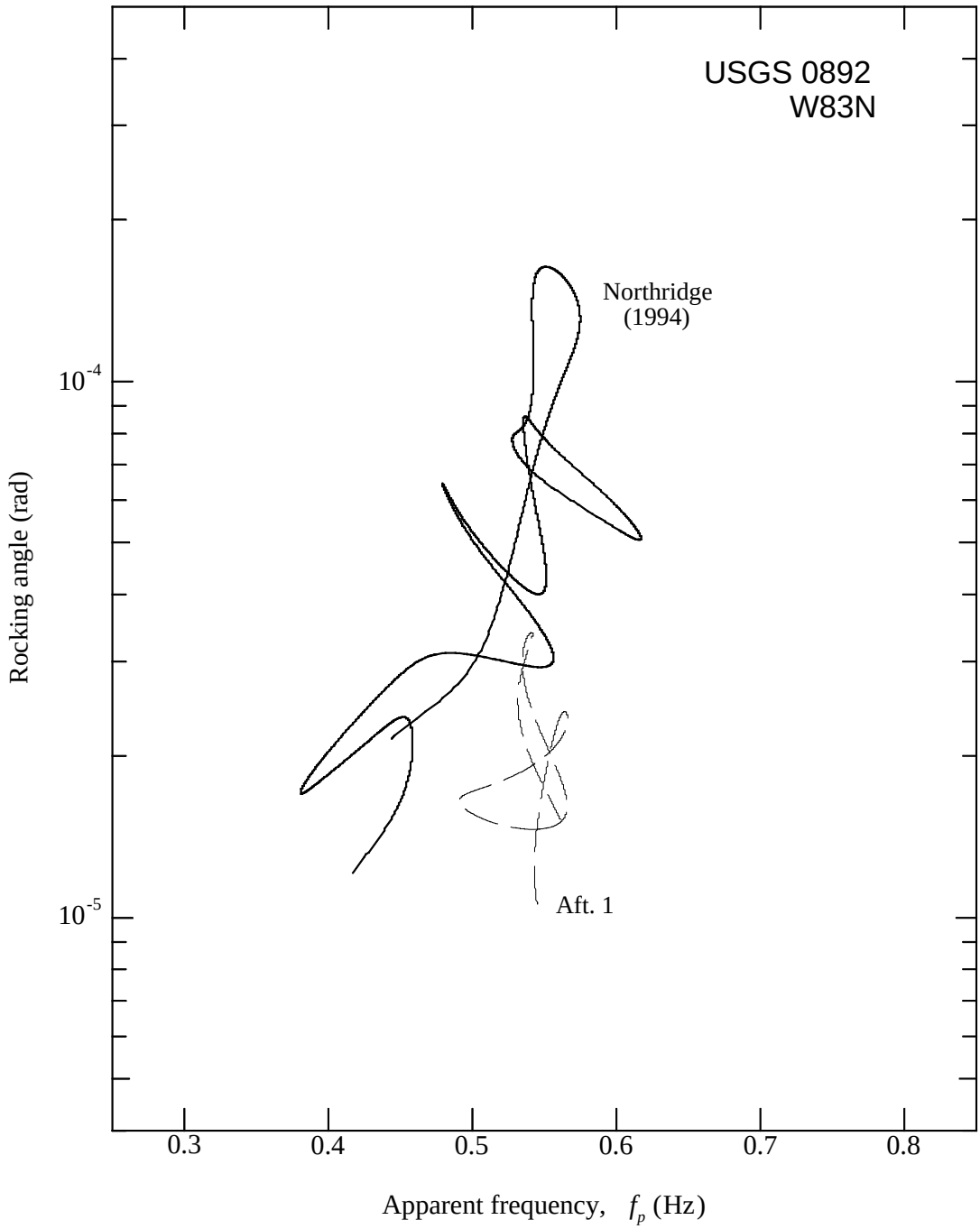

Figure B.08d

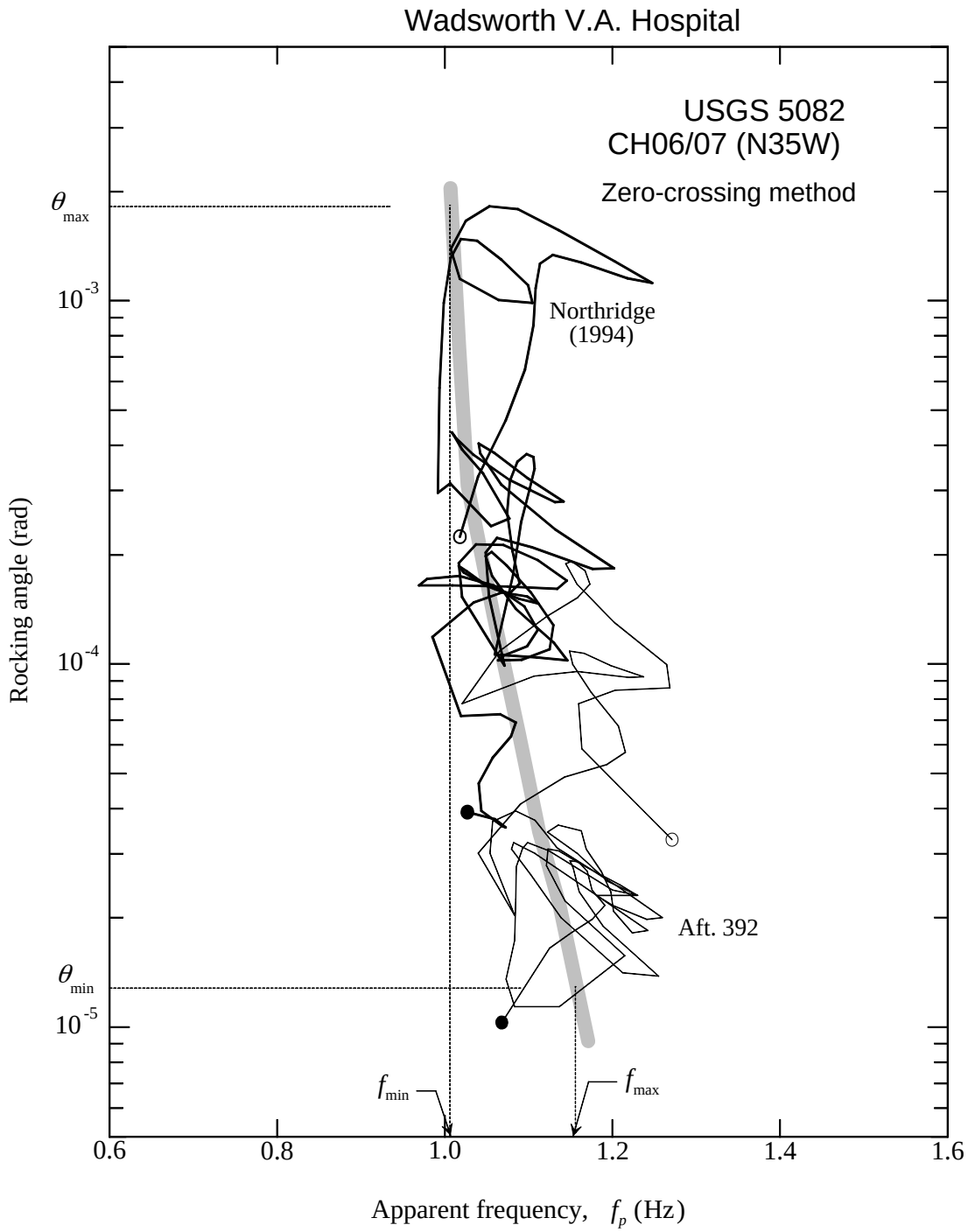
Wadsworth V.A. Hospital
USGS 5082
CH06/07 (N35W)
Zero-crossing method
Northridge
(1994)
Aft. 392
θmax
θmin
10-3
10-4
10-5
fmin
fmax
Rocking angle (rad)
0.6
0.8
1.0
1.2
1.4
1.6
Apparent frequency, fp (Hz)

Figure B.09a

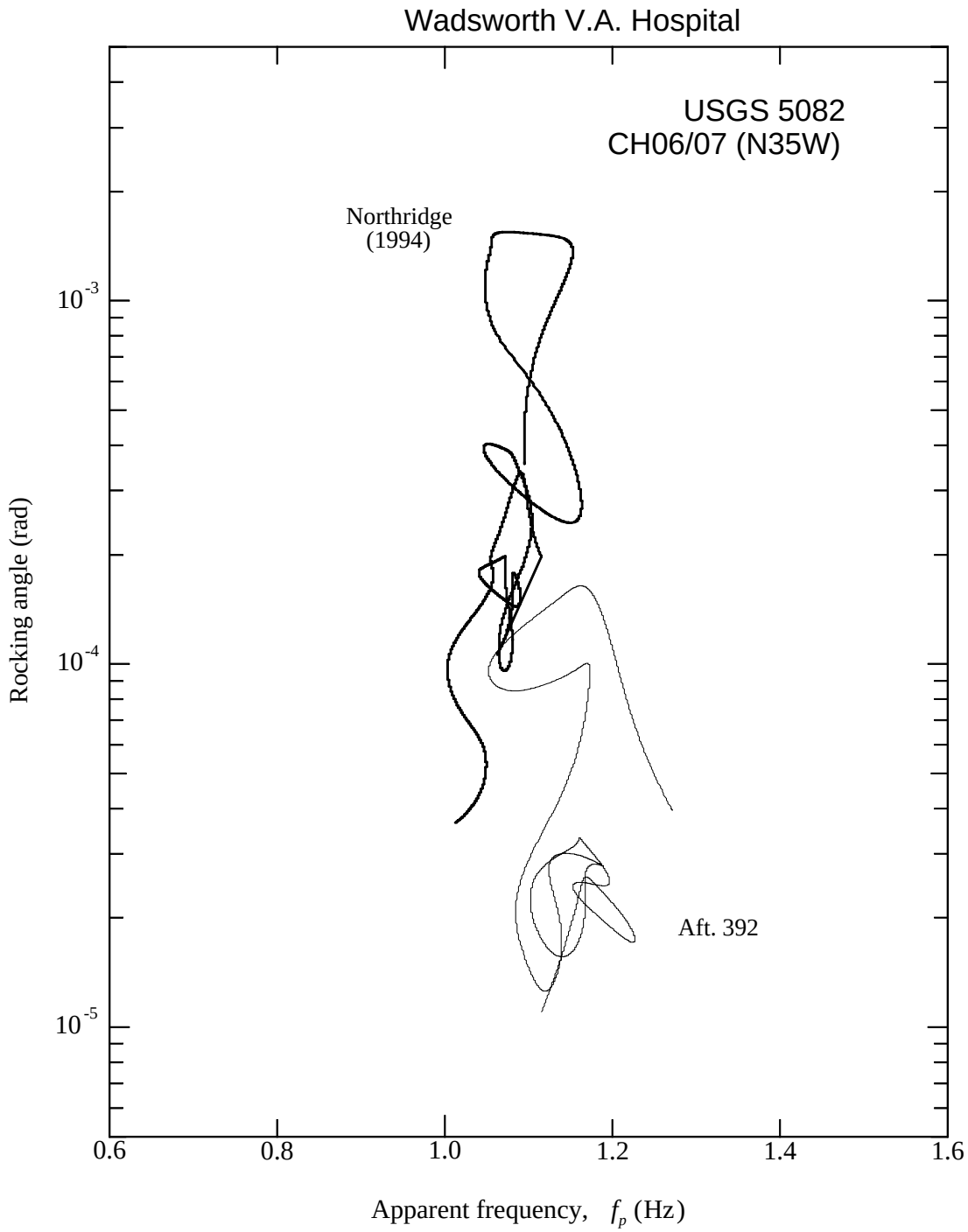
Wadsworth V.A. Hospital
USGS 5082
CH06/07 (N35W)
Northridge
(1994)
Aft. 392
Rocking angle (rad)
10-3
10-4
10-5
0.6
0.8
1.0
1.2
1.4
1.6
Apparent frequency, fp (Hz)

Figure B.09b

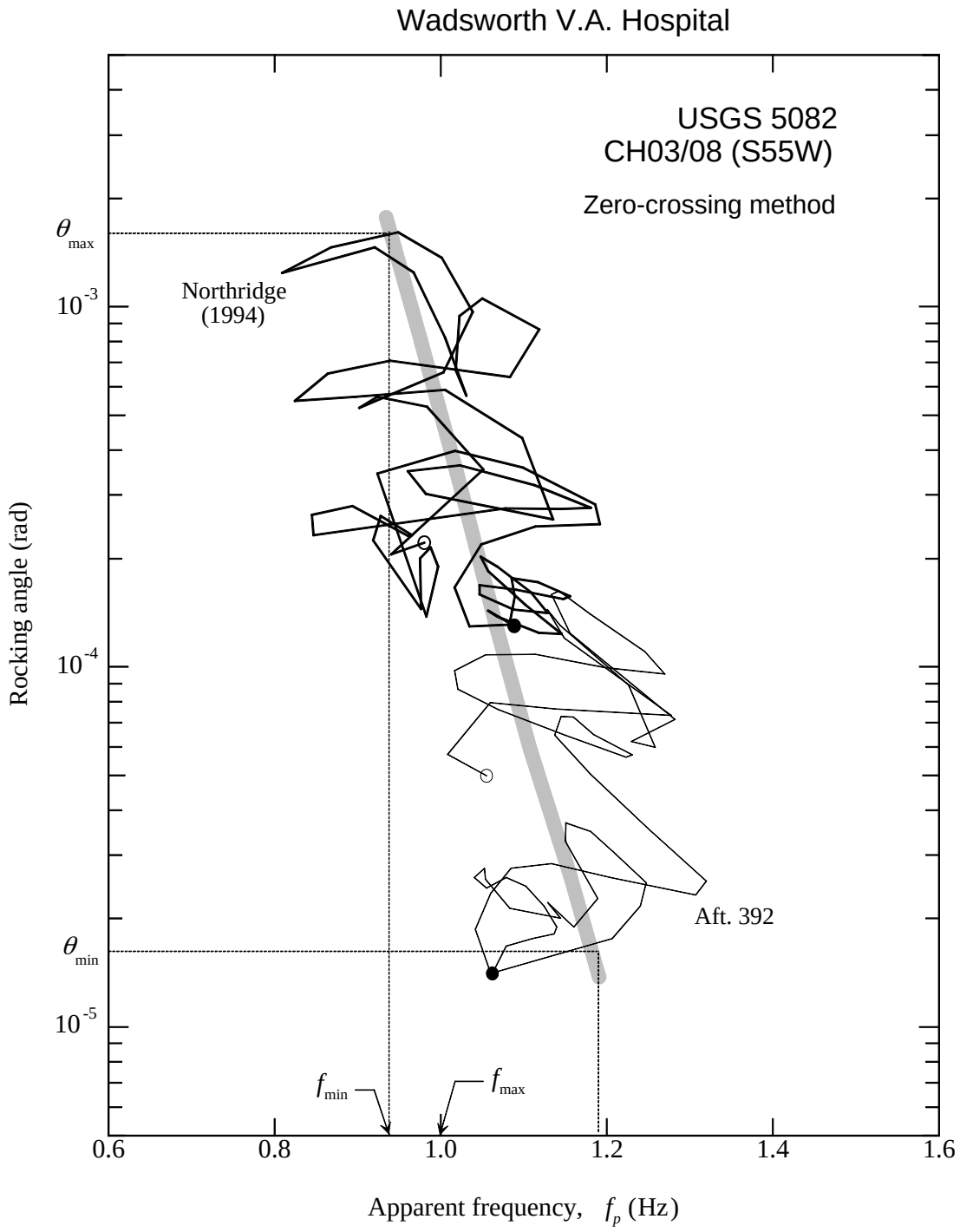
Wadsworth V.A. Hospital
USGS 5082
CH03/08 (S55W)
Zero-crossing method
θmax
10-3
Northridge
(1994)
10-4
θmin
10-5
Aft. 392
fmin
fmax
0.6
0.8
1.0
1.2
1.4
1.6
Rocking angle (rad)
Apparent frequency, fp (Hz)

Figure B.09c

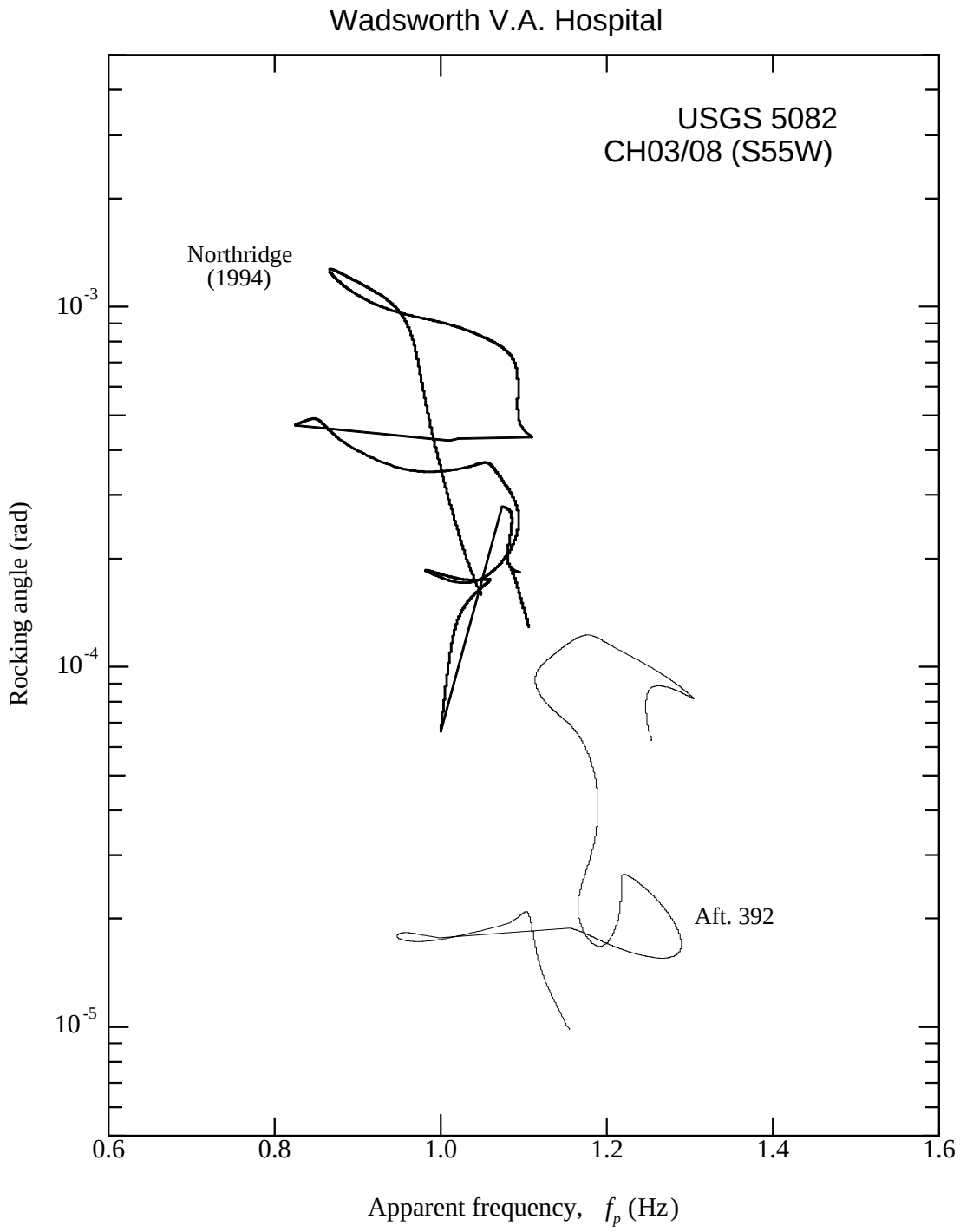
Wadsworth V.A. Hospital
USGS 5082
CH03/08 (S55W)
Northridge
(1994)
Aft. 392
Rocking angle (rad)
10-3
10-4
10-5
0.6
0.8
1.0
1.2
1.4
1.6
Apparent frequency, fp (Hz)

Figure B.09d

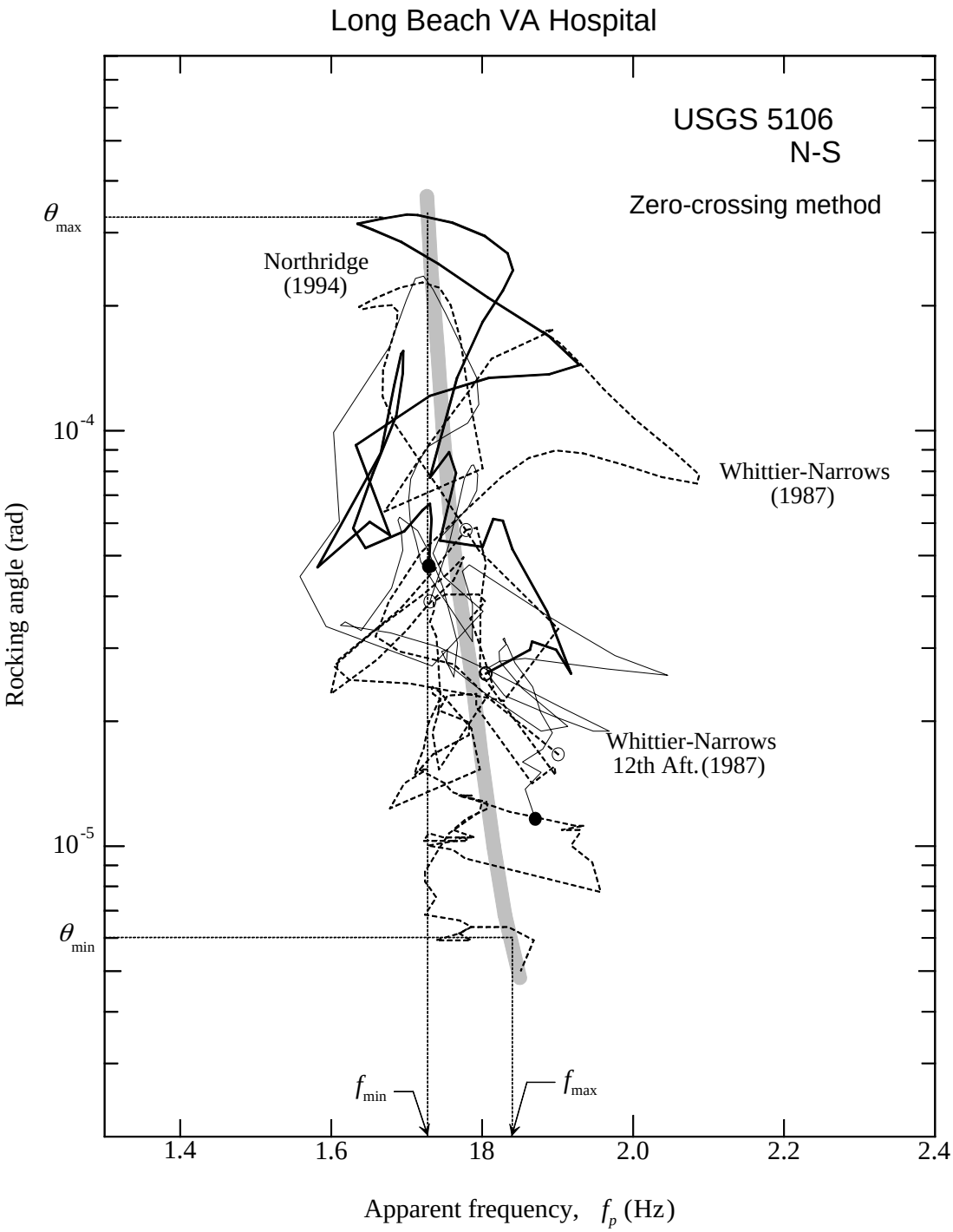
Long Beach VA Hospital
USGS 5106
N-S
Zero-crossing method
θmax
Northridge
(1994)
10-4
Whittier-Narrows
(1987)
Rocking angle (rad)
Whittier-Narrows
12th Aft.(1987)
10-5
θmin
fmin
fmax
1.4
1.6
18
2.0
2.2
2.4
Apparent frequency, fp (Hz)

Figure B.10a

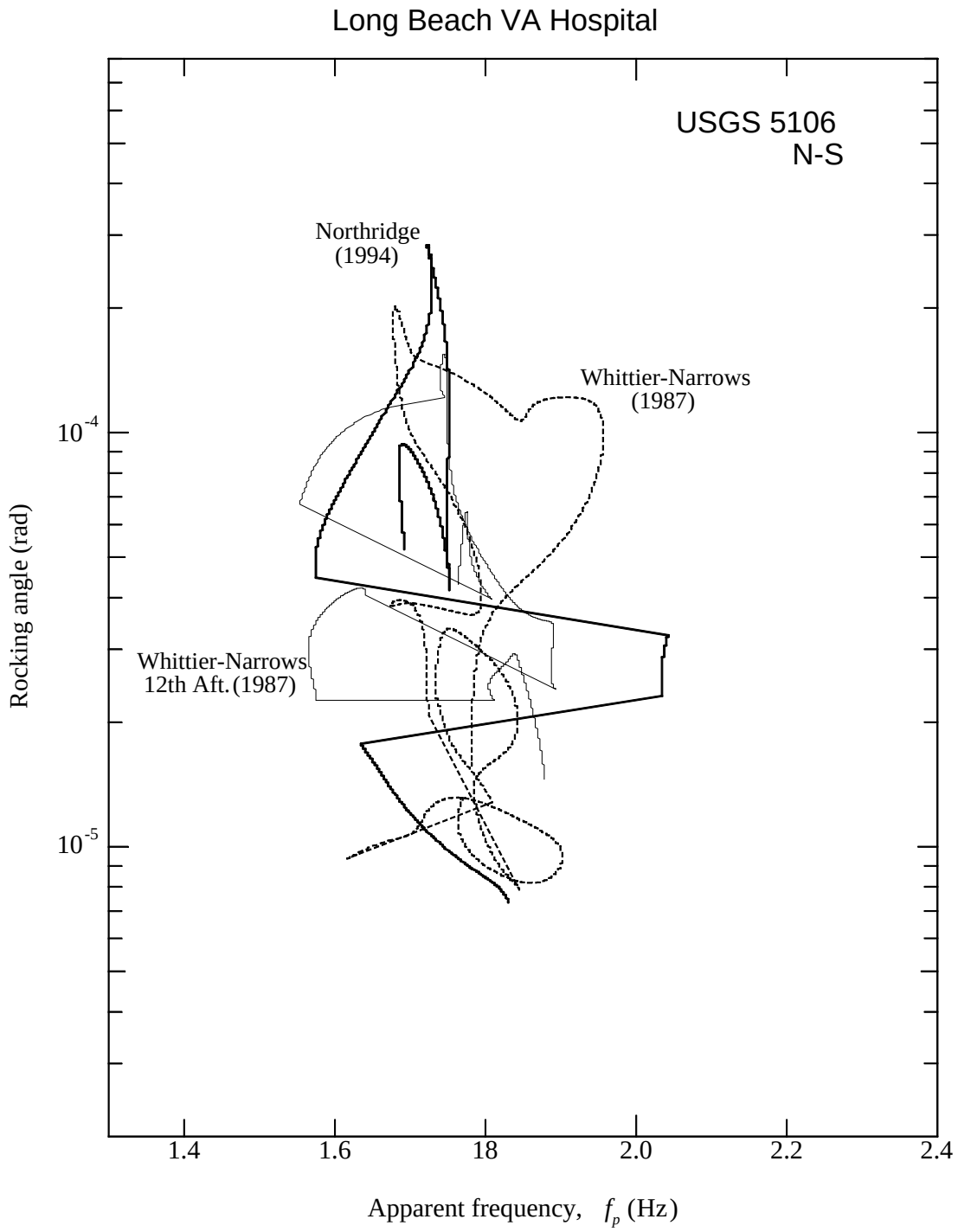
Long Beach VA Hospital
USGS 5106
N-S
Northridge
(1994)
Whittier-Narrows
(1987)
Whittier-Narrows
12th Aft.(1987)
10^{-4}
10^{-5}
Rocking angle (rad)
1.4
1.6
18
2.0
2.2
2.4
Apparent frequency, f_p (Hz)

Figure B.10b

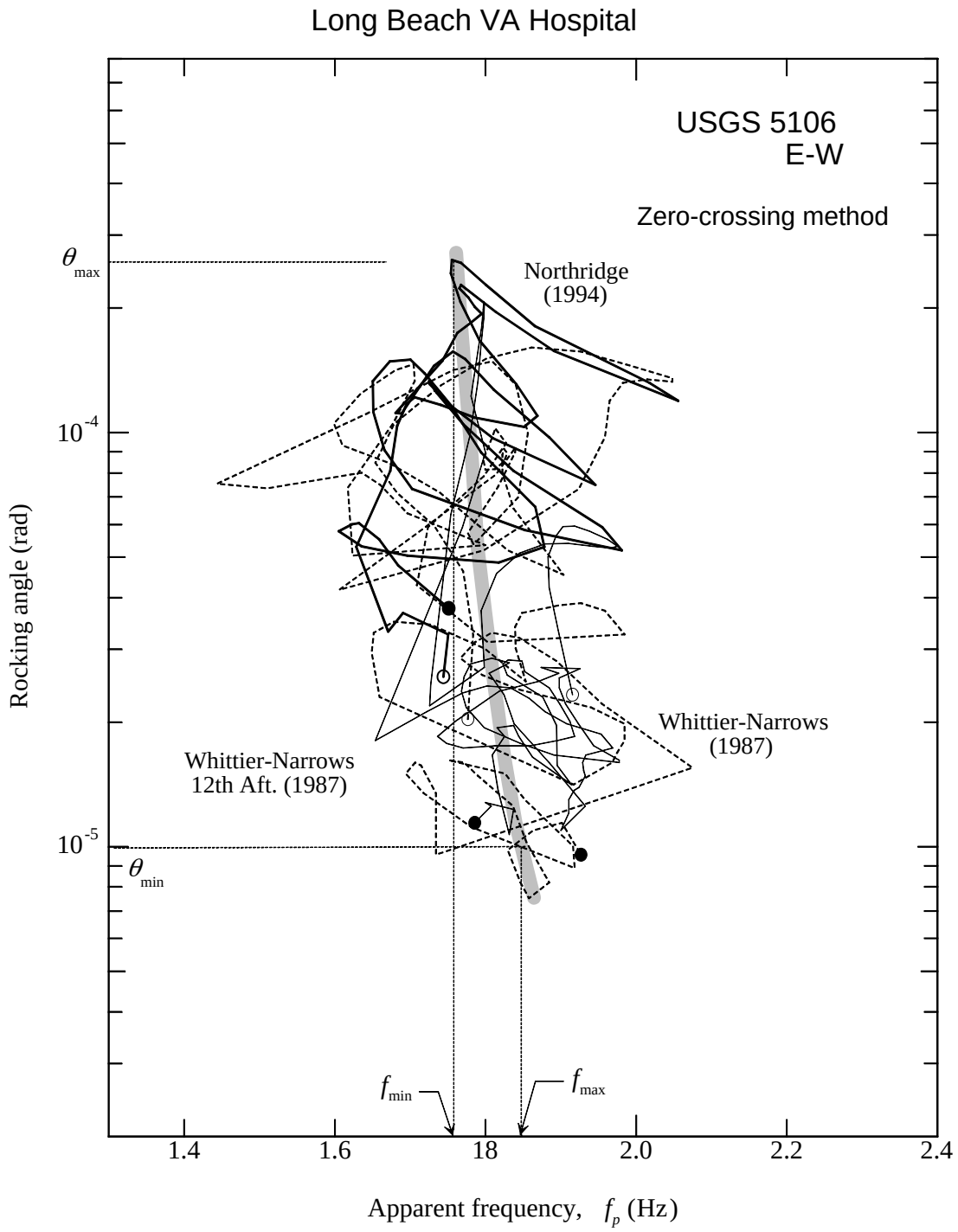
Long Beach VA Hospital
USGS 5106
E-W
Zero-crossing method
Northridge
(1994)
Whittier-Narrows
(1987)
Whittier-Narrows
12th Aft. (1987)
θmax
θmin
10-4
10-5
fmin
fmax
1.4
1.6
18
2.0
2.2
2.4
Rocking angle (rad)
Apparent frequency, fp (Hz)

Figure B.10c

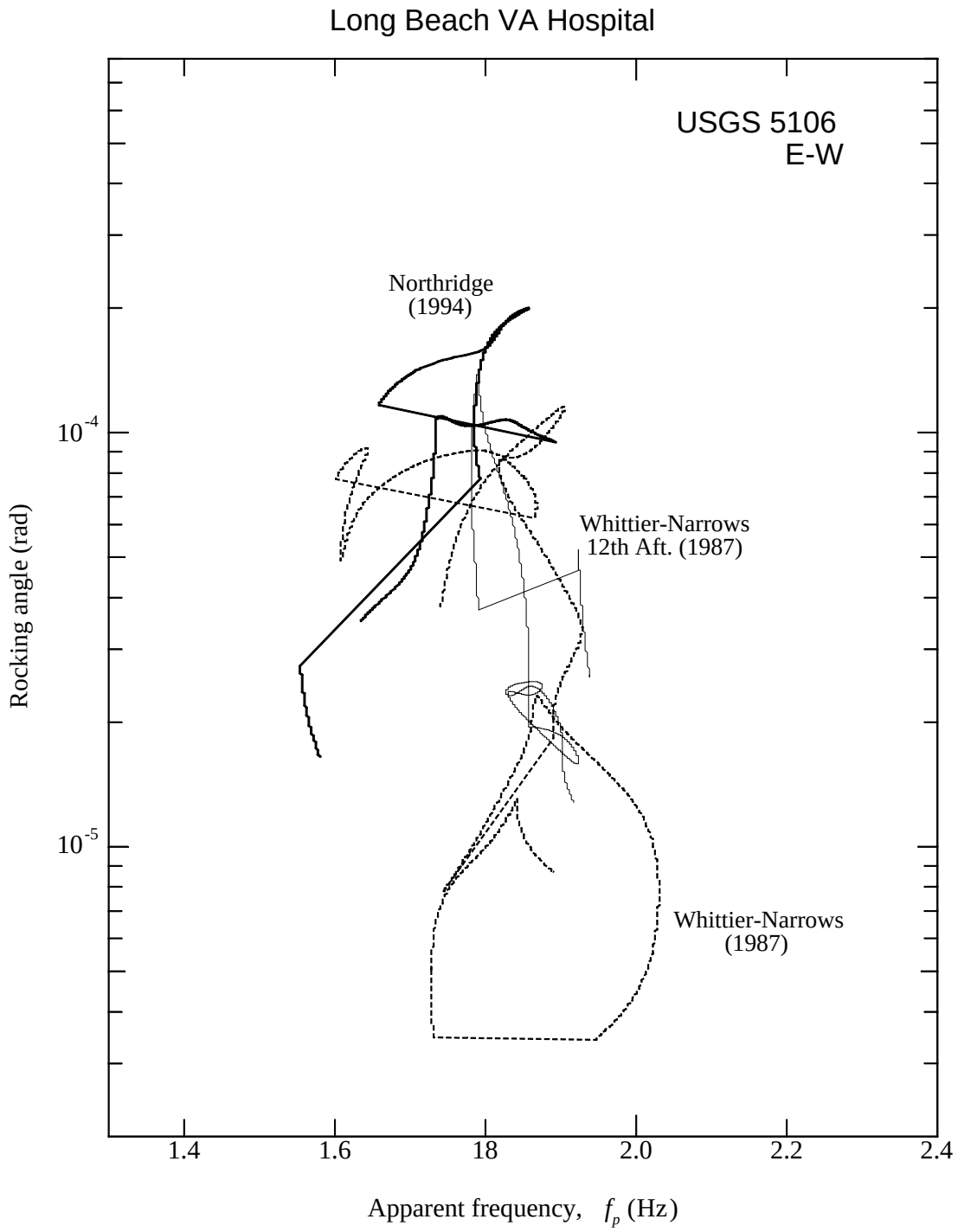
Long Beach VA Hospital
USGS 5106
E-W
Northridge
(1994)
Whittier-Narrows
12th Aft. (1987)
Whittier-Narrows
(1987)
Rocking angle (rad)
10-4
10-5
1.4
1.6
18
2.0
2.2
2.4
Apparent frequency, fp (Hz)

Figure B.10d

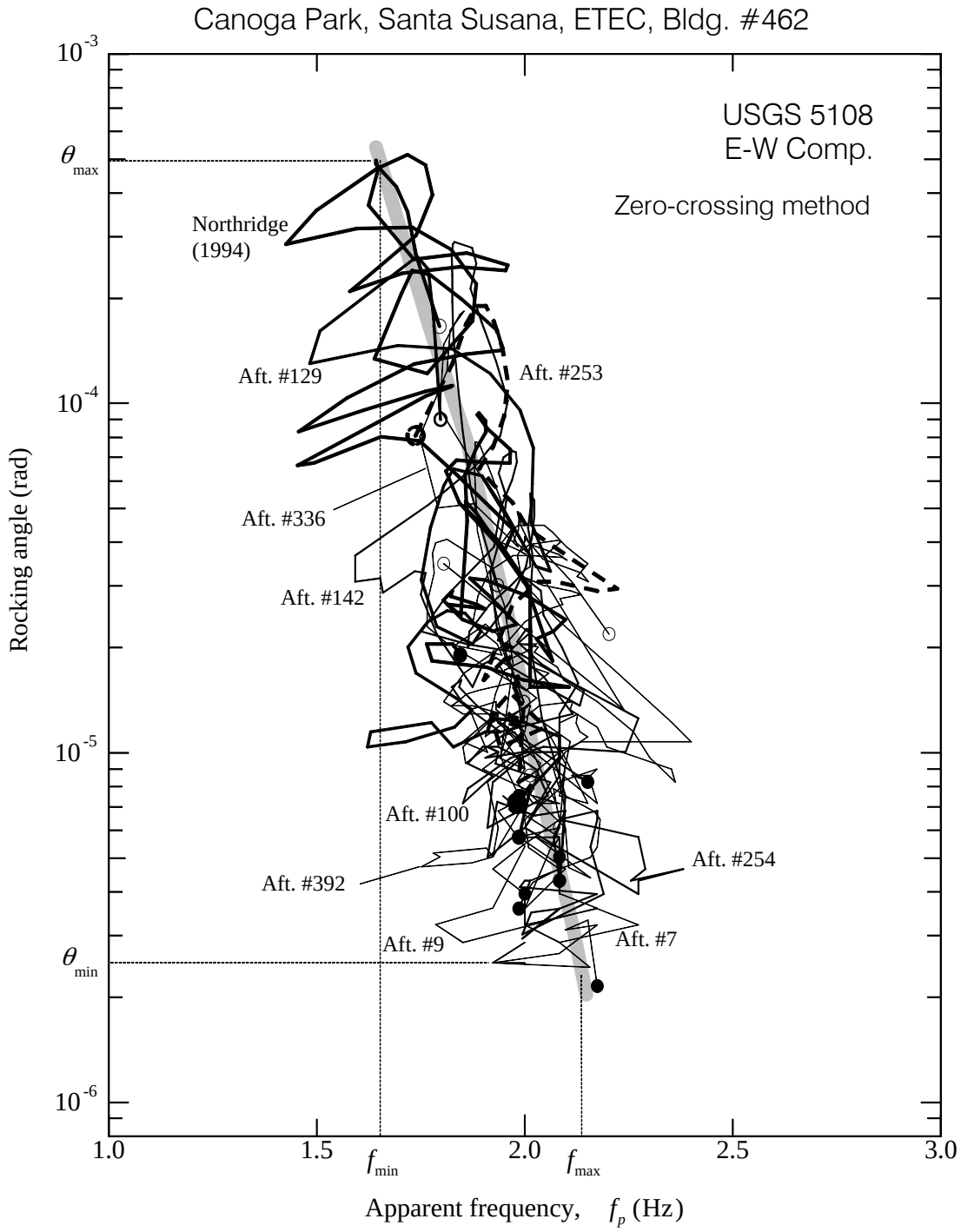
Canoga Park, Santa Susana, ETEC, Bldg. #462
USGS 5108
E-W Comp.
Zero-crossing method
Northridge
(1994)
Aft. #129
Aft. #253
Aft. #336
Aft. #142
Aft. #100
Aft. #392
Aft. #254
Aft. #9
Aft. #7
θ_{max}
θ_{min}
10^{-3}
10^{-4}
10^{-5}
10^{-6}
Rocking angle (rad)
1.0
1.5
2.0
2.5
3.0
f_{min}
f_{max}
Apparent frequency, f_p (Hz)

Figure B.11a

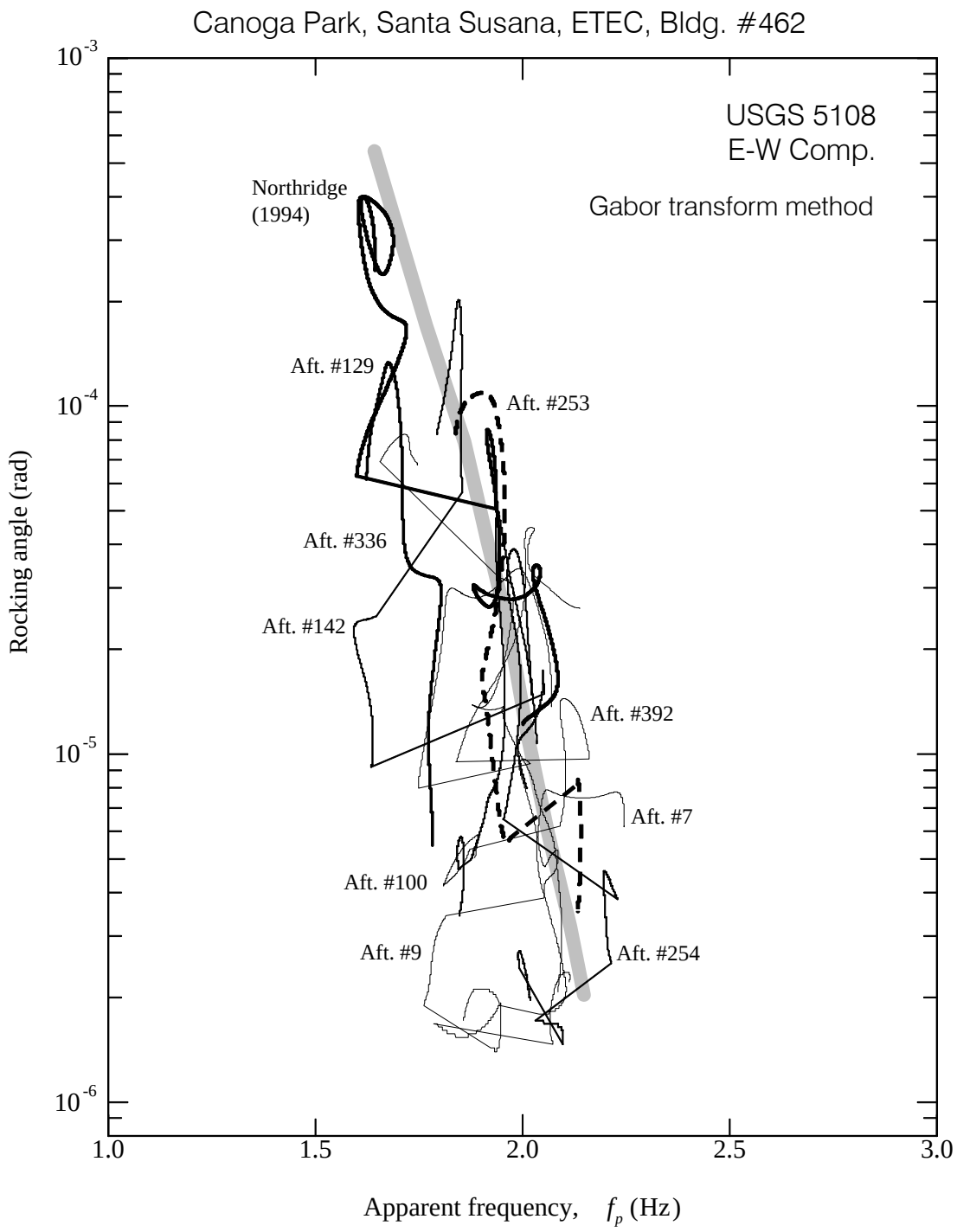
Canoga Park, Santa Susana, ETEC, Bldg. #462
USGS 5108
E-W Comp.
Gabor transform method
Northridge
(1994)
Aft. #129
Aft. #253
Aft. #336
Aft. #142
Aft. #392
Aft. #7
Aft. #100
Aft. #9
Aft. #254
Rocking angle (rad)
Apparent frequency, f_p (Hz)
10^{-3}
10^{-4}
10^{-5}
10^{-6}
1.0
1.5
2.0
2.5
3.0

Figure B.11b

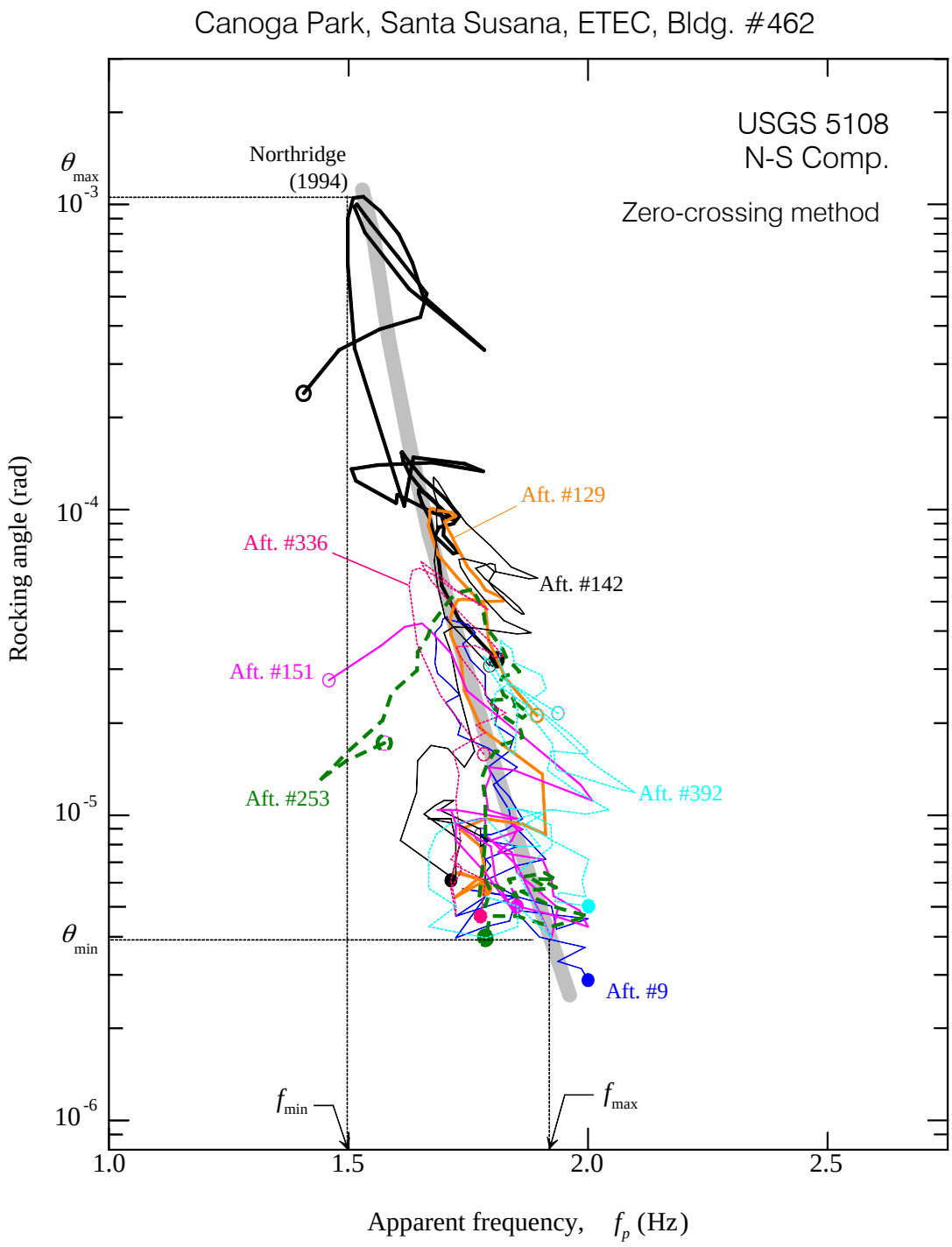
Canoga Park, Santa Susana, ETEC, Bldg. #462
USGS 5108
N-S Comp.
Zero-crossing method
Northridge
(1994)
θ_{max}
10^{-3}
10^{-4}
10^{-5}
θ_{min}
10^{-6}
Rocking angle (rad)
Aft. #129
Aft. #336
Aft. #142
Aft. #151
Aft. #253
Aft. #392
Aft. #9
f_{min}
f_{max}
1.0
1.5
2.0
2.5
Apparent frequency, f_p (Hz)

.Figure B.11c

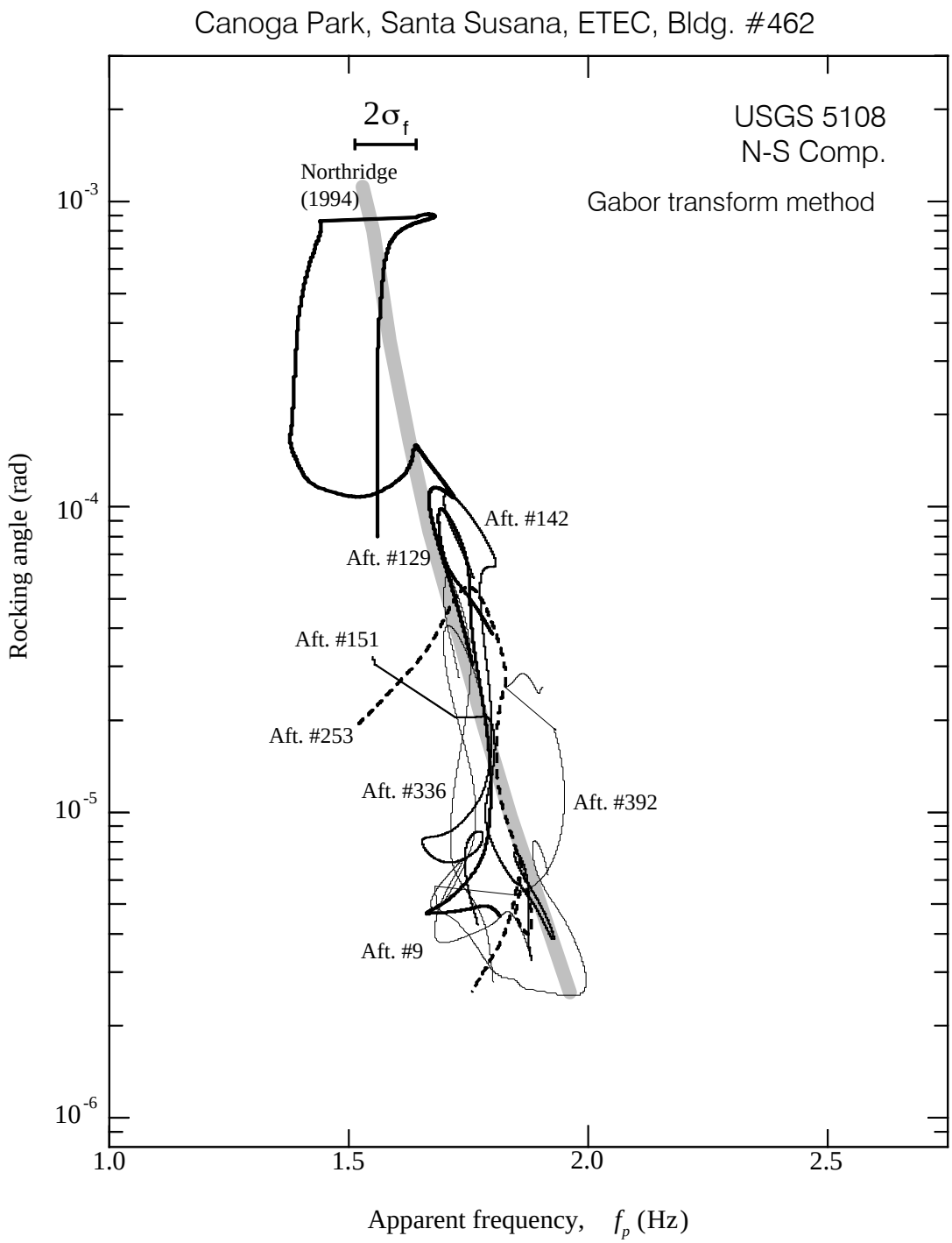
Canoga Park, Santa Susana, ETEC, Bldg. #462
2σf
USGS 5108
N-S Comp.
Gabor transform method
Northridge
(1994)
Aft. #142
Aft. #129
Aft. #151
Aft. #253
Aft. #336
Aft. #392
Aft. #9
Rocking angle (rad)
10-3
10-4
10-5
10-6
1.0
1.5
2.0
2.5
Apparent frequency, fp (Hz)

Figure B.11d

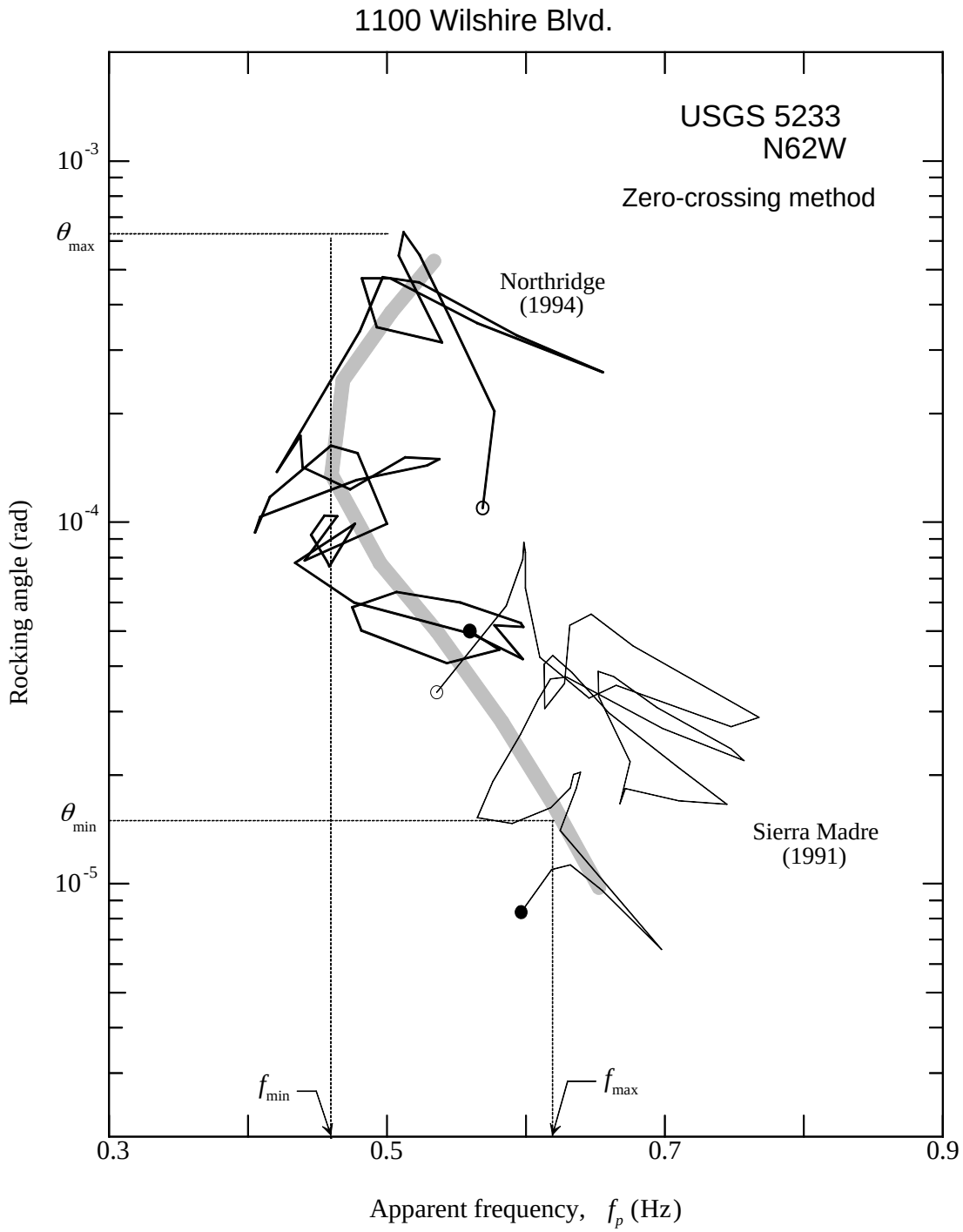
1100 Wilshire Blvd.
USGS 5233
N62W
Zero-crossing method
Northridge
(1994)
Sierra Madre
(1991)
10^{-3}
θ_{max}
10^{-4}
θ_{min}
10^{-5}
Rocking angle (rad)
f_{min}
f_{max}
0.3
0.5
0.7
0.9
Apparent frequency, f_p (Hz)

Figure B.12a

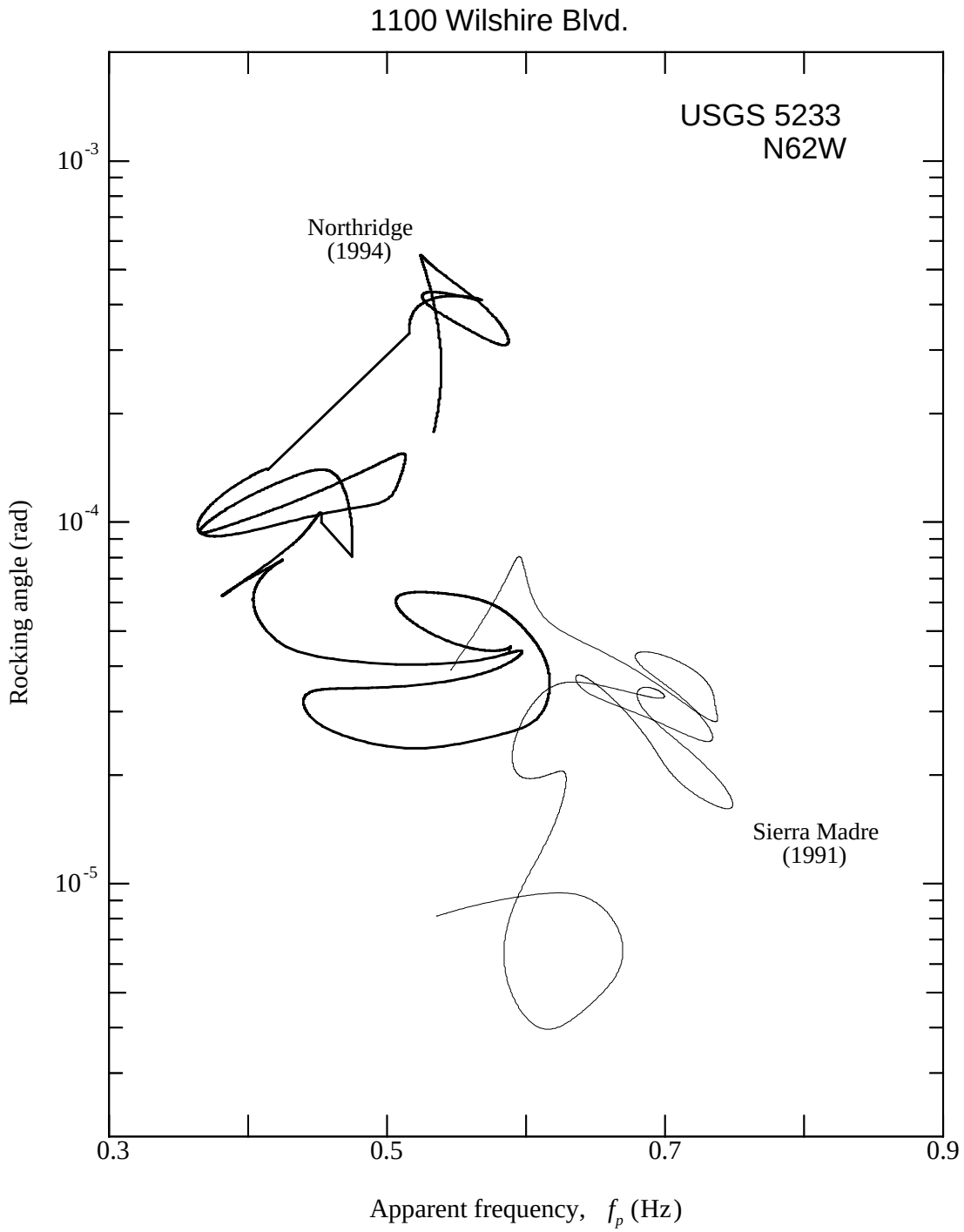
1100 Wilshire Blvd.
USGS 5233
N62W
Northridge
(1994)
Sierra Madre
(1991)
Rocking angle (rad)
10-3
10-4
10-5
0.3
0.5
0.7
0.9
Apparent frequency, fp (Hz)

Figure B.12b

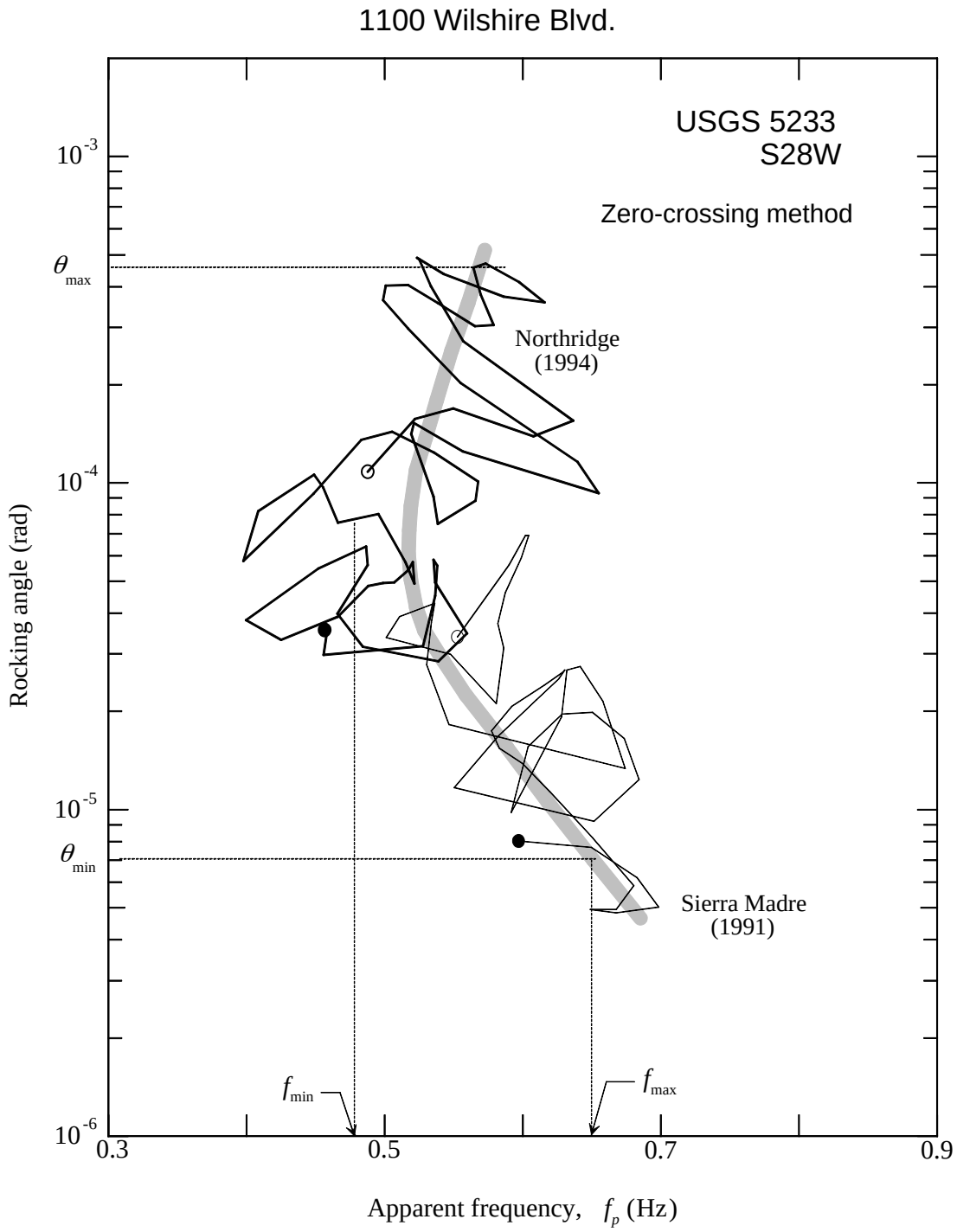
1100 Wilshire Blvd.
USGS 5233
S28W
Zero-crossing method
Northridge
(1994)
Sierra Madre
(1991)
θ_{max}
θ_{min}
f_{min}
f_{max}
10^{-3}
10^{-4}
10^{-5}
10^{-6}
0.3
0.5
0.7
0.9
Rocking angle (rad)
Apparent frequency, f_p (Hz)

Figure B.12c

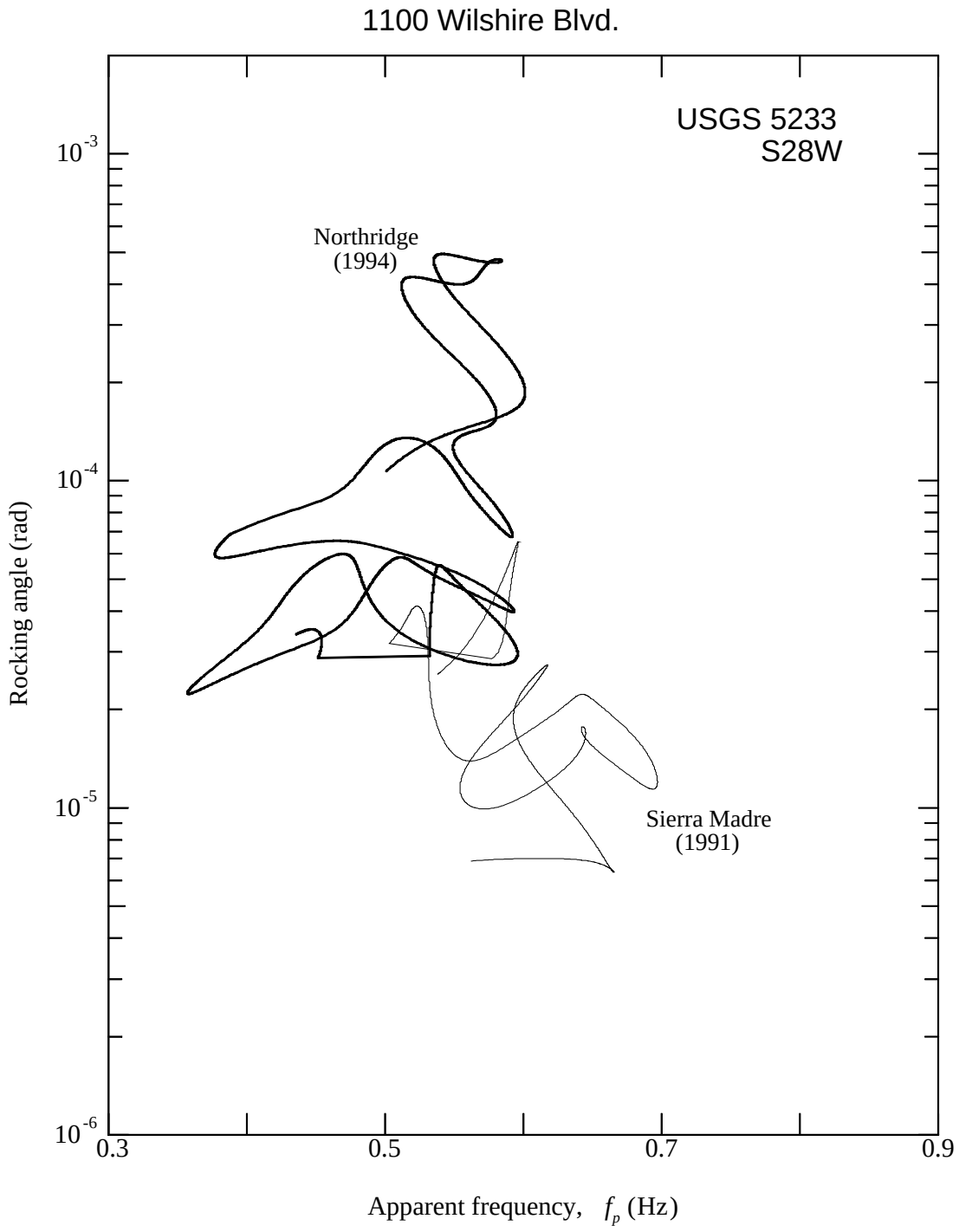
1100 Wilshire Blvd.
USGS 5233
S28W
Northridge
(1994)
Sierra Madre
(1991)
Rocking angle (rad)
10-3
10-4
10-5
10-6
0.3
0.5
0.7
0.9
Apparent frequency, fp (Hz)

Figure B.12d

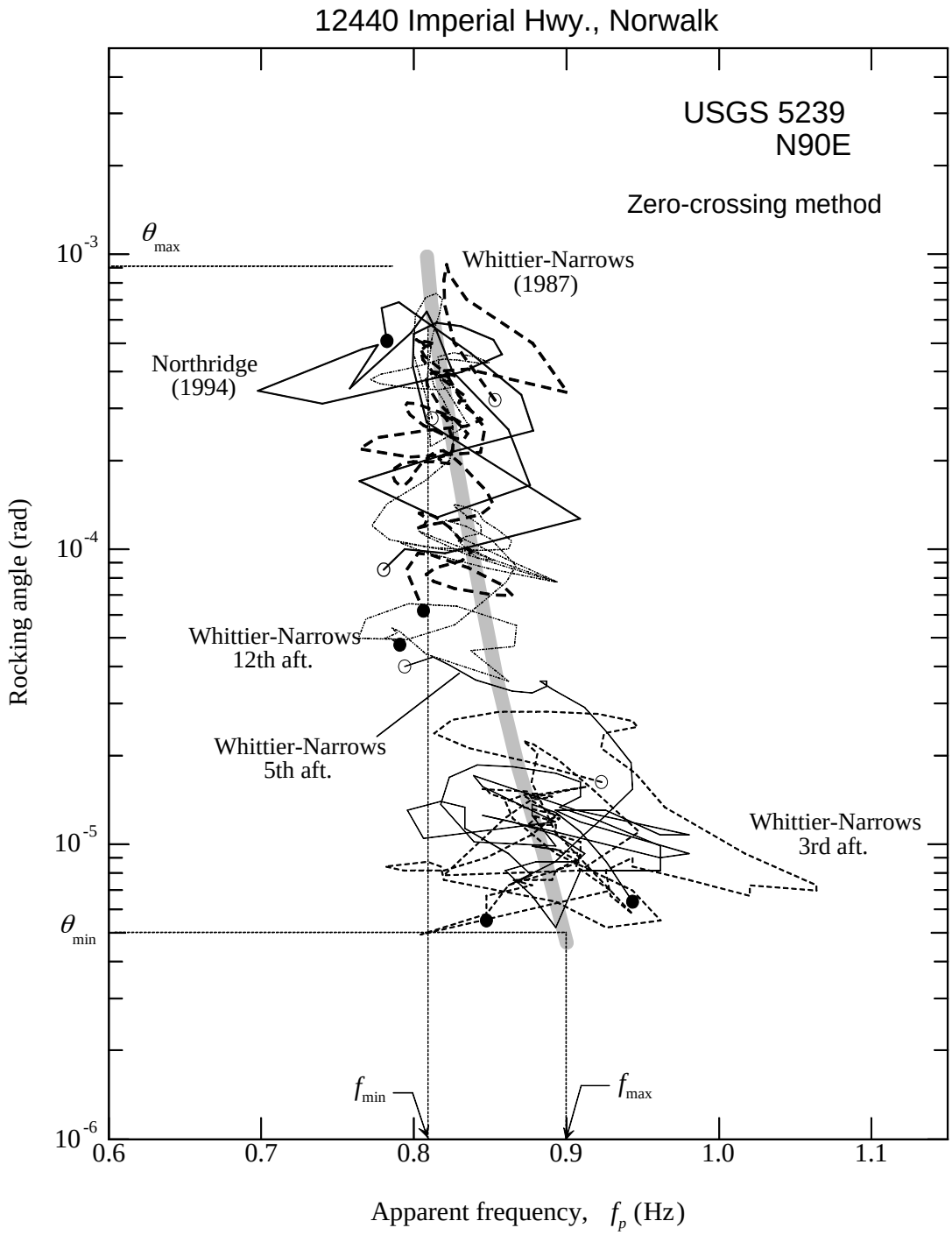
12440 Imperial Hwy., Norwalk
USGS 5239
N90E
Zero-crossing method
θ_{max}
10^{-3}
10^{-4}
10^{-5}
θ_{min}
10^{-6}
Whittier-Narrows
(1987)
Northridge
(1994)
Whittier-Narrows
12th aft.
Whittier-Narrows
5th aft.
Whittier-Narrows
3rd aft.
f_{min}
f_{max}
0.6
0.7
0.8
0.9
1.0
1.1
Rocking angle (rad)
Apparent frequency, f_p (Hz)

Figure B.13a

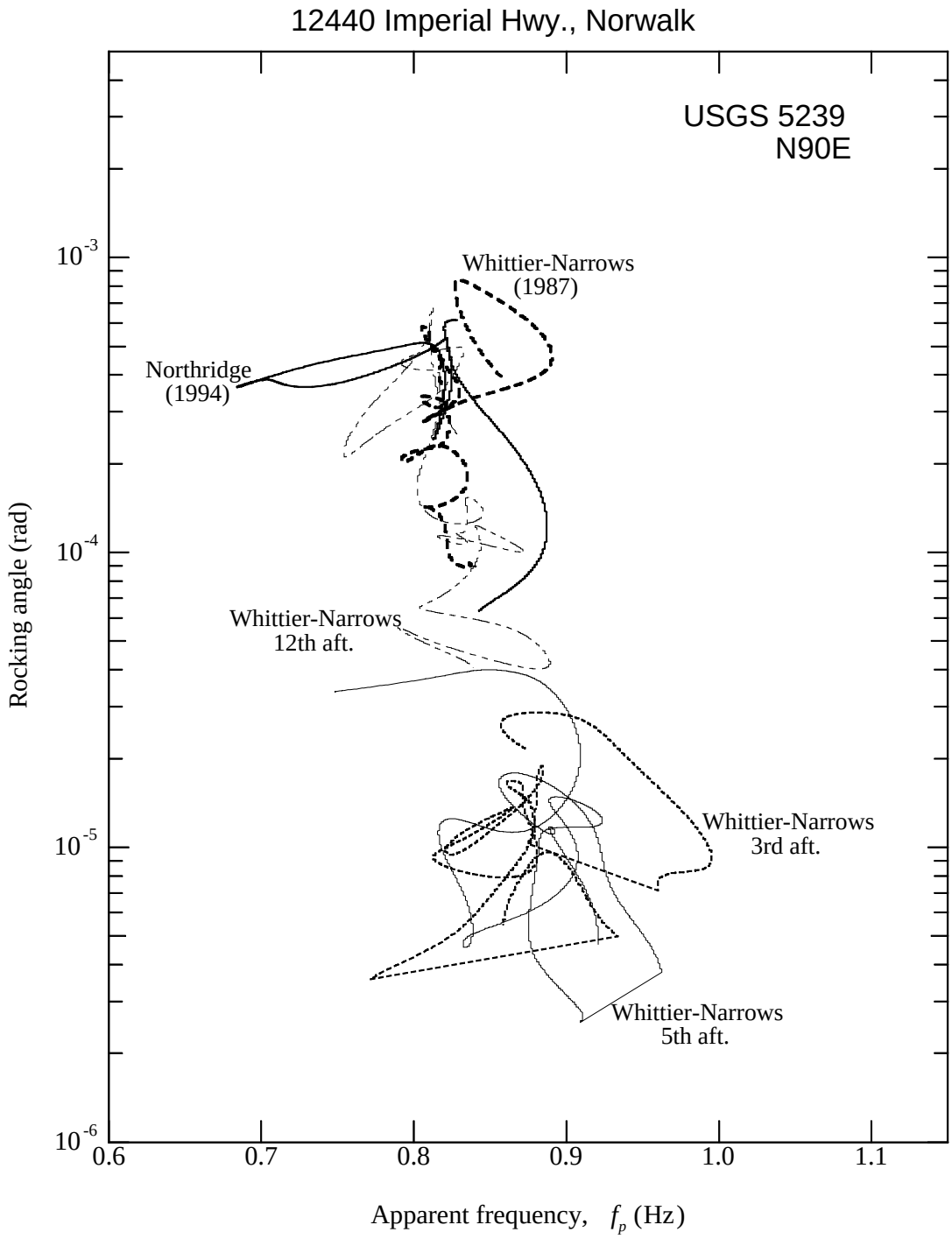
12440 Imperial Hwy., Norwalk
USGS 5239
N90E
Whittier-Narrows
(1987)
Northridge
(1994)
Whittier-Narrows
12th aft.
Whittier-Narrows
3rd aft.
Whittier-Narrows
5th aft.
Rocking angle (rad)
10-3
10-4
10-5
10-6
0.6
0.7
0.8
0.9
1.0
1.1
Apparent frequency, f_p (Hz)

Figure B.13b

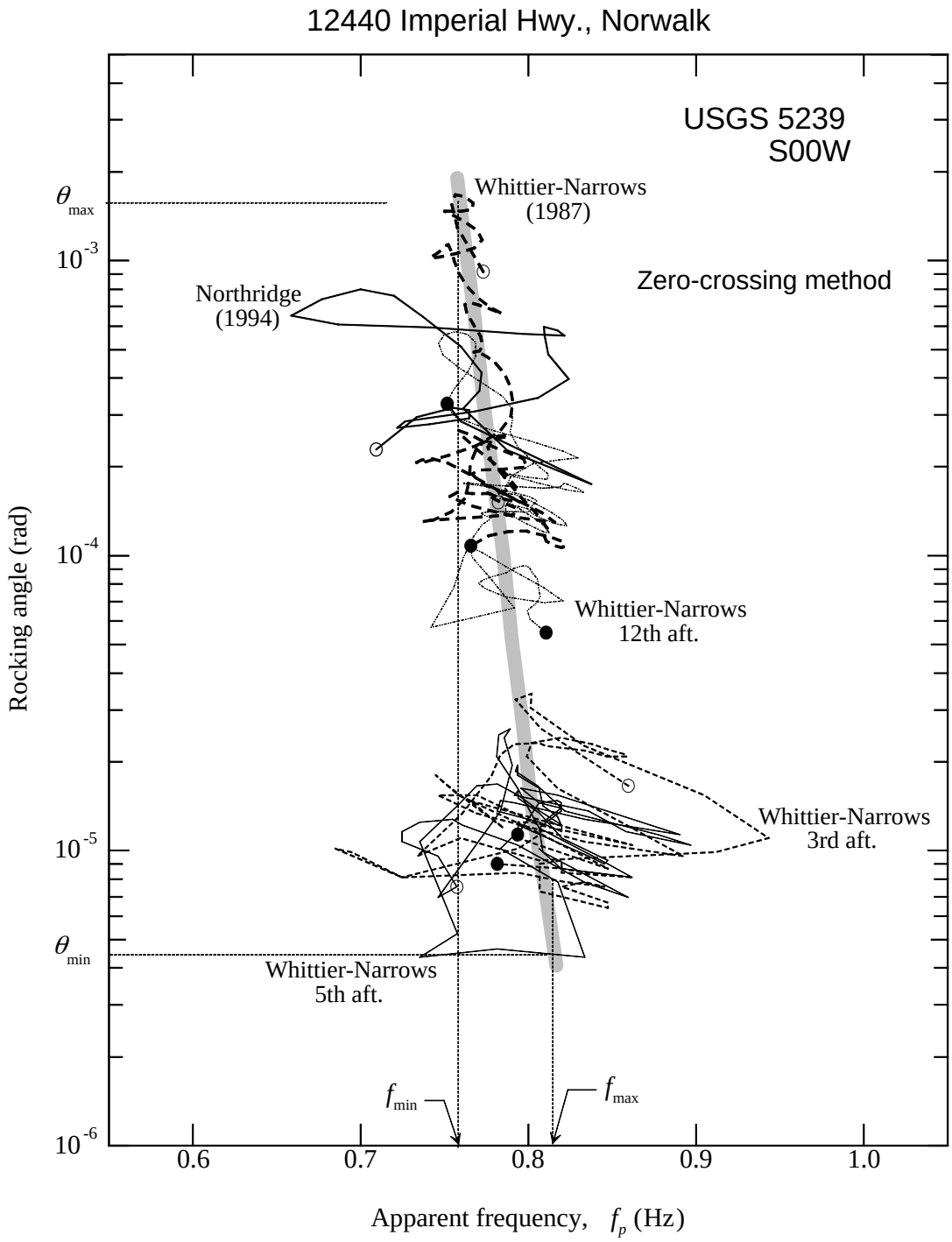
12440 Imperial Hwy., Norwalk
USGS 5239
S00W
Zero-crossing method
Whittier-Narrows
(1987)
Northridge
(1994)
Whittier-Narrows
12th aft.
Whittier-Narrows
3rd aft.
Whittier-Narrows
5th aft.
θmax
θmin
fmin
fmax
10-3
10-4
10-5
10-6
0.6
0.7
0.8
0.9
1.0
Rocking angle (rad)
Apparent frequency, fp (Hz)

Figure B.13c

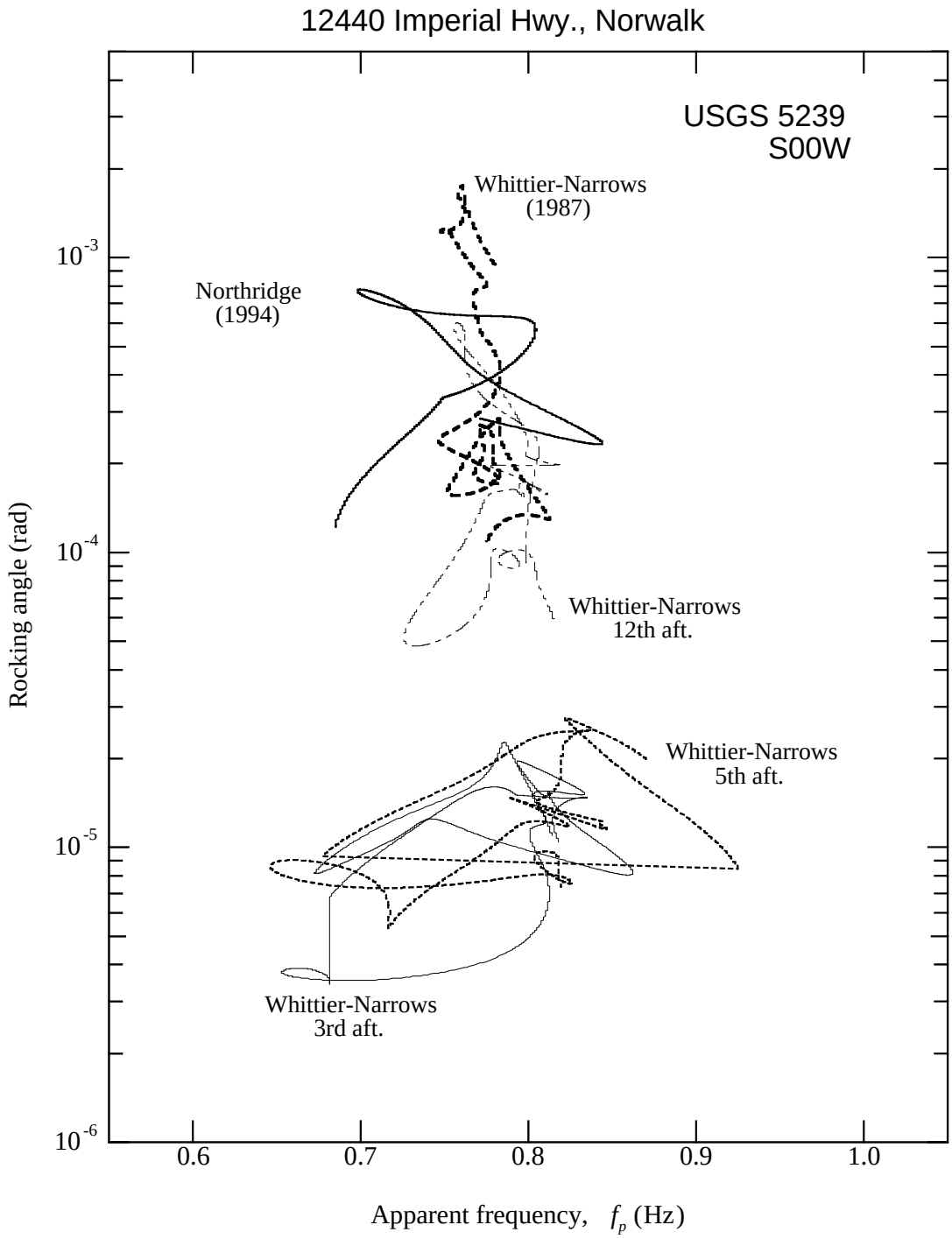
12440 Imperial Hwy., Norwalk
USGS 5239
S00W
Whittier-Narrows
(1987)
Northridge
(1994)
Whittier-Narrows
12th aft.
Whittier-Narrows
5th aft.
Whittier-Narrows
3rd aft.
Rocking angle (rad)
10-3
10-4
10-5
10-6
0.6
0.7
0.8
0.9
1.0
Apparent frequency, fp (Hz)

Figure B.13d

2005 N. Highland Ave.

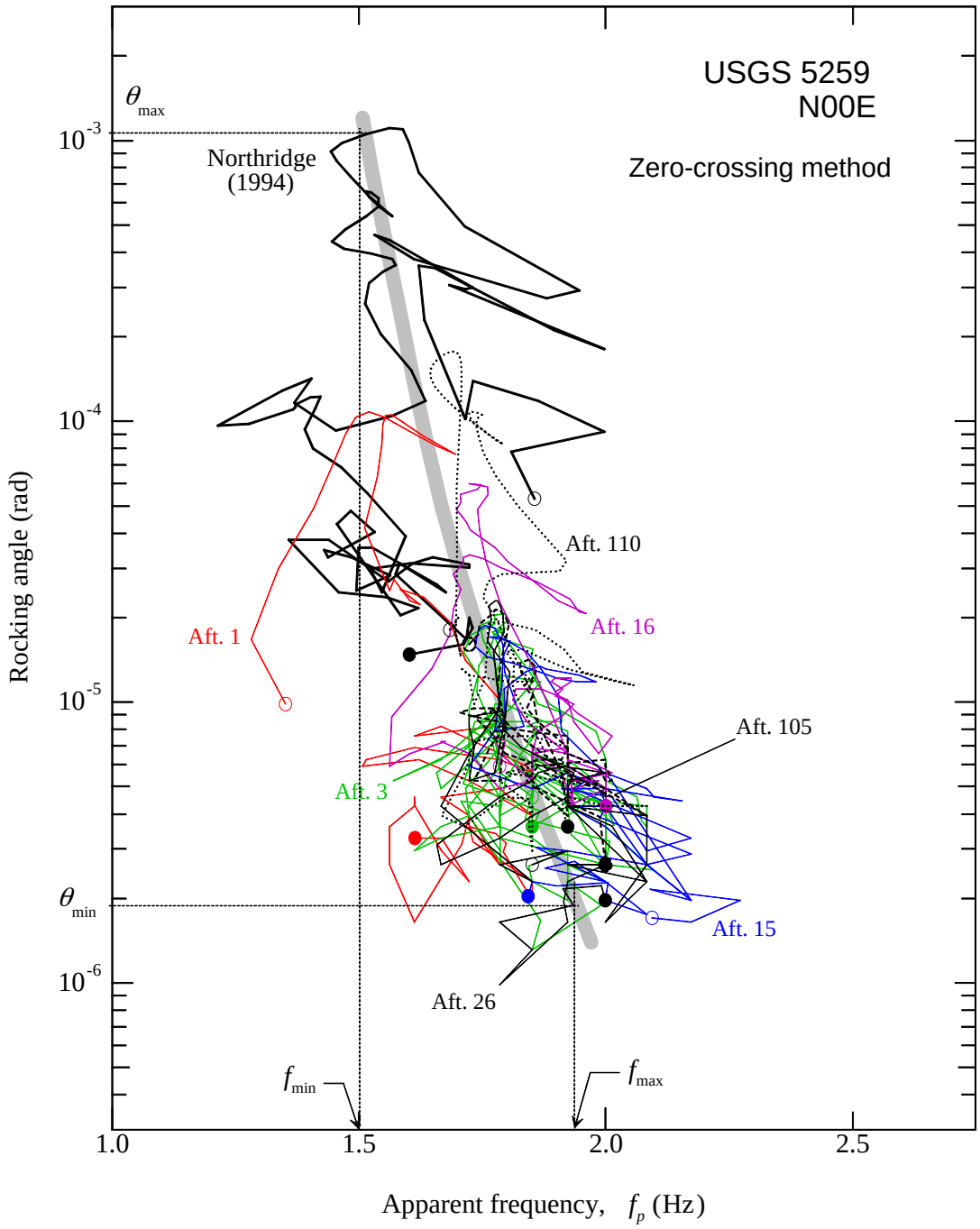

Figure B.14a

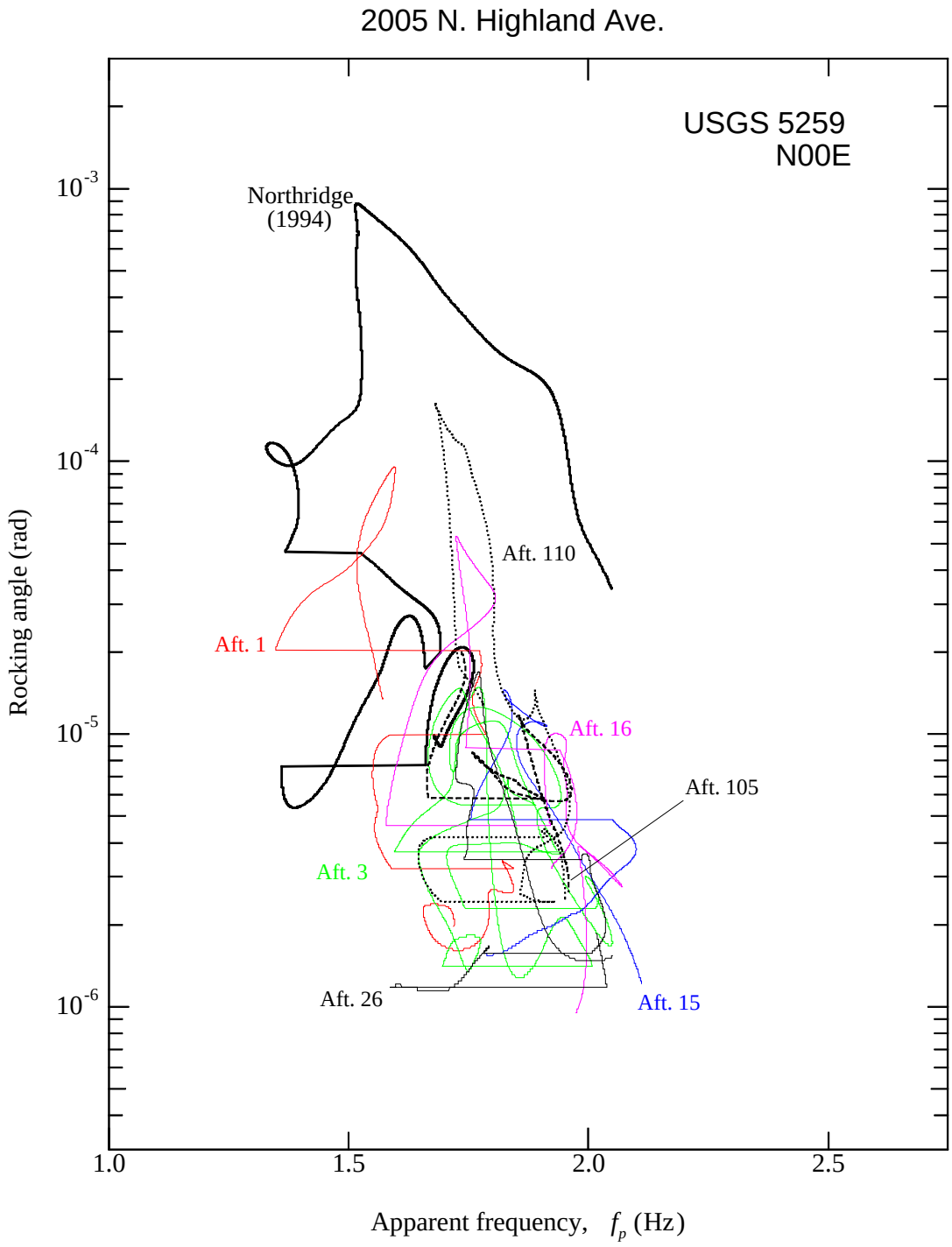
2005 N. Highland Ave.
USGS 5259
N00E
Northridge
(1994)
Aft. 110
Aft. 1
Aft. 16
Aft. 105
Aft. 3
Aft. 26
Aft. 15
Rocking angle (rad)
10^{-3}
10^{-4}
10^{-5}
10^{-6}
1.0
1.5
2.0
2.5
Apparent frequency, f_p (Hz)

Figure B.14b

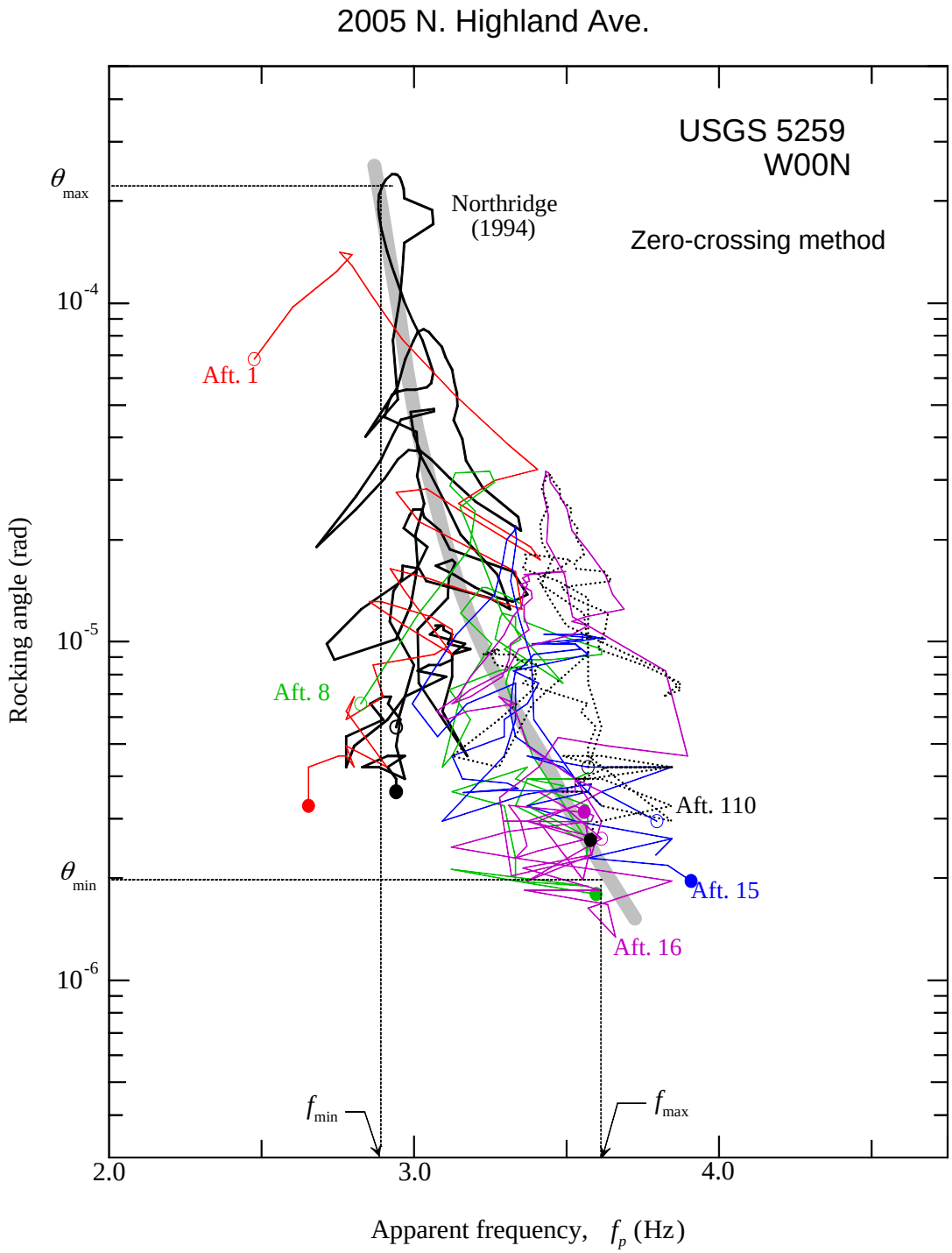
2005 N. Highland Ave.
USGS 5259
W00N
Zero-crossing method
Northridge
(1994)
Aft. 1
Aft. 8
Aft. 110
Aft. 15
Aft. 16
θ_{max}
θ_{min}
10^{-4}
10^{-5}
10^{-6}
Rocking angle (rad)
f_{min}
f_{max}
2.0
3.0
4.0
Apparent frequency, f_p (Hz)

Figure B.14c

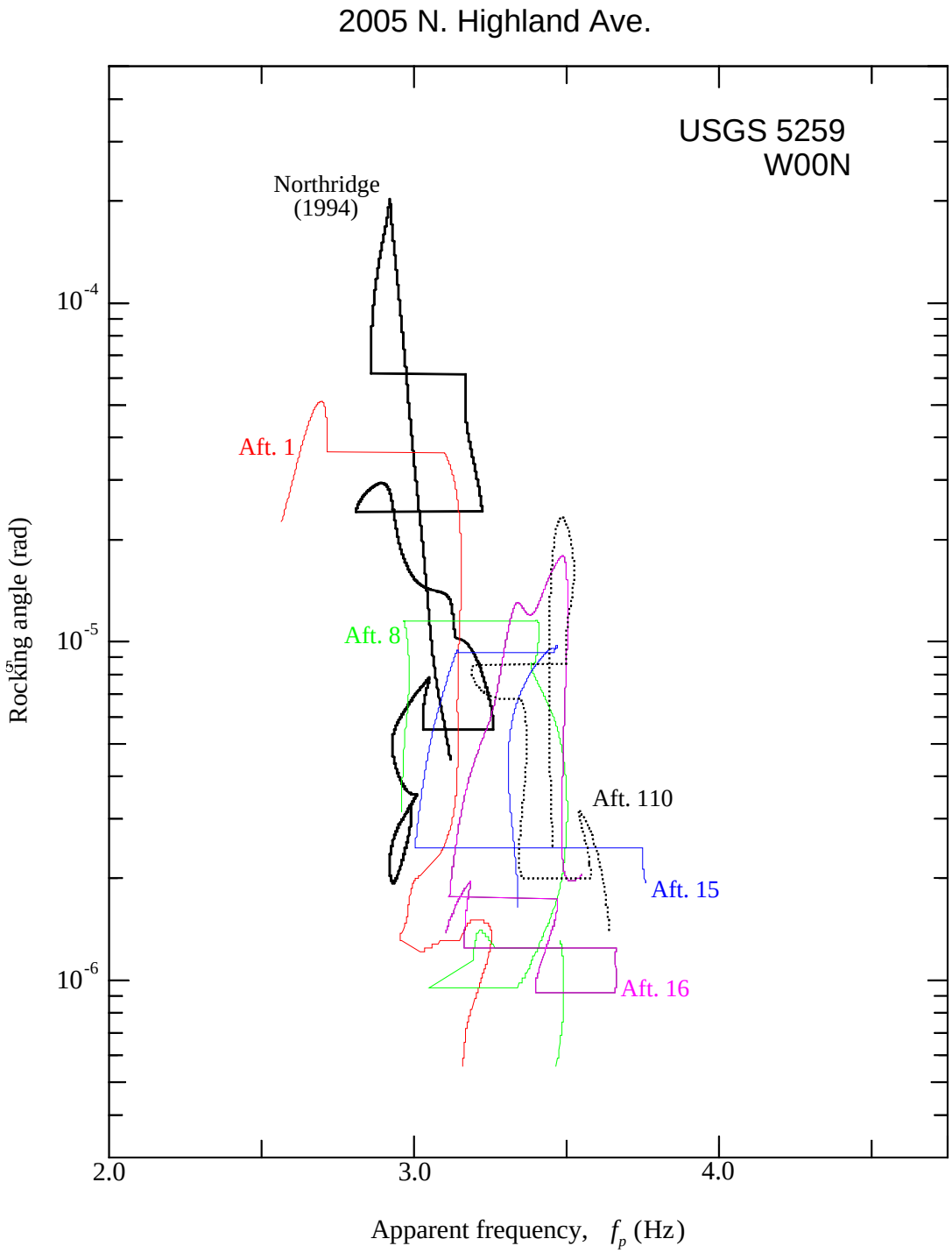
2005 N. Highland Ave.
USGS 5259
W00N
Northridge
(1994)
Aft. 1
Aft. 8
Aft. 110
Aft. 15
Aft. 16
10^{-4}
10^{-5}
10^{-6}
Rocking angle (rad)
2.0
3.0
4.0
Apparent frequency, f_p (Hz)

Figure B.14d

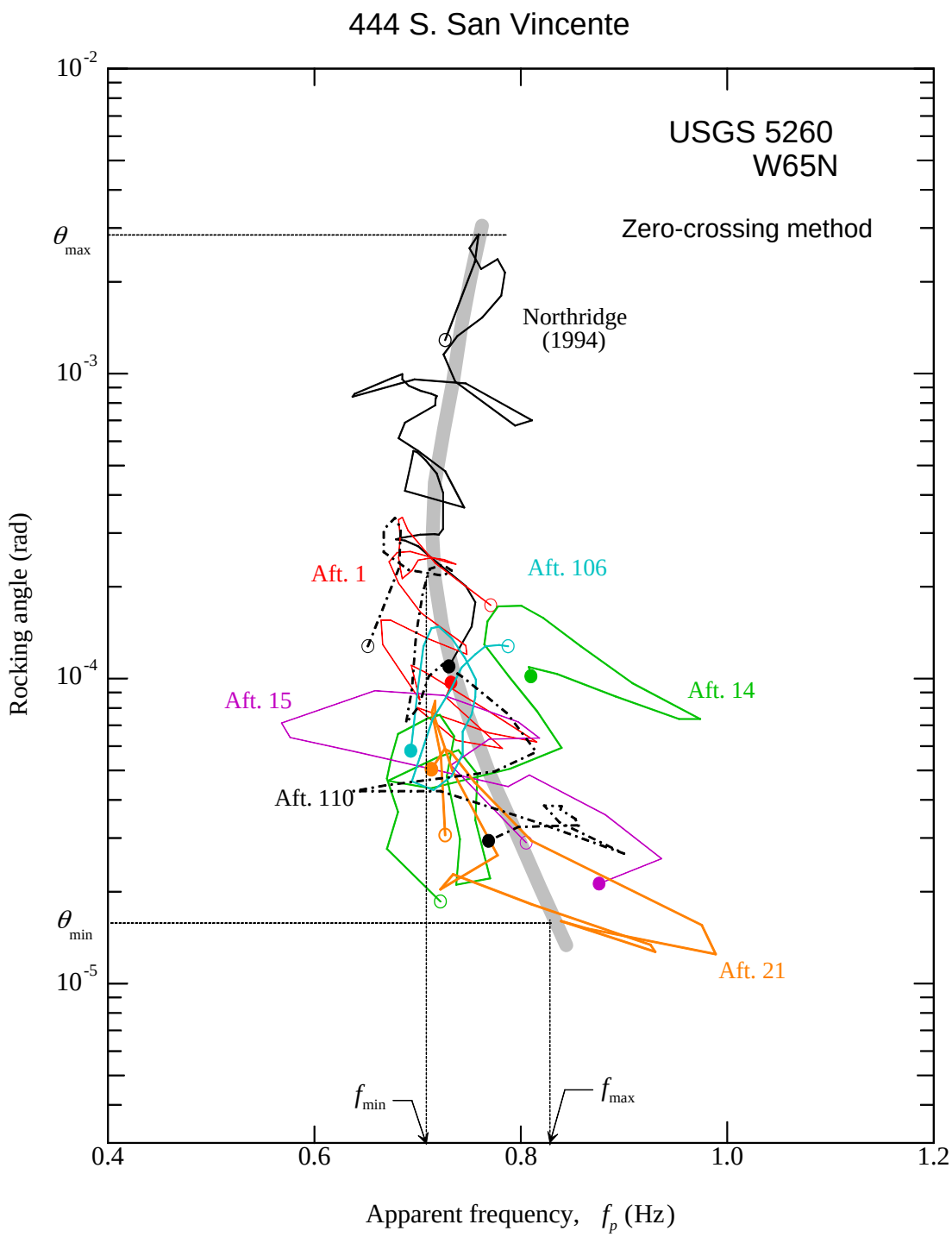
444 S. San Vincente
USGS 5260
W65N
Zero-crossing method
Northridge
(1994)
Aft. 1
Aft. 106
Aft. 14
Aft. 15
Aft. 110
Aft. 21
θ_{max}
θ_{min}
f_{min}
f_{max}
10^{-2}
10^{-3}
10^{-4}
10^{-5}
0.4
0.6
0.8
1.0
1.2
Rocking angle (rad)
Apparent frequency, f_p (Hz)

Figure B.15a

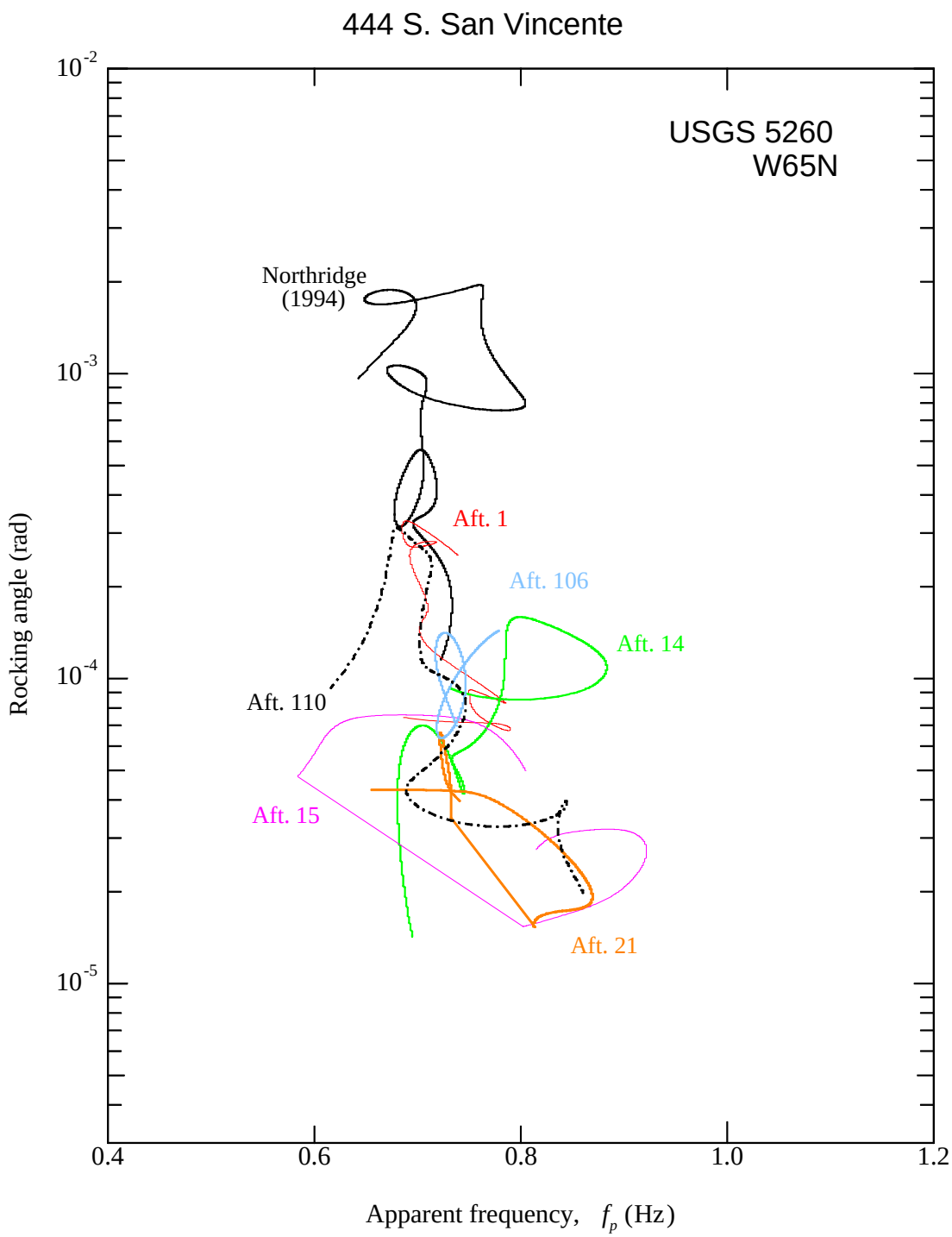
444 S. San Vincente
USGS 5260
W65N
Northridge
(1994)
Aft. 1
Aft. 106
Aft. 14
Aft. 110
Aft. 15
Aft. 21
Rocking angle (rad)
Apparent frequency, f_p (Hz)
10^{-2}
10^{-3}
10^{-4}
10^{-5}
0.4
0.6
0.8
1.0
1.2

Figure B.15b

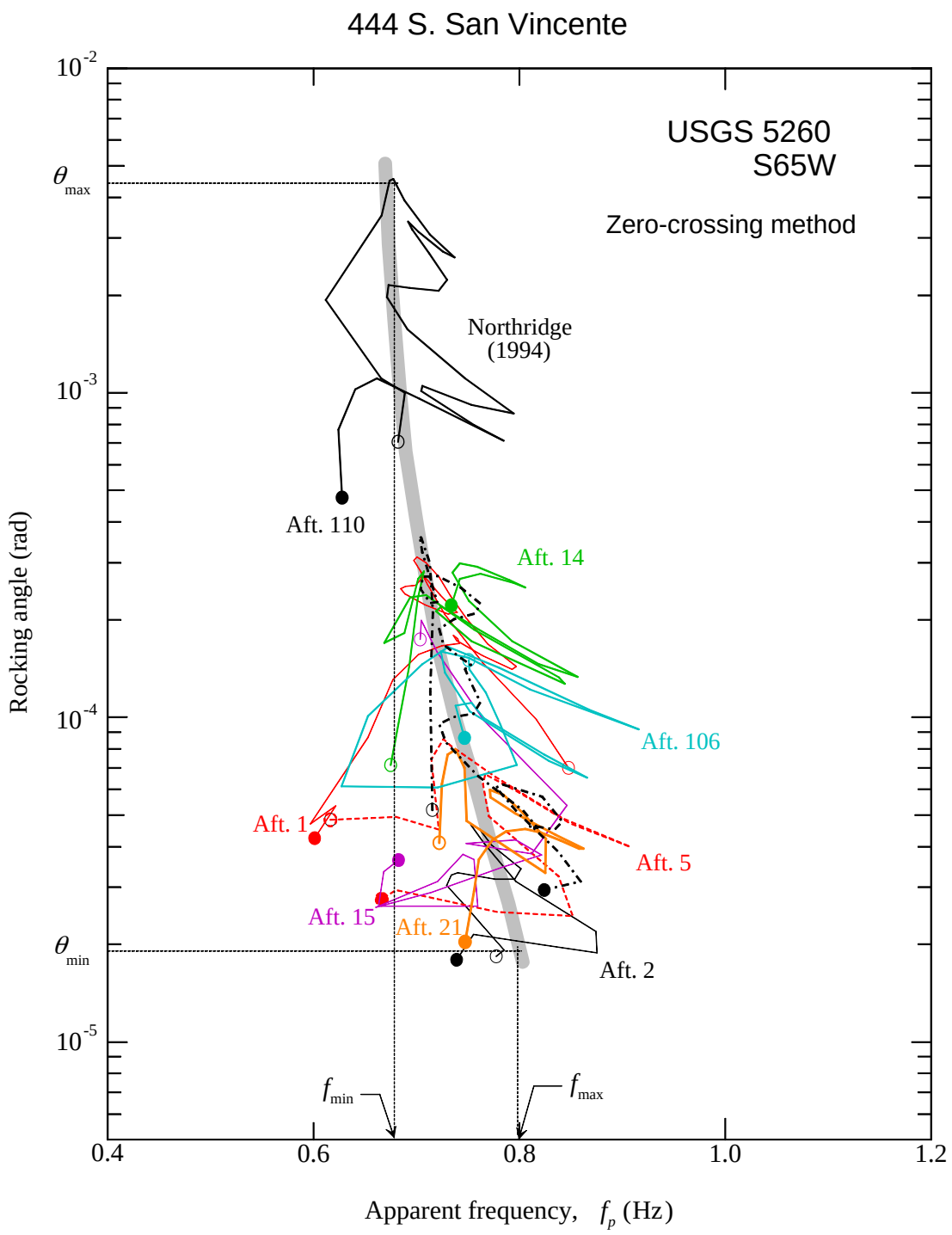
444 S. San Vincente
USGS 5260
S65W
Zero-crossing method
Northridge
(1994)
Aft. 110
Aft. 14
Aft. 106
Aft. 1
Aft. 5
Aft. 15
Aft. 21
Aft. 2
θ_{max}
θ_{min}
f_{min}
f_{max}
10^{-2}
10^{-3}
10^{-4}
10^{-5}
0.4
0.6
0.8
1.0
1.2
Rocking angle (rad)
Apparent frequency, f_p (Hz)

Figure B.15c

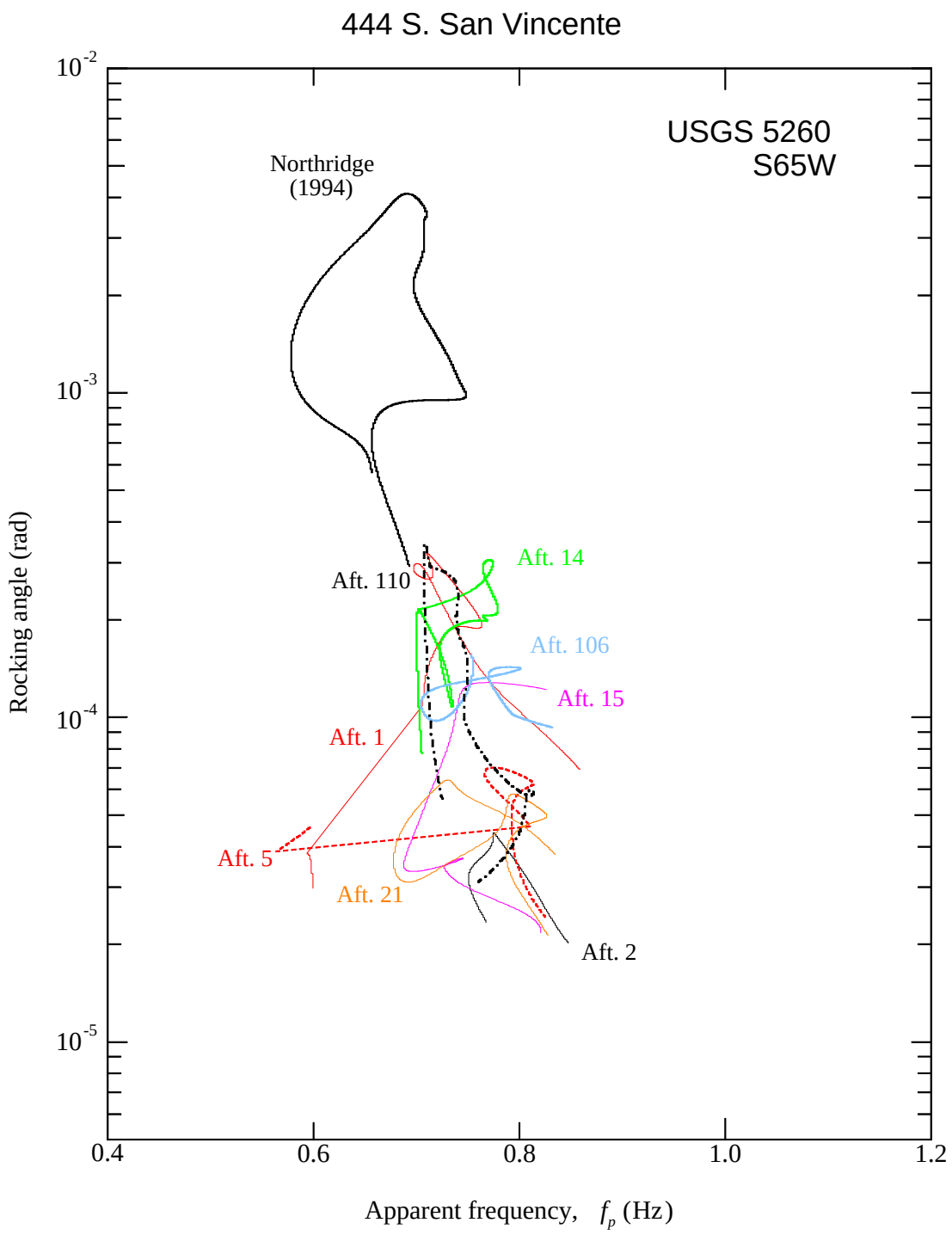
444 S. San Vincente
USGS 5260
S65W
Northridge
(1994)
Aft. 110
Aft. 14
Aft. 106
Aft. 15
Aft. 1
Aft. 5
Aft. 21
Aft. 2
Rocking angle (rad)
Apparent frequency, f_p (Hz)
10^{-2}
10^{-3}
10^{-4}
10^{-5}
0.4
0.6
0.8
1.0
1.2

Figure B.15d

10660 Wilshire Blvd.

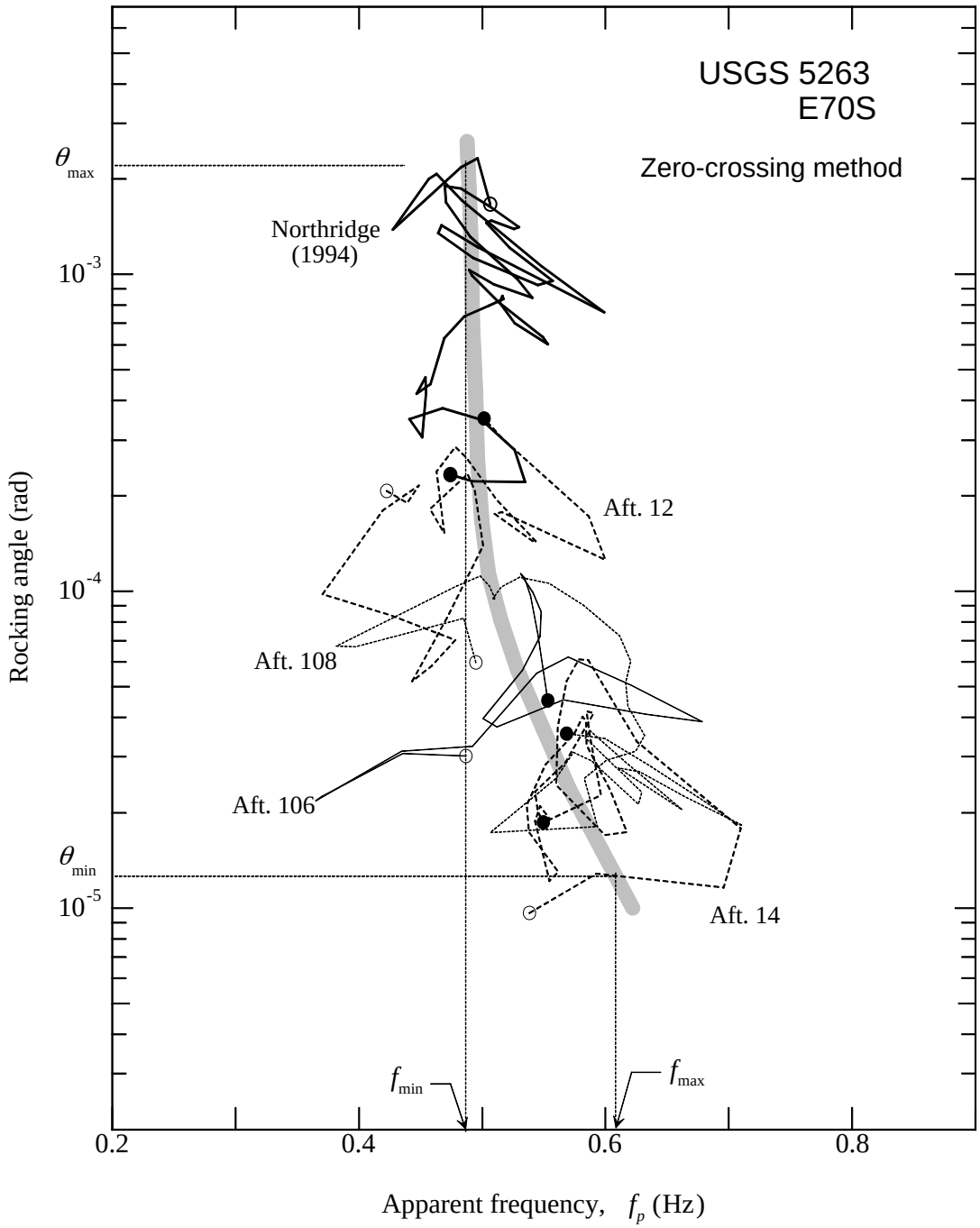

Figure B.16a

10660 Wilshire Blvd.

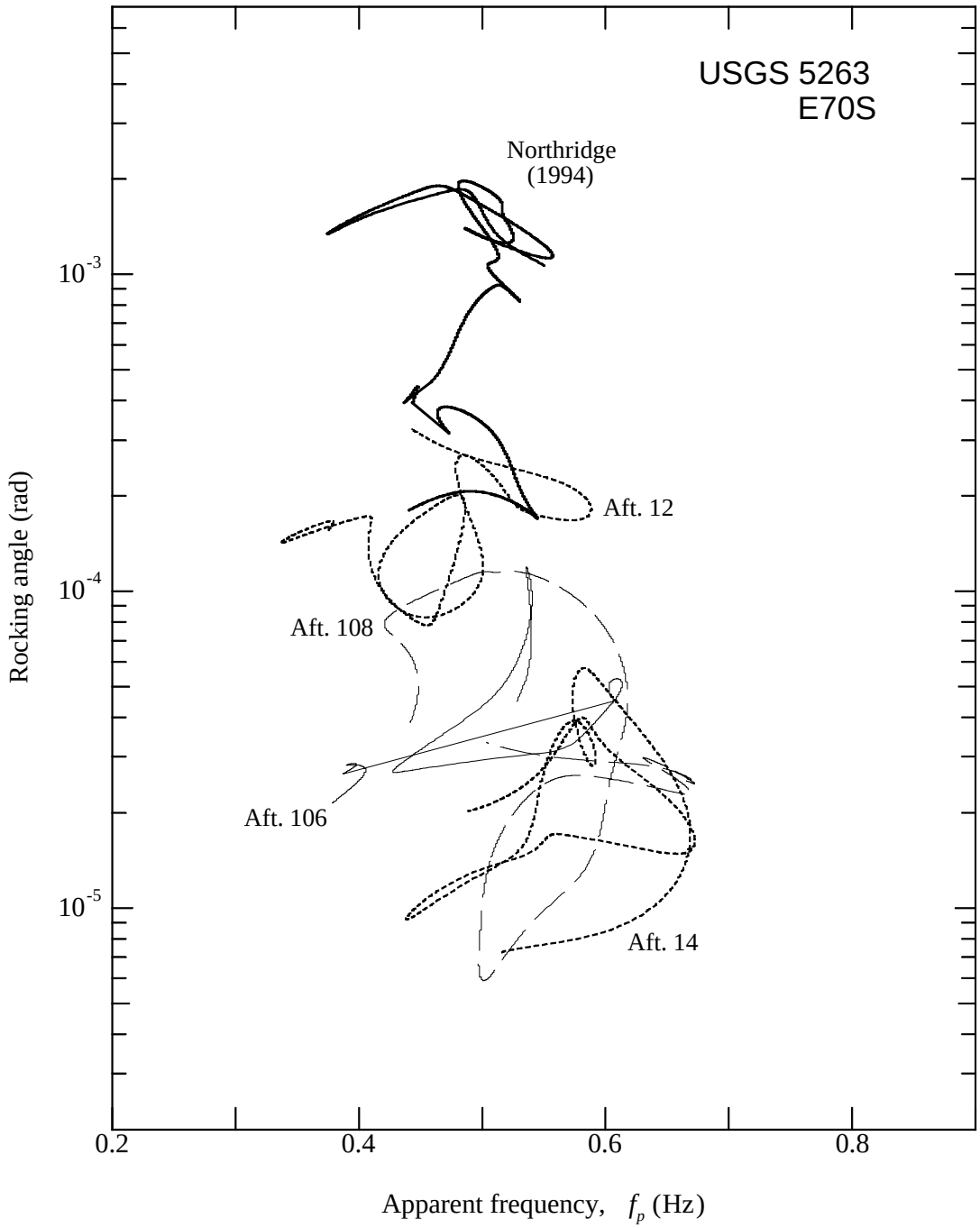

Figure B.16b

10660 Wilshire Blvd.

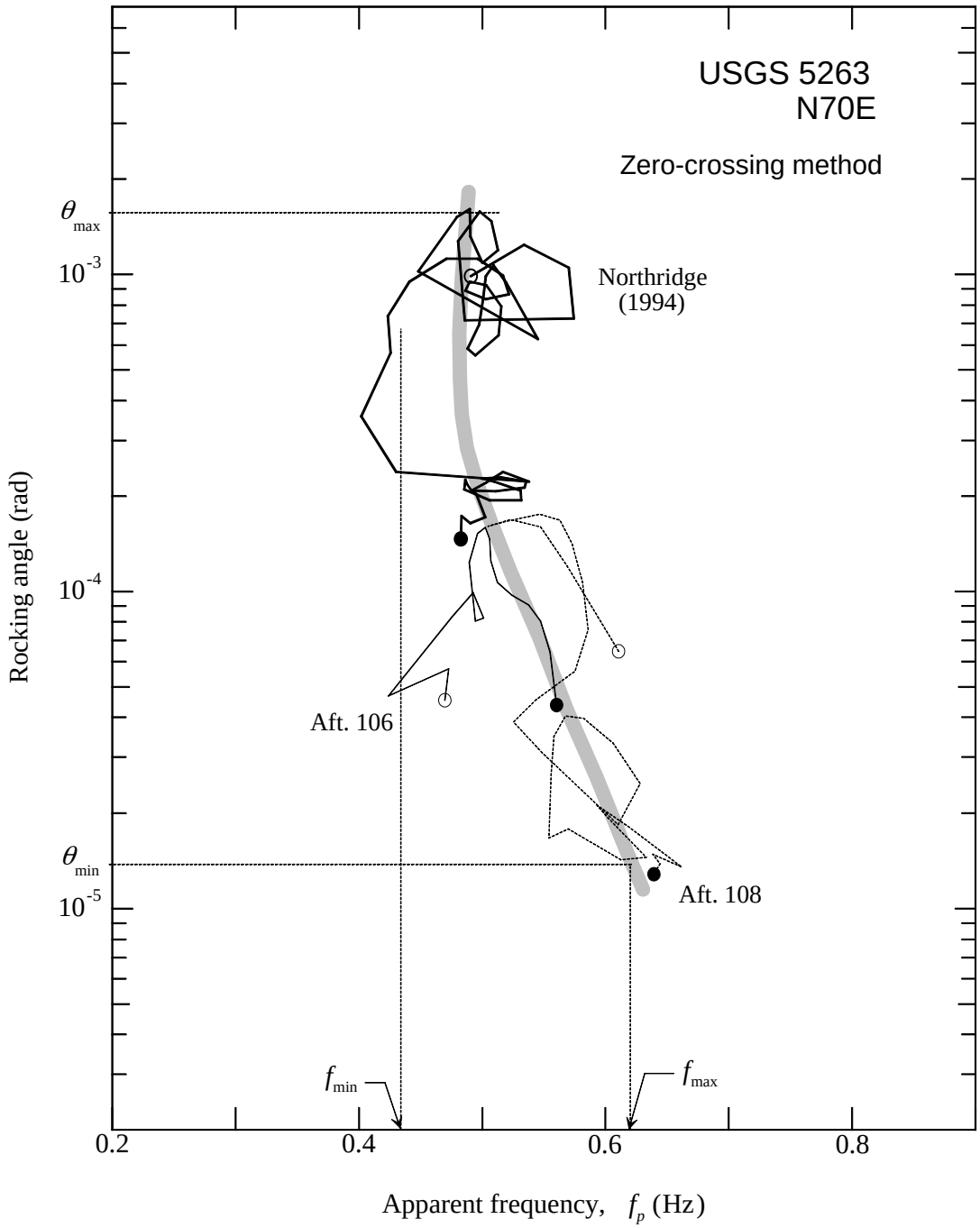

Figure B.16c

10660 Wilshire Blvd.

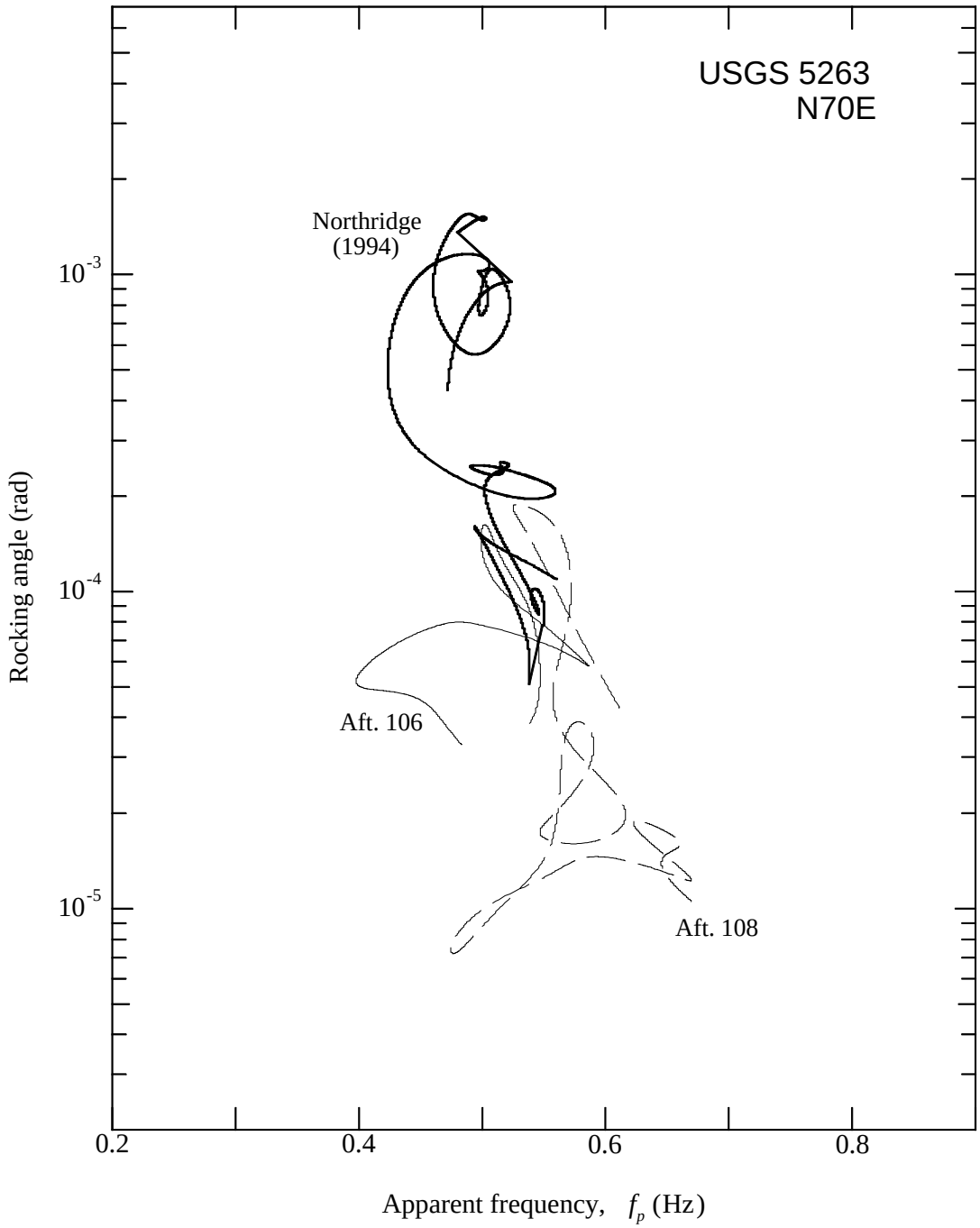

Figure B.16d

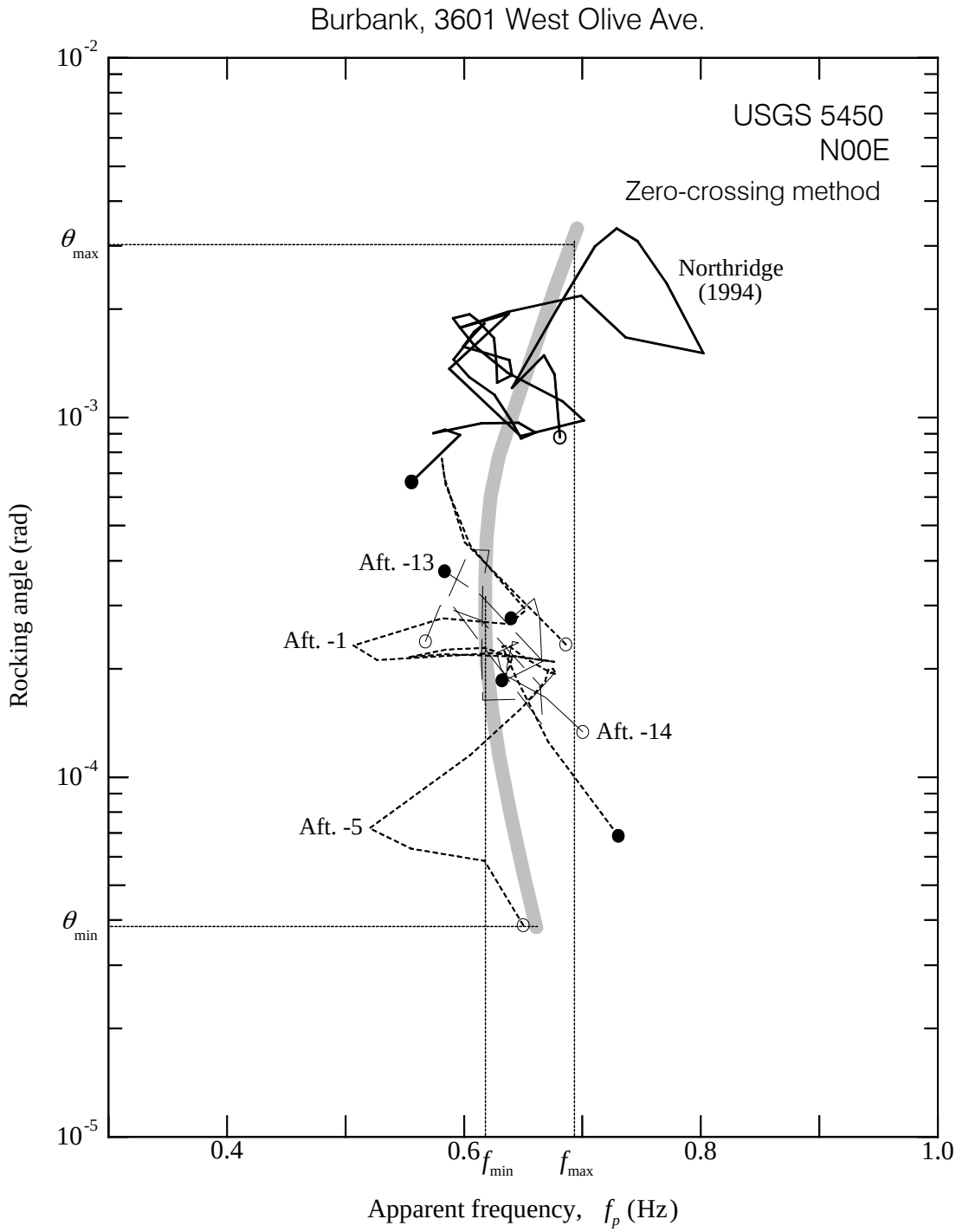
Burbank, 3601 West Olive Ave.
USGS 5450
N00E
Zero-crossing method
Northridge
(1994)
Aft. -13
Aft. -1
Aft. -14
Aft. -5
θ_{max}
θ_{min}
10^{-2}
10^{-3}
10^{-4}
10^{-5}
Rocking angle (rad)
0.4
0.6
0.8
1.0
f_{min}
f_{max}
Apparent frequency, f_p (Hz)

Figure B.17a

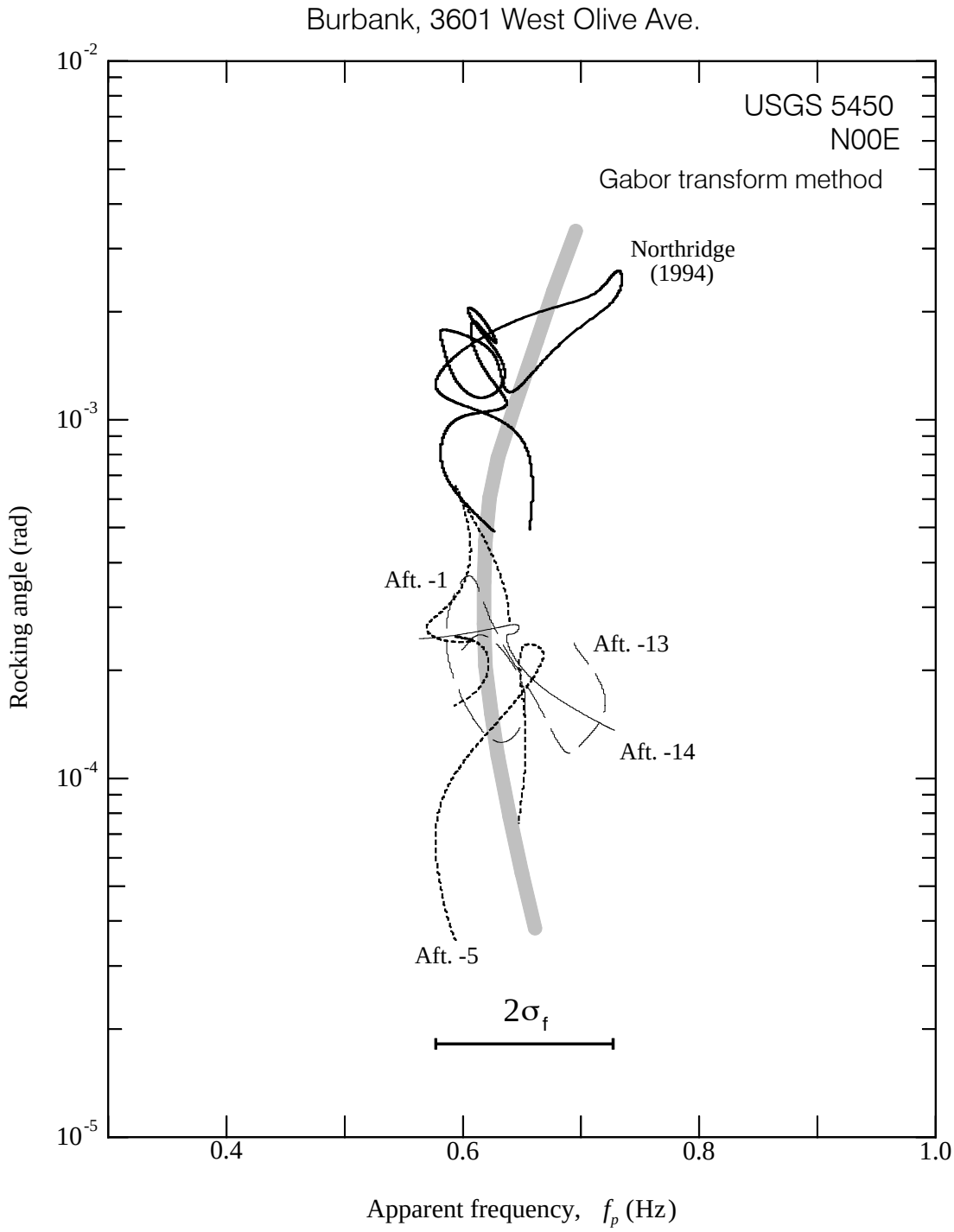
Burbank, 3601 West Olive Ave.
USGS 5450
N00E
Gabor transform method
Northridge
(1994)
Aft. -1
Aft. -13
Aft. -14
Aft. -5
2σf
Rocking angle (rad)
Apparent frequency, fp (Hz)
10-2
10-3
10-4
10-5
0.4
0.6
0.8
1.0

.Figure B.17b

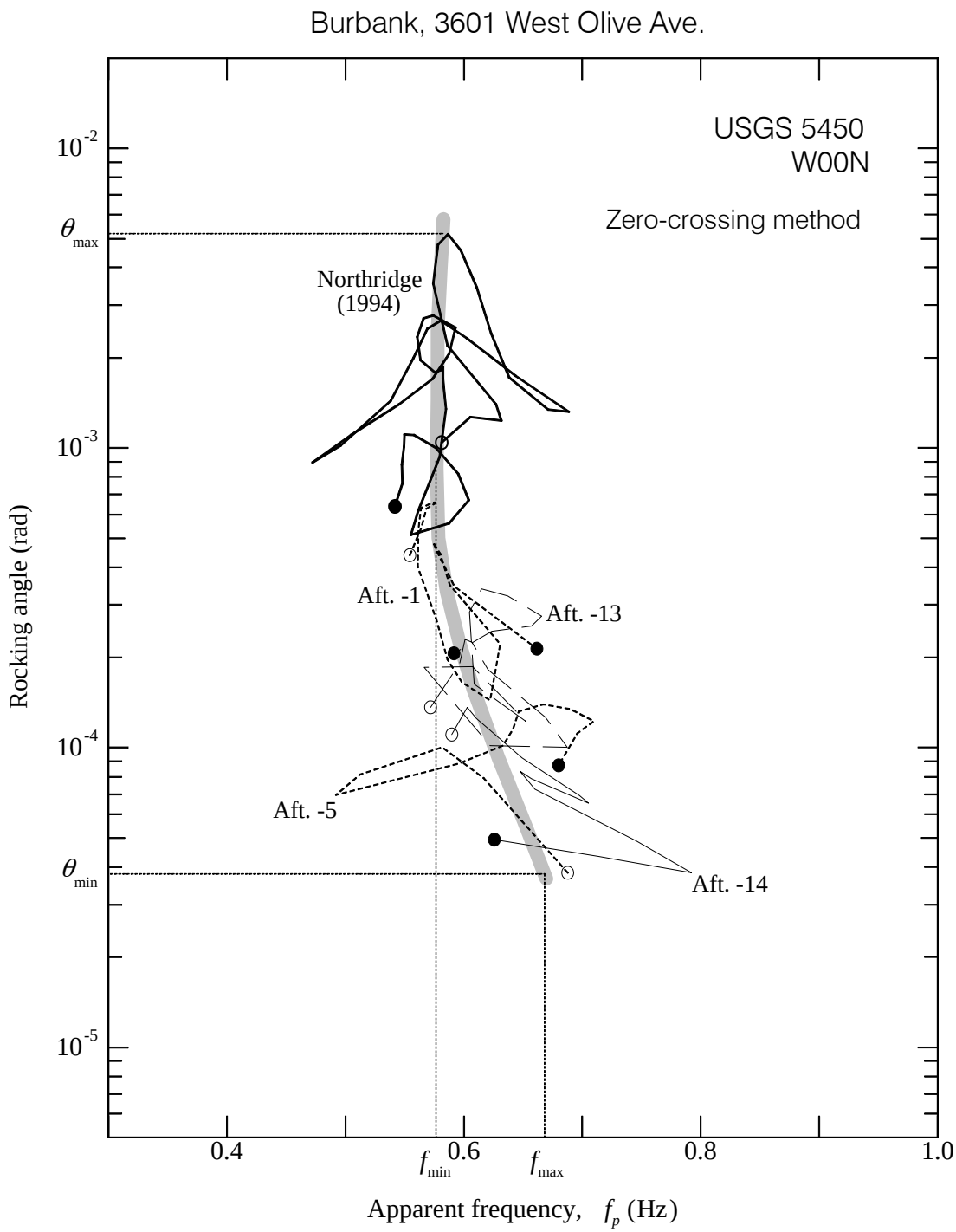
Burbank, 3601 West Olive Ave.
USGS 5450
W00N
Zero-crossing method
Northridge
(1994)
Aft. -1
Aft. -13
Aft. -5
Aft. -14
θ_{max}
θ_{min}
10^{-2}
10^{-3}
10^{-4}
10^{-5}
Rocking angle (rad)
0.4
0.6
0.8
1.0
f_{min}
f_{max}
Apparent frequency, f_p (Hz)

.

Figure B.17c

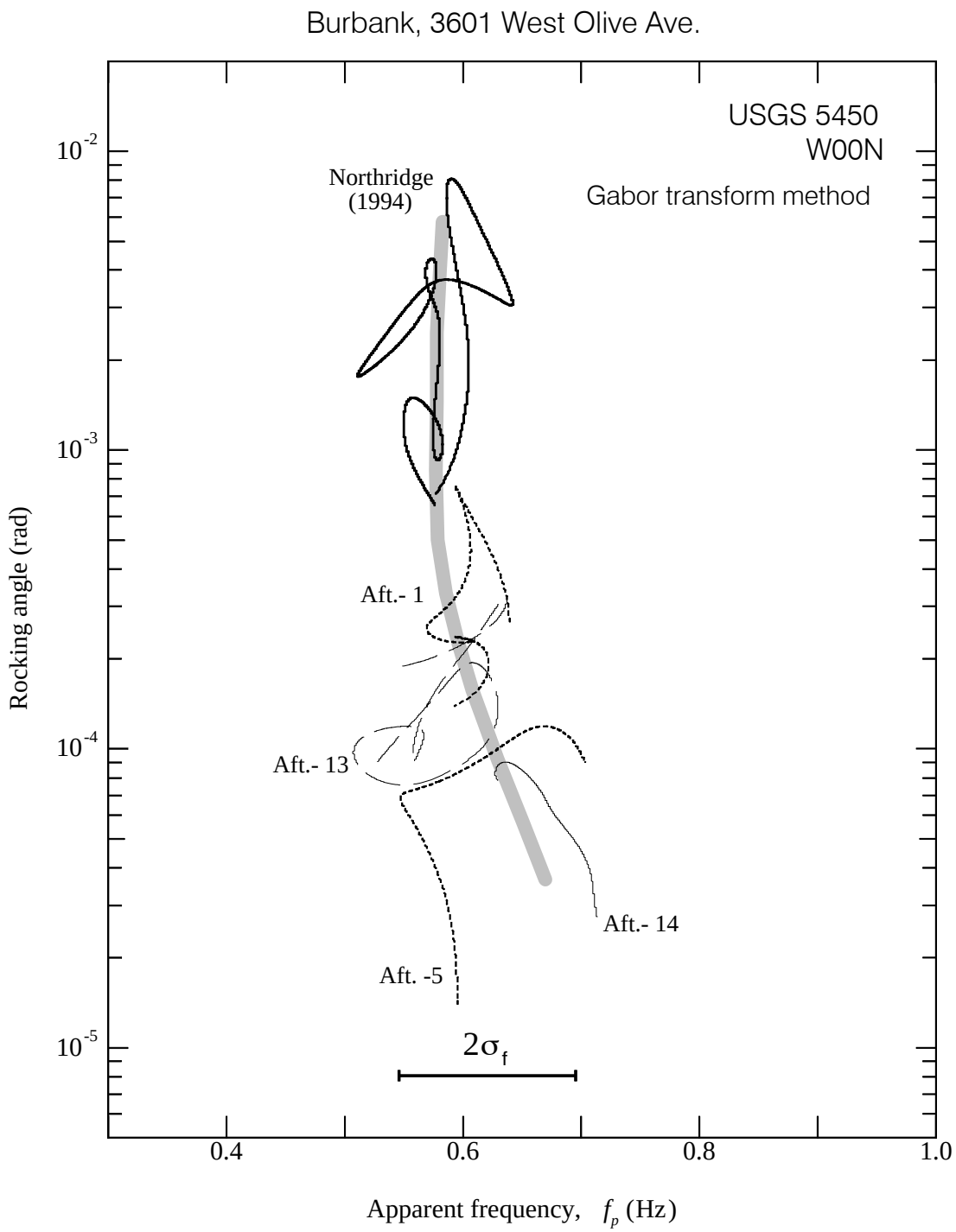
Burbank, 3601 West Olive Ave.
USGS 5450
W00N
Gabor transform method
Northridge
(1994)
Aft.- 1
Aft.- 13
Aft.- 14
Aft. -5
2σf
10-2
10-3
10-4
10-5
Rocking angle (rad)
0.4
0.6
0.8
1.0
Apparent frequency, fp (Hz)

Figure B.17d

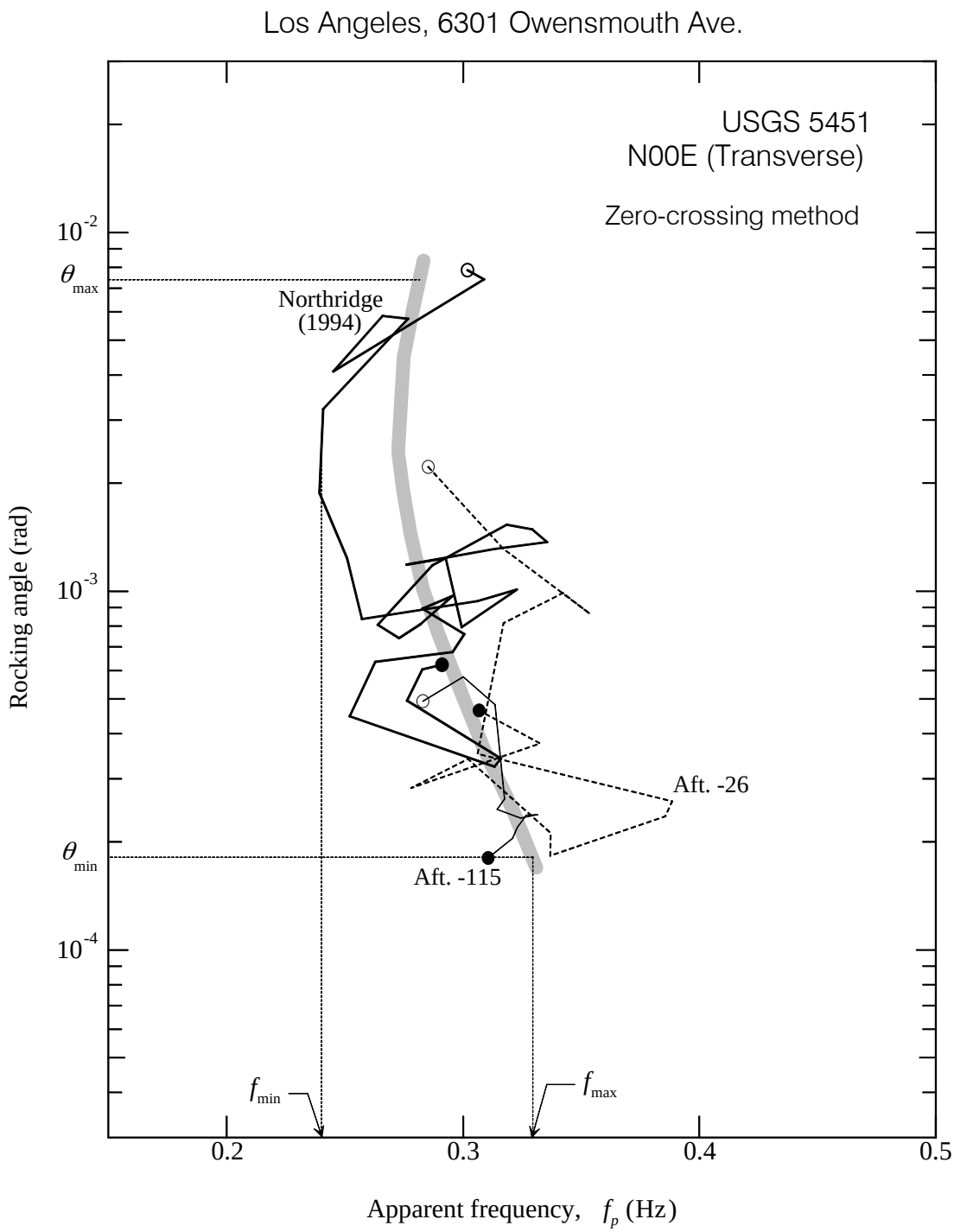
Los Angeles, 6301 Owensmouth Ave.
USGS 5451
N00E (Transverse)
Zero-crossing method
Northridge
(1994)
Aft. -26
Aft. -115
θ_{max}
θ_{min}
10^{-2}
10^{-3}
10^{-4}
f_{min}
f_{max}
0.2
0.3
0.4
0.5
Rocking angle (rad)
Apparent frequency, f_p (Hz)

.

Figure B.18a

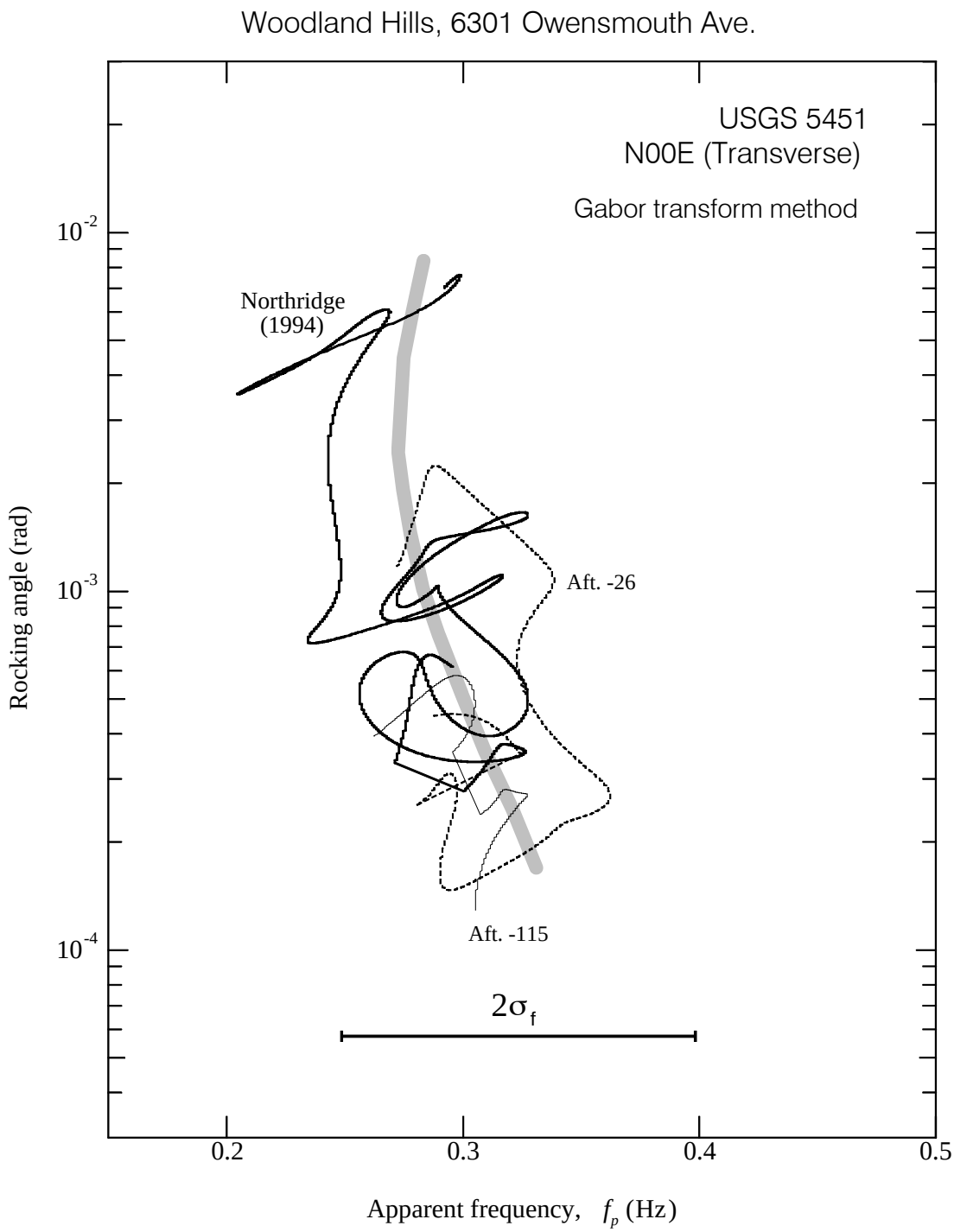
Woodland Hills, 6301 Owensmouth Ave.
USGS 5451
N00E (Transverse)
Gabor transform method
Northridge
(1994)
Aft. -26
Aft. -115
2σf
10-2
10-3
10-4
Rocking angle (rad)
0.2
0.3
0.4
0.5
Apparent frequency, fp (Hz)

Figure B.18b

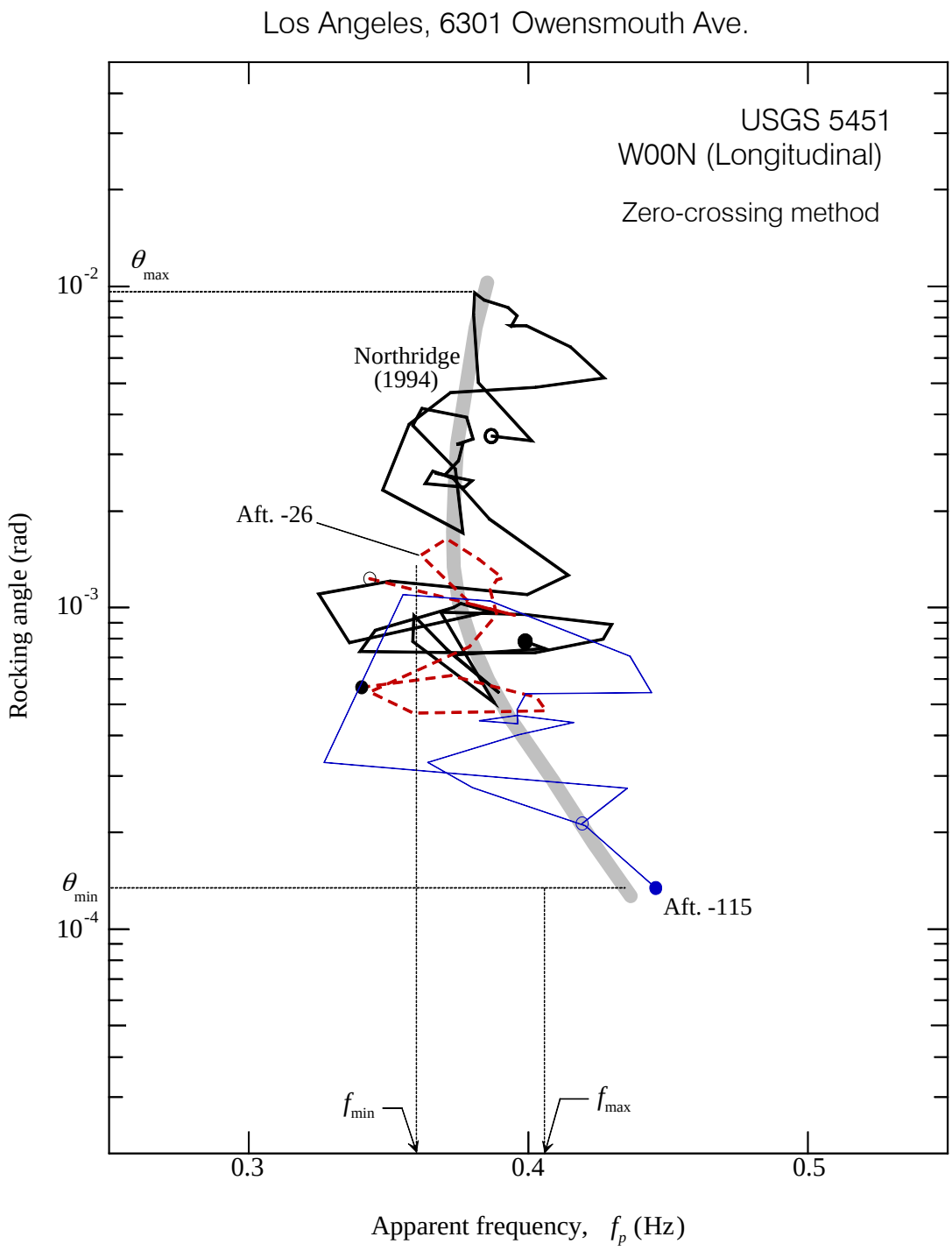
Los Angeles, 6301 Owensmouth Ave.
USGS 5451
W00N (Longitudinal)
Zero-crossing method
θmax
10-2
Northridge
(1994)
Aft. -26
10-3
θmin
10-4
Aft. -115
fmin
fmax
0.3
0.4
0.5
Rocking angle (rad)
Apparent frequency, fp (Hz)

Figure B.18c

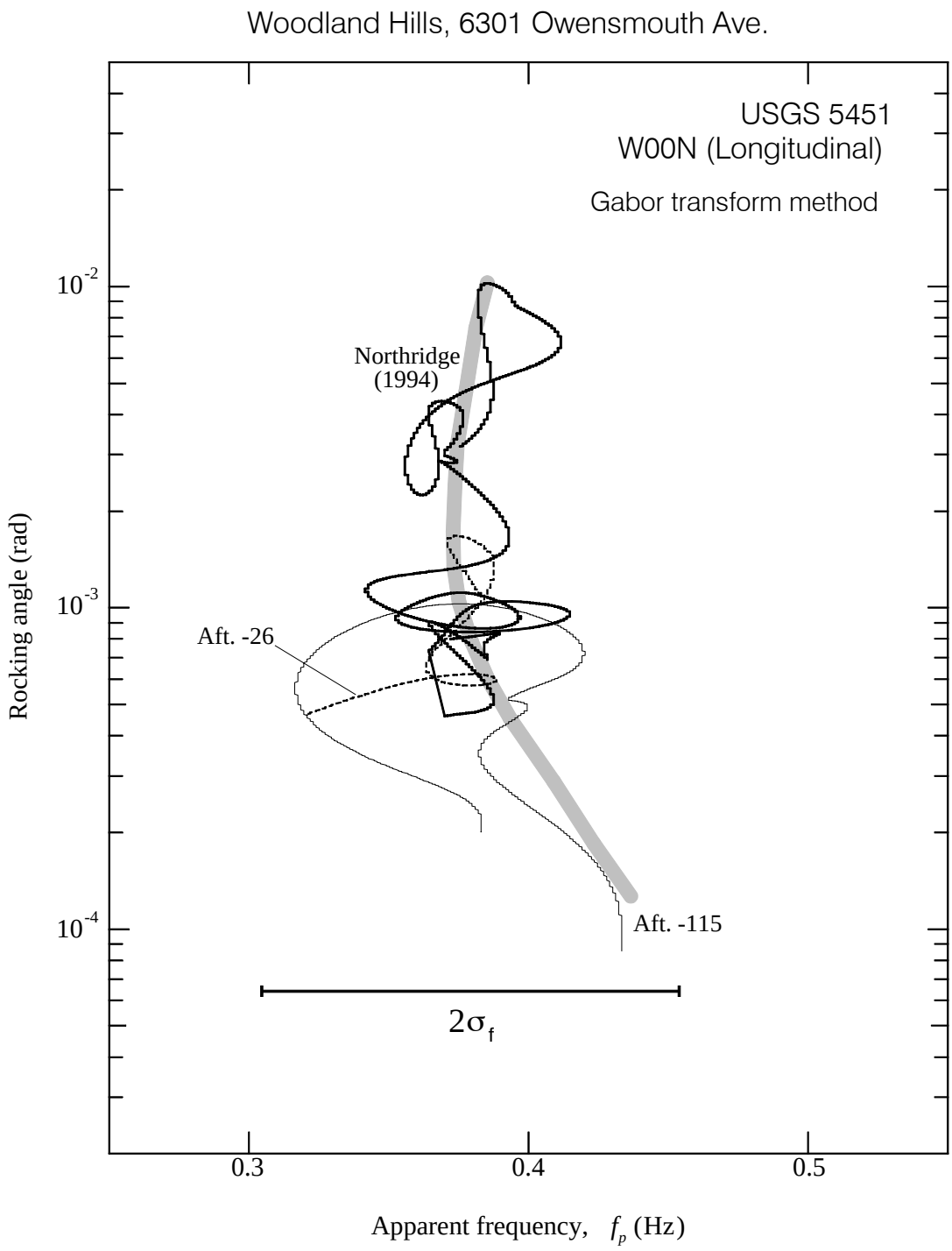
Woodland Hills, 6301 Owensmouth Ave.
USGS 5451
W00N (Longitudinal)
Gabor transform method
Northridge
(1994)
Aft. -26
Aft. -115
$2\sigma_f$
10^{-2}
10^{-3}
10^{-4}
Rocking angle (rad)
0.3
0.4
0.5
Apparent frequency, f_p (Hz)

Figure B.18d

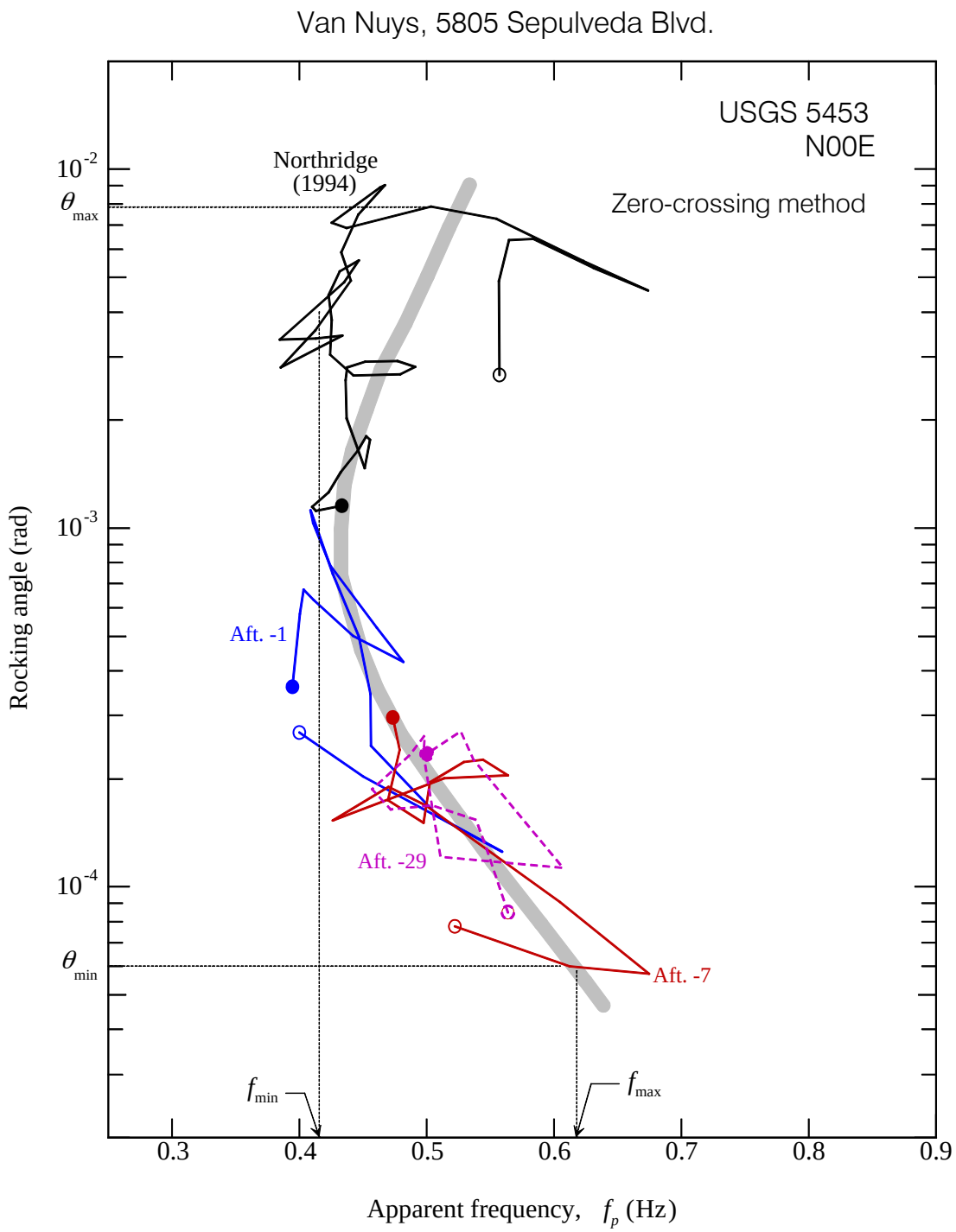
Van Nuys, 5805 Sepulveda Blvd.
USGS 5453
N00E
Zero-crossing method
Northridge
(1994)
Aft. -1
Aft. -29
Aft. -7
10^{-2}
θ_{max}
10^{-3}
10^{-4}
θ_{min}
f_{min}
f_{max}
0.3
0.4
0.5
0.6
0.7
0.8
0.9
Rocking angle (rad)
Apparent frequency, f_p (Hz)

Figure B.19a

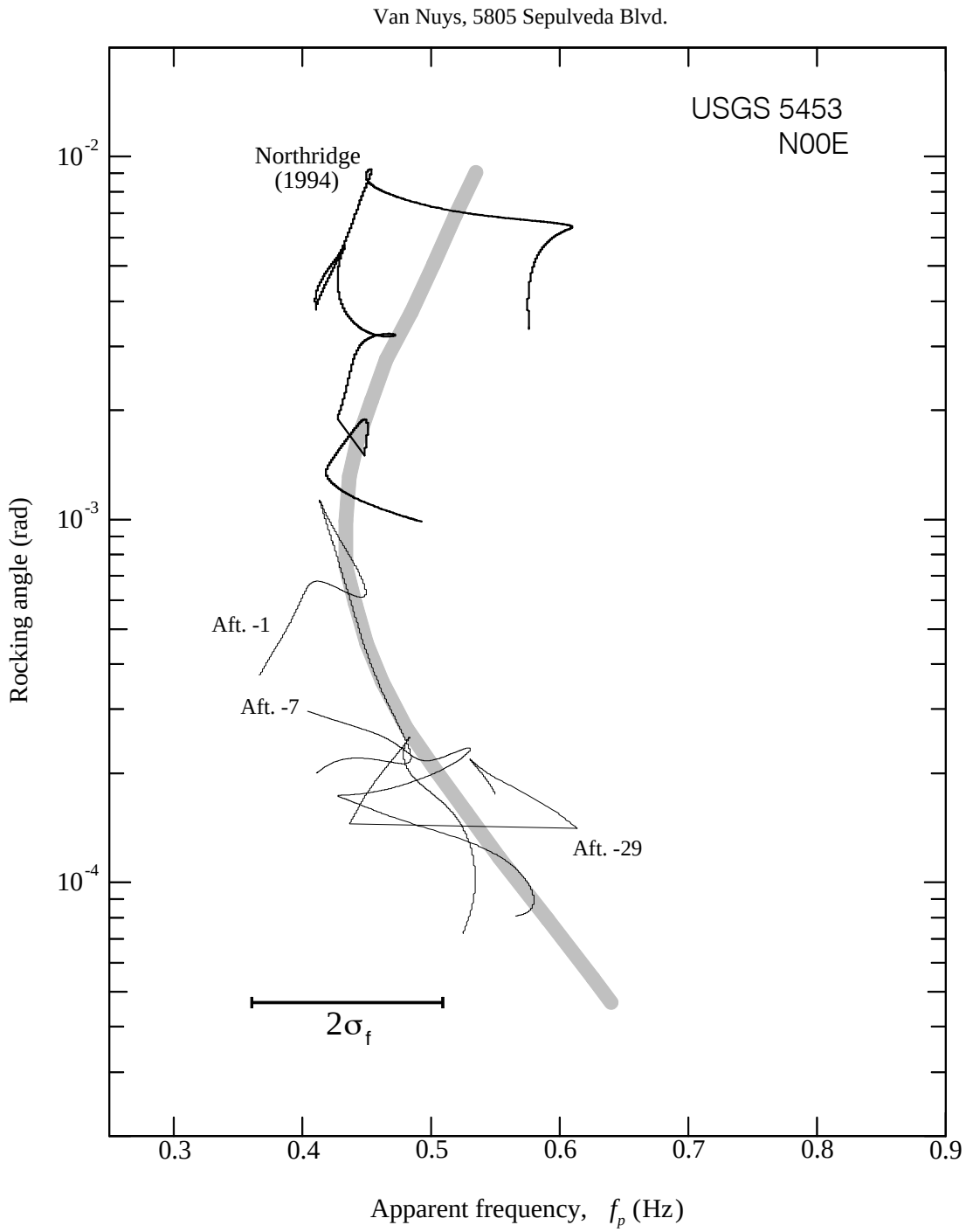
Van Nuys, 5805 Sepulveda Blvd.
USGS 5453
N00E
Northridge
(1994)
Aft. -1
Aft. -7
Aft. -29
$2\sigma_f$
10^{-2}
10^{-3}
10^{-4}
Rocking angle (rad)
0.3
0.4
0.5
0.6
0.7
0.8
0.9
Apparent frequency, f_p (Hz)

Figure B.19b

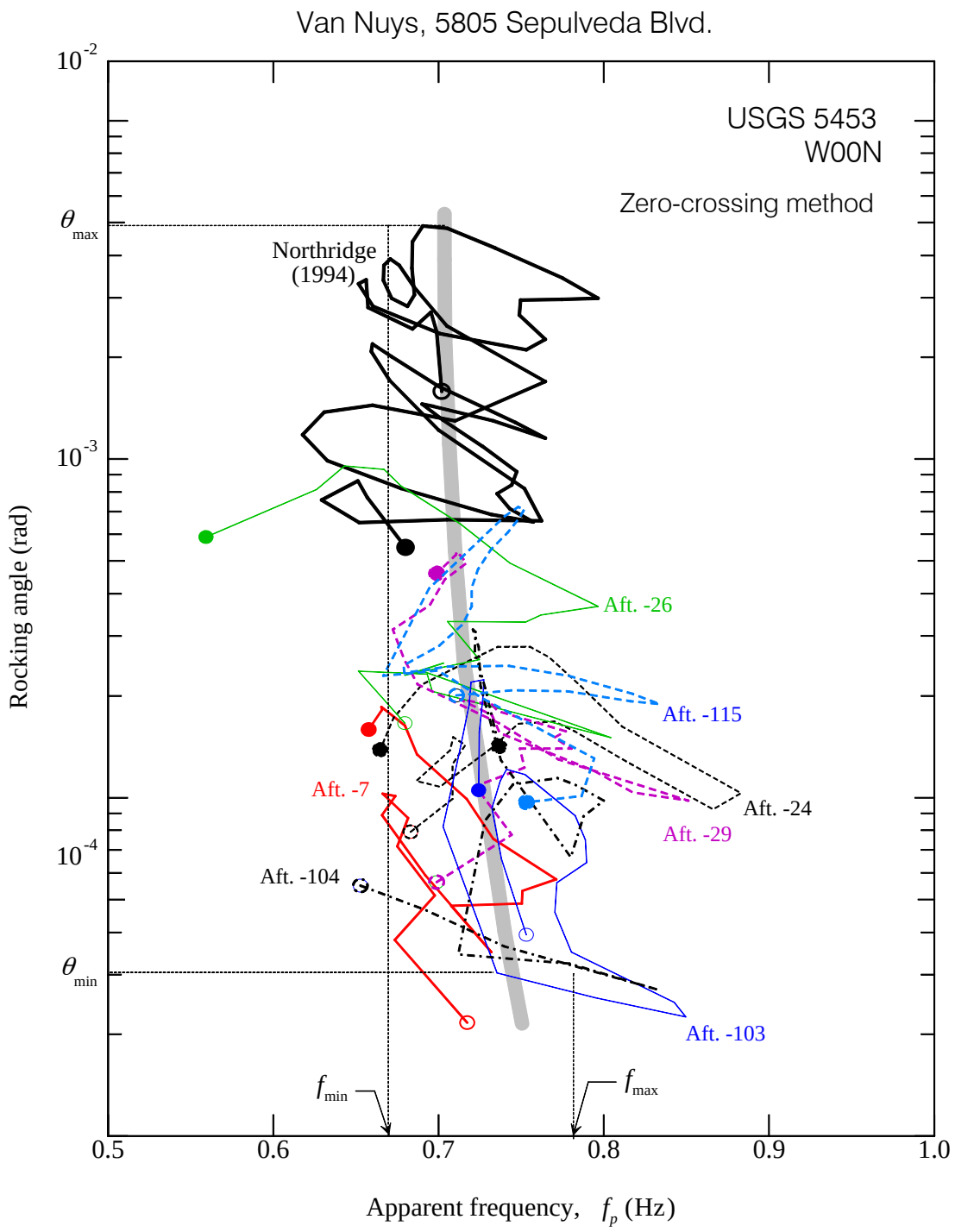
Van Nuys, 5805 Sepulveda Blvd.
USGS 5453
W00N
Zero-crossing method
Northridge
(1994)
Aft. -26
Aft. -115
Aft. -7
Aft. -24
Aft. -29
Aft. -104
Aft. -103
θ_{max}
θ_{min}
f_{min}
f_{max}
10^{-2}
10^{-3}
10^{-4}
0.5
0.6
0.7
0.8
0.9
1.0
Rocking angle (rad)
Apparent frequency, f_p (Hz)

Figure B.19c

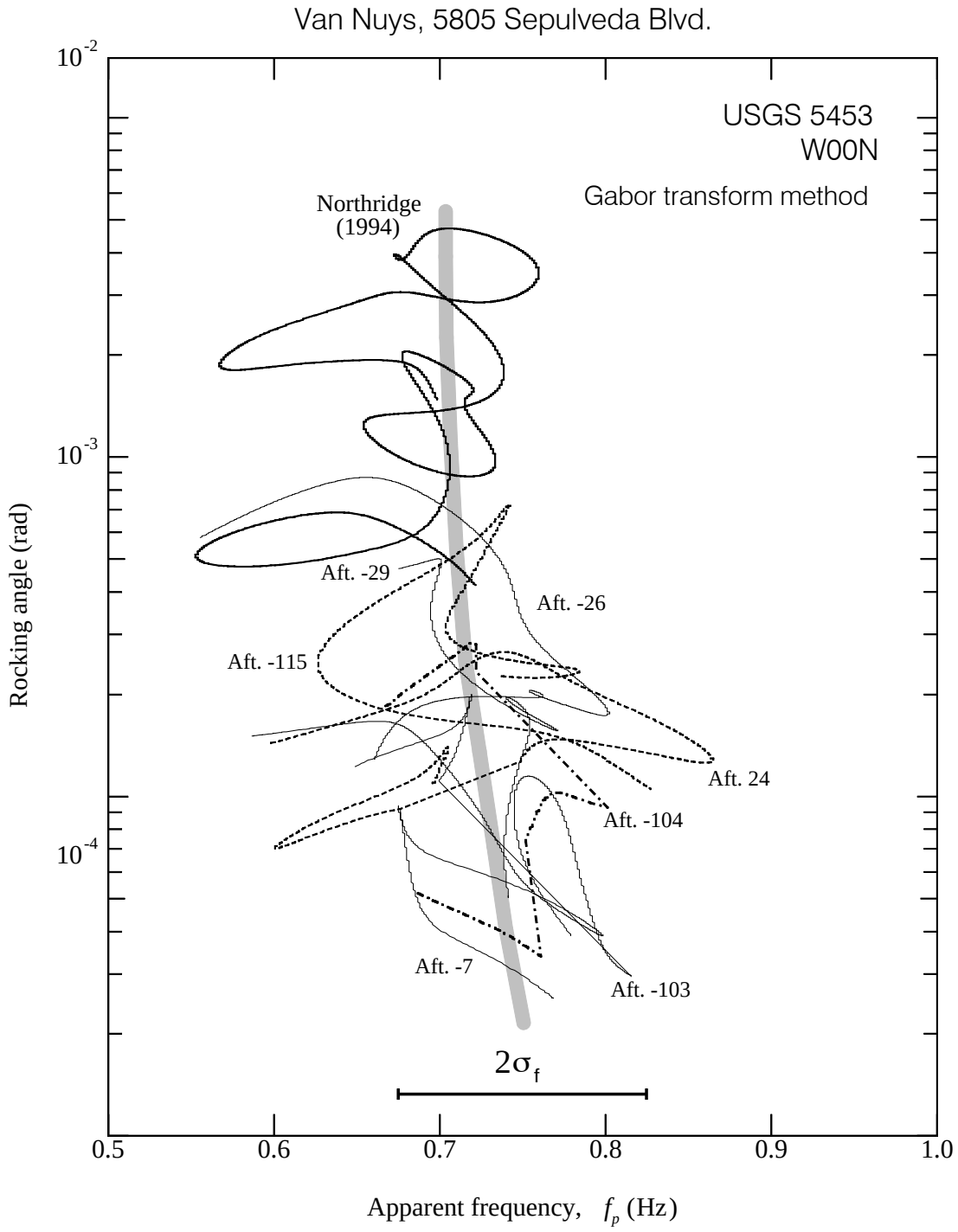
Van Nuys, 5805 Sepulveda Blvd.
USGS 5453
W00N
Gabor transform method
Northridge
(1994)
Aft. -29
Aft. -26
Aft. -115
Aft. 24
Aft. -104
Aft. -7
Aft. -103
2σf
Rocking angle (rad)
Apparent frequency, fp (Hz)
10-2
10-3
10-4
0.5
0.6
0.7
0.8
0.9
1.0

Figure B.19d

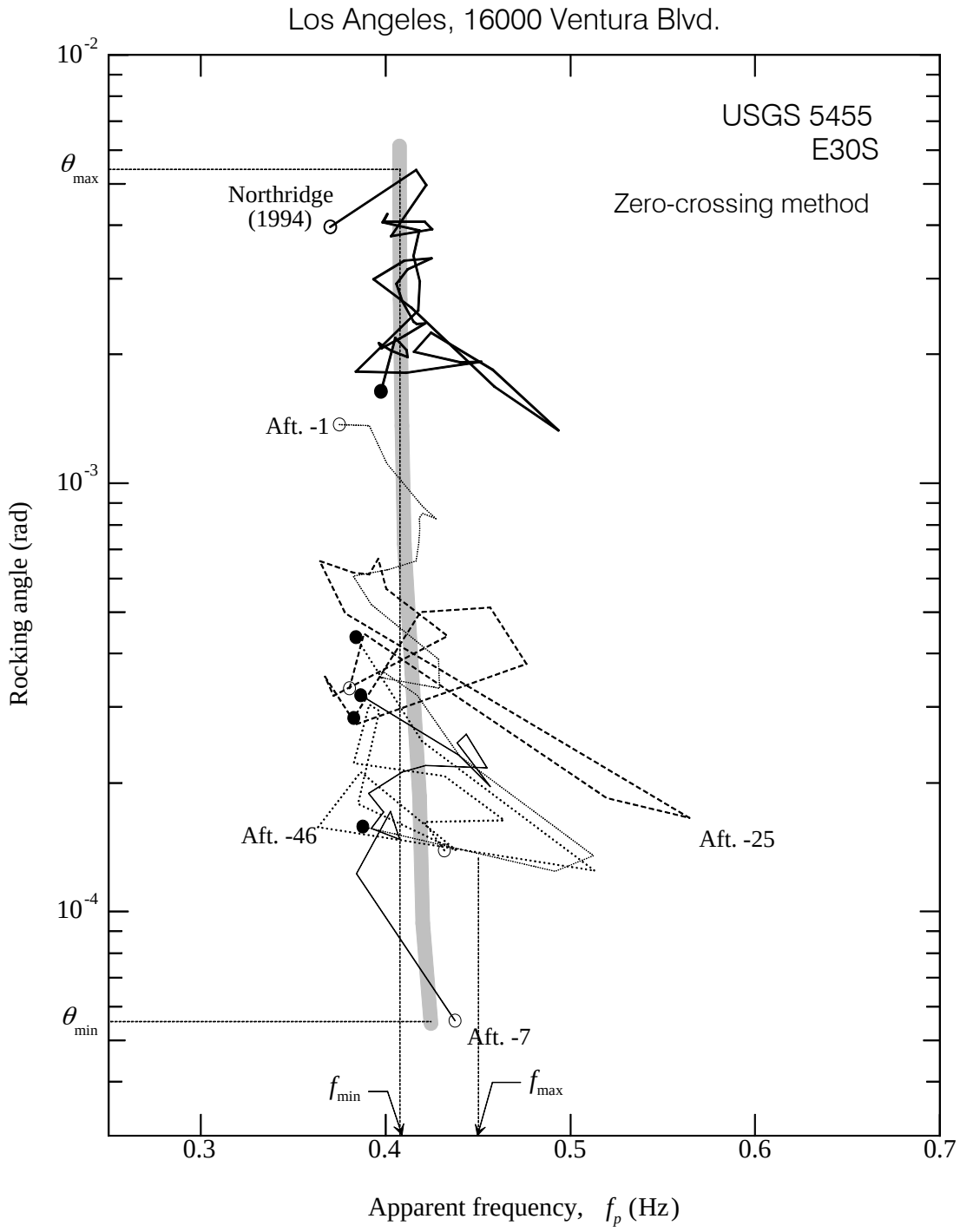
Los Angeles, 16000 Ventura Blvd.
USGS 5455
E30S
Zero-crossing method
Northridge
(1994)
Aft. -1
Aft. -46
Aft. -25
Aft. -7
θ_{max}
θ_{min}
f_{min}
f_{max}
10^{-2}
10^{-3}
10^{-4}
Rocking angle (rad)
0.3
0.4
0.5
0.6
0.7
Apparent frequency, f_p (Hz)

Figure B.20a

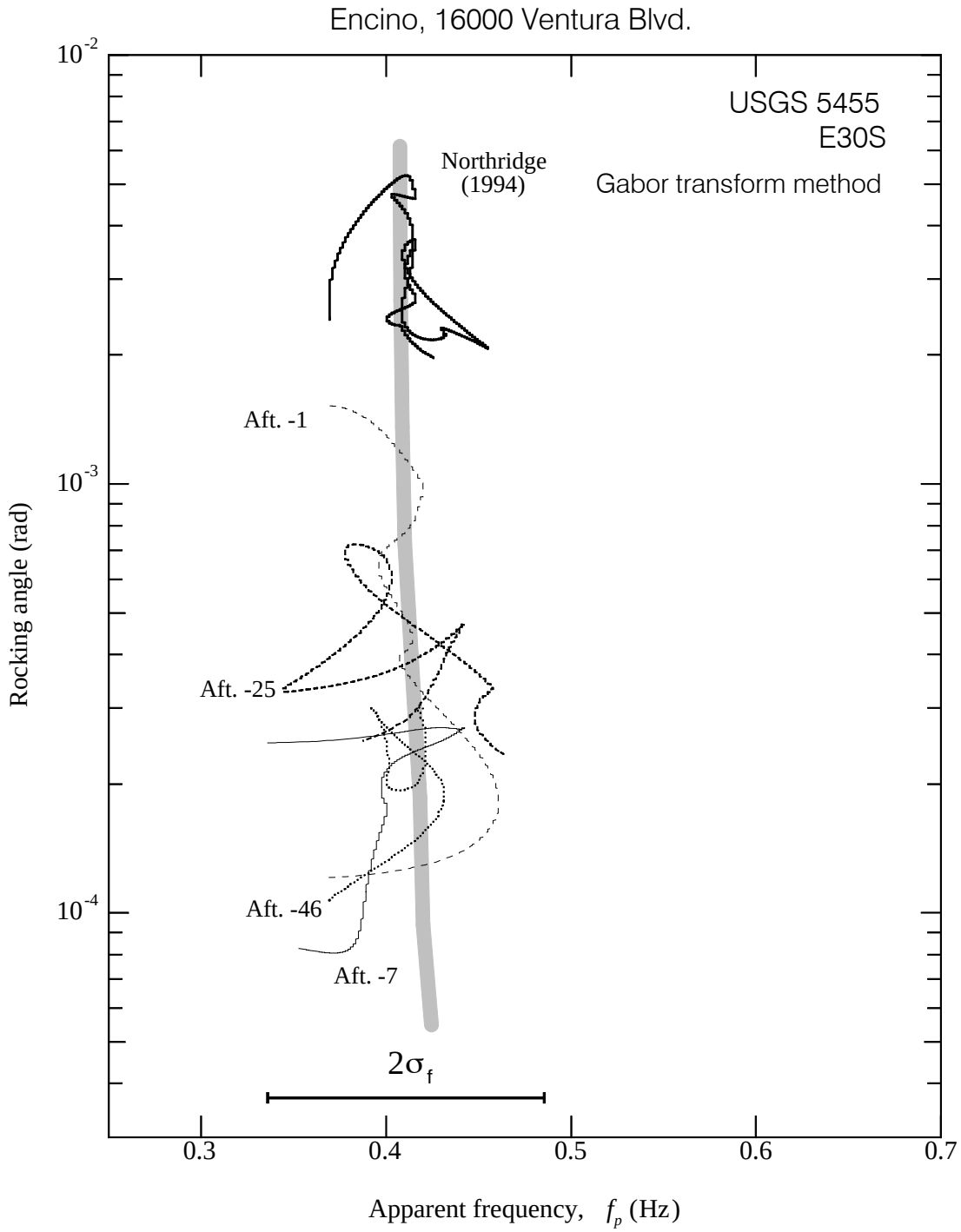
Encino, 16000 Ventura Blvd.
USGS 5455
E30S
Gabor transform method
Northridge
(1994)
Aft. -1
Aft. -25
Aft. -46
Aft. -7
$2\sigma_f$
10^{-2}
10^{-3}
10^{-4}
Rocking angle (rad)
0.3
0.4
0.5
0.6
0.7
Apparent frequency, f_p (Hz)

Figure B.20b

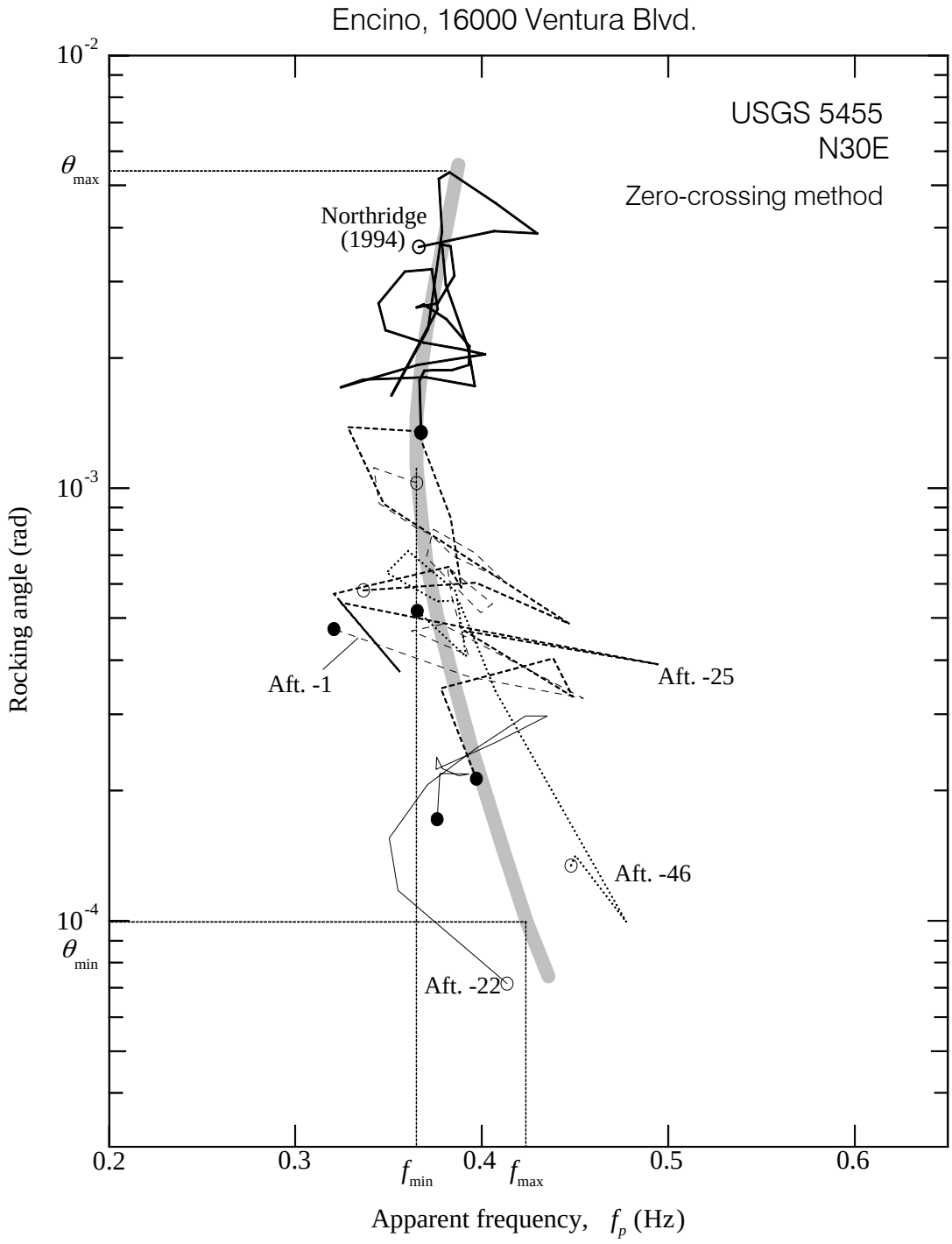
Encino, 16000 Ventura Blvd.
USGS 5455
N30E
Zero-crossing method
Northridge
(1994)
Aft. -1
Aft. -25
Aft. -46
Aft. -22
10^{-2}
θ_{max}
10^{-3}
10^{-4}
θ_{min}
Rocking angle (rad)
0.2
0.3
0.4
0.5
0.6
f_{min}
f_{max}
Apparent frequency, f_p (Hz)

Figure B.20c

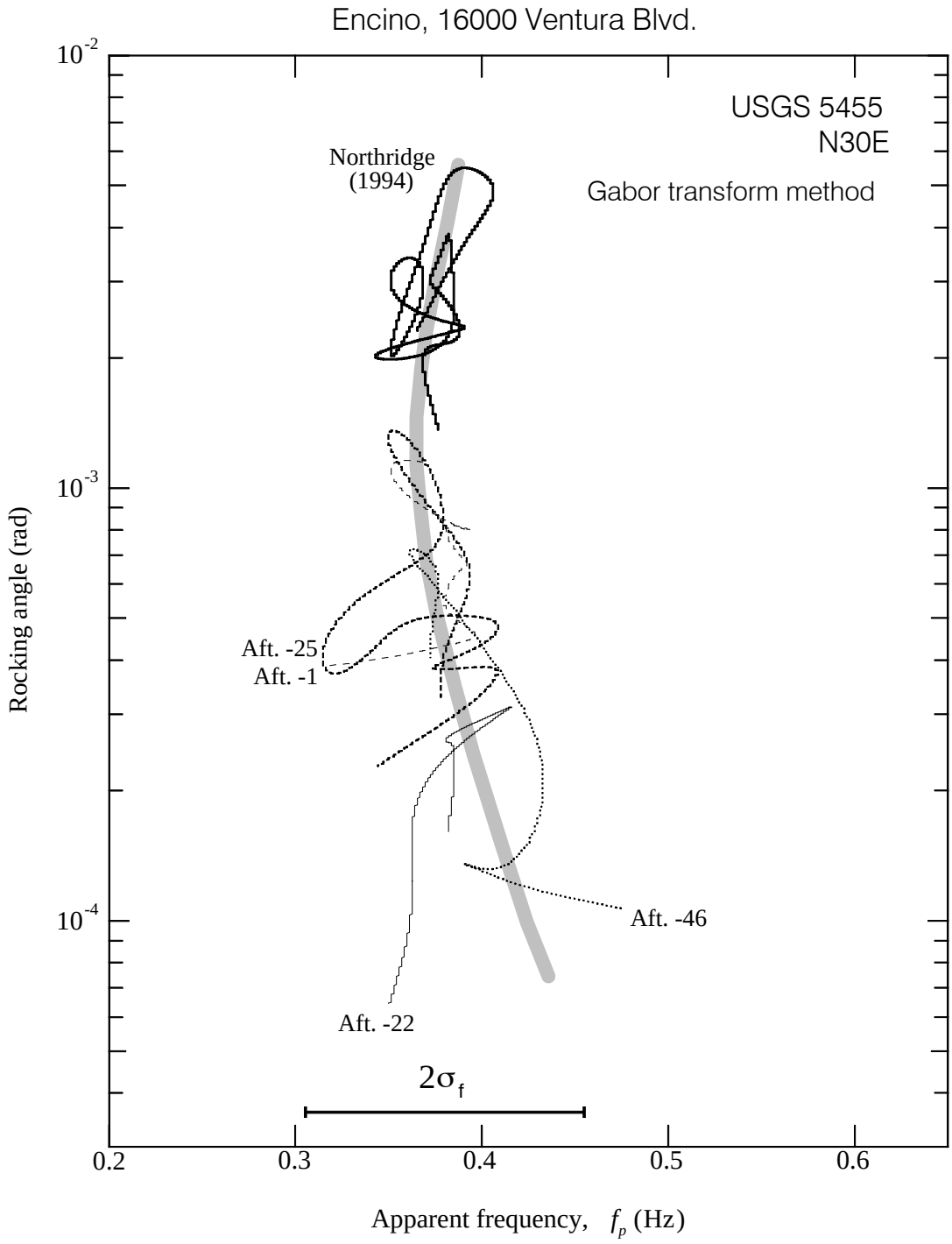
Encino, 16000 Ventura Blvd.
USGS 5455
N30E
Gabor transform method
Northridge
(1994)
Aft. -25
Aft. -1
Aft. -46
Aft. -22
2σf
10-2
10-3
10-4
0.2
0.3
0.4
0.5
0.6
Rocking angle (rad)
Apparent frequency, fp (Hz)

Figure B.20d

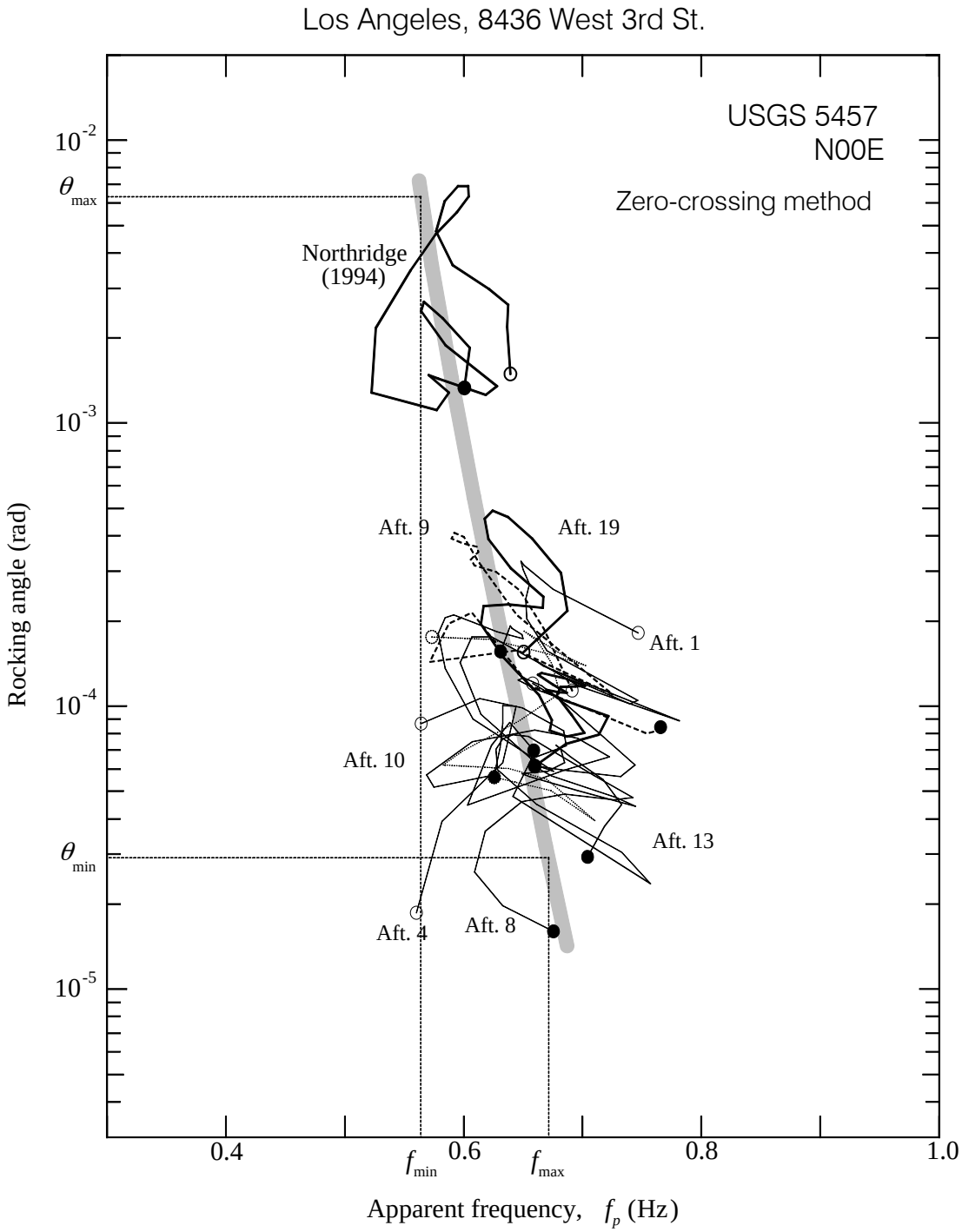
Los Angeles, 8436 West 3rd St.
USGS 5457
N00E
Zero-crossing method
Northridge
(1994)
Aft. 9
Aft. 19
Aft. 1
Aft. 10
Aft. 13
Aft. 4
Aft. 8
θ_{max}
θ_{min}
10^{-2}
10^{-3}
10^{-4}
10^{-5}
Rocking angle (rad)
0.4
0.6
0.8
1.0
f_{min}
f_{max}
Apparent frequency, f_p (Hz)

Figure B.21a

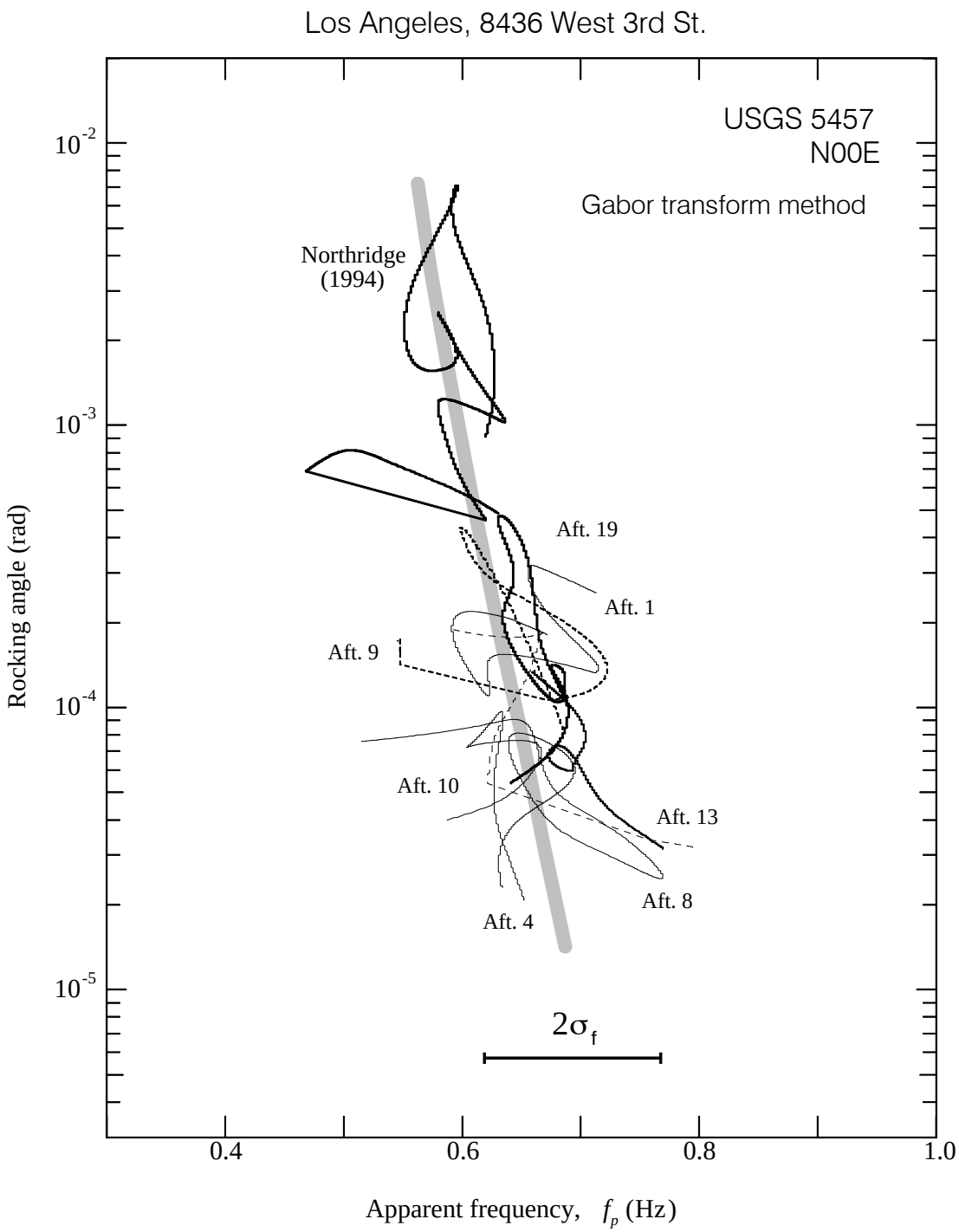
Los Angeles, 8436 West 3rd St.
USGS 5457
N00E
Gabor transform method
Northridge
(1994)
Aft. 19
Aft. 1
Aft. 9
Aft. 10
Aft. 13
Aft. 8
Aft. 4
2σf
10-2
10-3
10-4
10-5
Rocking angle (rad)
0.4
0.6
0.8
1.0
Apparent frequency, fp (Hz)

Figure B.21b

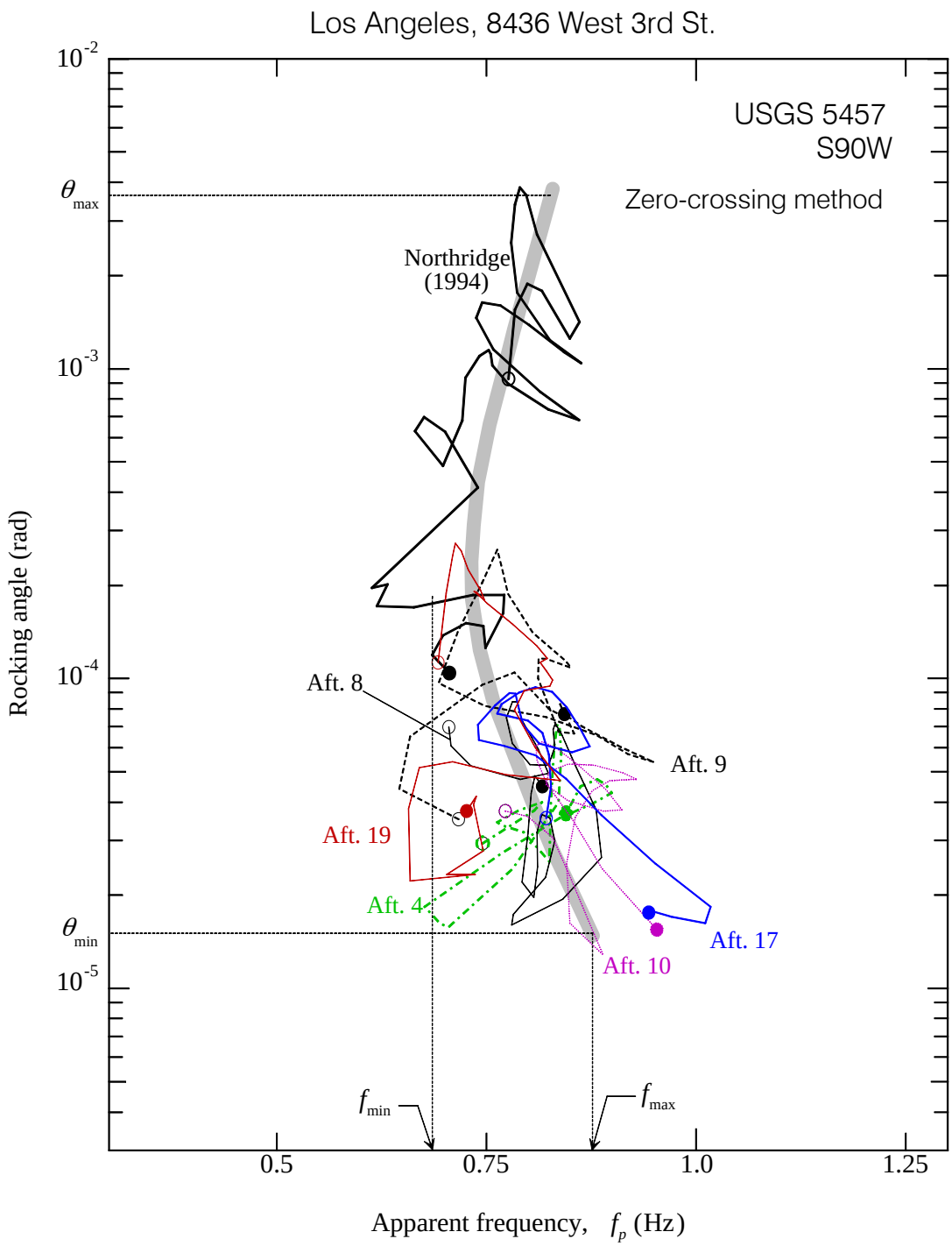
Los Angeles, 8436 West 3rd St.
USGS 5457
S90W
Zero-crossing method
Northridge
(1994)
Aft. 8
Aft. 9
Aft. 19
Aft. 4
Aft. 17
Aft. 10
θ_{max}
θ_{min}
f_{min}
f_{max}
10^{-2}
10^{-3}
10^{-4}
10^{-5}
0.5
0.75
1.0
1.25
Rocking angle (rad)
Apparent frequency, f_p (Hz)

Figure B.21c

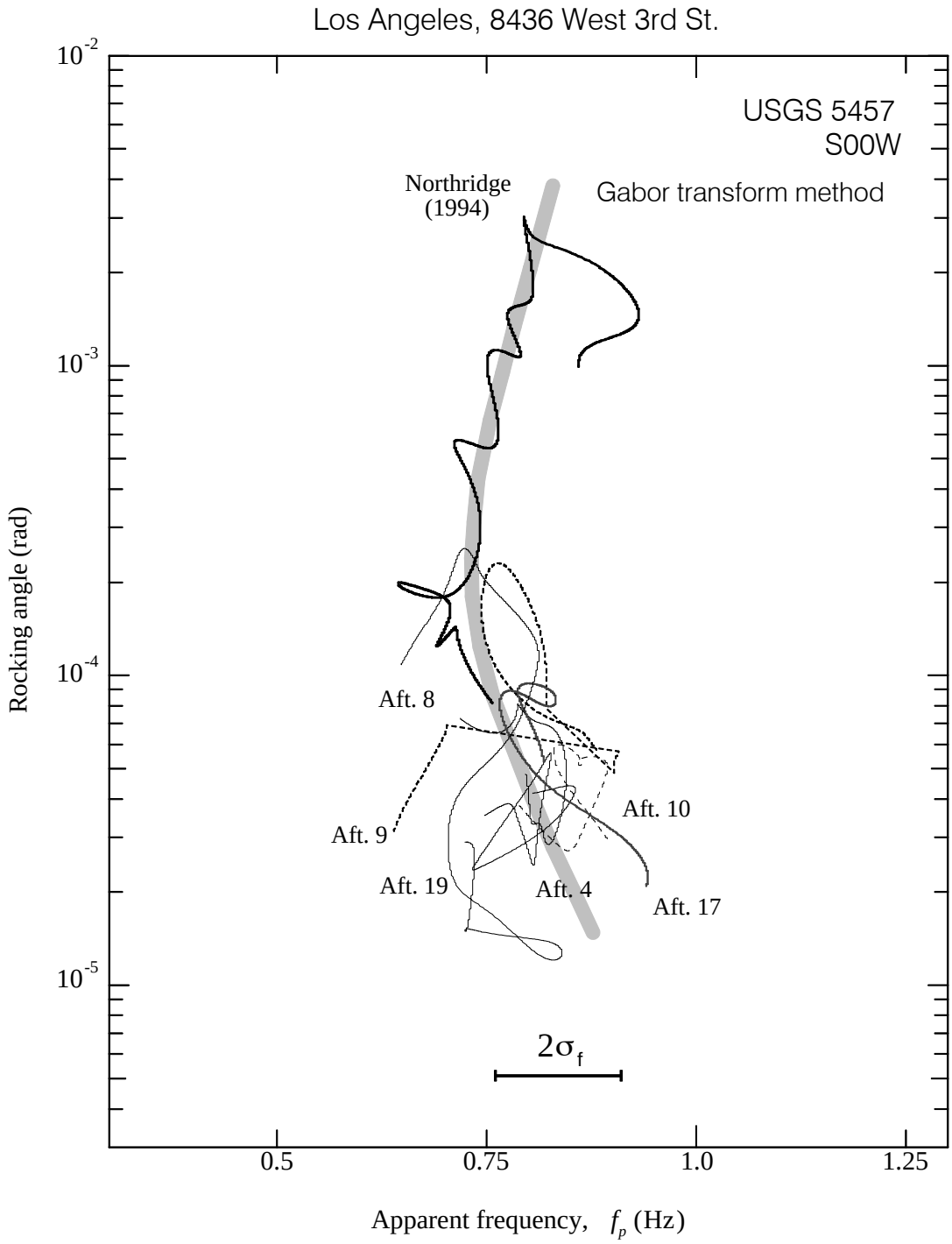
Los Angeles, 8436 West 3rd St.
USGS 5457
S00W
Northridge
(1994)
Gabor transform method
Aft. 8
Aft. 9
Aft. 10
Aft. 19
Aft. 4
Aft. 17
2σf
Rocking angle (rad)
Apparent frequency, fp (Hz)
10-2
10-3
10-4
10-5
0.5
0.75
1.0
1.25

Figure B.21d